C_3-symmetric Discotic Liquid Crystalline Materials for Molecular Electronics: Versatile Synthesis and Self-organization

Dissertation

zur Erlangung des Grades
"Doktor der Naturwissenschaften"

dem Fachbereich Chemie und Pharmazie der
Johannes Gutenberg-Universität Mainz
vorgelegt von

Xinliang Feng
geboren in Anhui Province / P. R. China

Mainz, 2008

Decan: Herr Prof. Dr.

1. Berichterstatter: Herr Prof. Dr.

2. Berichterstatter: Herr Prof. Dr.

Tag der mündlichen Prüfung:

Die vorliegende Arbeit wurde in der Zeit von September 2004 bis Februar 2008 im Max-Planck-Institut für Polymerforschung in Mainz unter Anleitung von Herrn Prof. Dr. Müllen ausgeführt.

Ich danke Herrn Prof. Dr. K. Müllen für seine wissenschaftliche und persönliche Unterstützung sowie für seine ständige Diskussionsbereitschaft.

Table of Contents

Index of Abbreviations

2D-WAXS	two-dimensional wide angle X-ray scattering
AFM	atomic force microscopy
DCM	dichloromethane
DSC	differential scanning calorimetry
EA	elemental analysis
FD MS	field desorption mass spectroscopy
FET	field effect transistor
HBC	hexa-*peri*-hexabenzocoronene
HOMO	highest occupied molecular orbital
h	hour
LED	light emitting diode
LUMO	lowest unoccupied molecular orbital
MeOH	methanol
MS	mass spectroscopy
min	minute
m.p.	melting point
MALDI-TOF	matrix-assisted laser desorption ionization –time of flight
NMR	nuclear magnetic resonance
PE	petroleum ether
PAH	polycyclic aromatic hydrocarbons
POM	polarized optical microscopy
RT	room temperature
STM	scanning tunneling microscopy
TCNQ	7,7,8,8-tetracyanoquinodimethane
THF	tetrahydrofuran
TLC	thin layer chromatography
TMS	trimethylsilyl
Tolane	diphenylacetylene
UV-vis	ultraviolet/visible

Chapter 1. Introduction

1.1 Polycyclic Aromatic Hydrocarbons

Polycyclic aromatic hydrocarbons (PAHs) are chemical compounds that consist of fused conjugated aromatic rings and do not contain heteroatoms or carry substituents.[1] These compounds can be point source (e.g. oil spill) or non-point source (e.g. atmospheric deposition) and are one of the most widespread organic pollutants. Some of them are known or suspected carcinogens, and are linked to other health problems. They are primarily formed by incomplete combustion of carbon-containing fuels such as wood, coal, diesel, fat, tobacco, or incense.[2] Tar also contains PAHs. Different types of combustion yield different distributions of PAHs of individual PAHs which can also give rise to isomers. Thus, those produced from coal combustion are different from those produced by motor-fuel combustion, which differ from those produced by forest fires. Some PAHs occur within crude oil, arising from chemical conversion of natural product molecules, such as steroids, to aromatic hydrocarbons. They are also found in the interstellar medium, in comets, and in meteorites and are a candidate molecule to act as a basis for the earliest forms of life.[3]

The simplest PAHs, as defined by the International Union on Pure and Applied Chemistry (IUPAC), are phenanthrene and anthracene. Smaller molecules, such as benzene and naphthalene, are not formally PAHs, although they are chemically related they are called one-ring (or mono) and two-ring (or di) aromatics. PAHs may contain four-, five-, six- or seven-member rings, but those with five or six are most common. PAHs composed only of six-membered rings are called alternant PAHs. Certain alternant PAHs are called "benzenoid" PAHs. PAHs containing up to six fused aromatic rings are often known as "small" PAHs and those containing more than six aromatic rings are called "large" PAHs. Due to the availability of samples of various small PAHs, the main research on PAHs has been focused on those of up to six rings. Examples of well-known PAHs are shown in Scheme 1-1.

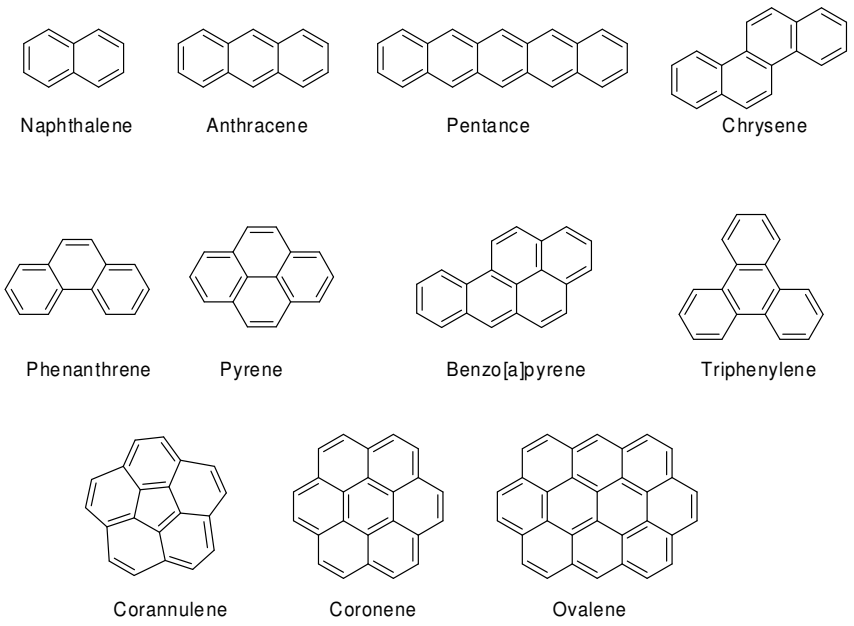

Scheme 1-1. Examples of prominent PAHs.

In graphene, the PAH motif is extended to large 2D sheets, which can be regarded as graphite segments (Figure 1-1), and represents one of the most intensively investigated class of compounds in synthetic chemistry and material sciences. The systematic study of PAHs and their application as materials have spurred scientist for several decades, however, only few selective synthetic methods have been established so far. Fundamental contributions to the directed synthesis and characterization of polycyclic aromatics were pioneered by R. Scholl, E. Clar and M. Zander, who achieved the synthesis of numerous aromatic compounds under drastic conditions at high temperatures with strong oxidation.[4] The synthetic breakthrough was achieved as a result of progress of analytical techniques and made the selective synthesis of various PAHs under mild conditions possible.[5]

One of the intrinsic properties of the PAHs is their aromaticity, which has attracted great interest in theoretic chemistry,[6] different theoretical methods have been applied to estimate the electronic properties of graphite based on PAHs with increasing size and varying topologies. As a result of the development of organic semiconductors,[7] PAHs with unique electronic and optoelectronic properties have received great attention in the scientific community. Large PAHs with different functionality, which

endow a facile fabrication, are promising candidates in organic devices such as light-emitting diodes (LEDs), field effect transistors (FETs), and photovolatic cells.[8] Additionally, two-dimensional all-benzenoid graphitic molecules with appropriate substituents are fascinating due to their highly stable columnar mesophases, which are desirable for device processing.[9] Furthermore, well-defined nanostructures resulting from supramolecular self-assembly of PAHs, such as nanotubes and nanowires, have a great potential in nanotechnology.[10]

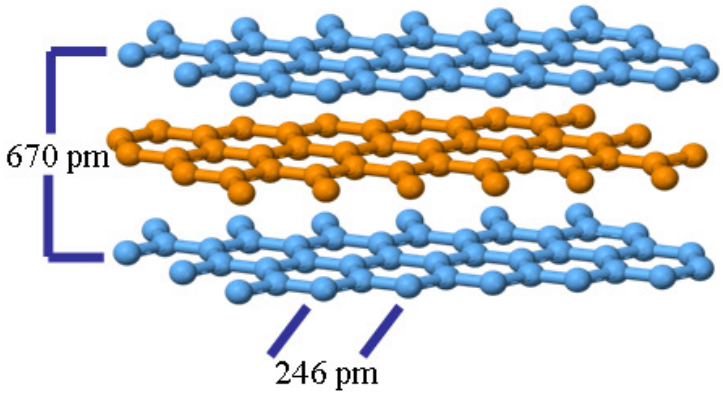

Figure 1-1. Layer structure of graphite.

1.1.1 Synthesis

Besides small PAHs, which have been isolated from coal tar and catalytic hydrocarcking of petroleum, a far more defined preparation of PAHs is possible by the means of synthetic organic chemistry, as shown by the pioneering work of R. Scholl, E. Clar and M. Zander. The most generally used methods for the construction of PAH ring systems are summarized in the following, including the most recently developed synthetic methodologies, and indicate the trend of this research field towards the development of milder methods, which proceed with high regioselectivity and yields.

1.1.1.1 Intra- and intermolecular Diels-Alder reaction

Diels-Alder reaction is surely one of the most efficient synthetic methods to create carbon-carbon bonds. One of the recent examples is to synthesize the attractive

pentacene derivative as illustrated in Scheme 1-2. Maleic anhydride and quinones, such as benzoquinone, are frequently employed as dienophiles for this purpose. Here the double Diels-Alder strategy of Danieshefsky's diene with anthradiquinone affords a cycloadduct that is finally converted to the substituted pentacene **1-1** by reductive deoxgygenation/aromatization.[11]

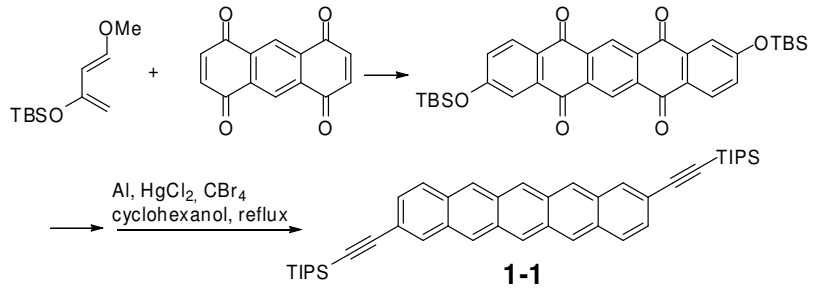

Scheme 1-2. Example of Diels-Alder cycloaddtion for the synthesis of PAHs.

An elegant entry to oligophenylene structures can be achieved by intramolcular [4+2] cycloaddition of suitable phenylene-vinylene derivatives, followed by aromatization of the newly formed cyclohexene structures. An example for such strategy is developed by M. Müller in the Müllen group, who constructed a suitable precursor for a 60 carbon containing, rhombus-shaped PAH **1-5** (Scheme 1-3).[12] The

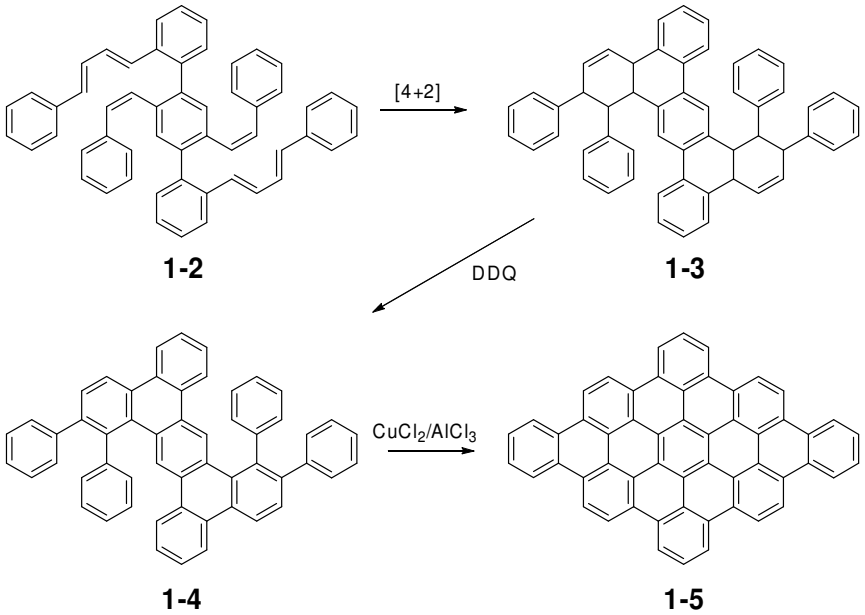

Scheme 1-3. Synthesis of rhombus-shaped PAH **1-5**.

para-terphenyl derivative **1-2** is subjected to a nearly quantitative intramolecular [4+2] cycloaddition at 135 ^{o}C to form the cyclohexene derivative **1-3**. Following the mild oxidation with 2,3-dichloro-4,5-dicyanoquinone (DDQ) and $CuCl_2/AlCl_3$, the precursor is planarized to the desired molecule **1-5**.

1.1.1.2 Ring-closing olefin metathesis (RCM)

Strategies involving transition metal catalysis are attractive because of the mild reaction conditions. For example, palladium-catalyzed cross-coupling is popular for the formation of aryl-aryl σ-bonds. Ring-closing olefin metathesis has emerged as a powerful tool for the preparation of double bonds in cyclic organic compounds but has only recently been applied to PAHs. The first preparative utility of RCM to generate functionalized phenanthrenes from 2,2'-divinylbiphenyl derivatives. As a typical example shown in Scheme 1-4, the double RCM of terphenyl precursors affords dibenz[a,j]anthracene **1-6** and dibenz[a,h]-anthracene **1-7** in good yields.[13]

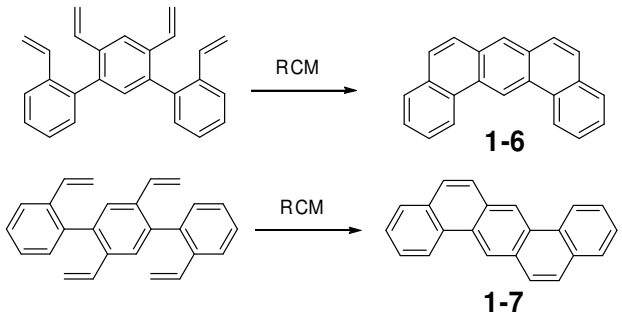

Scheme 1-4. Double RCM synthesis of acenes.

The need for more highly substituted and structurally varied helicenes has led to the development of new methods as replacements of the classical synthesis by the photocyclization of stilbenes. As a result, very recently, RCM has also been used to synthesize the substituted [5]helicenes **1-8** and even [6]- and [7]helicenes in good to high yields (Scheme 1-5).[14]

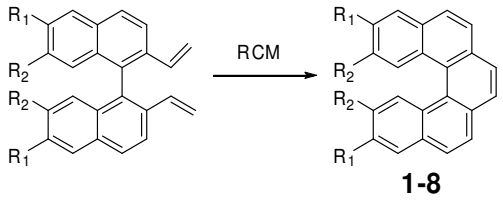

Scheme 1-5. Preparation of substituted helicenes

1.1.1.3 Benzannulation and electrophilic cyclization

The published methods for the synthesis of coronenes **1-9** are plagued with long procedures and inefficiency, typically including a pyrolysis step at high temperatures. The lack of a convenient and efficient synthesis of coronenes impedes their progress in organic chemistry. Scott and co-workers firstly proposed a short synthesis of coronenes from metal-catalyzed benzannulation of bis(1,1-ethynyl)alkene species,[15] which was a useful precursor for the flash-vaccum pyrolysis (FVP) synthesis of coronenes and could be prepared conveniently in three steps from commercially available anthraquinone (Scheme 1-6). By using 20 mol% $RuPPh_3(cymene)Cl_2$ catalyst, a 15~20% yield of coronene was the first time obtained by chemical reactions in solution, which is already much higher than that of the FVP method. Liu and co-workers optimized the reaction conditions by using $TpRuPPh_3(CH_3CN)_2PF_6$ as catalyst, amazingly 86% yield of coronene could be achieved.[16] By using their conditions, differently substituted coronene derivatives could be synthesized for the first time. This synthetic strategy is also useful for the synthesis of oligoacene derivatives, such as **1-7**.

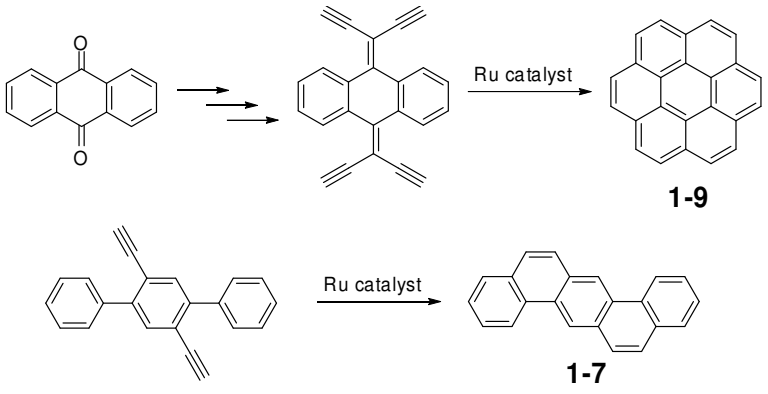

Scheme 1-6. Examples for the synthesis of PAHs by benzannulation.

With the goal of ultimately preparing polymeric fused or ribbon like PAHs, Swager and co-workers have successfully developed the electrophilic cyclization of polyacences by using of the strong electrophilic iodine reagent $I(pyridine)_2BF_4$ or trifluoroacetic acid.[17] The reaction conditions were very mild and mostly provided high yields. The typical example is shown in Scheme 1-7, starting from the conjugated polymers with 2,5-substituted diphenylacetylene units, conjugated ladder polymers or graphite ribbon **1-10** could be synthesized in quantitative yields. The same synthetic protocol is also useful for the building of related oligoacenes and thioacenes. Larock and co-workers observed that ICl was a strong electrophilic reagent for this reaction, and could be widely used under mild conditions with high yields.[18]

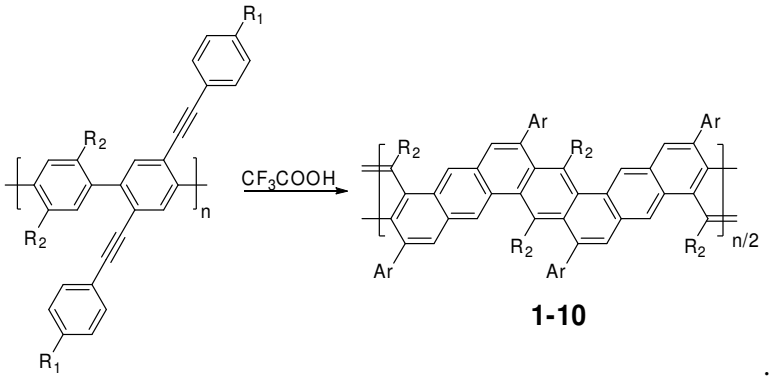

Scheme 1-7. Synthesis of polyacene by electrophilic cyclization.

1.1.1.4 Intramolecular photocyclization of stilbene type compounds

The photo-induced ring closure of stilbene type compounds has been extensively used in the preparation of condensed PAHs.[19] Different stilbenes can be conveniently prepared by employing Wittig, Heck as well as McMurry coupling reactions. Therefore various PAHs can be easily made, for example circumanthracene **1-11** (Scheme 1-8)**.**

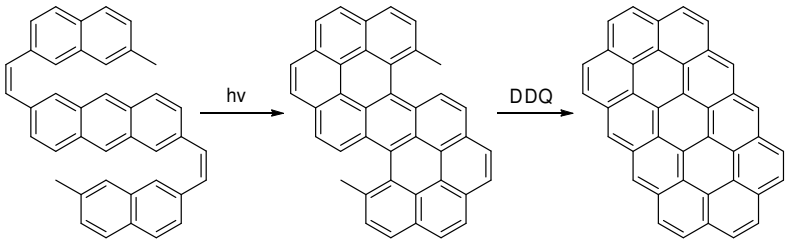

1-11

Scheme 1-8. Synthesis of circumanthracene.

Very recently, Nuckolls and co-workers have developed a novel approach towards a phase forming, distorted hexa-*cata*-hexabenzocoronene derivative **1-12** (Scheme 1-9),[20] whereby the decisive step is accomplished by the photocyclization. The material formed columnar liquid-crystalline phases with high charge carrier mobilities as determined in FETs.

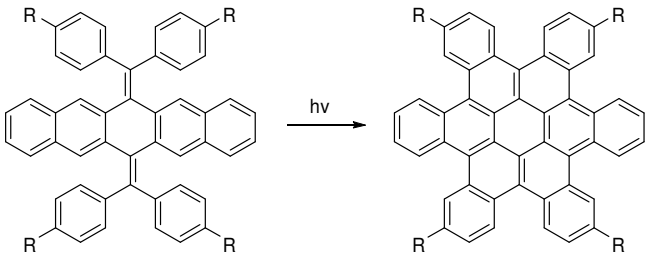

1-12

Scheme 1-9. Synthesis of hexa-*cata*-hexabenzocoronenes.

1.1.1.5 Flash vacuum pyrolysis

The conversion of appropriate precursors to condensed PAHs at high temperature with short contact time in the hot zone, is referred to as flash vacuum pyrolysis (FVP). The key point is the design of the precursors, which should have a good thermal stability and reactive sites. A typical example is the synthesis of corannulene **1-13** in good yield (Scheme 1-10) upon the treatment of 7,10-bis(1-chlorovinyl)fluoranthene under FVP condition.[21] This synthetic method has been successfully developed to yield different bowl-shaped PAHs and fullerene.[22]

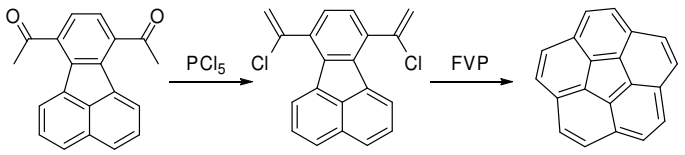

1-13

Scheme 1-10. Syntehsis of corannulene by FVP method.

1.1.1.6 Oxidative cyclodehydrogenation

In the presence of Lewis acid catalysts, the intermolecular or intramolecular coupling of two aromatic rings is called the "Scholl reaction". The detail mechanism for this reaction is however still not yet clearly understood. A stepwise arenium cation mechanism and radical cation mechanism are suggested theoretically.[23] With appropriate oligophenylene precursors, the Scholl reaction has been developed as a powerful tool to produce various all-benzenoid PAHs in the Müllen group.[9b,9d] A typical example is the synthesis of hexa-*peri*-hexabenzocoronenes (HBCs) **1-14** and their derivatives (Scheme 1-11) from substituted hexaphenylbenzene precursors by treatment with iron (III) chloride or $AlCl_3$-$Cu(OTf)_2$.

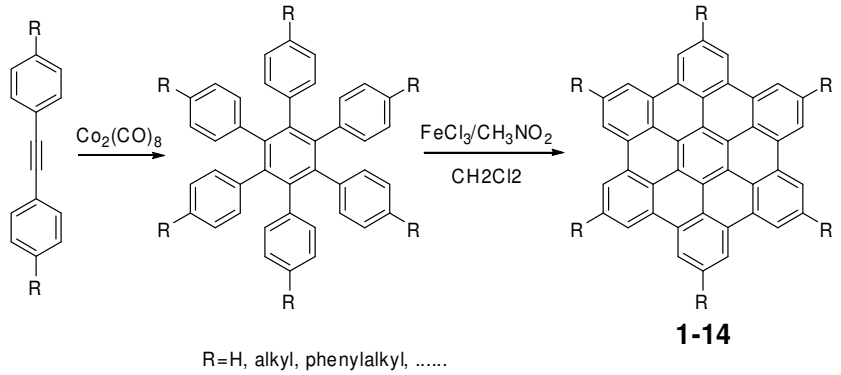

1-14

Scheme 1-11. General synthesis of D_{6h} symmetric HBCs.

A simple approach to HBCs with D_{6h} symmetry is starting from the $Co_2(CO)_8$ catalyzed cyclotrimerization of diphenylacetylenes to afford hexaphenylbenzene derivatives (Scheme 1-11). It opens the possibility to introduce solubilising alkyl side chains as well as functional groups on HBCs, and renders them into ordered columnar liquid-crystalline phases. An extraordinary versatile route to prepare differently symmetric hexaphenylbenzenes is the Diels-Alder reaction of

tetraphenylcyclopentadienones (CP) with diphenylacetylenes. The versatility of this concept becomes obvious regarding the defined preparation of HBC derivatives of different substitution types. By variation of the substituents in the diphenylacetylene or CP, it is possible to furnish different substitution patterns as shown in Scheme 1-12, such as mono substituted, "ortho" disubstituted (C_2 symmetry), and "para" disubstituted (D_2 symmetry) HBCs.

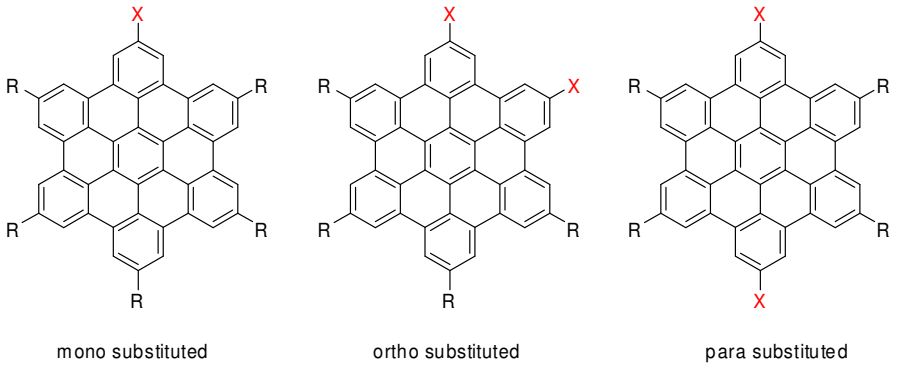

Scheme 1-12. Different substitution patterns of HBC derivatives (X indicates alkyl substituents or functional groups).

One of the major goals of PAH synthesis is to produce improved of ever molecularly defined model compounds of graphite. By employing the previous concept, large dendritic oligophenylene precursors with different size and shape were firstly designed by using the Diels-Alder reaction or cyclotrimerization of suitable building blocks, after planarization of the precursors, all kinds of large benzenoid PAHs with different molecular sizes, symmetries and peripheries have been available in the Müllen group. Up to now, the largest PAH with disc shape containing up to 222 carbon atoms is accessible.[24] Other large PAHs with e.g. linear ribbon-shape, cordite-shape, square-shape and others are also attainable.[25]

The most recent progress in the synthesis of large PAHs is the inclusion of additional double bonds on the periphery of HBCs, which act as the "zig/zag" armchair. It is well-known that the armchair with double bond like characteristics will dramatically influence the electronic and optoelectronic properties of PAHs, as well as their

reactivities.[26] Up to now, HBCs with mono-zigzag, double-zigzag and tri-zigzag are well designed and synthesized by the pioneering work of Z. Wang and M. Kastler in the Müllen group (Scheme 1-13).[27] The further functionalization and modification based on these building blocks will be the next focus.

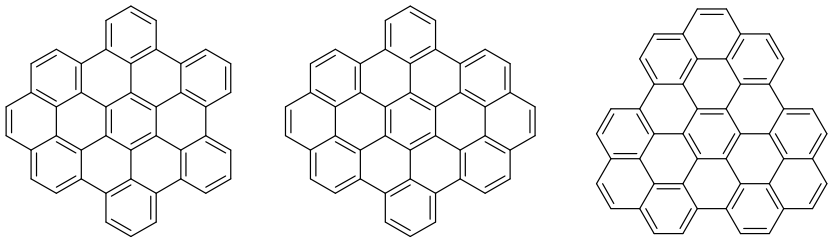

Scheme 1-13. HBCs with different zig/zag peripheries.

1.2 Self-organization and Discotic Liquid Crystals

1.2.1. Introduction and materials

Life on earth begins with the self-organization of molecules. No life would be possible without the self-assembly of lipids into bilayers within the cell membrane. Numerous biological supramolecular structures, e.g., the spontaneous formation of the double helix of nucleic acids, collagen, microtubules, ribosomes, multisubnit enzymes, etc., result from self-assembly of organic molecules.[28] In materials science, non-covalent interactions have been used to obtain well-defined self-assembled architectures in neat systems as well as in solvents. Liquid crystals (LCs) are important examples. Supramolecular interactions such as van der Waals forces, dipolar interactions, π-π interactions and hydrogen bonding play a crucial role in the formation of LCs and in the determination of their mesomorphic properties. Liquid crystals are unique nanostructures with remarkable electronic and optoelectronic properties. Liquid crystal phases share some of the properties of isotropic liquids and crystalline solids. While the molecules in these phases exhibit some positional and orientational order, they also behave as fluids. They combine both the fluidity of liquids and the anisotropy of crystals.

The serendipitous discovery of LCs in 1888 marks an important milestone in the

history of scientific discoveries.[29] When determining the melting point of cholesteryl benzoate, Friedrich Reinitzer, an Austrian botanist, noticed the unusual melting behavior of this compound. This strange phenomenon of the existence of two melting points was explained by the German physicist Otto Lehmann and the term "fluid crystals" or "liquid crystals" was introduced.

Liquid crystalline materials are divided into two categories, the thermotropic and the lyotropic. When a substance passes between the solid, liquid crystal and liquid state and vice versa as a function of temperature and in the absence of solvent, the liquid crystalline phases are classified as thermotropic, while lyotropic phases form in the presence of a suitable solvent. Thus, lyotropic mesophases, found abundantly in biological systems, are always mixtures, whereas thermotropic LCs could consist of a single component or a mixture of many compounds.

The hierarchical self-assembly of disc-shaped molecules leads to the formation of discotic liquid crystls (DLCs).[30] Vorlander in 1908 established his rule that liquid crystalline compounds must have a molecular shape as linear as possible. All the liquid crystalline materials prepared over about 90 years belonged to this family. However, in 1977 S. Chandrasekhar reported that not only rod-like molecules, but also compounds with disc-like molecular shape are able to form mesophases.[31] He prepared a number of benzene-hexa-*n*-alkanonates and from thermodynamic, optical and X-ray studies, it was established that these materials form a new class of LCs in which molecules are stacked one on top of the other in columns that assemble in a hexagonal arrangement. DLCs essentially show three types of mesophase, with varying degrees of organization: columnar (col), nematic-discotic (N_d) and lamellar discotic, where the structure of the latter has not yet been completely elucidated (Figure 1-2).[32] Three 2D lattices are possible in a mesophase: hexagonal, rectangle or oblique as shown in Figure 1-3. The discs are either perpendicular or slightly tilted with respect to the columnar axis.

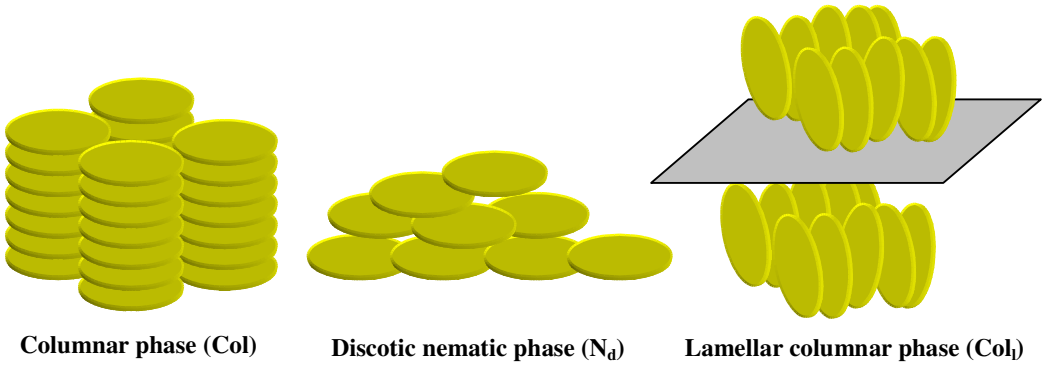

Figure 1-2. Schematic representation of different mesophases of DLCs.

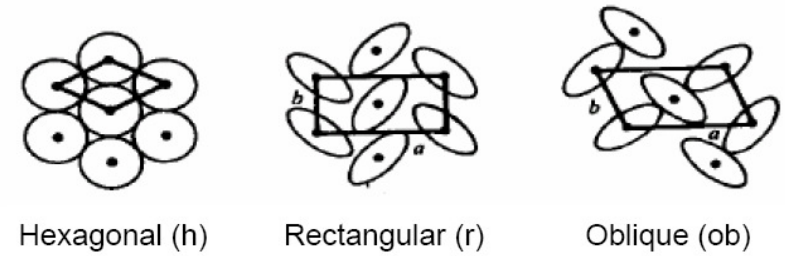

Figure 1-3. Top view of two-dimensional lattices of columnar phases. The ellipses denote discs that are tilted with respect to the columnar axis.

A majority of DLCs form columnar mesophases probably due to the phase separation between aromatic core and peripheral alkyl chains as well as intense π-π interactions of polyaromatic cores. The core-core separation in a columnar mesophase is usually of the order of 3.5 Å so that there is considerable overlap of π-orbitals. As flexible long aliphatic chains surround the core, the intercolumnar distance is usually 20-40 Å, depending on the lateral chain length. Therefore, the interactions between neighbouring molecules within the same column would be much stronger than interactions between neighbouring columns. Consequently charge migration in these materials is expected to be quasi one-dimensional. Conductivity along the columns in the columnar mesophases has been reported to be several orders of magnitude greater than in the perpendicular direction.[33] Thus, the columns maybe described as molecular wires (Figure 1-4). So far charge carrier mobility as high as 1.1 $cm^2V^{-1}s^{-1}$

along the columns has been observed for HBC at the crystalline phase.[34]

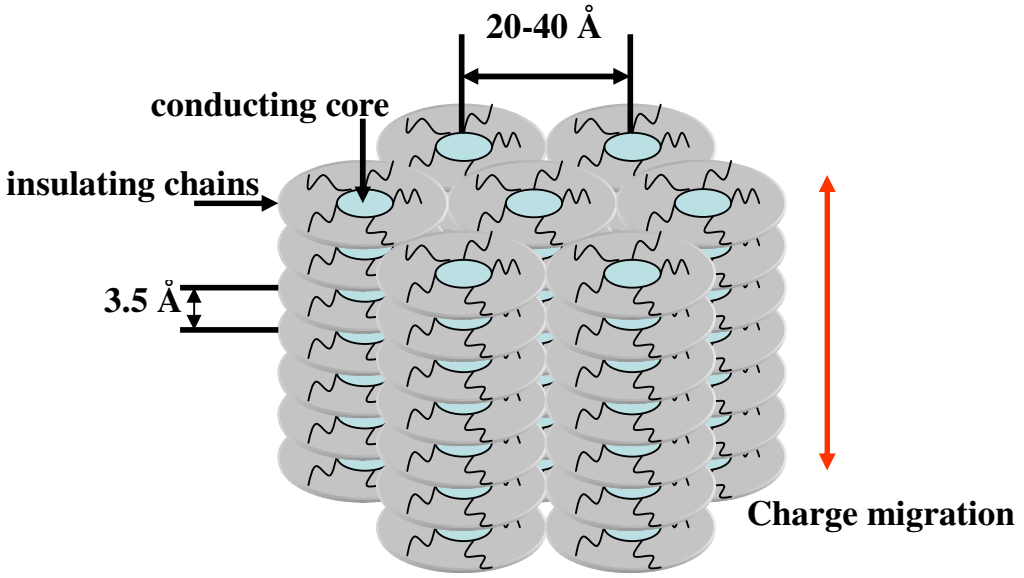

Figure 1-4. Schematic view of charge migration in columnar phase.

The supramolecular assemblies of disc-shaped molecules have been extensively studied for the energy and charge migration in organized systems and their device applications such as, one-dimensional conductors, photoconductors, light emitting diodes, photovoltaic solar cells, field-effect transistors and gas sensors have been sought.[35] Currently the number of DLCs derived from more than 50 different cores comes to about 3000. In Figure 1-5, some of the most prominent DLCs are shown, which range from the first reported hexa-alkanoyloxy-benzenes, to porphyrins, phthalocyanines, triphenylenes, hexaazatriphenylenes, perylenes, macrocycles, HBCs and others.[36]

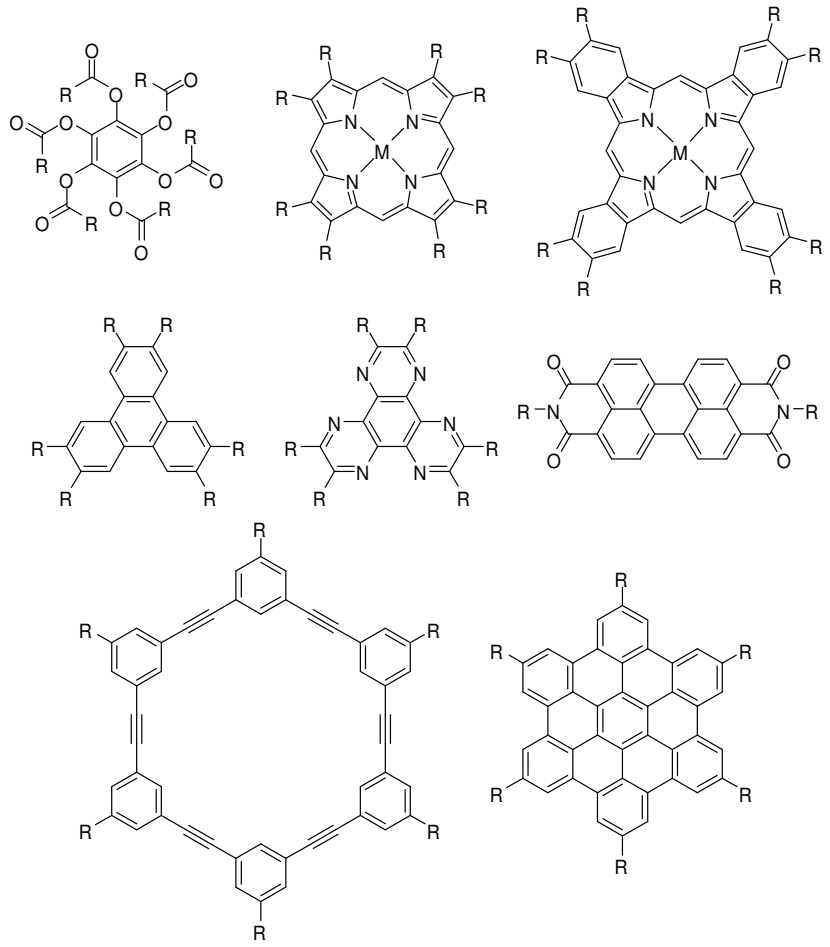

Figure 1-5. Selection of prominent discotic liquid crystals.

1.2.2. Characterization of the self-organization

In order to gain deep understanding of the molecular ordering in the bulk phase of discotics, thermgravimetric analysis (TGA), differential scanning calorimetry (DSC), polarized optical microscopy (POM), and X-ray diffractometry are necessary tools for structural characterizations. DSC, POM and X-ray reveal the columnar packing in different phases. Solid state NMR spectroscopy is an additional valuable tool to probe the packing mode at the molecular scale. Sometimes, solid state UV-vis spectroscopy, atomic force microscopy (AFM), scanning electron microscopy (SEM), and transmission electron microscopy (TEM) can also be combined to understand the phase transitions, and self-organization in thin layers upon the thermal annealing in the mesophase.

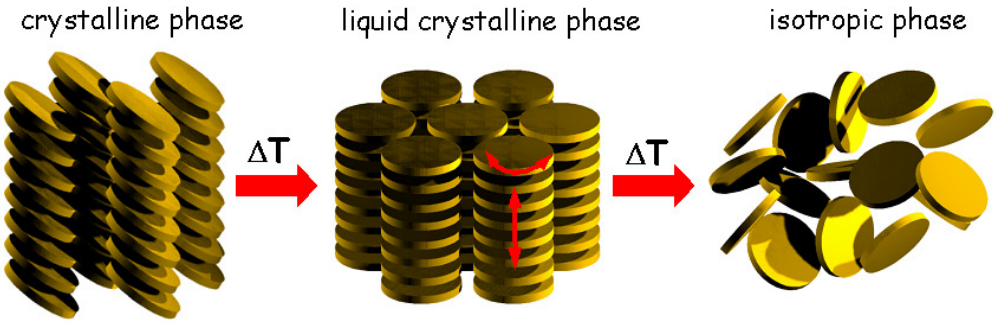

Figure 1-6. Schematic representation of the self-organization within three phases of substituted HBCs.

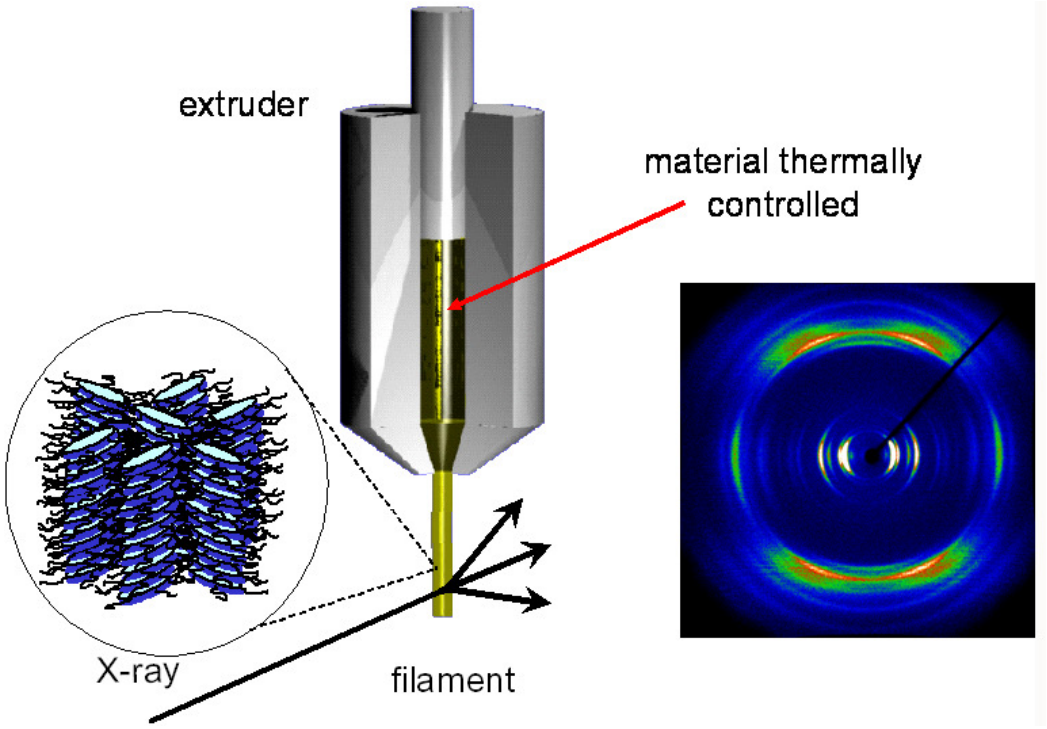

Figure 1-7. Schematic illustration of the experimental set up and principle for 2D-WAXS measurements on extruded filaments.

For the alkyl substituted HBCs, TGA revealed that the derivatives are stable up to 400°C, at which temperature decomposition of the substituted alkyl chains starts. Three phases are typically observed (Figure 1-6); both X-ray and solid state NMR experiments revealed a tilted columnar organization in the crystalline phase, in which

the aromatic core is crystallized and positioned on fixed lattice points. In the mesophase, the rotation of HBC discs around the column axis is possible, and the discs are perpendicular to the columnar axis. In the isotropic phase, the materials behave like the normal liquid without anisotropy. Two-dimensional wide-angle X-ray scattering measurements of extruded fibers are surely one of the most important methods to extract detail information about supramolecular organization of HBCs in the solid state (Figure 1-7).[37] The 2D diffractograms with information regarding the stacking within the columns and the intercolumnar arrangement in different phases are then obtained.

1.2.3. Self-assembly of discotics on the surface

In the quest for the fabrication of miniaturized devices based on molecular objects and nanostructures, the self-assembly of conjugated π-molecules on the surfaces are essentially important. There are basically two approaches to this research field, the first one is based on the visualization and manipulation of single molecules or small aggregates, which is named as single molecular electronics; the second field is based on the fabrication of nanostructures in the device, such as nanofibers (nanowires), nanotubes, and nanoshperes, which has been spurred intensively in the recent years.

In 1982, the invention of scanning tunnelling microscope (STM) represented a breakthrough for nanoscience by making it possible for the first time to generate real-space images with a resolution at the sub-micrometer scale. The ultra-high vacuum deposition (UHV) STM is limited to small molecules which are easy to be sublimed. Therefore only few HBC derivatives could be deposited due to the relative high sublimation temperature.

Using soluble, alkyl substituted HBC derivatives, face-on monomolecular layers could be prepared by self-assembly from solution on highly oriented pyrolytic graphite (HOPG), and could be analyzed with STM at the liquid-solid interface.[38] This methodology represents a useful approach to study the self-assembly behavior of molecules on the surface which can be solution processable. Figure 1-8 shows the ordering pattern of hexadodecyl-HBC on HOPG. Because of their specific areas of

the molecule could be studied by scanning tunnelling spectroscopy (STS), which resulted in different current-voltage curves for the aromatic and the aliphatic areas.[39] Very recently, C_3 symmetrical triangle-shaped discotics are observed to self-assemble into ordered honeycomb networks,[40] the driving force could be ascribed to the molecular-interface and molecular-molecular interactions, therefore allowing potential applications in molecular-switches and host-guest recognitions.[40]

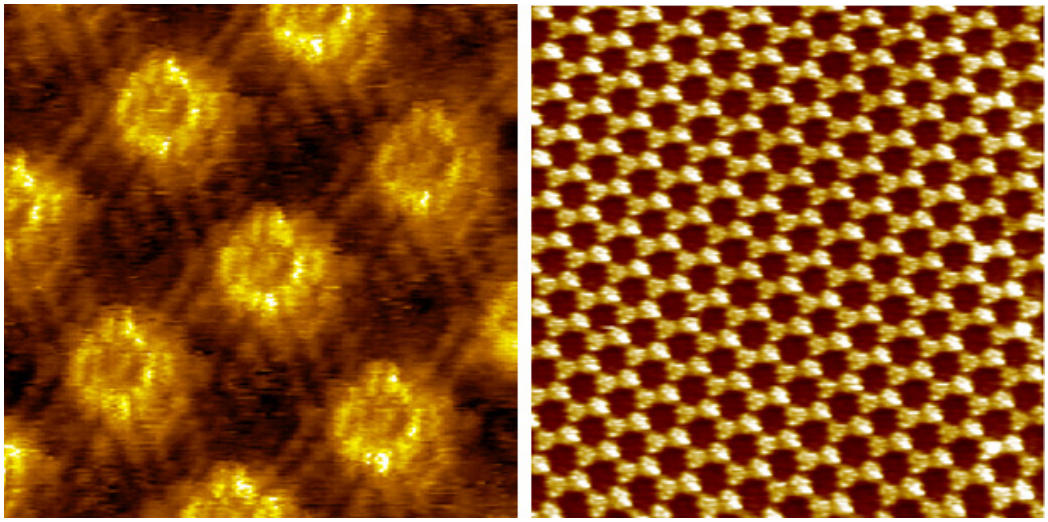

Figure 1-8. Self-assembly of hexadecyl-HBC (left) and triangle-shaped PAHs (right) on the liquid-solid interface.

In general, columnar nanostructures growth through strong π-stacking of alkylated discotic building blocks combined with additional intermolecular forces are attractive, both as "nanowires" and as molecular systems forming uniform films with a high degree of columnar orientation.[41] Recently, HBCs, self-assembled into well-defined nanotubular or fibrous objects with a large number of π-stacked HBC units, have gained wide attention due to their semiconducting character.[10]

In Figure 1-9a, the optical microscopy depicts a pronounced aggregation propensity of a hexadodecyl-HBC after solution casting. The resulting drop-cast film consists of fiber-like structures when deposited on a field-effect transistor. Each microfiber consists of the typical columnar stacks that form due to the π-stacking interactions of

the HBC-C_{12} molecules. Charge carrier transport takes place along the axis of the columns, the transistor shows a saturated hole mobility of $\mu_{sat} = 3 \times 10^{-4}$ cm^2/Vs and a source drain current on/off ratio of $I_{on}/I_{off} = 2 \times 10^5$. This moderate charge carrier mobility can be related to macroscopical columns connecting the source and drain electrodes.[42]

Since the above method for fiber growth is strongly dependent on the nature of molecules, an appropriate way to fabricate the fiber formation on the surface is to design new HBC molecules which can combine the strong π-stacking accompanied by additional non-covalent interactions. C_3 symmetric HBCs with alternating hydrophilic/hydrophobic substituents are good candidates for this application. Figure 1-9b shows the fiber formation of this kind of HBCs on the surface by facile casting from appropriate CH_2Cl_2/MeOH co-solvents.

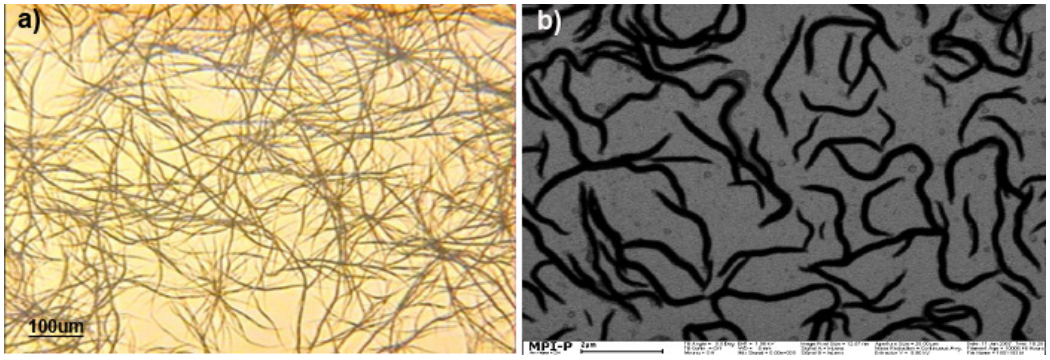

Figure 1-9. Self-assembly of HBCs into fibrous nanostructure on the surface.

1.2.4 DLCs for electronic devices

DLCs, which are formed by large PAHs, are attractive as charge carrier transporting materials due to the formation of quasi one-dimensional columnar structure. The hexahexylthioether substituted triphenylenes were the first examples of DLCs with high one-dimensional charge carrier mobility, whereby the highly ordered helical packing of discotics was expected to be the reason.[43] HBC and derivatives with larger rigid core compared with other mesogens allowing large π-orbital overlap between the discs in the column. As a result, alkyl and alkylphenyl substituted HBCs possess a number of excellent properties such as high order, the highest charge carrier mobility

(up to 1.13 $cm^2V^{-1}s^{-1}$) of all known DLC materials, and good solubility for device fabrication. Considerable scientific and technological efforts have been devoted to DLCs for applications as active components in field-effect transistors (FETs), photovoltaic cells, and light-emitting diodes (LED).

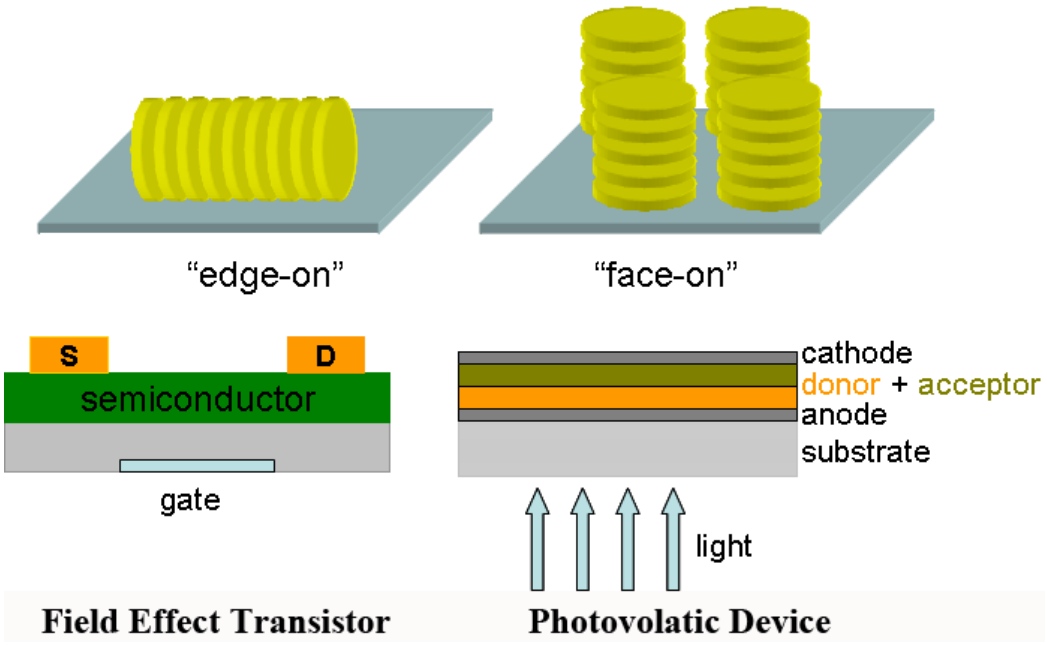

Figure 1-10. Schematic representation of two different electronic device types and their desired arrangement of discotics as electronic materials.

1.2.4.1 Organic field effect transistors (OFETs)

The widespread interest in OFETs is based on the large-area coverage, high charge carrier mobility and facile fabrication.[44] The self-assembly properties of columnar DLCs, in combination with their ability to provide anisotropic charge-carrier transport along the channel, make them viable candidates for OFETs. A typical OFET device is shown in Figure 1-10 (left). For a p-type semiconductor, conduction of charge between the source and the drain electrodes is governed by the gate voltage. When the gate is positive with respect to the source, the semiconductor is depleted of carriers. When the gate is biased negatively, carriers accumulate in the channel between source and drain. The drain current is then proportional to the charge mobility. Long range

and edge-on organized discotic materials are crucial for the device application. The orientation of the disc can be controlled by different methods, such as shearing on a PTFE surface or zone-casting on the substrate.[45] The FET devices based on both methods show mobilities for aligned HBCs approaching 10^{-2} $cm^2V^{-1}s^{-1}$.

1.2.4.2 Bulk heterojunction photovolatic cells

The photovoltaic effect requires:[46] 1) absorption of solar radiation and the photogeneration of excitions (electrons and holes); 2) polarization of the bound electron-hole pairs at the hetero-interface between donor and acceptor species; 3) charge separation, and the transport of the free charge carriers for collection at the cathode and anode. The typical bulk heterojunction photovoltaic device is shown in Figure 1-10 (right).

Discotic materials based on HBC as donor together with perylene dyes as acceptor component have been successfully implemented in photovoltaic devices.[47] High external quantum efficiencies of greater than 34% at 490 nm and power efficiencies up to 2% have been achieved. The high efficiencies result from an efficient photoinduced charge transfer between HBC layers and perylene layers and an effective charge transport through the layered structure.

1.2.4.3 Organic light emitting diodes (OLEDs)

Conjugated organic materials are capable of electroluminescence and over recent years they have been of great interest to investigate their potential applications in OLEDs. In a single layer OLED, a thin film of an organic emitter is sandwiched between a transparent anode (ITO) and a metallic cathode. A multilayer device consists of separate hole-transporting layer, emitter layer and electron transporting layer. Electrons and holes, which are injected into the LUMO and HOMO, respectively, drift through the organic film under the influence of an applied electric field. The columbic attraction between an electron and hole at the same chromophore site results in the formation of an exciton, a bound electron-hole pair, whose recombination produces luminescence. Efficient devices require the matching of

energy levels to minimize the barriers for carrier injection and to trap both electron and holes exclusively in the emitter region. Initially triphenylene based DLCs were employed as hole transport materials.[48] More recently, OLEDs have been constructed using DLCs based on pyrene and perylene derivatives.[49] Some groups have explored the electroluminescence and charge transport properties of photo-crosslinked and conjugated-bridged triphenylene derivatives in OLED applications.[50]

1.3 Motivation

As reviewed in previous sections, discotic liquid crystals, especially graphitic materials based on HBCs, show excellent electronic and optoelectronic properties, low-cost solution processing with good film-formation, fabrication by standard techniques, capability of self-healing as well as facile self-assembly on the surface. However, despite the great achievements in the synthesis of functional HBC derivatives and related large PAHs, there are still further spaces and challenges left for improvement of the properties of large DLCs based on new graphitic materials. The understanding of large DLCs as semiconductor materials, both from the self-assembly point view and device applications are still far away from their intrinsic properties. Here the main objectives are briefly summarized as follows:

(1) While the synthesis of alkyl or alkylphenyl substituted HBCs has been widely achieved by the standard route, most of them are restricted to the D_{6h} symmetry or asymmetry. This is because most HBCs so far have been synthesized via the cyclodehydrogenation from hexaphenylbenzene derivatives, where their precursors are only available for D_{6h} symmetry or low symmetry from cyclotrimerizations or Diels-Alder reactions. Therefore, it is necessary to develop new oligophenylene precursors such as 1,3,5-tris-(2'-biphenyl)benzene (**1-15**) or 1,4-bis-(2'-biphenyl)yl-2,5-diphenylbenzene (**1-16**) in Scheme 1-14, although they differ from hexaphenylbenzene in topology, they can undergo similar intramolecular cyclodehydrogenations to afford HBC molecules.[51]

Following this concept, we have the opportunity to synthesize C_3 symmetric HBCs with three substituents at the meta position. Additionally the synthetic route also allows the synthesis of C_2 symmetric HBC with two substituents.

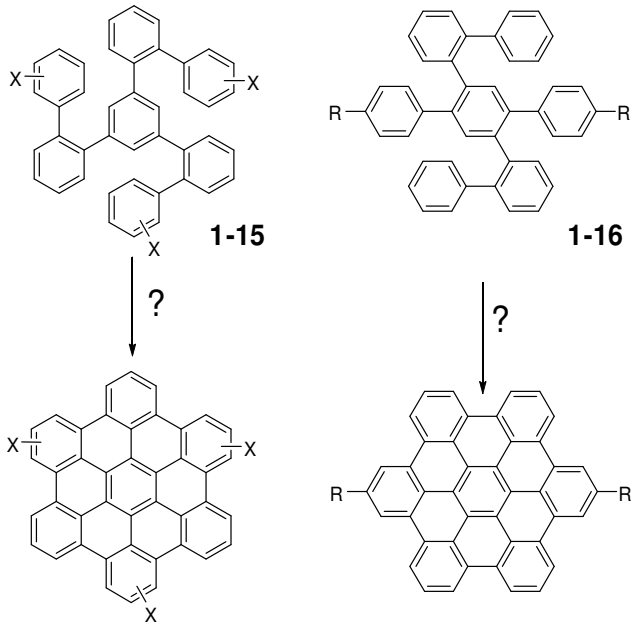

Scheme 1-14. From other oligophenylene precursors to HBCs.

(2) While the cyclotrimerization of symmetric diphenylacetylenes allows the synthesis of D_{6h} symmetric hexaphenylbenzenes and thus D_{6h} symmetric HBCs, two isomers are formed when asymmetric diphenylacetylenes are used and are normally difficult to be separated. By optimizing the different polarity between two substituents on the asymmetric diphenylacetylenes, after cyclotrimerzation, the isomers can be separated by columnar chromatography (Scheme 1-15). Following this concept, we have the opportunity to attain novel C_3 symmetric HBCs with alternating polar/apolar substituents. The new HBCs are expected not only to exhibit a different self-assembly behavior with respect to their D_{6h} symmetric analogues, but also bear the different functionalities, such as ester groups, methoxy groups and others. Furthermore, asymmetric HBCs can also be derived by this synthetic route.

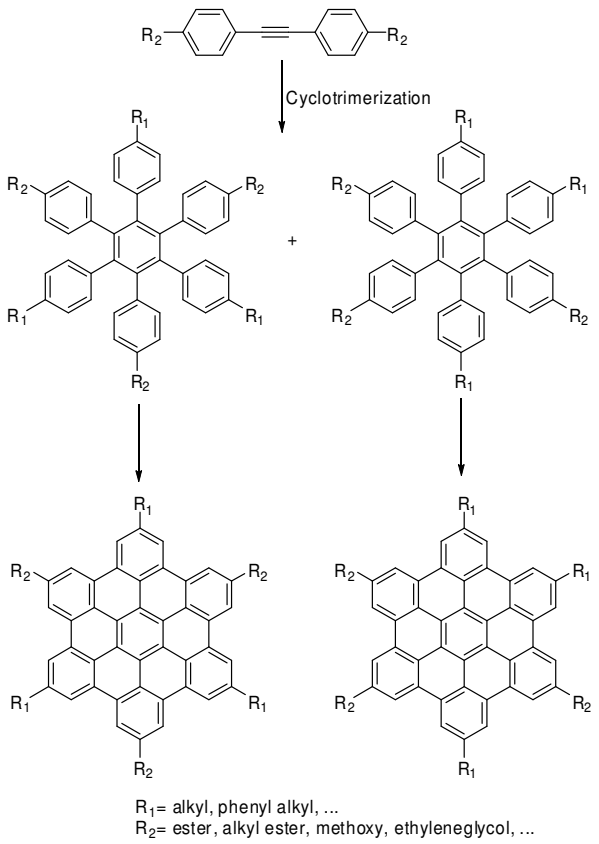

Scheme 1-15. Synthetic route towards C_3 symmetric HBCs with alternating polar/apolar substituents.

(3) The supramolecular organization of HBCs is interesting because they can form long-range one-dimensional columnar structures. The construction of supramolecular assemblies of π-conjugated systems in the 5~100 nm length scale offers an attractive bottom-up strategy to construct semiconducting wires in the nanometer range. HBC is one of the most attractive candidates due to their strong π-stacking along the columns and semiconductor properties.[10] C_3 symmetric HBCs with alternating hydrophilic/hydrophobic substituents are therefore promising materials for this application. Hydrophilic/hydrophobic interactions combined with π-stacking as driving force, allow a facile engineering of fibrous nanostructures from these materials on the surfaces.

(4) Large polycyclic aromatic hydrocarbons with various sizes, shapes and peripheral substituents have continuously attracted the interest of organic

chemists and materials scientists. These molecules have not only been used as models to investigate the electronic properties of aromatic compounds, but have also been applied as active semiconductors in organic electronics. Except HBCs, other large benzenoid PAH analogues with different size and molecular symmetry have been synthesized and studied. However, the typical benzenoid PAHs with triangle shape belong to a less studied class due to synthetic challenge which they present.[52] This work will present a facile synthesis of triangle-shaped PAHs with the same carbon number as fullerene, which reveal different electronic and optoelectronic properties with respect to HBC analogues (Scheme 1-16). Branched alkyl chains are necessary to introduce solubility of triangle shaped discotics, which are not only important for the purification, but also for the device fabrications. HBC combined with three conjugated benzothiophene units has been synthesized, and shows also the triangle-shape with novel optoelectronic properties.

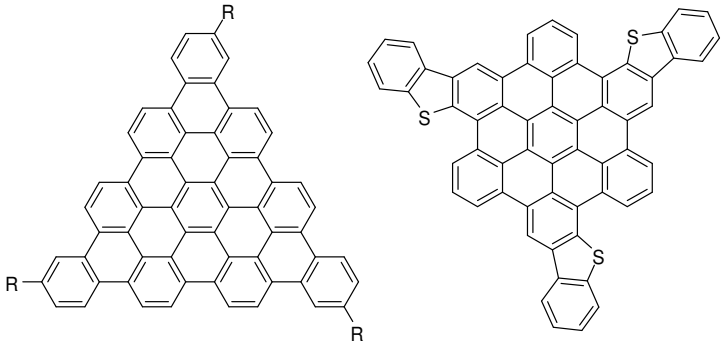

Scheme 1-16. Examples of triangle-shaped discotics.

(5) To date, only few large PAHs with "zig/zag" periphery have been selectively synthesized. The double bond behavior of "zig/zag" periphery can significantly influence the electronic properties, reactivities, as well as self-assembly behavior. C_3 symmetric HBC combined three "zig/zag" peripheries is so called trizigzagHBC (Scheme 1-17), with a semi-triangle shape. We will present the versatile synthesis of this new type of discotics, which not only show the interesting optoelectronic properties, but also remarkable self-organization

behavior in the solid state with ordered helical superstructures and self-assembly on the liquid-solid interface with novel honeycomb patterns.

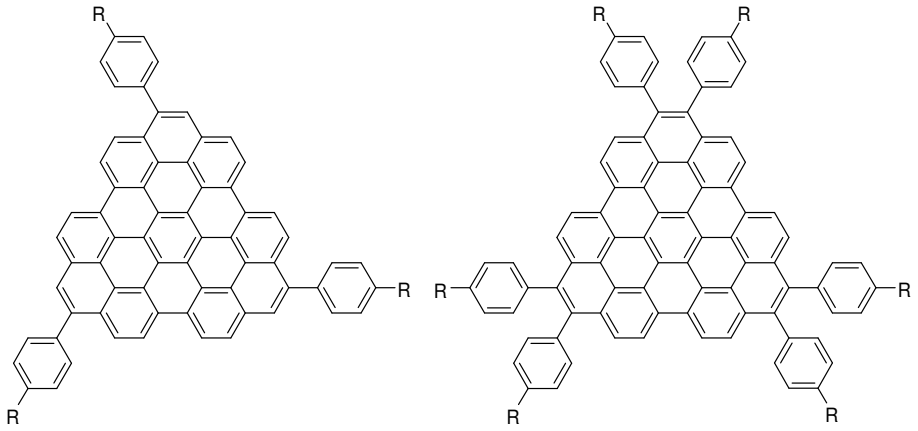

Scheme 1-17. Examples of C_3 symmetric trizigzagHBC derivatives.

(6) In the liquid crystalline phase, discotics molecules are rotated from each other inside the column. However, in the other phases, such as in plastic crystalline phase, sometimes helical superstructures are observed,[53] but they are just coming from the nature of molecular self-organization. The systematic understanding and facile manipulation of their helical pitches in the system is a great challenge.[54] The trizigzagHBC derivatives exhibit highly ordered helical superstructures with every three molecules in one helical pitch, corresponding to 40^o rotation for each disc molecules. The introduction of alternating hydrophilic/hydrophobic substituents in the system (in Scheme 1-18, substituent R_1 is hydrophilic, R_2 is hydrophobic), where the weak non-covalent interactions will significantly influence the supramolecular organization in the bulk, highly ordered staggered stacking is achieved, which corresponds to 60^o rotation for every two molecules. Theoretical simulations confirm the experimental results and furthermore predict for this packing higher charge carrier mobility in comparison to other discotics, with even one order higher than that of HBCs.

In another system, two "zig/zag" peripheries are introduced into the HBCs. The so formed D_2 symmetric bizigzagHBCs (Scheme 1-18, right structure) not only

shows interesting electronic properties, but also allows a facile control of the supramolecular organization from helical stacking to the staggered stacking of discs.

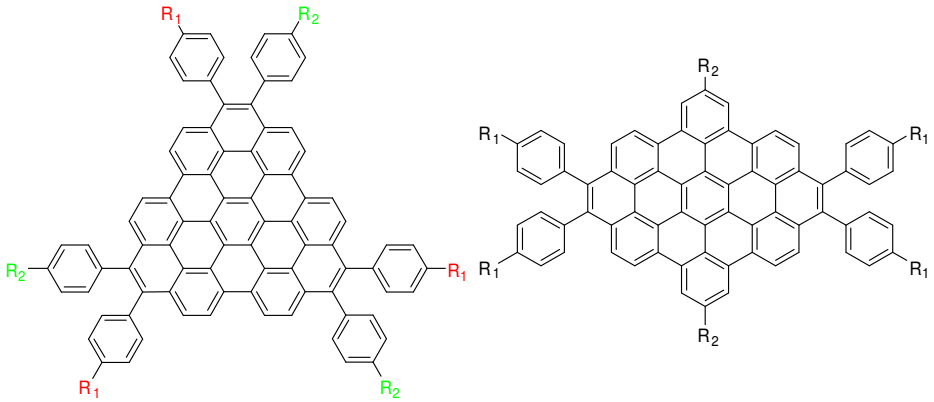

Scheme 1-18. Examples of two systems of discotics can be controlled from helical to staggered stacking.

References:

[1] Fetzer, J. C. *The Chemistry and Analysis of the Large Polycyclic Aromatic Hydrocarbons*. New York: Wiley, **2000**.

[2] (a) Lang, K. F.; Kalowy, J.; Buffleb, H. *Chem. Ber. Recl.* **1964**, *97*, 494; (b) Lang, K. F.; Kalowy, J.; Buffleb, H. *Chem. Ber. Recl.* **1962**, *95*, 1052

[3] Cook, D. J.; Schlemmer, S.; Balucani, N.; Wagner, D. R.; Steiner, B.; Saykally, R. J. *Nature*. **1996**, *380*, 227-229.

[4] (a) Scholl, R.; Seer, C. *Justus Liebigs Ann. Chem.* **1912**, *394*, 111-177; (b) Scholl, R.; Seer, C. *Ber. Dtsch. Chem. Ges.* **1911**, *44*, 1233-1240; (c) Scholl, R.; Seer, C.; Weitzenbock, R. *Ber. Dtsch. Chem. Ges.* **1910**, *43*, 2202-2209; (d) Clar, E. *Ber. Dtsch. Chem. Ges.* **1929**, *62*, 1574-1582; (e) Clar, E.; Wallenstein, H.; Avenarius, R. *Ber. Dtsch. Chem. Ges.* **1929**, *62*, 950-955; (f) Clar, E.; John, F.; Hawran, B. *Ber. Dtsch. Chem. Ges.* **1929**, *62*, 940-950; (g) Clar, E. *Ber. Dtsch. Chem. Ges.* **1929**, *62*, 50-359; (h) Clar, E. *Polycyclic Hydrocarbons*; John Wiley and Sons: New York, 1964; Vol. 1+2; (i) Clar, E.; Ironside, C. T.; Zander, M. *Tetrahedron* **1959**, *6*, 358-363; (j) Clar, E.; Zander, M. *J. Chem. Soc.* **1958**, 1577-1579; (k) Clar, E.; Zander, M. *J. Chem. Soc.*

1957, 4616-4619; (l) Zander, M. *Handbook of Polycyclic Aromatic Hydrocarbons*; Marcel Dekker:New York, **1983**.

[5] Hagen, S.; Hopf, H. *Top. Curr. Chem.* **1998**, *196*, 44-89.

[6] (a) Schleyer, P. V. R. *Chem. Rev.* **2001**, *101*, 1115-1118; (b) De Proft, F.; Geerlings, P. *Chem. Rev.* **2001**, *101*, 1451-1464; (c) Buhl, M.; Hirsch, A. *Chem. Rev.* **2001**, *101*, 1153-1184; (d) Gomes, J. A. N. F.; Mallion, R. B. *Chem. Rev.* **2001**, *101*, 1349-1384; (e) Randic, M. *Chem. Rev.***2003**, *103*, 3449-3606.

[7] See 2000 Nobel Prize lectures: (a) Shirakawa, H. *Angew. Chem. Int. Ed.* **2001**, *40*, 2574-2580; (b)

MaDiamid, A. G. *Angew. Chem. Int. Ed.* **2001**, *40*, 2581-2590; Heeger, A. J. *Angew. Chem. Int. Ed.* **2001**, *40*, 2591-2611.

[8] (a) Skotheim, T.A.; Elsenbaumer, R. L.; Reynolds, J. R. Ed. *Handbook of Conducting Polymers* 2nd Ed.

Marcel Dekker, Inc., New York, **1998**; (b) Hadziioannou, G.; van Hutten, P. F. *Semiconducting Polymers.* Wiley-VCH, Weiheim, **2000**.

[9] (a) Sage, I. C. in *Handbook of Liquid Crystals*; Demus, D.; Goodby, J.; Gray, G. W.; Spiess, H. W.; Vill, V.Eds, Wiley-VCH: Weinheim, **1998**, Vol. 1, 731-762; (b) Watson, M.; Fechtenkötter, A.; Müllen, K. *Chem.Rev.* **2001**, *101*, 1267-1300; (c) Bushby, R. J.; Lozman, O. R. *Curr. Opi. Solid. StateMater. Sci.* **2002**, *6*,569-578. (d) Wu, J.; Pisula, W.; Müllen, K. *Chem. Rev*. **2007**, *107*, 718-747; (e) Laschat, S.; Baro, A.; Steinke, N.; Giesselmann, F.; Hagele, C.; Scalia, G.; Judele, R.; Kapatsina, E.; Sauer, S.; Schreivogel, A.; Tosoni, M. *Angew. Chem. Int. Ed*. **2007**, *46*, 4837-4887.

[10] (a) Hill, J. P.; Jin, W.; Kosaka, A.; Fukushima, T.; Ichihara, H.; Shimomura, T.; Ito, K.; Hashizume, T.; Ishii, N.; Aida, T. *Science*. **2004**, *304*, 1481-1483; b) Yamamoto, Y.; Fukushima, T.; Suna, Y.; Ishii, N.; Saeki, A.; Seki, S.; Tagawa, S.; Taniguchi, M.; Kawai, T.; Aida, T. *Science*. **2006**, *314*, 1761-1764; (c) Xiao, S.; Tang, J.; Beetz, T.; Guo, X.; Tremblay, N.; Siegrist, T.; Zhu, Y.; Steigerwald, M.; Nuckolls, C. *J. Am. Chem. Soc*. **2006**, *128*, 10700-10701.

[11] Benard, C. P.; Geng, Z.; Heuft, M. A.; VanCrey, K.; Fallis, A. G. *J. Org. Chem.* **2007**, *72*(19), 7229-7236.

[12] (a) Müller, M.; Petersen, J.; Strohmaier, R.; Günther, C.; Karl, N.; Müllen, K. *Angew. Chem. Int.*

Ed. Engl. **1996**, *35*, 886-888; (b) Müller, M.; Kübel, C.; Müllen, K. *Chem. Eur. J.* **1998**, *4*, 2099-2109.

[13] (a) Bonifacio, M. C.; Robertson, C. R.; Jung, J. Y.; King, B. T. *J. Org. Chem.* **2005**, *70*, 8522-8526; (b) Iuliano, a.; Piccioli, P.; Fabbri, D. *Org. Lett.* **2004**, *6*, 3711-3714.

[14] Collins, S. K.; Grandbois, A.; Vachon, M. P. ; Cote, J. *Angew. Chem. Int. Ed.* **2006**, *45*, 2923-2926.

[15] Donovan, P. M.; Scott, L. T. *J. Am. Chem. Soc.* **2004**, *126*, 3108.

[16] Shen, H. C.; Tang, J. M.; Chang, H. K.; Yang, C. W.; Liu, R. S. *J. Org. Chem.* **2005**, *70*, 10113-10116.

[17] (a) Goldfinger, M. B.; Swager, T. M. *J. Am. Chem. Soc*, **1994**, *116*, 7985-7896; (b) Goldfinger, M. B.; Crawford, K. B.; Swager, T. M. *J. Am. Chem. Soc*, **1997**, *119*, 4578-4593.

[18] Yao, T.; Campo, M. A.; Larock, R. C. *J. Org. Chem.* **2005**, *70*, 3511-3517.

[19] (a) Bronene, R. D.; Diederich F. *Tetrahedron Lett.* 1991, 32, 5227; (b) Muszkat, K. A.; *Top. Curr. Chem.* **1981**, *88*, 89; (c) Meier, H. *Angew. Chem. Int. Ed.* **1992**, *31*, 1399.

[20] Xiao, S. X.; Myers, M.; Miao, Q.; Sanaur, S.; Pang, K. L.; Steigerwald, M. L.; Nuckolls, C. *Angew. Chem., Int. Ed.* **2005**, *44*, 7390-7394.

[21] (a) Scott, L. T.; Cheng, P. C.; Hashemi, M. M.; Bratcher, M. S.; Meyer, D. T.; Warren, H. B. *J. Am. Chem. Soc.* **1997**, *119*, 10963-10968; (b) Scott, L. T.; Hashemi, M. M.; Meyer, D. T.; Warren, H. B. *J. Am. Chem. Soc.* **1991**, *113*, 7082-7084.

[22] (a) Scott, L. T.; Boorum, M. M.; McMahon, B. J.; Hagen, S.; Mack, J.; Blank, J.; Wegner, H.; de Meijere, A. *Science* **2002**, *295*, 1500-1503; (b) Boorum, M. M.; Vasil'ev, Y. V.; Drewello, T.; Scott, L. T. *Science* **2001**, *294*, 828. (c) Tsefrikas, V. M.; Scott, L. T.; *Chem. Rev.* **2006**, *106*, 4868-4884.

[23] (a) Rempala, P.; Kroulik, J.; King, B. T. *J. Am. Chem. Soc.* **2004**, *126*, 15002-15003; (b) (b) Stefano, M. D.; Negri, F.; Carbone, P.; Mu¨llen, K. *Chem. Phys.* **2005**, *314*, 85.

[24] Simpson, C. D.; Brand, J. D.; Berresheim, A. J.; Przybilla, L.; Rader, H. J.; Müllen, K. *Chem. - Eur. J.* **2002**, *8*, 1424-1429.

[25] (a) Dötz, F.; Brand, J. D.; Ito, S.; Gherghel, L.; Müllen, K. *J. Am. Chem. Soc*. **2000**, *122*, 7707-

7717. (b) Tomovic, Z.; Watson, Müllen, K. *Angew. Chem. Int. Ed.* **2004**, *43*, 755-758.

[26] (a) Stein, S. E.; Brown, R. L. *J. Am. Chem. Soc.* **1987**, *109*, 3721-3729; (b) Wang, Z. H.; Tomovic, E.; Kastler, M.; Pretsch, R.; Negri, F.; Enkelmann, V.; Müllen, K. *J. Am. Chem. Soc.* **2004**, *126*, 7794-7795.

[27] (a) Kastler, M.; Schmidt, J.; Pisula, W.; Sebastiani, D.; Müllen, K. *J. Am. Chem. Soc*. **2006**, *128*, 9526-9534; (b) Feng, X.; Wu, J.; Ai, M.; Pisula, W.; Zhi, L.; Rabe, J. P.; Müllen, K. *Angew. Chem. Int. Ed*. **2007**, *46*, 3033-3046; (c) Feng, X.; Pisula, W.; Müllen, K. *J. Am. Chem. Soc*. **2007**, *129*, 14116-14117.

[28] (a) Lehn, J. M. Supramolecular Chemistry, VCH, Weinheim, **1995**; (b) Ringsdorf, H.; Schlarb, B.; Venzmer, J. *Angew. Chem., Int. Ed*., **1988**, *27*, 113; (c) Whitesides, G. M.; Grzybowski, B. *Science*, **2002**, *295*, 2418; (d) Kato, T. *Science*, **2002**, *295*, 2414.

[29] Reinitzer, F. *Monatsh. Chem.*, **1888**, *9*, 421; for English translation see *Liq. Cryst*., **1989**, *5*, 7.

[30] For the recent review: Kumar, S. *Chem. Soc. Rev*. **2006**, *35*, 83-109.

[31] Chandrasekhar, S.; Sadashiva, B. K.; Suresh, K. A. *Pramana*, **1977**, *9*, 471.

[32] (a) Dierking, I. *Textures of Liquid Crystals*; Wiley-VCH: Weinheim, 2003.; (b) Chandrasekhar, S.; Prasad, S. K. *Contemp. Phys.* **1999**, *40*, 237-245.

[33] (a) Balagurusamy, V. S. K.; Prasad, S. K.; Chandrasekhar, S.; Kumar, S.; Manickam, M.;Yelamaggad, C. V. *Pramana*. **1999**, *53,* 3; (b) Boden, N.; Bushby, R. J.; Cammidge, A. N.; Clements, J.; Luo, R. *Mol. Cryst. Liq. Cryst*. **1995**, *261*, 251; (c) Yamamoto, Y.; Fukushima, T.; Jin, W.; Kosaka, A.; Hara, T.; Nakamura, T.; Saeki, A.; Seki, S.; Tagawa, S.; Aida, T. *Adv. Mater*. **2006**, *18*, 1297-1300.

[34] van de Craats, A. M.; Warman, J. M.; Fechtenkötter, A.; Brand, J. D.; Harbison, M. A.; Müllen, K. *Adv. Mater*. **1999**, *11*, 1469-1472.

[35] (a) Boden, N.; Movaghar, B. in *Handbook of Liquid Crystals*, ed. Demus, D.; Goodby, J.; Gray, G. W.; Spiess, H. W.; Vill, V. Wiley-VCH, Weinheim, **1998**, Vol. 2B, Chapter IX; (b) O'Neill, M.; Kelly, S. M. *Adv. Mater*. **2003**, *15*, 1135-1146.

[36] (a) Eichorn, H. *J. Porphyrins Phthalocyanines* **2000**, *4*, 88-102; (b) Franck, B. *Angew. Chem. Int. Ed.* **1982**, *21*, 343-353; (c) Gregg, B. A.; Fox, M. A.; Bard, A. J. *J. Am.Chem. Soc.* **1989**, *111*, 3024-3029; (d) Roussel, O. Kestemont, G.; Tant, J. ; de Halleux, V. ; Aspe, R. G. ; Levin, J. ; Remacle, A. ; Gearba, I. R. ; Ivanov, D. ; Lehmann, M. ; Geerts, Y. *Mol. Cryst. Liq. Cryst*. **2003**, *396*, 35-39 ; (e) Bock, H.; Helfrich, W. *Liq. Cryst.* **1992**, *12*, 697-703; (f) Bodon, N.; Bushby, R. J.; Cammidge, A. N. J. *Chem. Soc. Chem. Commun.* **1994**, 465-466; (g) Boden, N.; Bushby, R. J.; Cammidge, A. N. *J. Am. Chem. Soc.* **1995**, *117*, 924-927; (h) Kreuder, W.; Rungsdorf, H. *Makromol. Chem. Rapid Commun.* **1983**, *4*, 807-815; (i) Zhang, J.; Moore, J. S. *J. Am. Chem. Soc.* **1994**, *116*, 2655-2656; (j) Hoger, S.; Enkelmann, V.; Bonrad, K.; Tschierske, C. *Angew. Chem. Int. Ed.* **2000**, *39*, 2268; (k) Rohr, U.; Schlichting, P.; Böhm, A.; Gross, M.; Meerholz, K.; Bräuchle, C.; Müllen, K. *Angew. Chem. Int. Ed.* **1998**, 37, 1434-1437; (l) Goltner, C.; Pressner, D.; Müllen, K.; Spiess, H. W. *Angew. Chem. Int. Ed.* **1993**, 32, 1660-1662; (m) Gregg, B. A.; Cormier, R. A. *J. Am. Chem. Soc.* **2001**, *123*, 7959-7960. (n) Boden, N.; Borner, R. C.; Bushby, R. J.; Clements, J. *J. Am. Chem. Soc.* **1994**, *116*, 10807-10808.

[37] Pisula, W.; Tomovic, Z.; Simpson, C.; Kastler, M.; Pakula, T.; Müllen, K. *Chem. Mater.* **2005**, *17*, 4296-4303.

[38] a) Stabel, A.; Herwig, P.; Müllen, K.; Rabe, J. P. *Angew. Chem. Int. Ed. Engl.* **1995**, *34*, 1609-1611. (b) Ito, S.; Wehmeier, M.; Brand, J. D.; Kübel, C.; Epsch, R.; Rabe, J. P.; Müllen, K. *Chem. Eur. J.* **2000**, *6*, 4327-4342. (c) Piot, L.; Marchenko, A.; Wu, J.; Müllen, K.; Fichou, D. *J. Am. Chem. Soc.* **2005**, *127*, 16245-16250.

[39] Jackel, F.; Watson, M. D.; Müllen, K.; Rabe, J. P. *Phys. Rev. Lett*. **2004**, *92*,

188303.

[40] (a) Tahara, K.; Furukawa, S.; Uji-i, H.; Uchino, T.; Ichikawa, T.; Zhang, J.; Mamdouh, W.; Sonoda, M.; De Schryver, F. C.; De Feyter, S.; Tobe, Y. *J. Am. Chem. Soc*. **2006**, *128*, 16613-16625; (b) Furukawa, S.; Uji-i, H.; Tahara, K.; Ichikawa, T.; Sonoda, M.; De Schryver, F. C.; Tobe, Y.; De Feyter, S. *J. Am. Chem. Soc*. **2006**, *128*, 3502-3503; (c) Schull, G.; Douillard, L.; Fiorini-Debuisschert, C.; Charra, F.; Mathevet, F.; Kreher, D.; Attias, A. J. *Nano. Lett*. **2006**, *6*, 1360-1363; (d) Schull, G.; Douillard, L.; Fiorini-Debuisschert, C.; Charra, F.; Mathevet, F.; Kreher, D.; Attias, A. J. *Adv. Mater*. **2006**, *18*, 2954-2957.

[41] (a) Palma, M.; Levin, J.; Lemaur, V.; Liscio, A.; Palermo, V.; Cornil, J.; Geerts, Y.; Lehmann, M.; Samori, P. *Adv. Mater*. **2006**, *18*, 3313-3317. (b) Hoeben, J. M.; Jonkheijm, P.; Meijer, E. W.; Schenning, A. P. H. J. *Chem. Rev*. **2005**, *105*, 1491-1546.

[42] Tsao, H. N.; Rader, H. J.; Pisula, W.; Rouhanipour, A.; Mullen, K. *Phys. Stat. Sol.* **2007**, in press.

[43] Adam, D.; Schuhmacher, P.; Simmerer, J.; Häussling, L.; Siemensmeyer, K.; Etzbach, K. H.; Ringsdorf, H.; Haarer, D. *Nature*. **1994**, *371*, 141-143.

[44] Dimitrakopoulos, C. D.; Malenfant, P. R. L. *Adv. Mater.* **2002**, *14*, 99-117.

[45] (a) Pisula, W.; Menon, A.; Stepputat, M.; Lieberwirth, I.; Kolb, U.; Tracz, A.; Sirringhaus, H.; Pakula, T.; Müllen, K. *Adv. Mater.* **2005**, *17*, 684; (b) van de Crass, A. M.; Stutzmann, N.; Bunk, O.; Nielsen, M. M.; Watson, M. D.; Müllen, K.; Chanzy, H. D.; Sirringhaus, H.; Friend, R. H. *Adv. Mat.* **2003**, *15*, 495-499.

[46] (a) Winder, C.; Sariciftci, N. S. *Chem. Commun.* **2004**, *14*, 1077-1086; (b) Muhlbacher, D.; Scharbac, M.; Morana, M.; Zhu, Z.; Waller, D.; Gaudiana, R.; Brabec, C. *Adv. Mater*. **2006**, *18*, 2884-2889. (c) Gunes, S.; Neugebauer, H.; Saricifci, N. S. *Chem. Rev*. **2007**, *107*, 1324-1338; (d) Lo, S. C.; Burn, P. L. *Chem. Rev*. **2007**, *107*, 1097-1116.

[47] (a) Schmidt-Mende, L.; Fechtenkotter, A.; Müllen, K.; Moons, E.; Friend, R. H.; MacKenzie, J. D. *Science* **2001**, *293*, 1119-1122; (b) Li, J.; Kastler, M.; Pisula, W.; Fobertson, J. W. F.; Wasserfallen, D.; Grimsdale, A. C.; Wu, J.; Müllen, K. *Adv. Funct.*

Mater. **2007**, *17*, 2528-2533.

[48] Christ, T.; Glüsen, B.; Greiner, A.; Kettner, A.; Sander, R.; Stümpflen, V.; Tsukruk, V.; Wendorff, J. H. *Adv. Mater.* **1997**, *9*, 48-51.

[49] van de Craats, A. M.; Warman, J. M.; Schlichting, P.; Rohr, J.; Geerts, Y.; Müllen, K. *Synth.Met.* **1999**, *102*, 1550-1551.

[50] Bacher, A.; Erdelen, C. H.; Paulus, W.; Ringsdorf, H.; Schmidt, H. W.; Schuhmacher, P. *Macromolecules* **1999**, *32*, 4551-4557.

[51] Feng, X.; Wu, J.; Enkelmann, V.; Müllen, K. *Org. Lett.* **2006**, *8*, 1145-1148.

[52] Feng, X.; Wu, J.; Ai, M.; Pisula, W.; Zhi, L.; Rabe, J. P.; Müllen, K. *Angew. Chem. Int. Ed.* **2007**, *46*, 3033-3046.

[53] (a) Fechtenkötter, A.; Saalwächter, K.; Harbison, M. A.; Müllen, K.; Spiess, H.W. *Angew. Chem. Int. Ed.* **1999**, *38*, 3039-3042; (b) Wu, J.; Watson, M. D.; Zhang, L.; Wang, Z.; Müllen, K. *J. Am. Chem. Soc.* **2004**, *126*, 177-186.

[54] (a) Cornil, J.; Lemaur, V.; Calbert, J. P.; Bredas, J. L. *Adv. Mater.* **2002**, *14*, 726-729; (b) Lemaur, V.; Filho, D. A. S.; Coropceanu, V.; Lehmann, M.; Geerts, Y.; Piris, J.; Debije, M. G.; van de Craats, A. M. ; Senthilkumar, K. ; Siebbeles, L. D. A.; Warmann, J. M.; Bredas, J. L.; Cornil, J. *J. Am. Chem. Soc.* **2004**, *126*, 3271-3279; (c) Kirkpatrick, J.; Marcon, V.; Nelson, J.; kremer, K.; Andrienko, D. *Phys. Rev. Lett.* **2007**, *98*, 227402.

Chapter 2. The Role of Oligophenylene Precursors for Oxidative Cyclodehydrogenation and Unusual Symmetry Effect on Thermal Behavior and Self-assembly of Hexa-*peri*-hexabenzocoronene

In this chapter, a novel concept to synthesize hexa-*peri*-hexabenzocoronene (HBC) derivatives starting from two new series of oligophenylene precursors will be presented. These precursors are different from hexaphenylbenzenes, and will be subjected to standard oxidative cyclodehydrogenation conditions. The substitution pattern strongly influenced the ring-fusion during the reactions. Some precursors allow the synthesis of target HBC derivatives, while some others only form partially ring-fused products. The new synthetic strategy is especially useful for the synthesis of D_3 symmetric HBC with three substituents and C_2 symmetric HBC with two substituents, which show an unusual thermal behavior and self-assembly properties at the solid-liquid interface.

2.1 Hexa-*peri*-hexabenzocoronenes by Efficient Oxidative Cyclodehydrogenation—the Role of the Oligophenylene Precursors

2.1.1 Introduction

As was discussed in Chapter 1, pioneering syntheses of polycyclic aromatic hydrocarbons (PAHs) were performed by Scholl and Clar et al. under harsh conditions.[1] However, previous synthetic methods have afforded HBCs in very low yields.[2] Our group has developed an efficient way for preparing a variety of HBCs **2-2** through a mild intramolecular oxidative cyclodehydrogenation of hexaphenylbenzene precursors **2-1** (Scheme 2-1).[3] Several suitable oxidant systems have been utilized for these transformations including $CuCl_2/AlCl_3$, $Cu(OTf)_2/AlCl_3/CS_2$ and $FeCl_3/CH_3NO_2$.[4] Through detailed studies of the oxidative cyclodehydrogenation, the parent hexaphenylbenzene (HPB) was found to exclusively

cyclodehydrogenize in an intramolecular fashion. Furthermore, the intermediate phenyldibenzo[fg,ij]-phenanthro[9,10,1,2,3-pqrst]pentaphene (**2-3**) could be separated, indicating that the cyclodehydrogenation proceeded in a step-wise process.[5] Recently, theoretical studies have pointed toward a radical cation mechanism for these intramolecular fusion reactions. The geometry, charge and spin distribution of the radical cation intermediates is decisive for the step-by-step bonding formation mechanism.[6]

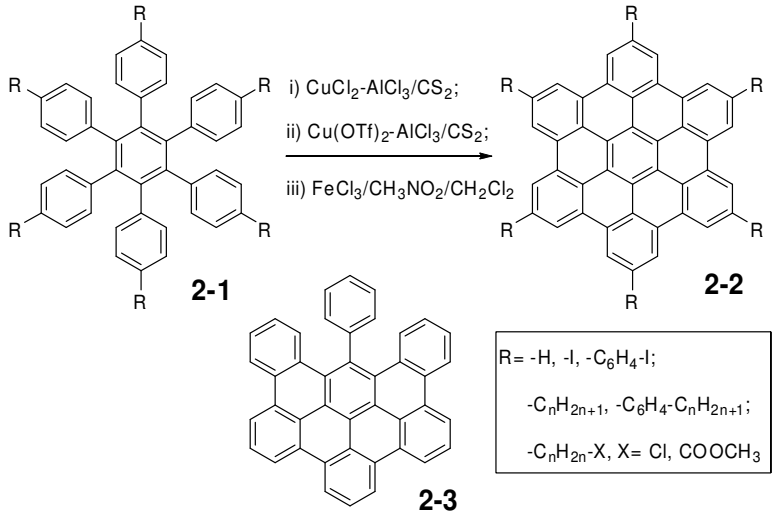

Scheme 2-1. General synthesis of HBCs by oxidative cyclodehydrogenation of hexaphenylbenzene precursors.

HPBs can be synthesized by the cyclotrimerization of diphenylacetylene or the Diels-Alder reaction between diphenylacetylene derivatives and tetraphenylcyclopentadienones.[7] D_{6h} symmetric or unsymmetric HBC molecules with iodo-, iodophenyl-, alkyl- and alkylphenyl- substitutions have been synthesized, and functional groups such as esters at the end of aliphatic chains can also be introduced. However, the synthesis of HBC molecules with lower symmetry such as D_3 met with difficulties.[8] In addition, the cyclodehydrogenation of HPB precursors, is sometimes limited by the electron-rich and -poor character of the substitutions. [9] To broaden the scope of HBC analogues, we propose the use of other oligophenylene

precursors such as 1,3,5-tris-(2'-biphenyl)benzene (**2-4)** or 1,4-bis-(2'-biphenyl)yl-2,5-diphenylbenzene (**2-5)** (Scheme 2-2). Although they differ from HPBs in topology, they can undergo similar intramolecular cyclodehydrogenations to afford HBC molecules. For example, J. Wu in the Müllen group observed that precursor **2-4b** can undergo the cyclodehydrogenation to give D_3 symmetric HBC **2-6b** with functional iodide groups at the *meta* positions in quantitative yield. Following this concept, here we describe an efficient synthetic method for the preparation of known HBCs (including **2-6a**) and unknown derivatives such as iodo compounds **2-6b-c** and the D_2 symmetric species **2-7**.

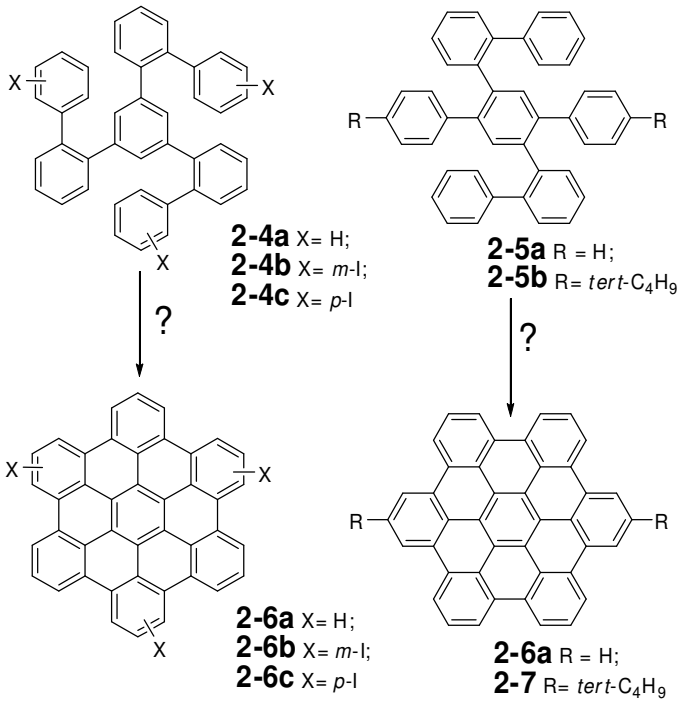

Scheme 2-2. Potential synthesis of HBCs from precursors **2-4a-c** and **2-5a-b**.

2.1.2 Synthesis

As shown in Scheme 2-3, 1,3,5-tris-(2'-bromophenyl)benzene (**2-9**) was firstly synthesized in 72% yield by trifluoromethanesulfonic acid-mediated trimerization of 2-bromoacetophenone (**2-8**). It is worthy to note that other Lewis acids typically used for condensation trimerizations of substituted acetophenones such as $SiCl_4$ and $TiCl_4$, were ineffective or problematic.[10] Molecule **2-9** constitutes an important building

block for subsequent palladium-catalyzed Suzuki, Stille and Negishi coupling reactions, and in our study led to various 1,3,5-tris-(2'-biphenyl)ylbenzene structures. Suzuki coupling of **2-9** with phenylboronic acid, 3-trimethylsilyl-1-phenyl boronic acid, and 4-trimethylsilyl-1-phenyl boronic acid afforded **2-4a**, **2-10a**, **2-10b** in 86%, 90%, and 93% yields, respectively. For comparison, it should be noted that **2-10a** was previously synthesized by J. Wu via a three-step procedure in only 48% yield.[8] The trimethylsilyl groups in **2-10a** and **2-10b** were then converted into iodo groups by treatment with iodine monochloride and gave **2-4b** and **2-4c** in 92% and 93% yields, respectively.

The intramolecular oxidative cyclodehydrogenation reactions were then performed on compounds **2-4a-c** using $FeCl_3$ as an oxidant. The parent HBC **2-6a** was obtained as yellow powder in 80% yield from compound **2-4a**. The MALDI-TOF mass spectra of the product revealed that no chlorination had occurred during this cyclodehydrogenation process, even after prolonged reaction times up to several hours. This result is important because chlorination was frequently observed with HPB cyclodehydrogenations,[4b, 11] and suggests that the present synthesis of parent HBC is superior. It also appears that the topology of the precursor plays an important role for cyclodehydrogenation. Likewise, compound **2-6b** can be prepared from **2-4b** under similar conditions and provides a useful building block for further functionalization.[8] Interestingly, the similar cyclodehydrogenation reaction of **2-4c** did not afford completely planarized HBC **2-6c**, even after prolongation of the reaction time up to 23 h**.** The MALDI-TOF mass spectrum of the obtained insoluble, yellow powder showed only a single species with a molecular ionic peak at 905, suggesting that only 6 hydrogen atoms had been removed (Figure 2-1). Though it was poorly soluble in normal organic solvents, compound **2-11** was then reacted with trimethylsilylacetylene under Hagihara-Sonogashira conditions to give a single soluble product **2-12**, whose structure could be confirmed by single-crystal structure analysis.[12] The crystal structure (Figure 2-2) clearly shows that the biphenyl group of **2-12** is highly twisted out of the central plane and has a dimeric oblique packing mode. Therefore, structure **2-11** was ascribed to the insoluble yellow powder where one of

the biphenyl units has not formed new C-C bonds during the reactions. Regarding the C_3 symmetry of precursors **2-4**, this result further supports a step-wise cyclodehydrogenation mechanism proceeding from **2-4a-c** to **2-6a-c**. We believe that **2-4c** can only be partially closed is due to the steric hindrance induced by the twist of the biphenyl units and the poor solubility of the product.

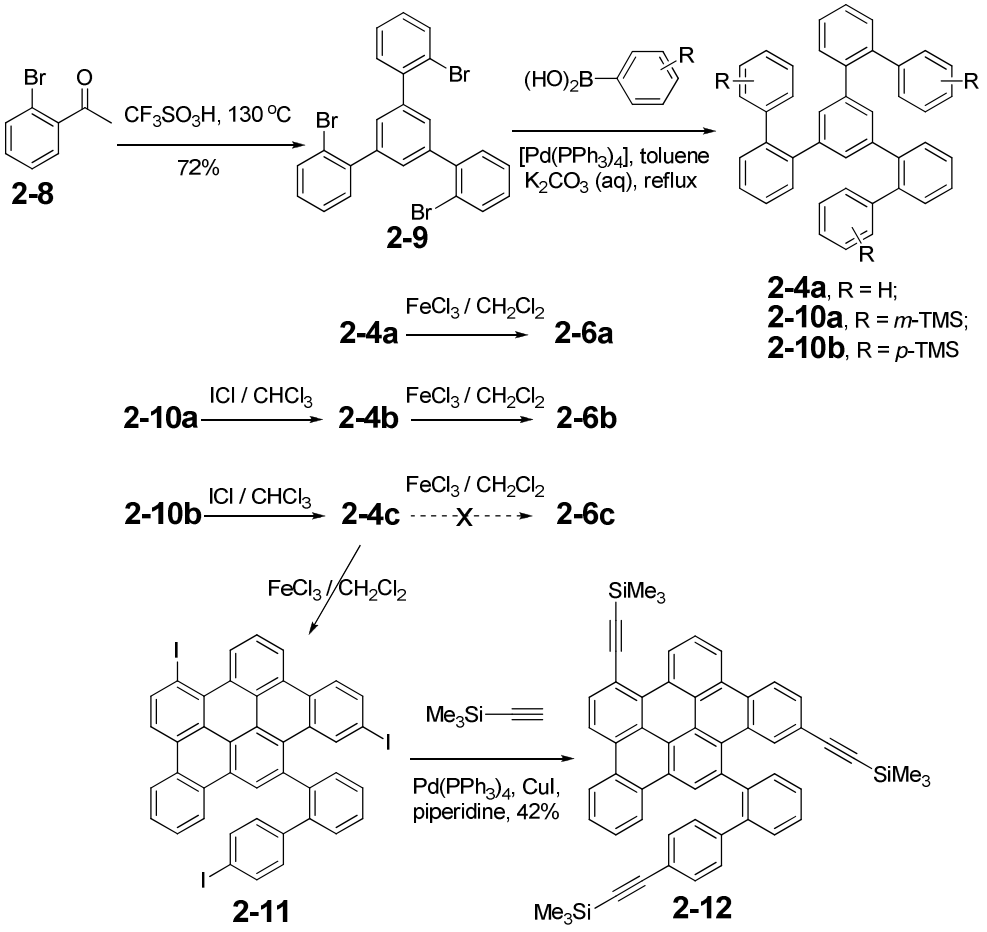

Scheme 2-3. Versatile synthesis start from efficient building block **2-9**.

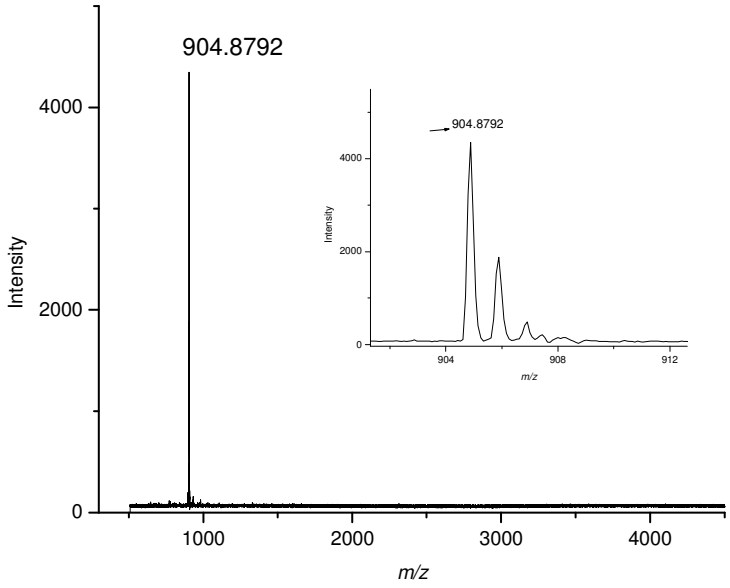

Figure 2-1. MALDI-TOF mass spectrum of compound **2-11.**

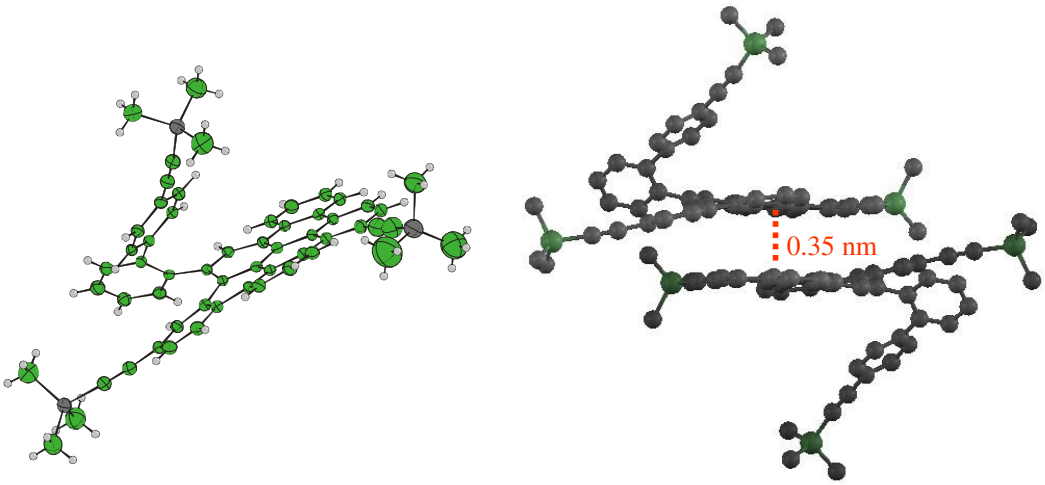

Figure 2-2. Single crystal structure (left) and dimmer packing mode (right) of **2-12**.

Encouraged by the efficient cyclodehydrogenation of 1,3,5-tris-(2'-biphenyl)ylbenzene precursors, we revisited a previously unsuccessful reaction, namely the cyclodehydrogenation of **2-5b** to compound **2-7**.[13] In this study we carefully controlled the quantity of oxidant and the reaction time. Interestingly, cyclodehydrogenation of **2-5b** by treatment with $FeCl_3$ in dichloromethane over 30 minutes up to 5 hours only yielded a partially closed intermediate **2-13**, which was

again supported by single-crystal analysis (Figure 2-3).[14] Alternatively, the analogous species, 1,4-bis(2'-biphenyl)yl-2,5-diphenylbenzene (**2-5a**) afforded complex mixtures under the same oxidation conditions. Comparing these two examples, we then assume that the *tert*-butyl groups in precursor **2-5b** stabilize the intermediate cation radical during the dehydrogenation process. This stabilizing effect in turn does not allow further cyclization and complete planarization to form HBC **2-7**. The stable cation radical of **2-13** was quenched by adding methanol to afford **2-13** in 68% yield. To support our hypothesis of cation radical stabilization, compound **2-13** was then further submitted to the oxidative cyclodehydrogenation by using 12 equivalents $FeCl_3$ for 30min. Amazingly, completely closed HBC molecule **2-7** was obtained in quantitative yield and without any chlorination as evidenced from MALDI-TOF MS spectrum (Figure 2-4)! Therefore, two independent steps of cyclodehydrogenations must be performed to clearly transform **2-5b** into **2-7**.

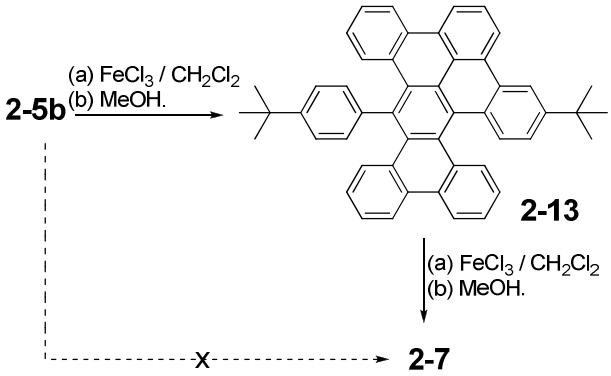

Scheme 2-4. Oxidation of **2-5b**.

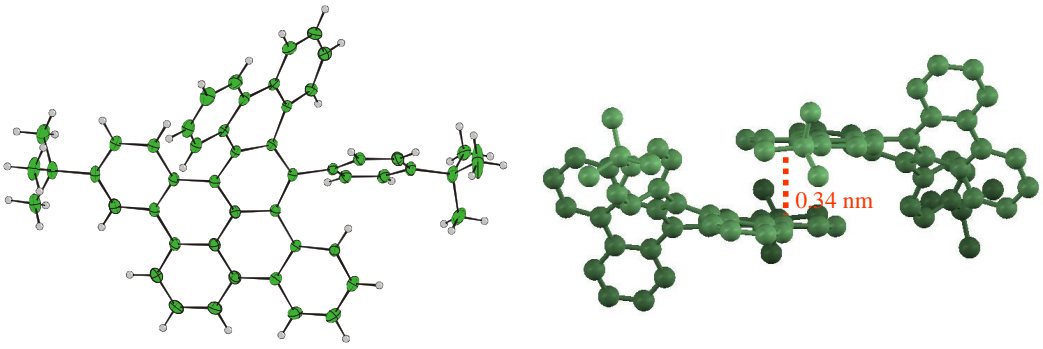

Figure 2-3. Single crystal structure and dimmer packing mode of **2-13**.

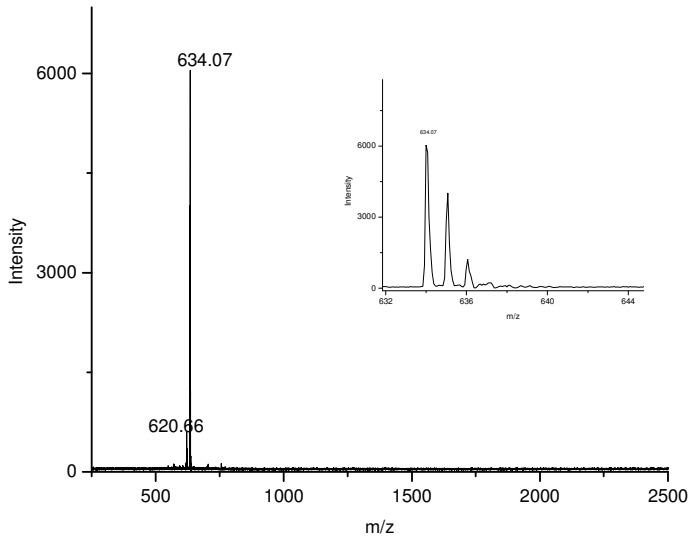

Figure.2-4. MALDI-TOF mass spectrum of compound **2-7** (the peak at 620.66 is ascribed to the scissor of *tert*-butyl group by MALDI-TOF spectrometer)

2.1.3 Summary

In conclusion, parent HBC **2-6a** was successfully synthesized from 1,3,5-tris-(2'-biphenyl)ylbenzene precursor using typical cyclodehydrogenation conditions. The new synthetic method starting from 1,3,5-tris-(2'-bromophenyl)benzene offers opportunities for synthesizing novel HBC derivatives. This route is especially attractive for D_3 symmetric HBCs that can otherwise not be obtained from typical hexaphenylbenzene precursors, which will be presented in the next section. The attachment of *tert*-butyl groups helps to change the spin density distribution and therefore requires a two-step procedure to prepare its HBC analogues. The partially cyclodehydrogenized products can be separated and characterized, further suggesting a step-wise ring closing mechanism including radical cations.

2.2 Unusual Symmetry Effect on Thermal behavior and Self-assembly of Hexa-*peri*-hexabenzocoronene

2.2.1 Introduction

Self-assembly of disc-like molecules on surfaces provides the opportunity to build

electronic devices at the nanoscale.[15,16] Many challenges have emerged in this area, such as the preparation of large PAHs, the controllability of molecular symmetry, and the peripheral substituents.[17] HBCs with hexagonal aromatic cores and extended π-conjugation are surly one of the prime concerns of large PAHs, such as the prominent D_{6h} symmetrically substituted **2-2**.[18, 19] The substitution of the aromatic core allows a control over the solubility, thermotropic properties and their self-assembly in the solid state and at a solid-liquid interface.[20] The material's prosperities can be modified through the architecture of the substituents, like e.g. the alkyl chain length, and the substitution symmetry at the disc corona.[19] For instance, longer and more flexible side chains are expected to decrease the thermal phase transitions. On the other hand, reducing the number of substituents, and maintaining a high substitution symmetry of the disc-shaped building blocks, for example the D_3 symmetry, which are believed to influence significantly their thermal and self-assembly behavior, are however restricted by their synthetic hitches.[21]

In this work, after cooperation with W. Pisula in the Müllen group on the study of thermal behavior and two-dimensional wide-angle X-ray scattering measurements for **2-14** and **2-15**, we present here a surprising effect on the isotropization temperatures (T_i) of the two HBC derivatives. The T_i of a D_3 symmetric HBC (**2-14**) and a C_2 symmetric HBC (**2-15**) with three and two dodecyl chains, respectively, have been dramatically reduced by ca. 250 °C and 200 °C with respect to the D_{6h} symmetric hexadodecyl HBC **2-2**. This provides an attractive, novel strategy for the implementation of these materials in organic electronics due to the three following reasons: I) the accessible phase transitions make thermal processing more facile, II) the reduction of alkyl substituents results in a higher concentration of the active chromophore, and III) the high substitution symmetry preserves pronounced supramolecular order important for the charge carrier transport. Finally, scanning tunneling microscopy (STM) experiments by M. Ai in the Rabe group reflected the significant effect of the substitution symmetry on the self-organized monolayer between highly oriented pyrolytic grahite (HOPG) and solution by displaying novel zigzag and flower-like patterns, which have never been observed for D_{6h}

symmetrically substituted HBCs.

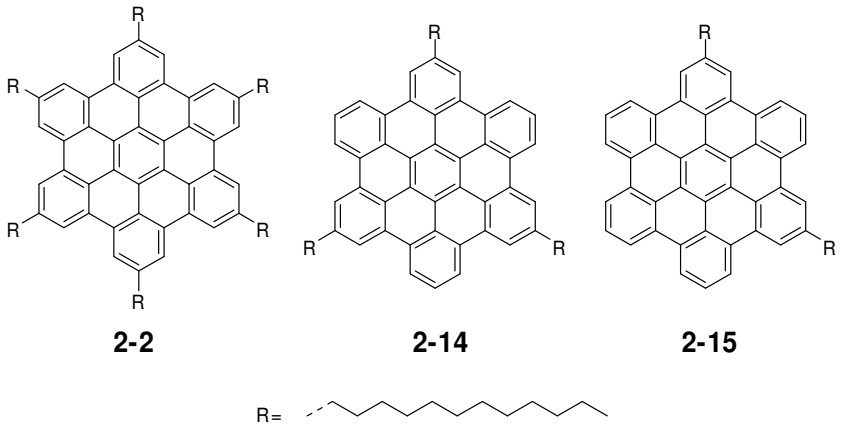

Chart 2-1. Molecular structures of different symmetric HBCs.

2.2.2 Synthesis

As was discussed previously, D_3 symmetric HBCs with alkyl substitutions at the *meta* positions have never been synthesized. Instead compound **2-6b** with functional iodide groups at the *meta* positions was available from the cyclodehydrogenation of precursor **2-4b**. Although **2-6b** was insoluble in normal organic solvents, J. Wu in the Müllen group demonstrated the opportunity to synthesize D_3 symmetric HBCs with arylamine substituents via Buchwald reaction. Here, the synthesis towards **2-14** and **2-15** took the same strategy as described above but directly starting from the building block **2-4b** (Scheme 2-5), where the functional group iodide allow the facile Kumada coupling with $C_{12}MgBr$ under the $Pd(dppf)Cl_2$ catalysis. Precursor 1,3,5-tris-2'-(3''-dodecyl)biphenylbenzene (**2-16**) was synthesized in reasonable yield (61%), while 1,3-bis-2'-(3''-dodecyl)biphenyl- 5-2'-biphenyl-benzene (**2-17)** was the side product (32%) during the reaction. Two precursors could be easily separated by column chromatography. It should be noted that the yield of **2-16** could be increased up to 85% when was strictly avoided from oxygen. The intramolecular cyclodehydrogenation of **2-16** and **2-17** was then performed by treatment with $FeCl_3$ under mild conditions affording **2-14** and **2-15** respectively as yellow solids. Both compounds were soluble in hot toluene and were purified by column chromatography

and precipitation from methanol. Further characterization by NMR, MALDI-TOF MS, and elemental analysis verified the purity of the compounds.

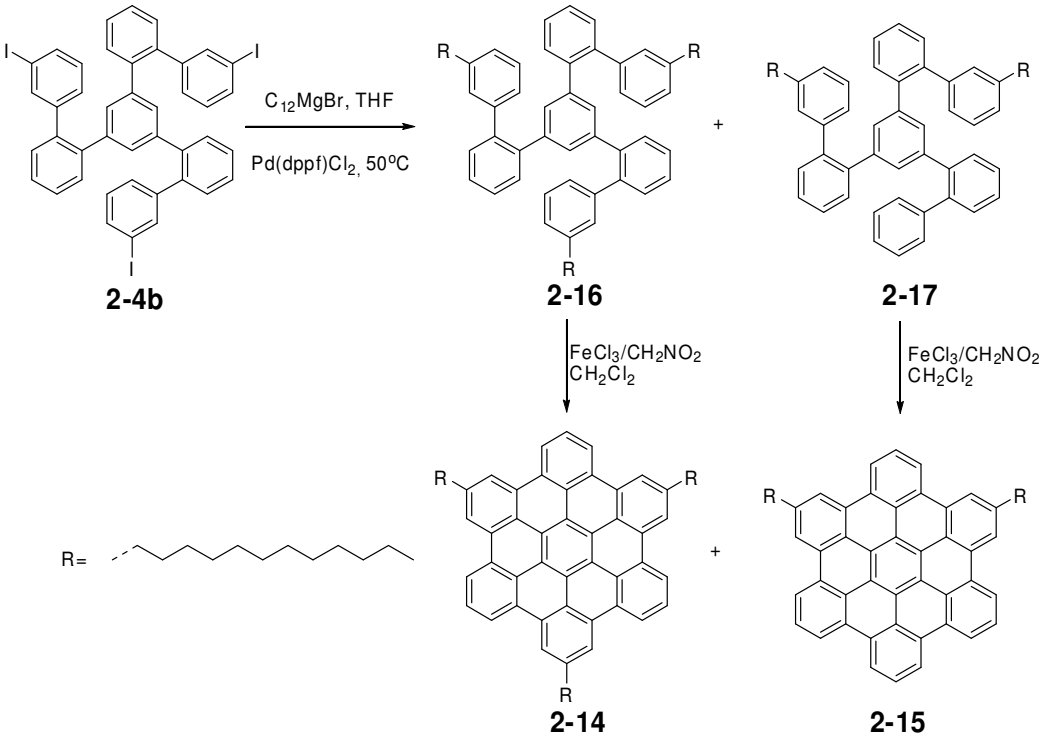

Scheme 2-5. Synthesis of **2-14** and **2-15**.

2.2.3 Thermal behavior and self-assembly at the solid-liquid interface

Differential scanning calorimetry (DSC) traces of **2-14** revealed two phase transitions (Figure 2-5). During the 2nd heating a broad first transition appeared at a temperature of 20 °C (maximum peak) which is attributed to the reorganization of the alkyl side chains, not affecting the supramolecular organization, as already reported for derivative **2-2**. Upon further heating, the second main transition at 171 °C (enthalpy 18.0 J/g) was observed. Two-dimensional wide-angle X-ray scattering (2D-WAXS) experiments of extruded samples of **2-14** indicated a self-assembly into columnar superstructures,[22] whereby the organization in the solid-state did not change with temperature (Figure 2-6 and Figure 2-7). The large number of distinct reflections in the 2D pattern and the highly birefringent optical textures observed by POM (inset in Figure 2-5) suggest, surprisingly, a crystalline phase of **2-14** over the whole solid-state phase up to the T_i of 171 °C.

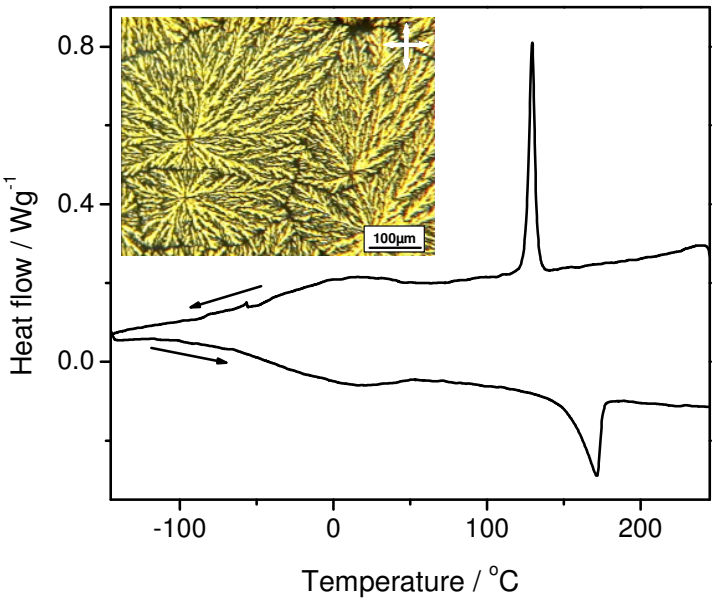

Figure 2-5. DSC traces of **2-14** during the first cooling and the second heating cycle at 10 °C/min; inset displays an image from polarized optical microscopy (POM) at cross-polarizers after cooling from the isotropic phase at 1 °C/min.

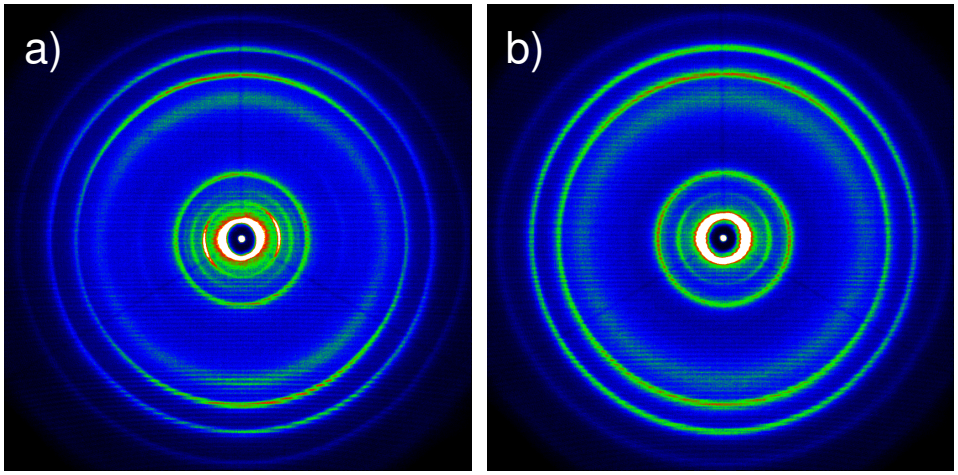

Figure 2-6. Room-temperature 2D-WAXS patterns of a) **2-14** and b) **2-15**.

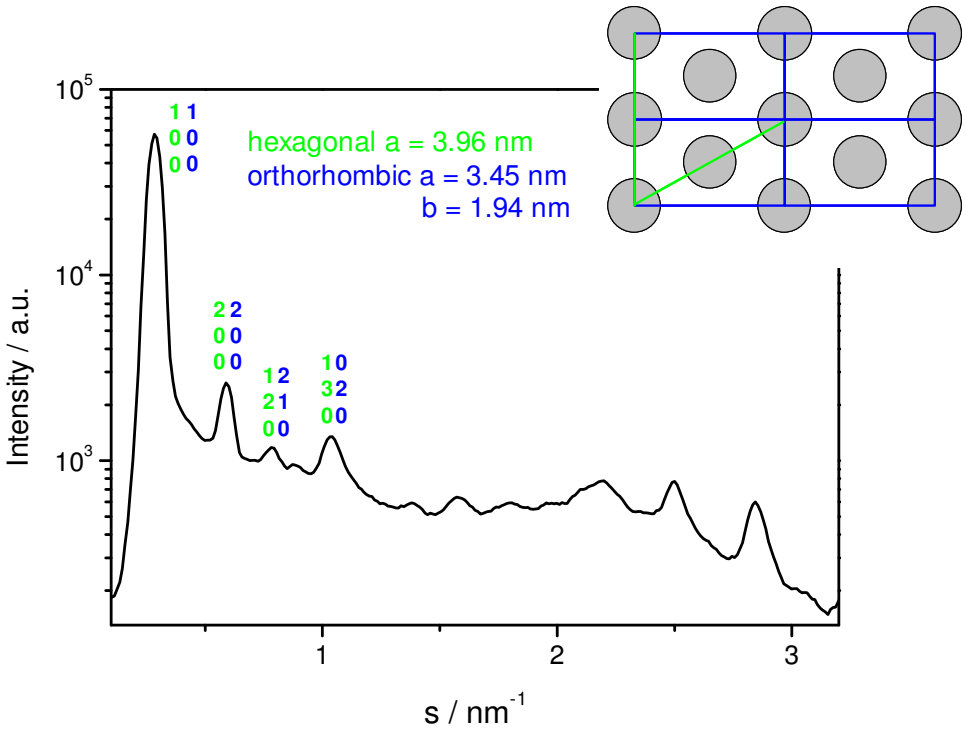

Figure 2-7. Equatorial integration of the 2D pattern of **2-14** plotted as the scattering intensity as a function of the scattering vector s. The reflections are assigned by the Miller's indices indicating two different unit cells, hexagonal and orthorhombic. The corresponding intercolumnar arrangement of **2-14** is illustrated in the inset.

This extraordinarily low T_i is in strong contrast to the thermal behavior of **2-2**, which exhibits a transition to a liquid crystalline phase at 107 °C and an isotropic phase at ca. 420 °C. Despite fewer dodecyl substituents, the T_i of **2-14** was decreased by ca. 250 °C with respect to **2-2**. A similar trend of the thermal behavior was discerned for **2-15**. During the 2nd heating **2-15** revealed a small first transition at 76 °C (1.6 J/g), which was also attributed to the side chains reorganization, and an isotropization point at 221 °C (4.9 J/g). Compound **2-15** exhibited an identical crystalline phase as **2-14** (see for 2D-WAXS and POM in Figure 2-5 and Figure 2-8). The dramatic T_i drop can only be explained in terms of the decrease of the molecular symmetry. In general, the aromatic cores approach each other via π-stacking interactions, while the alkyl side chains, bearing a certain steric demand, disturb these attractive non-covalent forces, which is usually reflected by enhanced solubility and decreased phase transition

temperatures. One might initially expect for the D_3 symmetric **2-14**, substituted by three alkyl substituents, a significant decrease of the T_i in comparison to **2-2**. The considerable impact of the lowered molecular symmetry from D_{6h} for **2-2** to D_3 of **2-14** on the thermal behavior, leading to the unexpectedly low isotropic phase transition, was confirmed by the lack of a mesophase. This phenomenon has so far only been observed for HBC derivatives carrying bulky 2-decyl-tetradecyl chains or asymmetrically substituted 1,2,3-tris-dodecyloxy HBC.[19,23] A lower T_i with decreasing number of aliphatic substitutions and maintaining the molecular symmetry has been only accounted for in discotic alkyloxy substituted triphenylenes, whereby the temperature decrease was relatively small.[24]

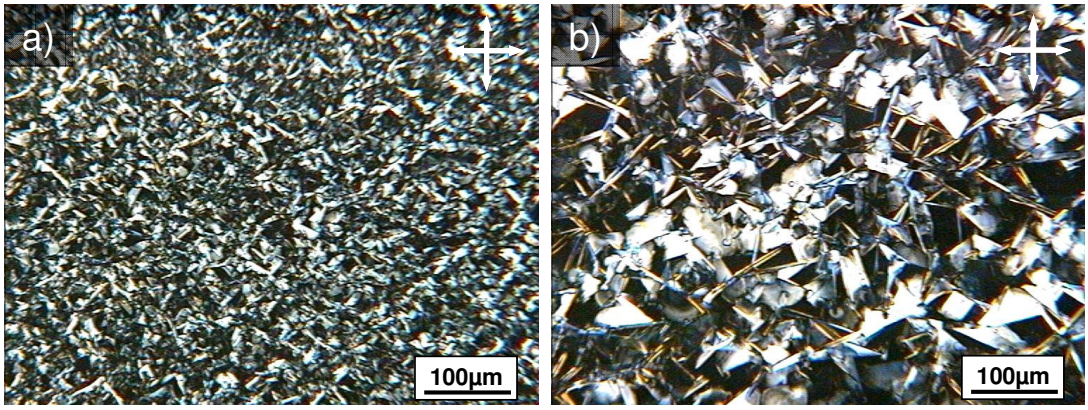

Figure 2-8. POM images with cross-polarizers of **2-15** cooled from the isotropic phase by a) 1 °C/min and b) 0.1 °C/min.

In the next step, the packing behavior of these two molecules in a quasi-2D system at an interface has been investgated by STM in order to study the influence of the symmetry of the aromatic cores on molecular self-assembly at the interface between their solutions and HOPG.[21b] D_{6h} symmetric **2-2** has already been found to self-assemble in oblique or dimer nanostructures on the basal plane of HOPG.[20] Here, for D_3 symmetric **2-14**, a significantly different packing besides dimer patterns (Figure 2-9b) was obtained, namely a zigzag pattern, as shown in Figure 2-9a. STM current image of **2** in the large scale revealed many domains (Figure 2-10). The zigzag

pattern comprises six bright features (corresponding to high tunneling probability) in a unit cell, which are ascribed to the π-conjugated HBC discs.[25] The aliphatic side chains have not been resolved, probably due to their high conformational mobility on a time scale faster than the STM imaging. The C_2 symmetric compound **2-15** was also assembled into two different coexisting crystallographic phases (Figure 2-10). In addition to a zigzag structure (Figure 2-9c), which was similar to **2-14**, a flower-like pattern was found (Figure 2-9d). The flower-like pattern consists of six triangle-shaped objects, each with three molecules of **2-15**. Noteworthy, the centers of the flowers were sometimes empty, but in few cases accommodated an object inside, marked by white and red hexagons correspondingly in Figure 2-9d. Fewer alkyl substituents and thus lower symmetry of **2-14** and **2-15** resulted in significantly distinguishable packings, i.e. the zigzag and flower-like nanostructures, in comparison with the D_{6h} symmetric HBC derivatives. The lattice constants of the two-dimensional crytal structures of **2-14** and **2-15** are shown in Table 2-1.

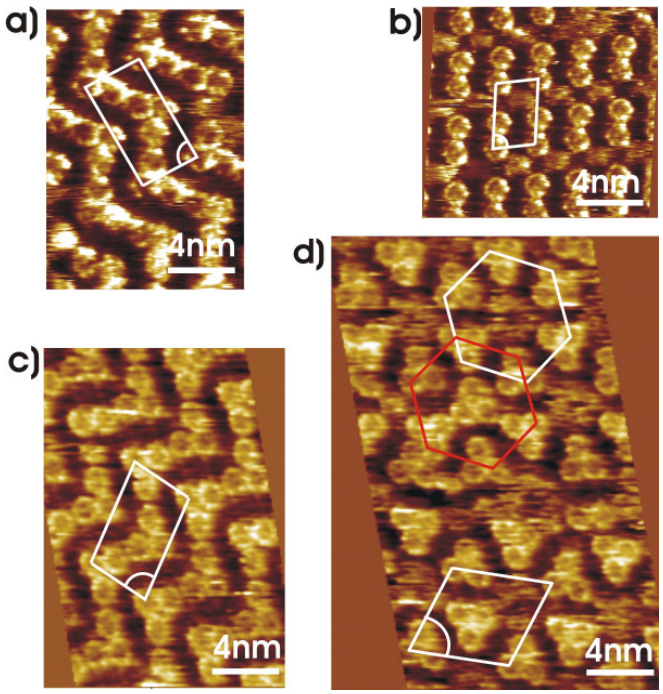

Figure 2-9. a) and b) STM current images of molecules **2-14**; c) and d) STM height images of molecules **2-15**.

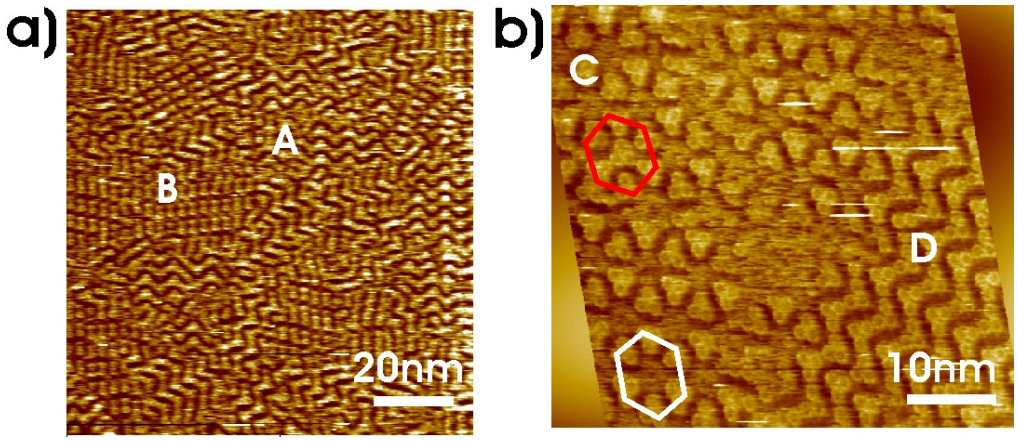

Figure 2-10. a) STM current image of molecules **2-14**, the "zigzag" structure marked by A, and the dimer structure by B. b) STM height image of molecules **2-15**, the flowerlike pattern in C domain, the zigzag in D domain.

Table 2-1. Lattice constants of the two-dimensional crytal structures of HBC derivatives

Molecule type	Lattice type	Lattice parameter	Area in nm^2
2-14	zigzag	a = 3.22 ± 0.21 nm b = 6.38 ± 0.43 nm α = 87 ± 3 °	20.49 ± 1.77
	dimer	a = 2.43 ± 0.12 nm b = 4.20 ± 0.25 nm α = 82 ± 2 °	10.11 ± 0.71
2-15	zigzag	a = 3.39 ± 0.06 nm b = 6.24 ± 0.43 nm α = 90 ± 3 °	21.14 ± 0.58
	flowerlike	a = 5.86 ± 0.27 nm b = 5.86± 0.25 nm α = 60 ± 3 °	29. 59 ± 1.78

2.2.4 Summary

In summary, we have synthesized D_3 symmetric (**2-14**) and C_2 symmetric (**2-15**) HBCs, which showed a surprisingly significant reduction of the isotropic temperatures with respect to their D_{6h} symmetric analogue. The accessible T_i may allow the fabrication of organic field-effect transistors by melt-processing.[26] A better

performance of the two compounds in devices is expected due to fewer insulating alkyl chains and an increase of the chromophore concentration, with a high degree of order at the same time. STM revealed additionally a strong effect of symmetry and substitutes on the self-assembly of both derivatives at the solid-liquid interface displaying novel zigzag and flower-like patterns with a lower symmetry than the D_{6h} symmetric analogue.

2.2.5 References:

(1) (a) *Polycyclic Hydrocarbons*, Clar, E. Academic Press, New York, 1964, Vol. I/II; (b) *The Aromatic Sextet*, Clar, E. Wiley-VCH, London, 1972; (c) Scholl, R.; Seer, C.; Weitzenbök, R. *Chem. Ber.* **1910**, *43*, 2202-2209; (d) Scholl, R.; Seer, C. *Liebigs Ann. Chem.* **1912**, *394*, 111-123; (e) Scholl, R.; Seer, C. *Chem. Ber.* **1922**, *55*, 330-341; (f) Clar, E.; Stewart, D. G. *J. Am. Chem. Soc.* **1953**, *75*, 2667-2672; (g) Clar, E.; Schmidt, W. *Tetrahedron* **1979**, *35*, 2673-2680.

(2) (a) Clar, E.; Ironside, C. T. *Proc. Chem. Soc.* **1958**, 150; (b) Clar, E.; Ironside, C. T.; Zander, M. *J. Chem. Soc.* **1959**, 142-147. (c) Halleux, A.; Martin, R. H.; King, G. S. D. *Helv. Chim. Acta* **1958**, *129*, 1177-1183. (d) Hendel, W.; Khan, Z. H.; Schmidt, W. *Tetrahedron* **1986**, *42*, 1127-1134.0

(3) Watson, M. D.; Fechtenköter, A.; Müllen, K. *Chem. Rev*. **2001**, *101*, 1267-1300.

(4) (a) Stabel, A.; Herwig, P.; Müllen, K.; Rabe, J. P. *Angew. Chem.*, **1995**, *107*, 1768-1770; *Angew. Chem. Int. Ed.* **1995**, *34*, 1609-1611; (b) Müller, M.; Kübel, C.; Müllen, K. *Chem. Eur. J.* **1998**, *4*, 2099-2109.

(5) Kübel, C.; Eckhardt, K.; Enkelmann, V.; Wegner, G.; Müllen, K. *J. Mater. Chem.* **2000**, *10*, 879-886.

(6) (a) Rempala, P.; Kroulik, J.; King, B. T. *J. Am. Chem. Soc.* **2004**, *126*, 15002-15003; (b) Stefano, M. D.; Negri, F.; Carbone, P.; Müllen, K. *Chem. Phys.*, **2005**, *314*, 85-99.

(7) (a) Hyatt, J. A. *Org. Prep. Proced. Int.* **1991**, *23*, 460-463. (b) Herwig, P.; Kayser, C. W.; Müllen, K.; Spiess, H. W. *Adv. Mater.* **1996**, *8*, 510-513. (c) Fechtenkötter, A.; Saalwächter, K.; Harbison, M. A.; Müllen, K.; Spiess, H. W. *Angew. Chem.*, **1999**, *111*,

3224-3228; *Angew. Chem. Int. Ed.* **1999**, *38*, 3039-3042. (d) Brand, J. D.; Kübel, C.; Ito, S.; Müllen, K. *Chem. Mater.* **2000**, *12*, 1638-1647.

(8) (a) Wu, J.; Watson, M. D.; Müllen, K. *Angew. Chem. Int. Ed.* **2003**, *42*, 5329-5333. (b) Wu, J.; Baumgarten, M.; Debije, M. G.; Warman, J. M.; Müllen, K. *Angew. Chem. Int. Ed.* **2004**, *43*, 5331-5335; (c) Wu, J.; Watson, M. D.; Zhang, L.; Wang, Z.; Müllen, K. *J. Am. Chem. Soc.* **2004**, *126*, 177-186.

(9) (a) Lambert, C.; Nöll, G. *Angew. Chem. Int. Ed.* **1998**, *37*, 2107-2110. *Angew. Chem.* **1998**, *110*, 2239-2242; (b) Lambert, C.; Nöll, G. *Chem. Eur. J.* **2002**, *8*, 3467-3477.

(10) (a) Elmorsy, S. S.; Pelter, A.; Smith, K. *Tetrahedron. Lett*. **1991**, *32(33)*, 4175. (b) Elmorsy, S.S.; Khalil, A. G. M.; Girges, M. M.; Salama, T. A. *Tetrahedron. Lett*. **1997**, *38(6)*, 1071. (c) Boorum, M. M.; Vasil'ev, Y. V.; Drewello, T.; Scott, L. T. *Science* **2001**, *294*, 828. (d) Scott, L. T.; Boorum, M. M.; McMahon, B. J.; Hagen, S.; Mack, J.; Blank, J.; Wegner, H.; de Meijere, A. *Science* **2002**, *295*, 1500. (e) Ansems, R. B. M.; Scott, L. T. *J. Am. Chem. Soc*. **2000**, *122*, 2719-2724. (f) Scott, L. T. *Angew. Chem. Int. Ed*. **2004**, *43*, 4994-5007.

(11) (a) Dötz, F.; Brand, J. D.; Ito, S.; Gherghel, L.; Müllen, K. *J. Am. Chem. Soc*. **2000**, *122*, 7707-7717. (b) Simpson, C. D.; Brand, J. D.; Berresheim, A. J.; Przybilla, L.; Räder, H. J.; Müllen, K. *Chem. Eur. J*. **2002**, *8(6)*, 1424-1429.

(12) Crystals suitable for X-ray structure analysis were obtained by slow evaporation of ethyl acetate/hexane solution of compound **2a** at room temperature. Crystal structure determination was carried out on a KCCD diffractometer with graphite-monochromated Mo Ka irradiation. The structure was solved by direct methods (SHELXS-97).

(13) Wu, J.; Gherghel, L.; Watson, M. D.; Li, J.; Wang, Z.; Simpson, C. D.; Kolb, U.; Müllen, K. *Macromolecules*. **2003**, *36*, 7082-7089.

(14) Crystal growth see ref 13.

(15) (a) Grimsdale, A. C.; Müllen, K. *Angew. Chem. Int. Ed.* **2005**, *44*, 5592-5629. (b) van de Crass, A. M.; Stutzmann, N.; Bunk, O.; Nielsen, M. M.; Watson, M. D.; Müllen, K.; Chanzy, H. D.; Sirringhaus, H.; Friend, R. H. *Adv. Mater*. **2003**, *15*, 495-499. (c) Schmidt-Mende, L.; Fechtenköter, A.; Müllen, K.; Moons, E.; Friend, R.

H.; MacKenzie, J. *Science*. **2001**, *293*, 1119-1122.

(16) (a) Pisula, W.; Menon, A.; Stepputat, M.; Lieberwirth, I.; Kolb, U.; Tracz, A.; Sirringhaus, H.; Pakula, T.; Müllen, K. *Adv. Mater.* **2005**, *17*, 684. (b) Jäckel, F.; Watson, M. D.; Müllen, K.; Rabe, J. P. *Phys. Rev. Lett.* **2004**, *92*, 188303. (c) Xiao, S.; Tang, J.; Beetz, T.; Guo, X.; Tremblay, N.; Siegrist, T.; Zhu, Y.; Stigerwald, M.; Nuckolls, C. *J. Am. Chem. Soc*. **2006**, *128*, 10700-10701.

(17) (a) Wu, J.; Pisula, W.; Müllen, K. *Chem. Rev*. **2007**, *107*, 718-747. (b) Feng, X.; Pisula, W.; Müllen, K. *J. Am. Chem. Soc*. **2007**, *129*, 14116-14117.

(18) Pisula, W.; Kastler, M.; Wasserfallen, D.; Mondeshki, M.; Piris, J.; Schnell, I.; Müllen, K. *Chem. Mater.* **2006**, *18*, 3634 -3640;

(19) Kastler, M.; Pisula, W.; Wasserfallen, D.; Pakula, T.; Müllen, K. *J. Am. Chem. Soc*. **2005**, *127*, 4286-4296.

(20) Ito, S.; Wehmeier, M.; Brand, J. D.; Kübel, C.; Epsch, R.; Rabe, J. P.; Müllen, K. *Chem. Eur. J.* **2000**, *6*, 4327-4342.

(21) (a) Feng, X.; Wu, J.; Enkelmann, V.; Müllen, K. *Org. Lett.* **2006**, *8*, 1145-1148; (b) Feng, X.; Wu, J.; Ai, M.; Pisula, W.; Zhi, L.; Rabe, J. P.; Müllen, K. *Angew. Chem. Int. Ed.* **2007**, *46*, 3033-3046.

(22) Pisula, W.; Tomovc, Z.; Simpson, C.; Kastler, M.; Pakula, T.; Müllen, K. *Chem. Mater.* **2005**, *17*, 4296 –4303.

(23) (a) Pisula, W.; Kastler, M.; Wasserfallen, D.; Davies, R. J.; García-Gutiérrez, M. C.; Müllen, K. *J. Am. Chem. Soc*. **2006**, *128*, 14424 –14425. (b) Wang, Z.; Watson, M. D.; Wu, J.; Müllen, K. *Chem. Commun*. **2004**, 336–337.

(24) (a) Allen, M. T.; Harris, K. D. M.; Kariuki, B. M.; Kumari, N.; Preece, J. A.; Diele, S.; Lose, D.; Hegmann, T.; Tschierske, C. *Liq. Cryst.* **2000**, *27*, 689- 692; (b) Closs, F.; Haussling, L.; Henderson, P.; Ringsdorf, H.; Schuhmacher, P. *J. Chem. Soc. Perkin Trans. 1*. **1995**, 829-387.

(25) Lazzaroni, R.; Calderone, A.; Brédas, J. L.; Rabe, J. P. *J. Chem. Phys.* **1997**, *107*, 99-105.

(26) Maunoury, J. C.; Howse, J. R.; Turner, M. L. *Adv. Mater.* **2007**, *19*, 805-809.

Chapter 3. C_3 symmetric Hexa-*peri*-hexabenzocoronenes with Alternating Polar/Apolar Substituents

In the last chapter, a novel synthetic strategy towards C_3 symmetric hexa-*peri*-hexabenzocorones (HBCs) with three substituents has been developed by oxidizing appropriate 1,3,5-tris-(2'-biphenyl)benzene precursors. Here a facile approach towards C_3 symmetric HBCs with alternating polar/apolar substituents will be presented. Functional groups such as ester and methoxy groups can be introduced directly on the HBC skeleton or via additional phenylene units. With the functional ester substitutions on the hexaphenyl-substituted HBCs, the local dipole moments and nanoscale phase separation between the polar and apolar substituents endow the new materials with strong self-association both in solution and the solid state; remarkably enough, they can also self-assemble into fibrous nanostructures on the surface upon drop casting from appropriate solutions. On the other hand, the methoxy-substituted HBC shows strong concentration and temperature dependant association in solution, the exceptional long-range helical packing in the solid state is for first time observed for HBC derivatives, which could be possibly due to the complex non-covalent interactions inside the columnar self-organization; moreover, the methoxy-substituted HBC can easily self-assembly into giant fibers with several hundred micrometers length when it is fabricated from a broad range of organic solvents.

3.1 Controlling Columnar Orientation of C_3-symmetric "Superbenzenes" by Alternating Polar/Apolar Substitutents

3.1.1 Introduction

Hexa-*peri*-hexabenzocoronene (HBC, "superbenzene") and its hexaphenyl derivatives have continuously attracted attention due to their large nanographene-type conjugated π-system,[1] making their applications in electronic devices appealing.[2] Control of supramolecular organization in the solid state and of the interfaces with substrates and

electrodes is therefore essential. This approach utilizes the complex interplay of weak intermolecular forces such as π-stacking, phase separation between aromatic cores and soft alkyl chain peripheries as well as hydrogen bonding.[3] Another key factor is the competition between substrate-adsorbate and adsorbate-adsorbate interactions. To achieve an even higher level of control we here introduce HBCs such as **3-1** with an alternating array of apolar (alkyl) and polar (ester) substituents. The local dipole moments and the nanophase separation between polar and apolar sites are expected to profoundly change the packing modes in both 2D and 3D arrangements.[4] While hexasubstituted HBCs with D_{6h} symmetry have been widely studied, the necessary HBCs with specified C_3 symmetry are difficult to be synthesized.[5] Therefore new efficient synthetic strategy is necessary. After successful synthesis of the C_3-symmetric title systems **3-1a** and **3-1b** and of their asymmetric analogues **3-2a** and **3-2b**, solution NMR, UV-vis, and fluorescence spectroscopy as well as X-ray scattering are applied to evaluate the self-assembly both in solution and the solid state. Further, the alternating attachment of polar ester and apolar alkyl chains and the profound influence of even subtle structural changes allow a remarkably facile growth of fibrous structures from solution.

3.1.2 Synthesis, structure characterization and self-aggregation in solution

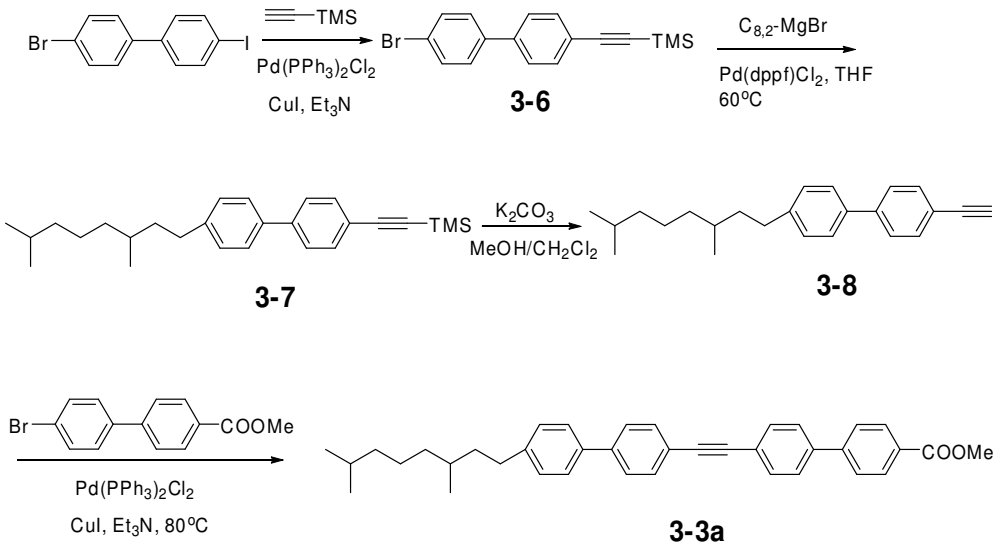

Scheme 3-1. Synthesis of **3a**.

Although in the last chapter, a new synthetic strategy is developed for D_3 symetric HBCs with three substituents at the *meta* positions starting from the precursor 1,3,5-tris(2'-biphenyl)benzene, the attempt to functionalize this building block with appropriate six substitutions is unsuccessful. Therefore, we come back to reconsider the hexaphenylbenzene precursors because more chemistry is available for their synthesis.

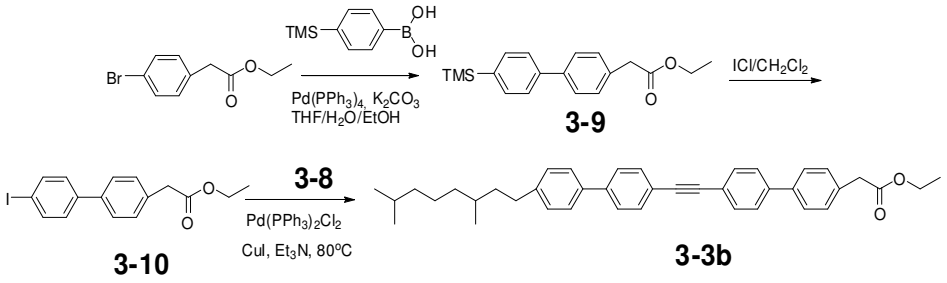

Scheme 3-2. Synthesis of **3-3b**.

Herein, the synthetic approach is based on the asymmetricly substituted diphenylacetylenes **3-3**, where one ester group and one alkyl group are introduced through the multi-step standard Hagihara-Sonogashira and Suzuki coupling reactions in good yields (Scheme 3-1 and Scheme 3-2). The different polarity of the substituents is important for the subsequent step, $Co_2(CO)_8$ catalysed cyclotrimerization, where the obtained two isomers **3-4** and **3-5** with high yield (>85%) could be separated by column chromatography. However the asymmetricly substituted diphenylacetylenes with tiny polarity difference of substituents only lead to a mixture of two isomers, which complicates the further purification by column chromatography. The yield of asymmetric isomer **3-5** dominates over that of the C_3 symmetric **3-4** (the ratio is around 2:1), thus the separated yield of desired **3-4** is generally larger than 25%. The key step of oxidative planarization toward the HBCs is accomplished by treatment of these precursors with $FeCl_3$ under mild conditions to obtain the final C_3 symmetric HBCs **3-1** and asymmetric HBCs **3-2** in good yields after purification with column chromatography and reprecipitation from methanol.[6] Since the synthesis of **3-3** is very facile within three steps and gives relatively large quantities, **3-1** could be synthesized on the gram scale. Compounds **3-1a** and **3-2a**,

where the ester groups are directly attached at the hexaphenyl-substituted HBCs show poor solubility in organic solvents including THF, dichloromethane and chloroform, already indicating a high aggregation tendency in solution (see below). In contrast, **3-1b** and **3-2b** with an additional methylene linkage are well soluble in the above solvents.

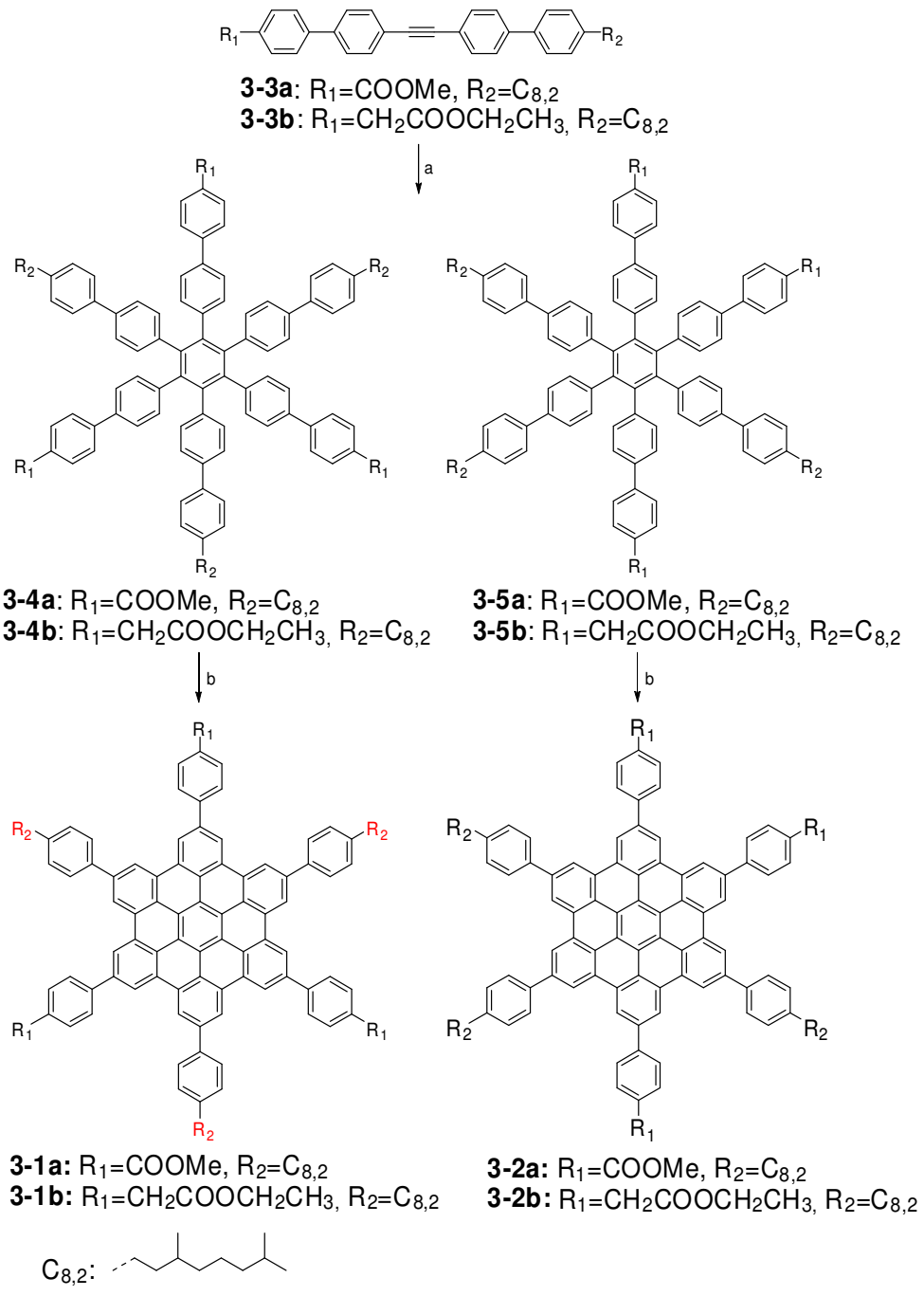

Scheme 3-3. General synthetic route toward **3-1** and **3-2**.

The relative tendencies of compounds **3-1a** and **3-1b** to aggregate in solution are qualitatively assessed by solution NMR and optical spectroscopy.[7] The temperature dependent ^{1}H NMR spectra (2.0×10^{-3} M in *d*-$CDCl_2CDCl_2$) indicate a strong tendency of all disc-type structures, **3-1** and **3-2**, to form aggregates in solution at low temperature, which causes significant line broadening and shielding (Figure 3-2 to Figure 3-5). With increasing temperature, as shown in Figure 3-1 and Figure 3-4, **3-1b** reveals a remarkably resolved spectrum at 140^{o}C, suggesting less aggregation at high temperature, whereas at the same condition, the ^{1}H NMR signals of **3-1a** are still broadened (Figure 3-1 and Figure 3-2). It is interesting to note that the entire proton signals of **3-1a** including the HBC core (7.58 ppm), peripheral phenyl protons (broaden at 6.70 ppm) and even substituted ester groups and alkyl chains are high field shifted, indicating that **3-1a** is strongly aggregated in solution even at high temperature. ^{1}H NMR spectra taken for different concentrations of **3-1a** and **3-1b** (5 times higher or 10 times lower) at high temperature support the above conclusions. On the other hand, at low temperatures, the spectra in all cases for **3-1a** and **3-1b** are met with significant line broadening and multiple signals, which are significantly different from the formerly hexa-alkylphenyl substituted HBCs reported by A. Fechtenkötter, where already showed clearly resolvable proton signals of the corona. The broadened phenyl proton signals could be possibly ascribed to the interlocking of pending phenyl rings and π-interactions.[2a] Therefore, the difference of the self-associations among **3-1a**, **3-1b** and hexa-alkylphenyl substituted HBCs in solution as reflected by ^{1}H NMR spectra, despite their similar molecular structure,

imply the important role of substituted ester functions, in which the nano-scale separated polar ester groups can impart the strong local intermolecular dipole-interactions, and thus enhance the aggregation in solution. Similarly, with the NMR spectroscopic studies, compounds **3-2a** and **3-2b** demonstrate an identical tendency as observed for **3-1a** and **3-1b**, a stronger aggregation in solution occurring for **3-2a** than for **3-2b**.

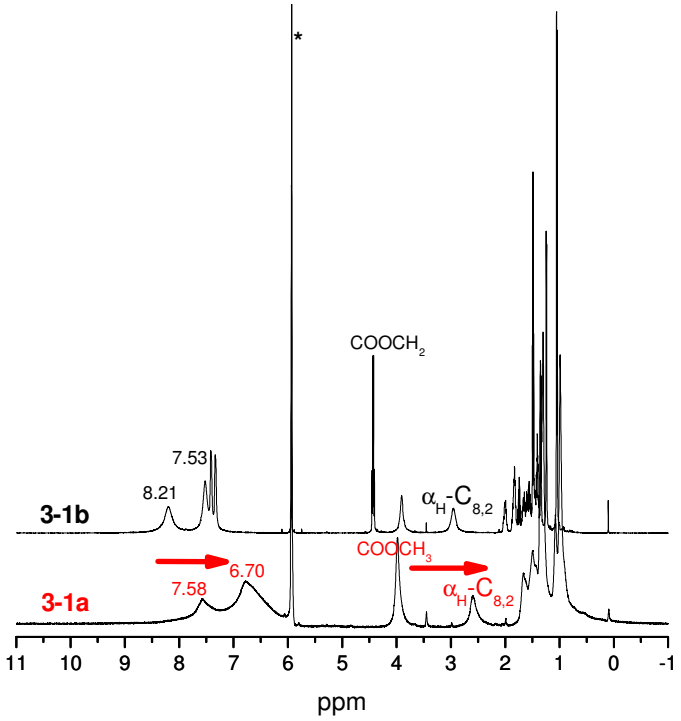

Figure 3-1. ^{1}H NMR spectra of **3-1a** (red) and **3-1b** (black) in *d*-tetrachloroethane at 140^{o}C.

In the solution UV-vis and fluorescence spectra (5.0×10^{-6} M, Figure 3-6), the broad and less structured emission spectra for **3-1a** and **3-1b** were also different from those of hexa-alkylphenyl substituted HBCs with more resolved absorptions. The UV-vis signals of **3-1a** (tailing to 490 nm) are broader than those of **3-1b**, and the emission at 549 nm for **3-1a** is bathochromically shifted by 26 nm compared to **3-1b** (523 nm).

Thus the different self-assembly of **3-1a** and **3-1b** in solution further emphasizes the role of ester groups directly attached to the central aromatic system.

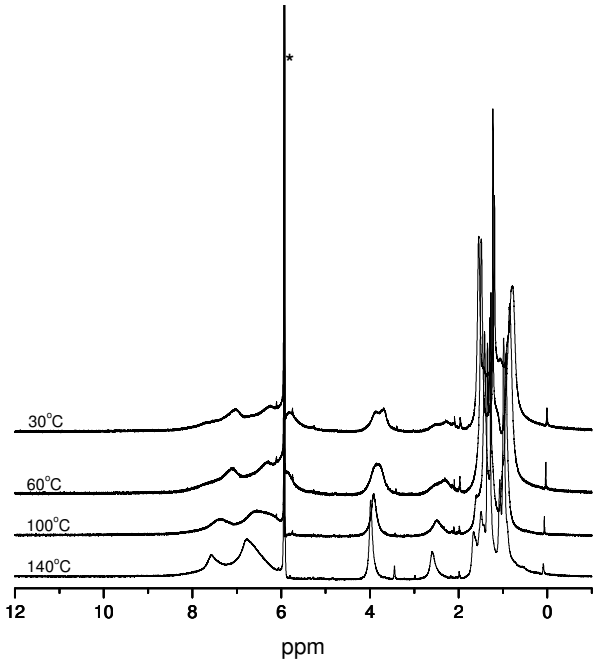

Figure 3-2. Temperature-dependant ^{1}H NMR (500 MHz) spectra of **3-1a** in *d*-tetrachloroethane (*)

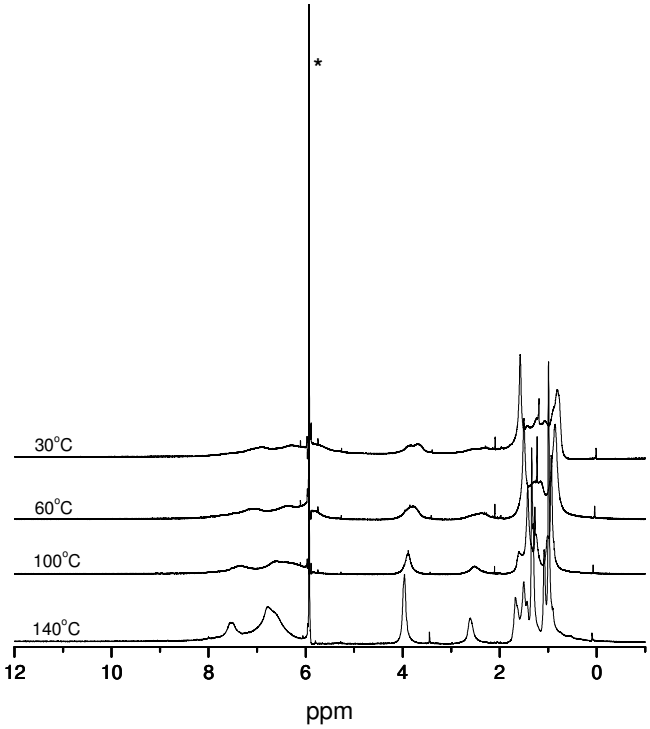

Figure 3-3. Temperature-dependant ^{1}H NMR (500 MHz) spectra of **3-2a** in *d*-tetrachloroethane (*)

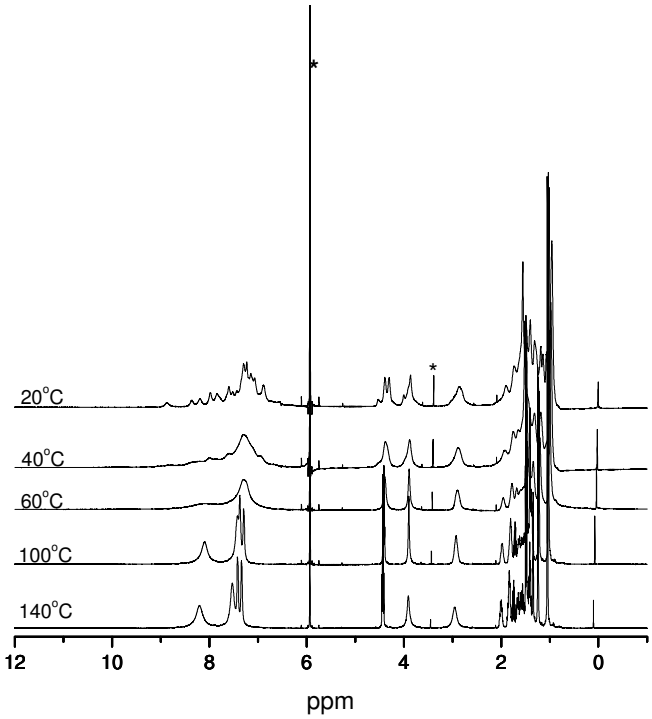

Figure 3-4. Temperature-dependant ^{1}H NMR (500 MHz) spectra of **3-1b** in *d*-tetrachloroethane (*)

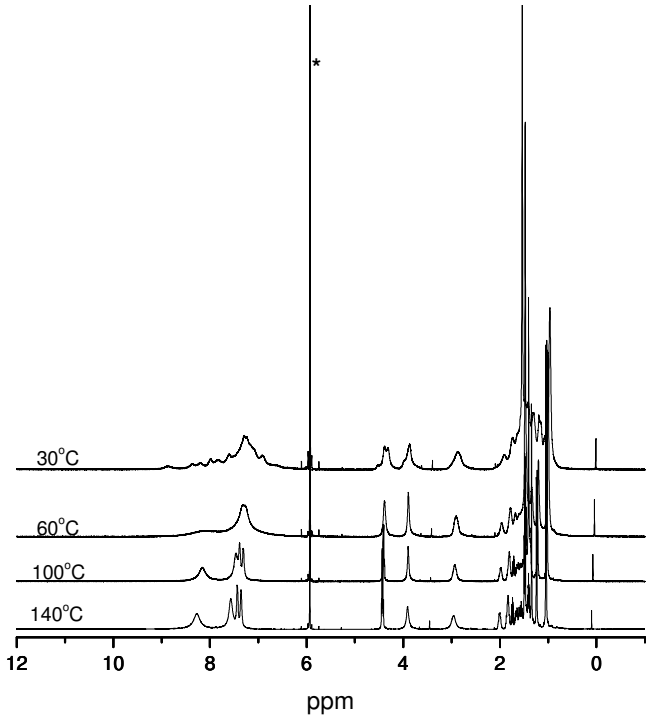

Figure 3-5. Temperature-dependant ^{1}H NMR (500 MHz) spectra of **3-2b** in *d*-tetrachloroethane (*)

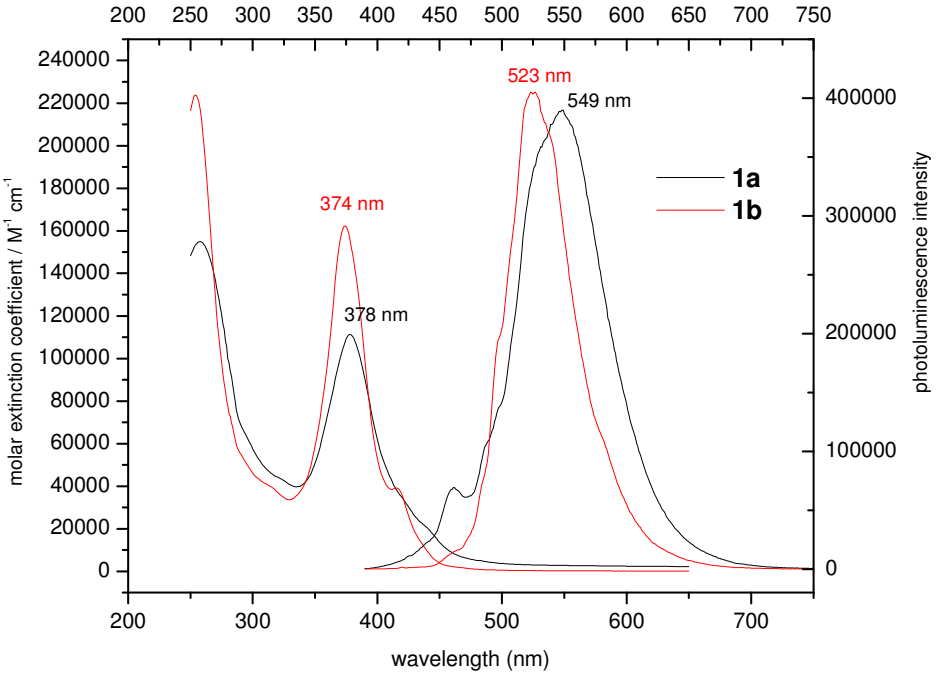

Figure 3-6. UV-vis and photoluminescence spectra for **3-1a** (black) and **3-1b** (red) in THF (5.0×10^{-6}M).

3.1.3 Bulk characterization in the solid state

Two-dimensional wide-angle X-ray scattering (2D-WAXS) experiments on mechanically oriented filaments were investigated in detail in cooperation with W. Pisula in the Müllen group, and revealed the self-assembly of all four investigated compounds, **3-1a**, **3-2a**, **3-1b** and **3-2b**, into discotic columnar arrays.[8] Within the hexagonal columnar unit cells the packing parameters (3.00 nm for **3-1a**, 2.90 nm for **3-2a**, 2.97 nm for **3-1b**, and 2.95 nm for **3-2b)** and the π-stacking distance of 0.35 nm are very close to those of hexaalkyl substituted hexaphenyl HBCs.[9] However, **3-1a** shows a unique columnar alignment in the extruded filaments since its columns are arranged perpendicular to the alignment direction (see Figure 3-7a). In general, columnar superstructures based on discotic molecules are aligned along the orientation direction, e.g. along the shearing direction and thus along the filament axis (Figure 3-7b).[10] The alignment of (macro)molecules usually depends strongly on

their molecular aspect ratio.[11] The larger the aspect ratio of the building blocks, the higher the possibility for an orientation of the molecules with their molecular axis along the shearing direction, as is in the case for conjugated polymers.[11] To our knowledge, this is the first case that low molecular weight discotic molecules are aligned with their planes along the mechanical alignment direction.[12] This unusual orientation of columns highlights not only (π-stacking) interactions between single building blocks leading to columnar structures, but also intercolumnar interactions as observed for **3-1a**. The unique role of **3-1a** with an alternating attachment of the polar ester groups and apolar alkyl chains can be ascribed to a phase separation of the substituents in the disc periphery of **3-1a** and intermolecular dipole interactions induced by ester groups which are responsible for the observed in-plane interaction and the orientation of the discs. Neither **3-1b** (see Figure 3-9) nor **2a** (Figure 3-7b) reveal this unexpected orientation, indicating the crucial role of substitution pattern and molecular symmetry. This special alignment under shearing has been so far only observed for high molecular-weight main chain discotic polymers consisting of covalently linked triphenylenes, [13] where the columns are aligned perpendicularly to the oriented polymer chains, as schematically illustrated in Figure 3-8a. Our case utilizes a more complex supramolecular approach based on non-covalent forces between monomers. It can be assumed that the strong intermolecular dipole-dipole interactions between the ester groups of individual building blocks of **3-1a** lead to a 2D in-plane hexagonal network possessing the necessary aspect ratio to be oriented in the above described specific way (Figure 3-8b); during the further assembly step under alignment, a 3D hexagonal columnar array is thus formed *via* π-stacking interactions.

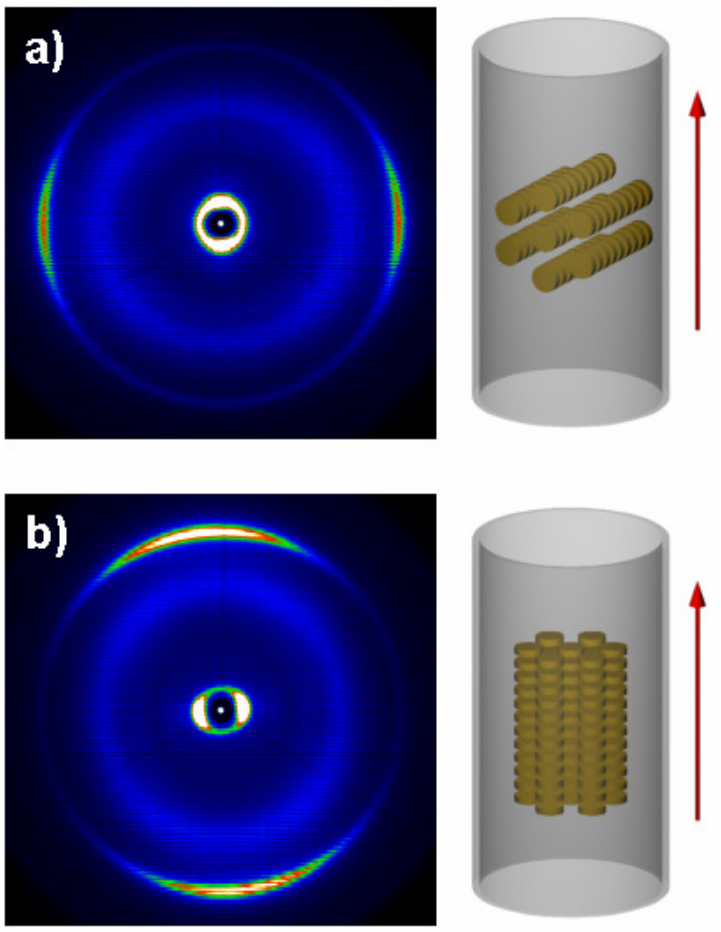

Figure 3-7. 2D-WAXS patterns and schematic illustration of the corresponding alignment of the columnar superstructures in the extruded filaments (red arrow indicates the extrusion direction) for a) **3-1a** and b) **3-2a**.

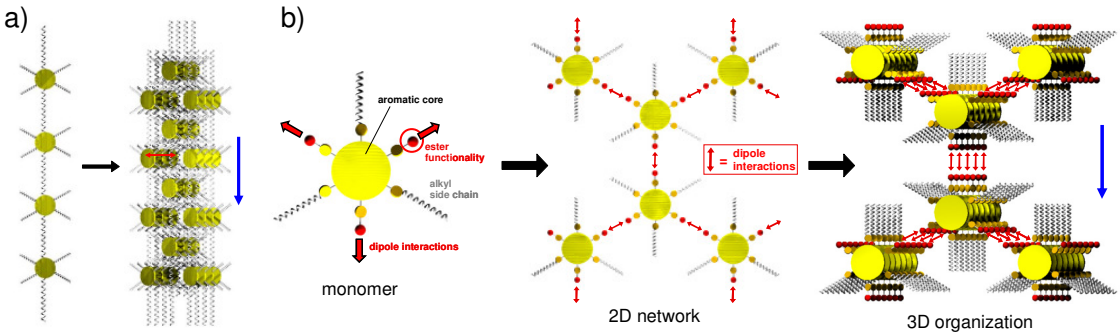

Figure 3-8. Schematic illustration of self-assembly and alignment orientation during mechanical processing of a) main chain discotic polymers (red arrow characterises π-stacking interactions), and b) compound **3-1a** which assembles first *via* dipole interactions into a 2D network and in a further step *via* π-stacking into a 3D hexagonal columnar organization. In both cases, the blue arrow indicates the alignment direction to which the columns are arranged perpendicularly.

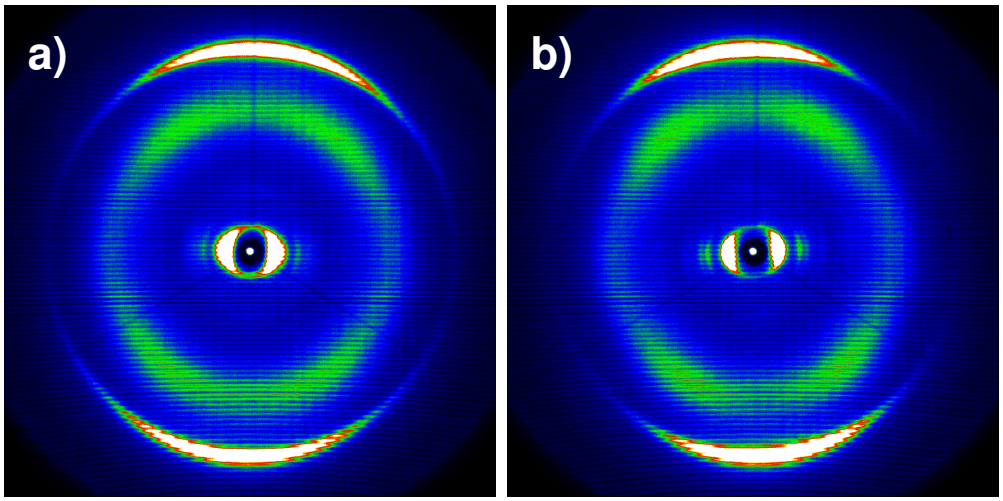

Figure 3-9. 2D-WAXS patterns of the corresponding alignment of the superstructures in the extruded filaments for a) **3-1b** and b) **3-2b**.

3.1.4 Self-assembly in solution and on the surface

The self-assembly of suitably decorated disc-type molecules does not only lead to columnar arrangements in the bulk, but also to the growth of fibrous nanostructures from solution.[14] Recently, HBCs, self-assembled into well-defined nanotubular or fibrous objects with a large number of π-stacked HBC units, have gained wide attention due to their semiconducting character.[14] Based on the above discussions, ester groups in **1a** and **1b** have played an important role for the pronounced self-aggregation properties both in solution and in the solid state, therefore, it can be expected that the joint effect of π-stacking, dipole-interactions of ester groups and nanoscale phase separation between polar and apolar substituents of **1a** and **1b** should allow the growth of fibrous nanostructures from solution via self-assembly. In the solution, the change of UV-vis and photoluminescence spectra upon variation of concentration, temperature as well as solvate conditions has been widely used to qualitatively evaluate the self-assembly behavior for the aromatic systems.[3] Thus, the polar solvent methanol is added to a solution of **3-1a** in THF (1.0×10^{-5} M). Although no gelation or precipitation are observed upon increasing the THF:MeOH ratio up to 1:1, the UV-vis spectrum is significantly broadened and a tailing to visible region

with a bathochromical shift of absorption maximum (3 nm) occurs, indicating the formation of aggregates at this condition (Figure 3-10a). The fluorescence spectra

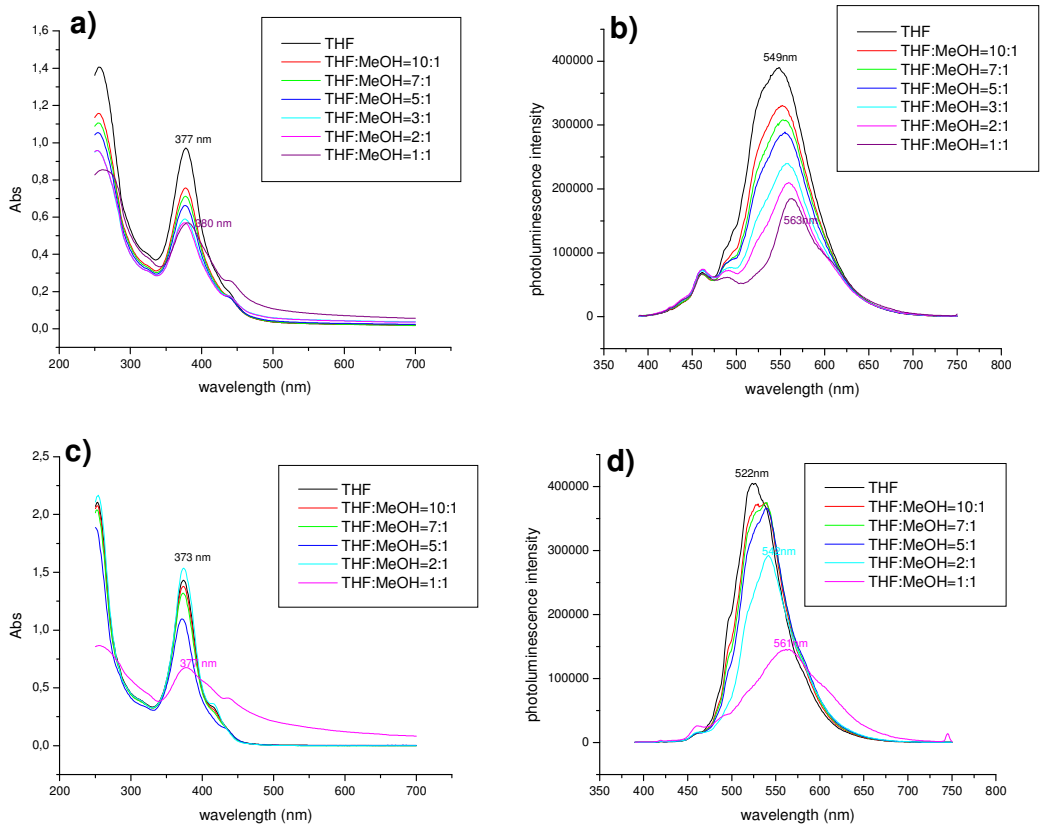

Figure 3-10. UV-vis and photoluminescence spectra for **3-1a** (a and b) and **3-1b** (c and d) in THF-MeOH mixed solvents (1.0×10^{-5} M).

reveal the same trend as UV-vis spectra (Figure 4b), upon increasing the THF:MeOH ratio to 1:1, the emission maximum is 15 nm bathochromically shifted with respect to the pure THF solution. Precipitated filaments are formed in several minutes, and then drop-cast at room temperature. Interestingly, fibrous structures are obtained with a diameter of around 100-200 nm and several micrometers length (Figure 3-11a and Figure 3-12a). Taking into account the molecular size, the submicron-sized fibers consist of 50~100 bundles of stacked molecular wire of **3-1a**. These results confirm again the strong aggregation and π-stacking tendency of **3-1a** allowing the growth of fibrous superstructures. High-resolution transmission electron microscopy (HRTEM)

images (Figure 3-11b) display individual columnar structures along the fiber direction, which are corresponding to the one-dimensional stacking of HBC discs, indicating the long range organization of disc molecules upon the self-assembly. It should be mentioned that this ordering of self-assembled disc molecules with columnar features inside the fibrous superstructure could be comparable to the zone-casting technique of HBCs molecules as revealed by HRTEM,[10a] indicating the promise for nanodevices. Sharp and distinct reflections in the small area-selected electron diffraction pattern indicate again the well-oriented columnar structures (inset of Figure 3-11b), which can be assigned to the π-stacking distance of 0.35 nm. The intercolumnar distance of 2.5 nm was calculated, which is slightly smaller than observed for the extruded samples.

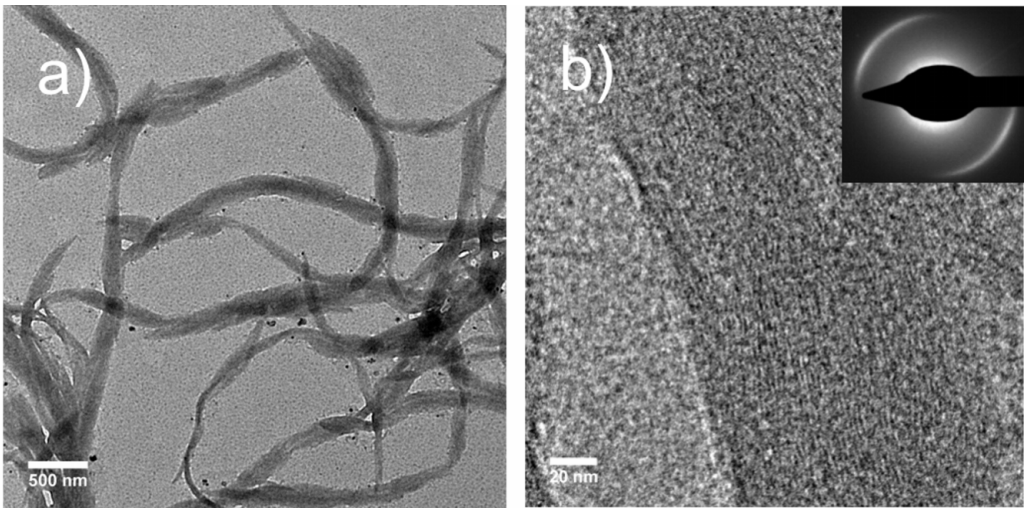

Figure 3-11. a) Electron microscopy of **3-1a** fibers grown from THF:MeOH=1:1 solution, b) HRTEM image of a fiber displaying columnar structures of **3-1a**, c) electron diffraction pattern with reflections assigned to the π-stacking distance of 0.35 nm.

Similarly, when the THF:MeOH ratio is increased up to 1:1 (Figure 3-10c and 3-10d), the bathochromic shift in the fluorescence spectra of **3-1b** is even more remarkable, suggesting, again, pronounced aggregate formation. After several minutes filaments precipitate, however, in this case, only large structures on the substrate are observed by scanning electron microscopy (SEM) (Figure 3-12b). The solution is further

allowed to stand for two days at room temperature and interestingly large bundles of fibrous structures (300-600 nm) are formed (Figure 3-13a). Furthermore, the high-resolution TEM also demonstrates the well-oriented columns along the fiber axis (Figure 3-13b). This behavior might be explained by the lower tendency toward phase separation between polar ester groups and apolar alkyl chains in **3-1b** that lead to a longer time necessary to self-assemble into ordered one-dimensional nanostructures.

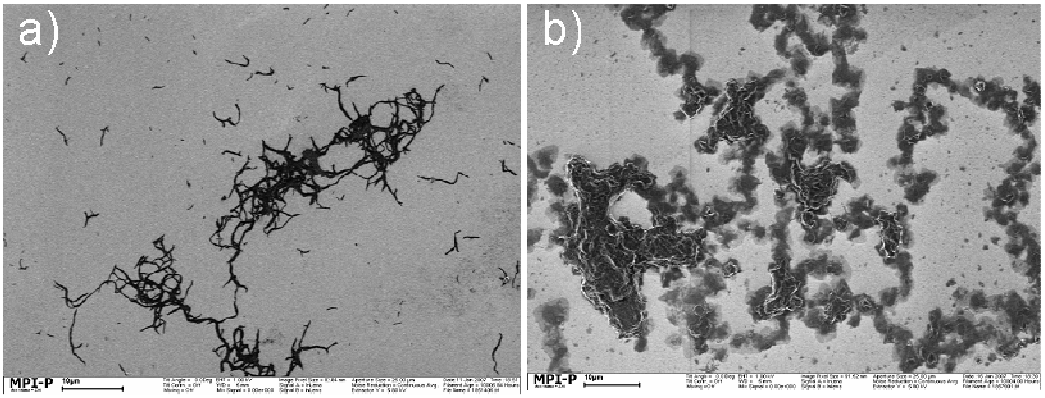

Figure 3-12. SEM pictures of **3-1a** (a) and **3-1b** (b) nanostructures grown from THF:MeOH = 1:1 solution.

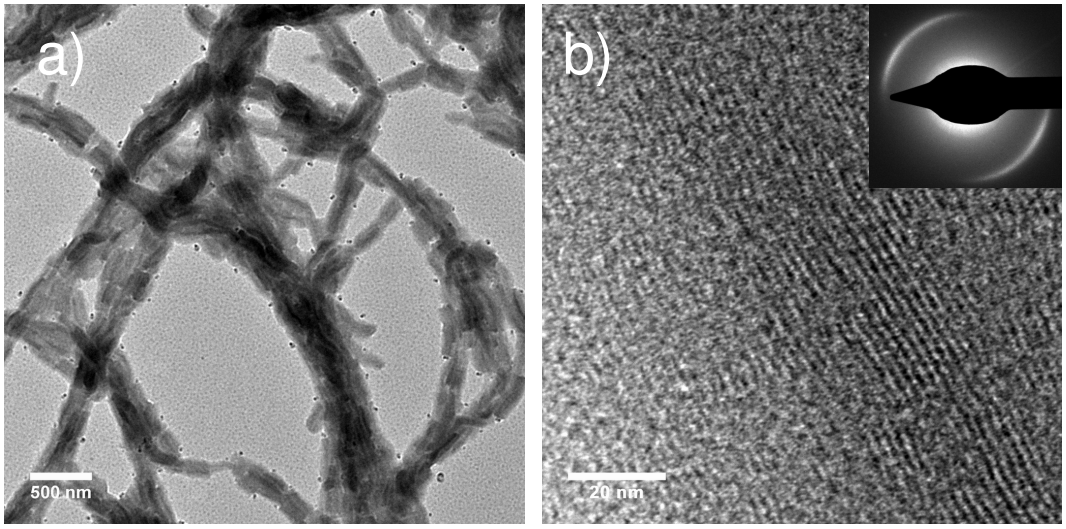

Figure 3-13. a) Electron microscopy of **3-1b** fibers grown from THF:MeOH=1:1 solution, b) HRTEM image of a fiber displaying columnar structures of **3-1b**, electron diffraction pattern with reflections (inset) assigned to the π-stacking distance of 0.35 nm.

3.1.5 Conclusion

In conclusion, we have developed a synthetic route toward novel C_3 symmetric HBCs with alternating polar and apolar substituents which are attached to the hexaphenyl-HBCs either directly or through a spacer. Spectroscopic studies reveal the stronger aggregation ability in solution of **3-1a** with respect to **3-1b** which can be ascribed to the strong intermolecular dipole interactions. These pronounced non-covalent forces lead to a perpendicular orientation of columnar superstructures of the discotic molecules to the applied alignment direction. Thereby, the substitution symmetry of the functional groups plays a key role for the self-assembly, indicating an opportunity to strongly enhance supramolecular assembly by introducing appropriate functional groups. Obviously, the corresponding C_3 symmetric HBCs with three acid functions open new opportunities for fiber formation from basic solution and for epitaxial growth of mono- and multilayers on surfaces.[15]

3.2 Synthesis, Helical Organization, and Long-range Fibrous Assembly of C_3 symmetric Hexa-*peri*-hexabenzocoronene with Methoxy Groups

3.2.1 Introduction

Hexa-*peri*-hexabenzocoronene (HBC) and its derivatives are important, not only due to their synthetic beauty as large conjugated aromatic system, but also because of their interesting self-organization behavior, as well as electronic and optoelectronic properties.[1] Considerable attention has been paid to the fabrication of unperturbed long-range oriented discotic molecules in devices.[16] For example, supramolecular nanoscale objects, such as nanowires and nanotubes from nanometer up to the millimeter length scale is of utmost importance for their practical applications in technology.[17] The synthetic strategy towards HBCs and their extended analogues has been spurred during the recent several years.[1] Thereby, different alkyl substituents and functional groups as well as a variety of topologies and molecular symmetries have been introduced and realized. Among them, C_3 symmetric discotics exhibited

distinctive self-assembly properties both in the solid-state and at the solid-liquid interface.[5] However, the incorporation of heteroatoms into the graphene core and the attachment of heteroatom-containing substituents to the HBC framework, which may influence the electronic properties and thermal behaviors, maintains a synthetic challenge.[18-23] So far, only few arylamine-substituted[19] and alkoxy-substituted[20-22] HBCs have been successfully synthesized through the functionalization of iodinated HBCs or via the oxidative cyclodehydrogenations of proper hexaphenylbenzene precursors. Very recently, a *meta*-dimethoxy substituted HBC instead of *para*-dimethoxy substitution was synthesized by a surprising rearrangement during the Scholl reaction from *para*-dimethoxy substituted hexaphenylbenzene precursor,[23] indicating that *meta*-dimethoxy substituted HBC was a stable product under the oxidation conditions. Otherwise, a new class of contorted HBCs with alkoxy substituents was obtained by photocyclizations and showed a distinct columnar self-assembly resulting in pronounced device properties.[2b,3b] Herein, we have designed appropriate C_3 symmetrically *meta*-trimethoxy substituted hexaphenylbenzene precursors which allowed the synthesis of novel C_3 symmetric HBCs **3-16** with three alternating methoxy and alkyl substituents under the Scholl reaction. The strong self-association propensity of **3-16b** in solution was firstly evaluated by NMR spectroscopy. In cooperation with W. Pisula in the Müllen group, two-dimensional wide angle X-ray scattering (2D-WAXS) demonstrated a helical organization with a surprisingly large intracolumnar correlation in the solid state. Due to this strong tendency to self-assemble, remarkably giant fibrous nanostructures with several hundred micrometers of length were easily fabricated from solution via simple drop-casting.

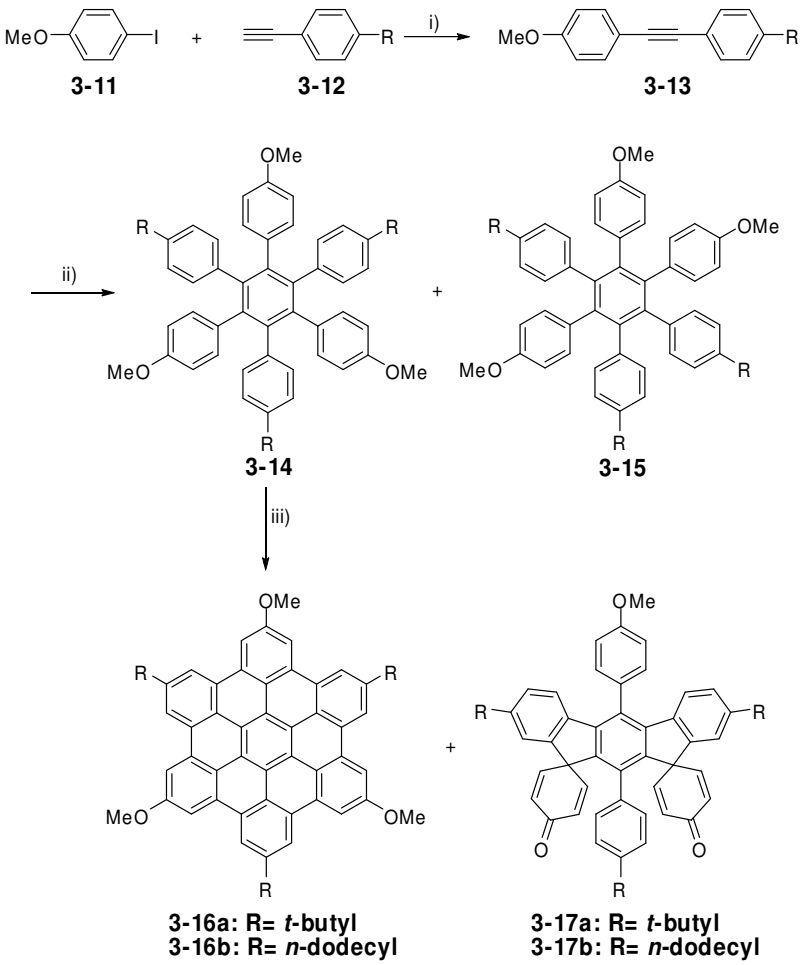

Scheme 3-4. Synthesis of C_3 symmetric HBCs **3-16** and bis-spirocyclic dienones **3-17**. i) $Pd(PPh_3)_2Cl_2$, CuI, Et_3N, r.t.; ii) $Co_2(CO)_8$, dioxane, reflux; iii) $FeCl_3/CH_3NO_2$, CH_2Cl_2.

3.2.2 Synthesis and self-assembly in the solution

The synthetic strategy is similar to the procedure as described in previous section. As outlined in Scheme 3-4, asymmetric diphenylacetylenes **3-13** were firstly synthesized via Sonogashira coupling in high yields. Afterwards $Co_2(CO)_8$ catalyzed cyclotrimerization gave two isomers (**3-14** and **3-15** at a ratio of around 1:2), which could be easily separated by column chromatography. The key step of planarization for **3-14** was carried out with $FeCl_3$ under mild conditions affording the desired HBCs **3-16** in around 40% yield, purification was accomplished by reprecipitation and washing repeatedly with methanol. It is noteworthy that **3-16a** with *t*-butyl groups led to strong chlorination according to the MALDI-TOF MS spectrum analysis

(Supporting Information). In contrast, the *n*-dodecyl group in **3-16b** lead to only minor chlorination probably due to the different electron-donating effect of *t*-butyl groups with respect to *n*-dodecyl groups.[24] Compound **3-16b** was soluble in organic solvents including THF, CH_2Cl_2 and toluene, and thus could be further purified by column chromatography and characterized by UV-vis, photoluminescence and NMR spectroscopy. The bis-spirocyclic dienones **3-17a** and **3-17b** were also separated, whereby their formation mechanisms were similar to the discussions within recent reports.[23,25] Their structures were confirmed additionally by single crystal X-ray diffraction.[13] The crystal structure clearly showed that **2a** adopted a oblique layered packing in the solid state, where the two cyclohexadienone rings were nearly perpendicular to the central indeno[1,2-b]fluorene plane (Figure 3-14).

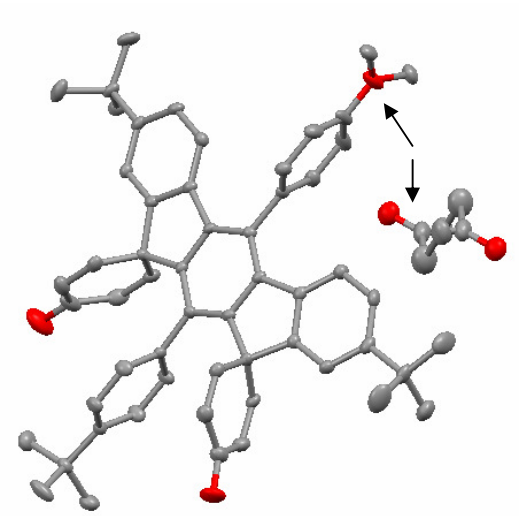

Figure 3-14. X-ray crystallographic structure of compound **3-17a** (the arrows indicated the disordering with two configurations).

The UV-vis and photoluminescence spectra of **3-16b** were recorded in chloroform solution (Figure 3-15), and showed similar types of bands as alkyl substituted HBCs, but with slightly bathochromic shift of the corresponding absorption maximum (λ_{max} = 367 nm). Proton NMR spectroscopy has been used as an efficient tool to evaluate the self-association of disc molecules in the solution,[26] the ^{1}H NMR spectrum of **3-16b** in d^2-1,1,2,2-tetrachloroethane was recorded over a range of temperatures and concentrations.. Two kinds of core protons (*a*, *b*) were recognized which are correlating to the neighboring with alkyl and methoxy substitutions. On heating from

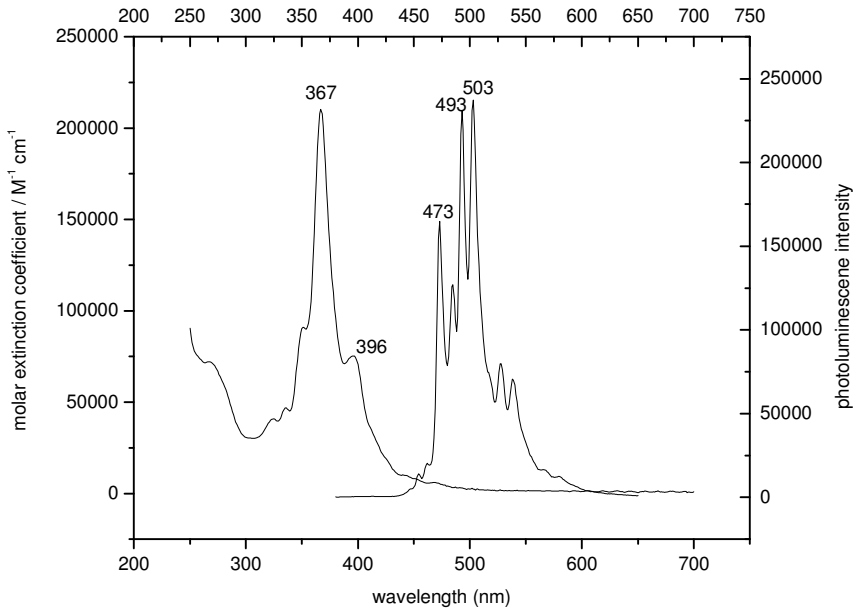

Figure 3-15. UV-vis and photoluminescence spectra of **3-16b** in $CHCl_3$ (1.0×10^{-6} M^{-1}).

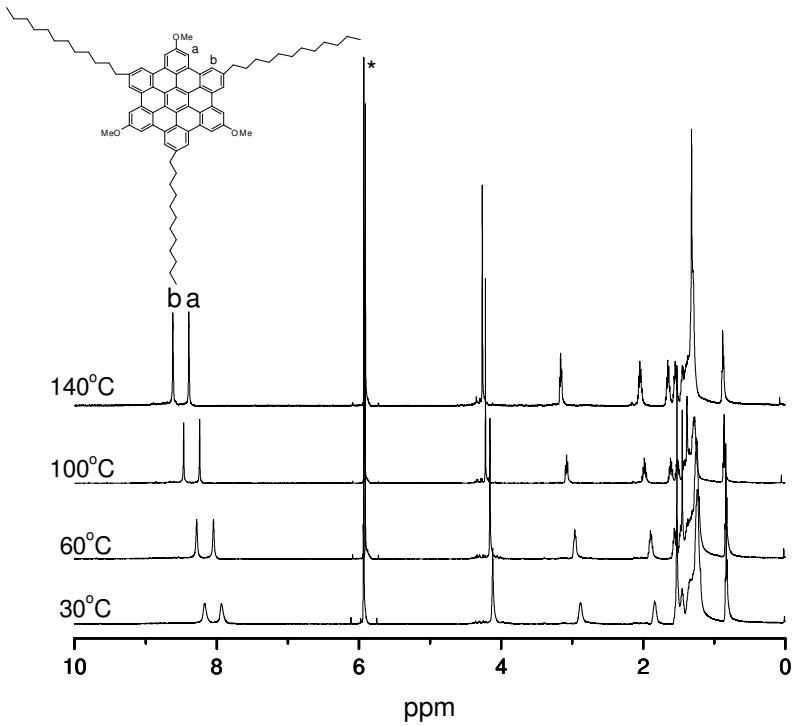

Figure 3-16. Temperature dependent ^{1}H NMR spectra of **3-16b** in d^2-1,1,2,2-tetrachloroethane (2.38×10^{-3} M).

30 °C to 140 °C, the aromatic signals assigned to the HBC core *a* experienced a

down-field shift of 0.47 ppm from δ = 8.15 ppm to 8.62 ppm, which could be comparable to the hexadodecyl substituted HBC (Figure 3-16).[26a] Furthermore, HBC core *b* exhibited a quite similar chemical down-field shift of δ = 0.49 ppm from δ = 7.91 ppm to 8.40 ppm. Likewise, decreasing the concentration from 11.9×10^{-3} M to 2.38×10^{-4} M at 60 °C resulted in a shift down field by 0.44 ppm. It is clear that such shifts corresponded to a strong face-to-face stacking of the discs, resulting in shielding effects.

3.2.3 Bulk characterization and self-assembly on the surface

Differential scanning calorimetry (DCS) indicated thermotropic properties of **3-16b**. Two peaks appeared in the DSC scan during second heating: one minor peak at 80 °C (3 J/g) and a major peak at 145 °C (13 J/g). The minor transition was related to a reorganization of the alkyl side chains as already observed for other HBC derivatives not influencing the supramolecular organization as implied by 2D-WAXS measurements on extruded fibers.[8] The second peak was assigned to a liquid crystalline (LC) phase transition. Figure 3-17a shows a characteristic 2D-WAXS pattern for the LC phase. The positions of equatorial reflections suggested a hexagonal arrangement of columnar structures, which were well oriented along the fiber extrusion direction and possessed a packing parameter of a_{hex} = 2.51 nm. The intracolumnar order of the disc-shaped molecules was represented by distinct meridional reflections related to a π-stacking distance of 0.36 nm. Thereby, the molecular planes were arranged perpendicular to the columnar axis. Remarkably, after cooling back the sample, the 2D pattern revealed a much more complex superstructure (Figure 3-17b). Additional X-ray measurements showed scattering intensities also in the small-angle range (Figure 3-17c). The hexagonal unit cell was maintained at 30 °C,

but with a significantly larger intercolumnar parameter of a_{hex} = 3.49 nm. The π-stacking distance of 0.35 nm remained identical as observed in the LC phase. The reciprocal spacing of the first layer line formed by the off-meridional reflections in the small-range indicated a period of 9.8 nm along the stacking direction (Figure 3-17c).[27] We attribute this distance to intermolecular correlations of discs possessing an identical lateral position within the columns.[28] This correlation is surprisingly large including 28 molecules, if taking into account the π-stacking of 0.35 nm between individual building blocks. Thereby, the molecules were slightly laterally rotated by an angle of *ca* 2.14° to each other resulting in a helical packing with pronounced order (Figure 3-17d).[29] The driving force of this unusual helical arrangement can be probably ascribed to the minor local dipole-interactions between the methoxy-substituted HBCs. Non-covalent π-stacking and dipole-interactions are known to play an important role for the cooperative self-assembly leading to complex superstructures.[30] Therefore, the introduction of methoxy units as functional groups in our case induced local dipole moments which improved the intermolecular interactions and led to better ordered superstructures. In contrast, hexalkyl substituted HBCs without local dipole moment do not reveal such pronounced intracolumnar packing. We assume that this enhanced organization of molecules to each other might have an additional effect on the charge carrier transport. As consequence, the small rotation angle resulted in a higher side chain density in the outer alkyl mantle and thus to a larger hexagonal unit cell at 30 °C in comparison to the LC phase.

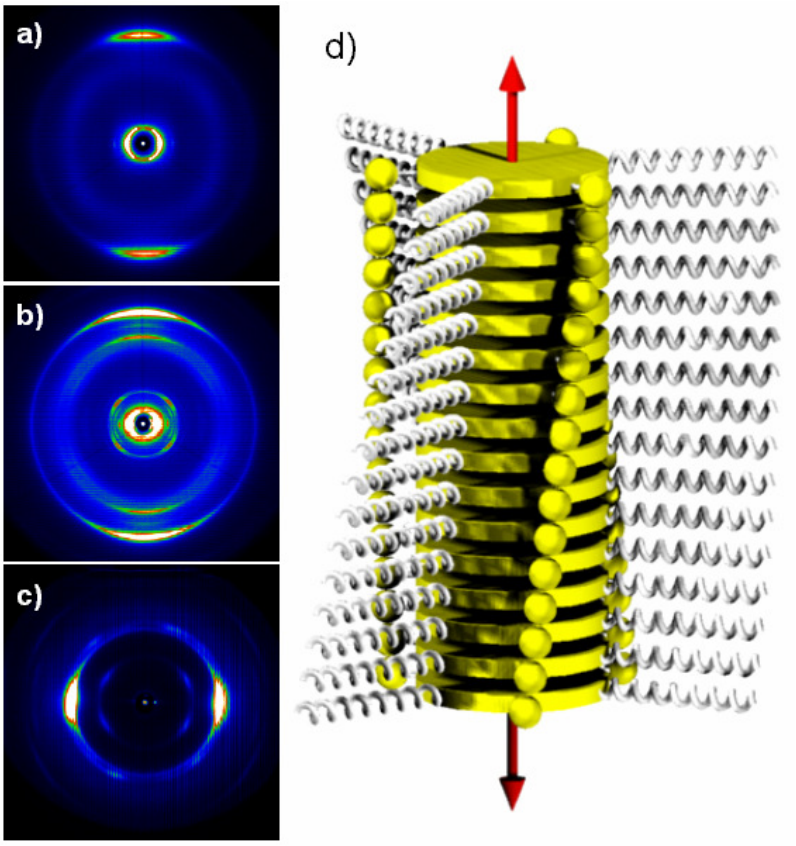

Figure 3-17. Structural characterization of **3-16b**; a) 2D-WAXS at 170 °C and b) at 30 °C after annealing; c) 2D-SAXS at 30 °C after annealing; d) schematic illustration of the intracolumnar arrangement of **3-16b** at 30 °C into a helical organization with a disc rotation of *ca* 2.14°.

For the solution processing of organic semiconductors in electronic devices, the control of the morphology formation on surfaces is an essential key procedure which determines in many cases the performance. Therefore, it is important to understand which role the molecular design plays for the self-assembly in solution and for the supramolecular organization in the bulk. The relation between the behavior in solution and bulk state as well as the morphology is quite apparent in the case of **3-16b**. The self-assembly of **3-16b** on the surface upon simple drop-casting was studied by optical microscopy. Surprisingly, the uniform thin film (1.0×10^{-4} M in *o*-dichlorobenzene) was composed of several hundred micrometers long fibers (Figure 3-18), indicating a strong one-dimensional self-assembly tendency of **3-16b**. The

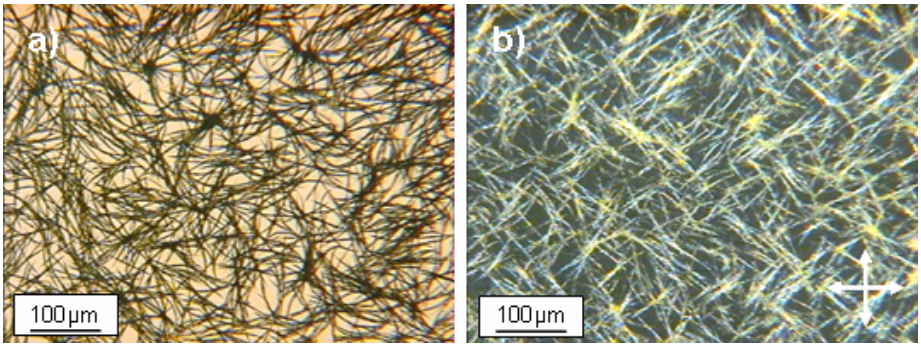

Figure 3-18. Optical images of the morphology of **3-16b** drop-cast from *o*-dichlorobenzene (1.0×10^{-4} M) in a) without and b) with cross-polarizers.

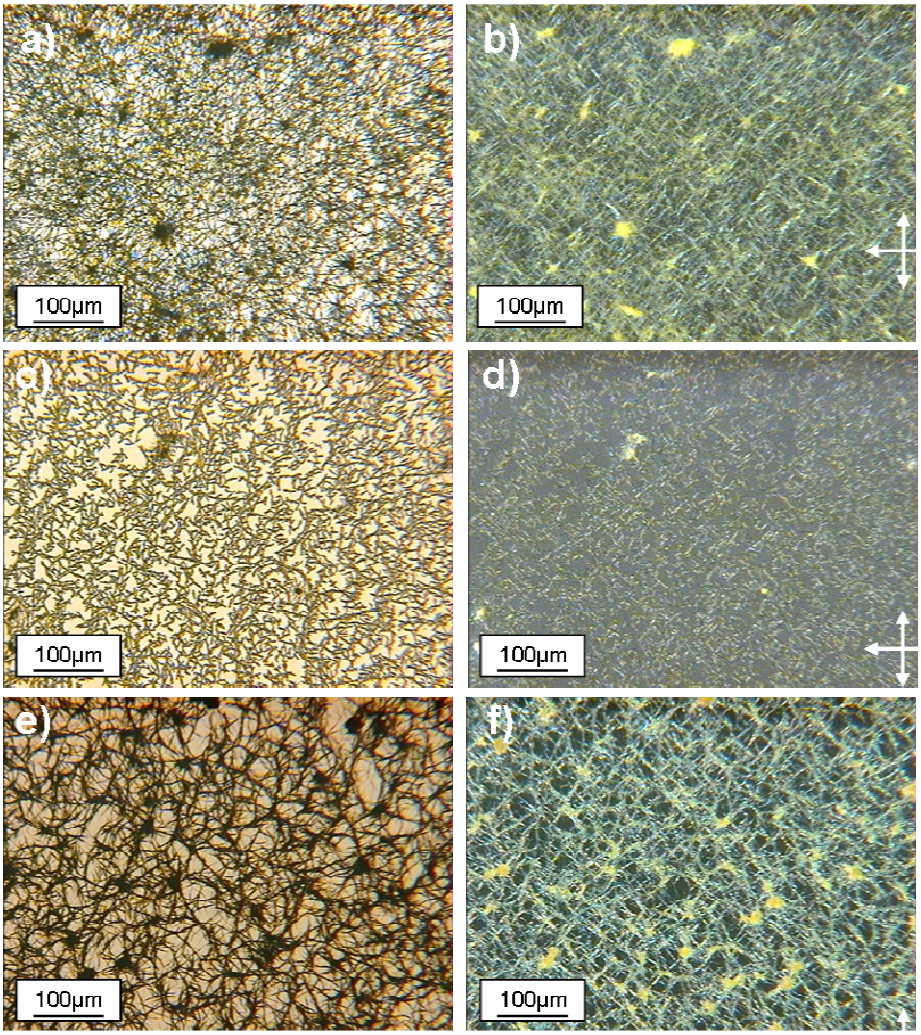

Figure 3-19. Optical images of the morphology of **1b** drop-cast from toluene (a and b), $CHCl_3$ (c and d), and THF (e and f) solution (1.0×10^{-4} M) without and with cross-polarizers.

birefringence of the fibers implied a high supramolecular order within these structures,

while optical anisotropy is characteristic for macroscopic orientation of the columnar structures along the fiber direction. The fibers revealed only birefringence at a relative arrangement of 45° towards the analyzer/polarizer. Further investigation upon solution drop-casting from different solvents, including toluene, THF and $CHCl_3$, displayed in all cases, a uniform morphology within the films, but different lengths of fibrous assemblies (Figure 3-19).

3.2.4 Conclusion

In conclusion, a novel C_3 symmetric HBC with three alternating dodecyl and methoxy substituents was successfully synthesized via the Scholl reaction from its hexaphenylbenzene precursor. It showed pronounced aggregation in solution as characterized by concentration and temperature dependant ^{1}H NMR measurements. Additionally, the distinct intermolecular interactions and the influence of methoxy units at the *meta* positions were manifested in the formation of a complex helical superstructure in the solid state as derived form X-ray scattering results. The fabrication of solution onto the surface resulted into formation of exceptionally long fibrous microstructures. The facile transformation of methoxy units into hydroxyl groups is expected to be further used for construction of new alkoxy-substituted HBC discotics.[31]

3.2.5. References:

[1] Wu, J.; Pisula, W.; Müllen, K. *Chem. Rev*. **2007**, *107*, 718-747.

[2] a) Fechtenkötter, A.; Saalwächter, K.; Harbison, M. A.; Müllen, K.; Spiess, H. W. *Angew. Chem*. **1999**, 111, 3224-3228; *Angew. Chem., Int. Ed.* **1999**, *38*, 3039-3042; b) Schmidt-Mende, L.; Fechtenkötter, A.; Müllen, K.; Moons, E.; Freind, R. H.; MacKenzie, J. D. *Science*. **2001**, *293*, 1119-1122; c) van de Craats, A. M.; Stutzmann, N.; Bunk, O.; Nielsen, M. M.; Watson, M.; Müllen, K.; Chanzy, H. D.; Sirringhaus, H.; Friend, R. H. *Adv. Mater*. **2003**, *15*, 495-499.

[3] a) Hoeben, F. J. M.; Jonkheijm, P.; Meijer, E. W.; Schenning, A. P. H. J. *Chem. Rev*. **2005**, *105*, 1491-1546; b) Schenning, A. P. H. J.; Meijer, E. W. *Chem. Commun*. **2005**, 3245-3258; c) Ajayaghosh, A.; Vijayakumar, C.; Varghese, R.; George, S. J. *Angew. Chem.* ***2006****, 118, 470-474; Angew. Chem. Int. Ed*. **2006**, *45*, 456-460; d) Ajayaghosh, A.; Varghese, R.; Praveen, V. K.; Mahesh, S. *Angew. Chem*. **2006**, *118*, 3339-3342; *Angew. Chem. Int. Ed*. **2006**, *45*, 3261-3264; e) Ajayaghosh, A.; Praveen, V. K. *Acc. Chem. Res*. **2007**, *40*, 644-656.

[4] Ester groups enhancing supramolecular organization: a) Hunter, C. A.; Sanders, J. K. M. *J. Am. Chem. Soc*. **1990**, *112*, 5525-5534; b) Enozawa, H.; Hasegawa, M.; Takamatsu, D.; Fukui, K.; Iyoda, M. *Org. Lett*. **2006**, *8*, 1917-1920; c) Andersson, A. S.; Kilsa, K.; Hassenkam, T.; Gisselbrecht, J.; Boudon, C.; Gross, M.; Nielsen, M. B.; Diederich, F.; *Chem. Eur. J*. **2006**, *12*, 8451-8459; d) Ajayaghosh, A.; Praveen, V. K.; Srinivasan, S.; Varghese, R. *Adv. Mater*. **2007**, *19*, 411-415.

[5] a) Feng, X.; Wu, J.; Enkelmann, V.; Müllen, K. *Org. Lett.* **2006**, *8*, 1145-1148; b) Wu, J.; Baumgarten, M.; Debije, M. G.; Warman, J. M.; Müllen, K. *Angew. Chem.* **2004**, *116*, 5445-5449; *Angew. Chem. Int. Ed.* **2004**, *43*, 5331-5335; c) Feng, X.; Wu, J.; Ai, M.; Pisula, W.; Zhi, L.; Rabe, J. P.; Müllen, K. *Angew. Chem*. **2007**, *119*, 3093-3096; *Angew. Chem. Int. Ed*. **2007**, *46*, 3033-3036.

[6] The structure and purity of the molecules are proven by MALDI-TOF mass spectrometry, elemental analysis, as well as NMR spectroscopy.

[7] a) Kastler, M.; Schmidt, J.; Pisula, W.; Sebastiani, D.; Müllen, K. *J. Am. Chem. Soc*. **2006**, *128*, 9526; b) Kastler, M. PhD Thesis, University of Mainz, 2006; c) Wu, J.; Watson, M. D.; Zhang, L.; Wang, Z.; Müllen, K. *J. Am. Chem. Soc.* **2004**, *126*, 177-186.

[8] Pisula, W.; Tomović, Z.; Simpson, C.; Kastler, M.; Pakula, T.; Müllen, K. *Chem. Mater*. **2005**, *17*, 4296.

[9] Pisula, W.; Tomović, Z.; Watson, M. D.; Müllen, K.; Kussmann, J.; Ochsenfeld, C.; Metzroth, T.; Gauss, J. *J. Phys. Chem. B*. **2007**, *111*, 7481-7487.

[10] a) Pisula, W.; Tomović, Z.; Stepputat, M.; Kolb, U.; Pakula, T.; Müllen, K. *Chem. Mater*. **2005**, *17*, 2641; b) Pisula, W.; Kastler, M.; Wasserfallen, D.; Nolde, F.; Kohl,

C.; Pakula, T.; Müllen, K. *Angew. Chem.* **2006**, *118*, 834-838; *Angew. Chem. Int. Ed.* **2006**, *45*, 819.

[11] a) Tokita, M.; Tokunaga, K.; Funaoka, S.; Osada, K.; Watanabe, J. *Macromolecules*. **2004**, *37*, 2527-2531; b) Abeysekera, R.; Bushby, R. J.; Caillet, C.; Hamley, I. W.; Lozman, O. R.; Lu, Z.; Robards, A. W. *Macromolecules* **2003**, *36*, 1526.

[12] Fischbach, I.; Pakula, T.; Minkin, P.; Fechtenkötter, A.; Müllen, K.; Spiess, H. W.; Saalwächter, K. *J. Phy. Chem. B.* **2002**, *106*, 6408-6418.

[13] Hsu, T. C.; Hüser, B.; Pakula, T.; Spiess, H. W.; Stamm, M. *Die Makromolekulare Chemie*. **1990**, *191*, 1597 – 1609.

[14] (a) Hill, J. P.; Jin, W.; Kosaka, A.; Fukushima, T.; Ichihara, H.; Shimomura, T.; Ito, K.; Hashizume, T.; Ishii, N.; Aida, T. *Science*. **2004**, *304*, 1481-1483; b) Yamamoto, Y.; Fukushima, T.; Suna, Y.; Ishii, N.; Saeki, A.; Seki, S.; Tagawa, S.; Taniguchi, M.; Kawai, T.; Aida, T. *Science*. **2006**, *314*, 1761-1764; (c) Xiao, S.; Tang, J.; Beetz, T.; Guo, X.; Tremblay, N.; Siegrist, T.; Zhu, Y.; Steigerwald, M.; Nuckolls, C. *J. Am. Chem. Soc*. **2006**, *128*, 10700-10701.

[15] Hydrogen-boding induced honeycomb templates on surface have been widely studied for small trimesic acid and isophthalic acid: a) Ishikawa, Y.; Ohira, A.; Sakata, M.; Hirayama, C.; Kunitake, M. *Chem. Commun*. **2002**, 2652-2653; b) Ruben, M.; Payer, D. ; Landa, A. ; Comisso, A. ; Gattinoni, C. ; Lin, N. ; Collin, J. P. ; Sauvage, J. P. ; De Vita, A. ; Kern, K. *J. Am. Chem. Soc*. **2006**, *128*, 15644-15651; c) De Feyter, S.; Gesquiere, A.; Klapper, M.; Müllen, K.; De Schryver, F. C. *Nano. Lett*. **2003**, *3*, 1485-1488.

[16] a) Pisula, W.; Menon, A.; Stepputat, M.; Lieberwirth, I.; Kolb, U.; Tracz, A.; Sirringhaus, H.; Pakula, T.; Müllen, K. *Adv. Mater.* **2005**, *17*, 684; b) Xiao, S.; Myers, M.; Miao, Q.; Sanaur, S.; Pang, K.; Steigerwald, M. L.; Nuckolls, C. *Angew. Chem. Int. Ed*. **2005**, *44*, 7390-7394.

[17] a) Palermo, V.; Samori, P., *Angew. Chem. Int. Ed.* **2007**, *46*, 4428-4432; b) Laschat, S.; Baro, A.; Steinke, N.; Giesselmann, F.; Hagele, C.; Scalia, G.; Judele, R.; Kapatsina, E.; Sauer, S.; Schreivogel, A.; Tosoni, M. *Angew. Chem. Int. Ed*. **2007**,

46, 4837-4887.

[18] Draper, S. M.; Gregg, D. J.; Madathil, R. *J. Am. Chem. Soc*. **2002**, *124*, 3486-3487.

[19] Wu, J.; Baumgarten, M.; Debije, M. G.; Warman, J. M.; Müllen, K. *Angew. Chem., Int. Ed.* **2004**, *43*, 5331-5335.

[20] Wang, Z.; Dotz, F.; Enkelmann, V.; Müllen, K. *Angew. Chem., Int. Ed.* **2005**, *44*, 1247-1250.

[21] Wang, Z.; Watson, M. D.; Wu, J.; Müllen, K. *Chem. Commun.* **2004**, 336-337.

[22] Zhang, Q.; Prins, P.; Jones, S. C.; Barlow, S.; Kondo, T.; An, Z.; Siebbeles, L. D. A.; Marder, S. R. *Org. Lett.* **2005**, *7*, 5019-5022.

[23] Dou, X.; Yang, X.; Bodwell, G. J.; Wagner, M.; Enkelmann, V.; Müllen, K. *Org. Lett*. **2007**, *9*, 2485-2488.

[24] King, B. T.; Kroulik, J.; Robertson, C. R.; Rempala, P.; Hilton, C. L.; Korinerk, J. D.; Gortari, K. M. *J. Org. Chem*. **2007**, *72*, 2279-2288.

[25] Gregg, D. J.; Ollagnier, C. M. A.; Fitchett, C. M.; Draper, S. M. *Chem. Eur. J*. **2006**, *12*, 3043-3052.

[26] a) Kastler, M.; Pisula, W.; Wasserfallen, D.; Pakula, T.; Müllen, K. *J. Am. Chem. Soc.* **2005**, *127*, 4286-4296; b) Shetty, A. S.; Zhang, J. S.; Moore, J. S. *J. Am. Chem. Soc.* **1996**. *118*, 1019-1027; c) Hoger, S.; Bonrad, K.; Mourran, A.; Beginn, U.; Moller, M. *J. Am. Chem. Soc.* **2001**. *123*, 5651-5659.

[27] Kakudo, M.; Kasai, N. *X-ray Diffraction by Polymers*, Kodansha Ltd: Tokyo, **1972**.

[28] Holst, H. C.; Pakula, T.; Meier, H. *Tetrahedron*. **2004**, *60*, 6765–6775

[29] Feng, X.; Pisula, W.; Müllen, K. *J. Am. Chem. Soc*. **2007**, *129*, 14116-14117.

[30] (a) Datta, A.; Pati, S. K. *Chem. Soc. Rev*. **2006**, *35*, 1305-1323; (b) Lim, G. S.; Jung, B. M.; Lee, S. J.; Song, H. H.; Kim, C.; Chang, J. Y. *Chem. Mater*. **2007**, *19*, 460-467; (c) Haino, T.; Tanaka, M.; Fukazawa, Y. *Chem. Commun*. **2008**, 468-470.

[31] Zelcer, A.; Donnio, B.; Bourgogne, C.; Cukiernik, F. D.; Guillon, D. *Chem. Mater*. **2007**, *19*, 1992-2006.

Chapter 4. Triangle-shaped Polycyclic Aromatic Hydrocarbons

Polycyclic aromatic hydrocarbons (PAHs) such as hexa-*peri*-hexabenzocoronenes (HBCs) have been widely synthesized and studied. In the last two chapters we also described the facile synthesis and self-assembly behavior of HBCs with C_3 symmetry. However, the nanographene core based on a D_3 symmetric triangle-shape is still hamperedly synthetic difficulties. By far now, only the chemistry of triphenylenes is well developed over the past 30 years. Herein, in this chapter, a novel synthetic strategy starting from C_3 symmetric dendritic polyphenylene precursors which are different from hexaphenylbenzenes will be made and subsequent planarization of these precursors towards novel triangle shaped and semi-triangle shaped PAHs will be demonstrated. Based on these new discotic graphene cores, different alkyl substituents and functional groups can be easily introduced, and endow the new molecules with phase forming behavior. The substituted semi-triangle shaped discotics show a novel mode of self-assembly with honeycomb pattern at the solid-liquid interface and highly ordered helical superstructures in the bulk. On the other hand, triangle shaped discotics with swallow-tailed substituetents display highly stable liquid crystalline phasess over a broad temperature range; further photovoltaic devices based on these new discotics show a good performance which is strongly dependant on the supramolecular organization in the solid state.

4.1 Versatile Synthesis and Self-assembly of Triangle-shaped Polycyclic Aromatic Hydrocarbons

4.1.1 Introduction

Triangle-shaped polycyclic aromatic hydrocarbons belong to a special class due to their D_3 symmetry of aromatic cores and the beauty of their molecular topology. Triphenylene is considered as the first generation of this series with fully benzenoid structure (Chart 4-1), therefore high chemical and thermal stability are the typical

characteristics. The chemistry of triphenylenes has been well developed since last thirty years due to their fascinating discotic liquid crystal properties.[1] Common synthetic methods towards symmetrically substituted triphenylene include the oxidative trimerization of 1,2-dialkoxybenzene, whereas the synthesis of unsymmetric triphenylenes proceeds via the biphenyl-phenyl coupling (Chart 4-2).[2]

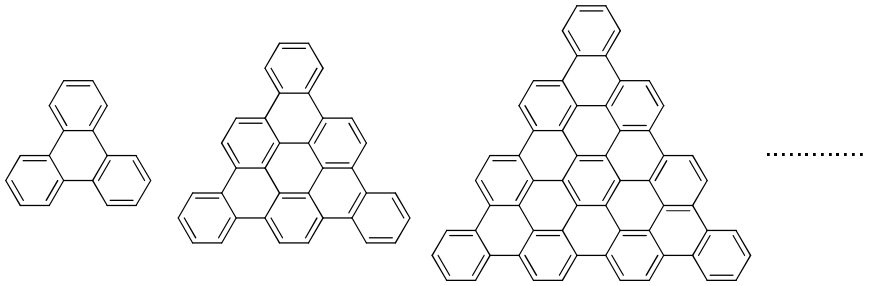

Chart 4-1. Molecular structures of the triangle-shaped benzenoid PAHs with different generations.

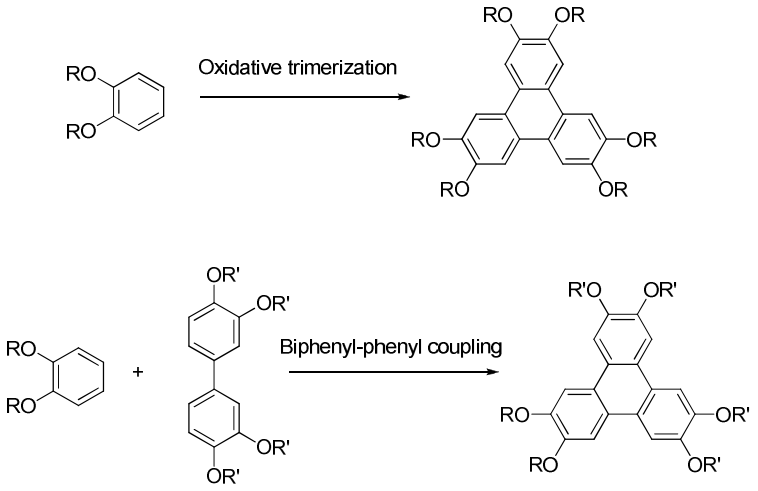

Chart 4-2. Common routes to triphenylenes.

Higher generation triangle-shaped PAHs have however not received great attention. This could be most probably due to the synthetic difficulties. For example, the second generation of triangle-shaped benzenoid PAHs, namely tribenzo[a,g,m]coronene (Chart 4-1 and Chart 4-3) is so far only available from the photochemical cyclodehydrogenation of its macrocycle precursor.[3] And indeed, the synthesis of the macrocyclis precursor in low yield is restricted by the difficult chemistry.

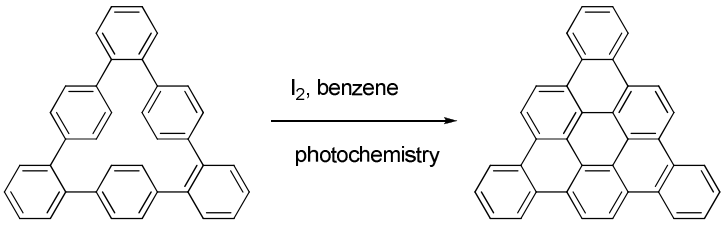

Chart 4-3. Synthesis of tribenzo[a,g,m]coronene

Nevertheless, the larger PAHs with C_3 symmetry are expected to be particularly interesting as theoretic models, molecular building blocks as well as organic functional materials.[4] It is therefore urgent for us to develop new synthetic strategy to make up the gaps within PAHs with different sizes, symmetries as well as peripheries. In the last two chapters, the synthetic approach towards HBCs with C_3 symmetry has been described. Here we present a versatile synthesis of a series of large triangle-shaped (third generation in Chart 4-1) and semi-triangle shaped PAH molecules **4-2—4-10** (Chart 4-4) with different substituents and peripheral structures. The D_{3h} symmetrical molecule **4-2** (benzo[o]bistriphenyleno[2,1,12,11-efghi:2',1',12',11'-uvabc]ovalene, **trinaphthoHBC**) is a simple triangle-shaped benzenoid PAH with the same number of carbons as fullerene. Molecule **4-4** (**tribenzothiopheneHBC**) can be regarded as a 1,7,13-triphenyl substituted HBC, where the peripheral phenyl rings are bridged by sulfur atoms. Molecules **4-5—4-10** (derivatives of diphenanthro[3',4'5,'6'-efghi:3,4,5,6-uvabc]ovalene, **trizigzagHBC**) possess three "zig-zag" peripheries with a semi-triangle shape, and have different optical and electronic properties from those of the PAHs with arm-chair peripheries.[5] As the typical example, the self-assembly of trizigzagHBC **4-10** is described. X-ray scattering experiments reveal an arrangement of **4-10** into highly ordered helical superstructures in the solid-state, and monolayers that consist of novel honeycomb patterns are observed by scanning tunneling microscopy (STM) at the liquid solid interface.

4.1.2 Synthesis and structural characterization

The synthesis of all triangle molecules **4-2—4-10** was based on the same precursor, 1,3,5-tris-(2'-bromophenyl)benzene (**4-11**), where the synthesis was described in the chapter 2.[6] As outlined in Scheme 4-1, subsequent Suzuki coupling reactions of **4-11** with 4-biphenylboronic acid or 4-dibenzothiopheneboronic acid afforded precursors **4-12** and **4-13** in 83% and 87% yields, respectively. The intramolecular oxidative cyclodehydrogenation reactions of **4-12** and **4-13** were then performed by using $FeCl_3$ as oxidant and monitored by MALDI-TOF MS spectrum until the quantitative removal of 18 or 12 hydrogens, gave trinaphthoHBC **4-2** as an insoluble brown-red powder and tribenzothiopheneHBC **4-4** as yellow powder after precipitation from

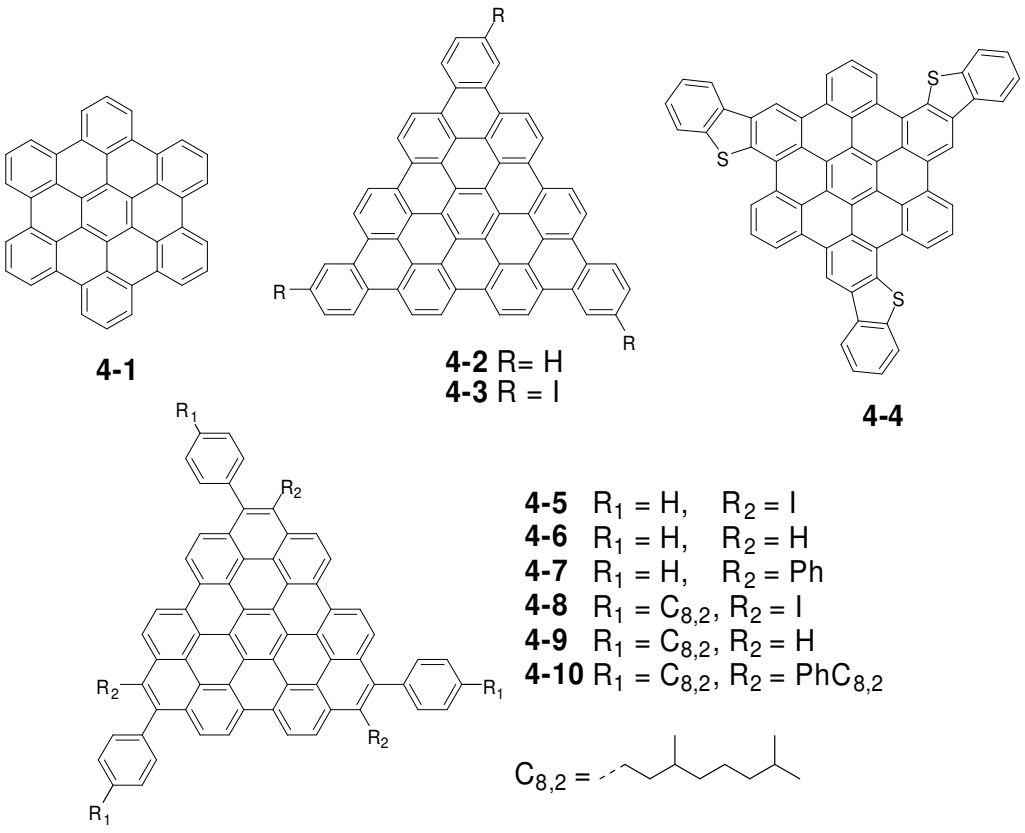

Chart 4-4. Molecular structures of HBC and triangle shaped PAHs.

the reaction mixture, the precipitate was further repeatedly washed by water and methanol until the filtrate was colorless, dried under vacuum to give **4-2** and **4-4** in

71% and 81% yields, respectively. Compound **4-14** was previously synthesized from

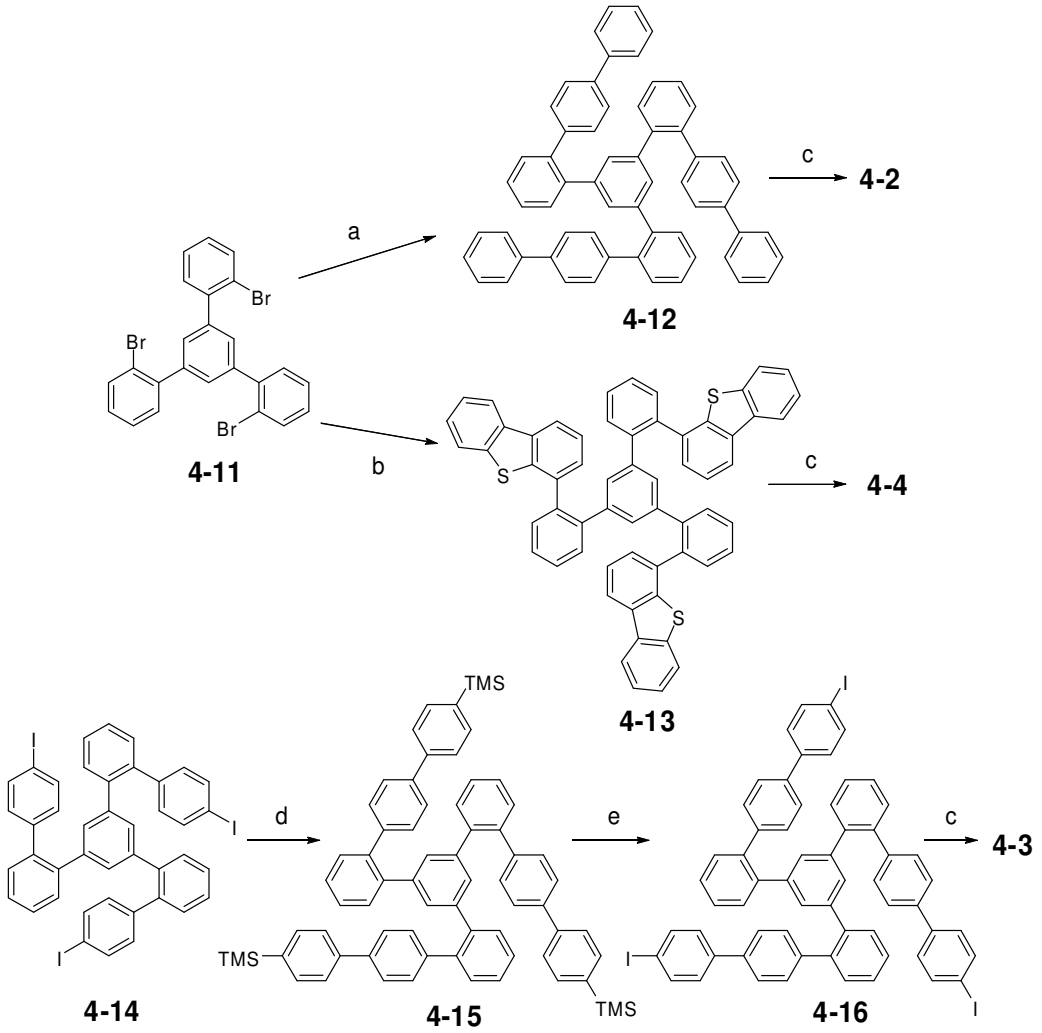

Scheme 4-1. Versatile synthesis of **4-2**, **4-3** and **4-4** based on **4-11**: a) 4-biphenylboronic acid, $Pd(PPh_3)_4$, toluene, K_2CO_3 (aq.), reflux, 83%; b) 4-dibenzothiopheneboronic acid, $Pd(PPh_3)_4$, toluene, K_2CO_3 (aq.), reflux, 87%; c) $FeCl_3$, CH_3NO_2/CH_2Cl_2, 71% for **4-2**, 83% for **4-3**, 81% for **4-4**; d) 4-trimethylsilyl-phenylboronic acid, $Pd(PPh_3)_4$, THF, K_2CO_3 (aq.), reflux, 70%; e) ICl, chloroform, 99%.

4-11 as shown in chapter 2. Subsequent reaction with 4-trimethylsilyl-phenylboronic acid afforded **4-15** in 70% yield. The trimethylsilyl (TMS) groups were then

converted into iodides by treatment with iodine monochloride to give the precursor **4-16** in 99% yield. Oxidative cyclodehydrogenation of **4-16** by treatment with $FeCl_3$ provided trinaphthoHBC **4-3** as an insoluble yellow powder in 83% yield with the same purification procedure as described above. Although virtually insoluble, **4-3** could be further functionalized under metal catalyzed coupling conditions.

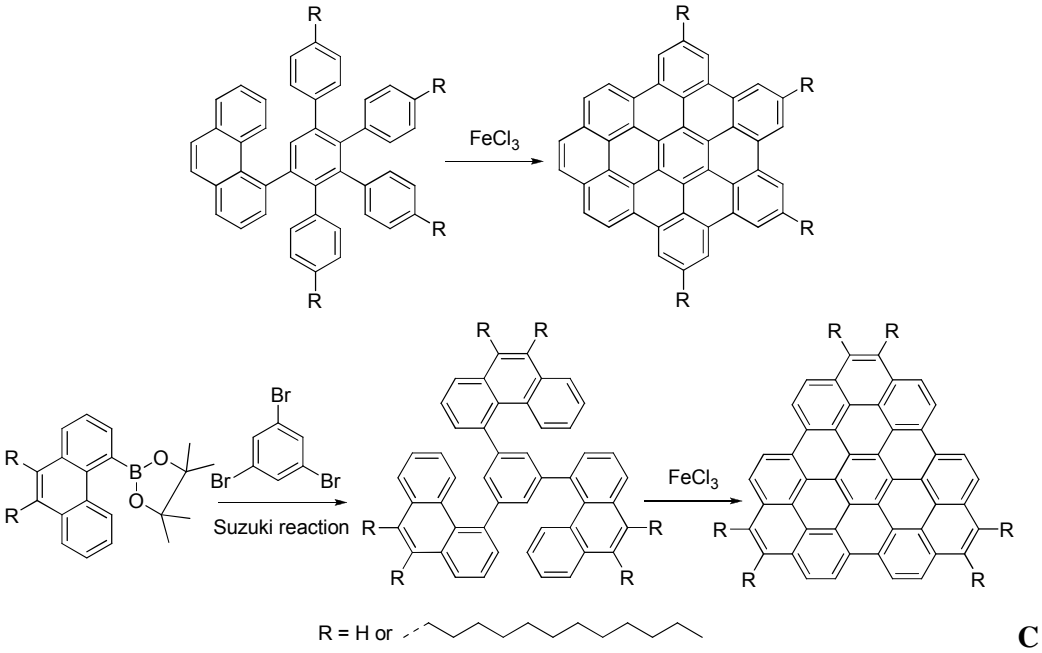

C

Chart 4-5. Synthetic route towards zigzagHBC by M. Kastler.

M. Kastler in the Müllen group demonstrated that polyphenylene dendrimers with phenanthrene units can undergo intramolecular cyclodehydrogenations,[5c] for example, the monozigzagHBC was synthesized from a 1-(9'-phenanthryl)-2,3,4,5-tetraphenylbenzene precursor (Chart 4-5). On the other hand, after a tedious multi-steps synthesis of corresponding phenanthrylboronic esters, 1,3,5-tris(9'-phenanthryl)benzene precursors were synthesized via the Suzuki coupling (Chart 4-5), subsequent $FeCl_3$ mediated oxidative cyclodehydrogenation gave the corresponding trizigzagHBCs with a semi-triangle shape. Nevertheless, this

synthetic protocol was restricted by the low yield due to the steric hindrance in the Suzuki coupling step; the difficulties for the synthesis of phenanthrylboronic ester with various functional groups additionally limit the multiplicate use.

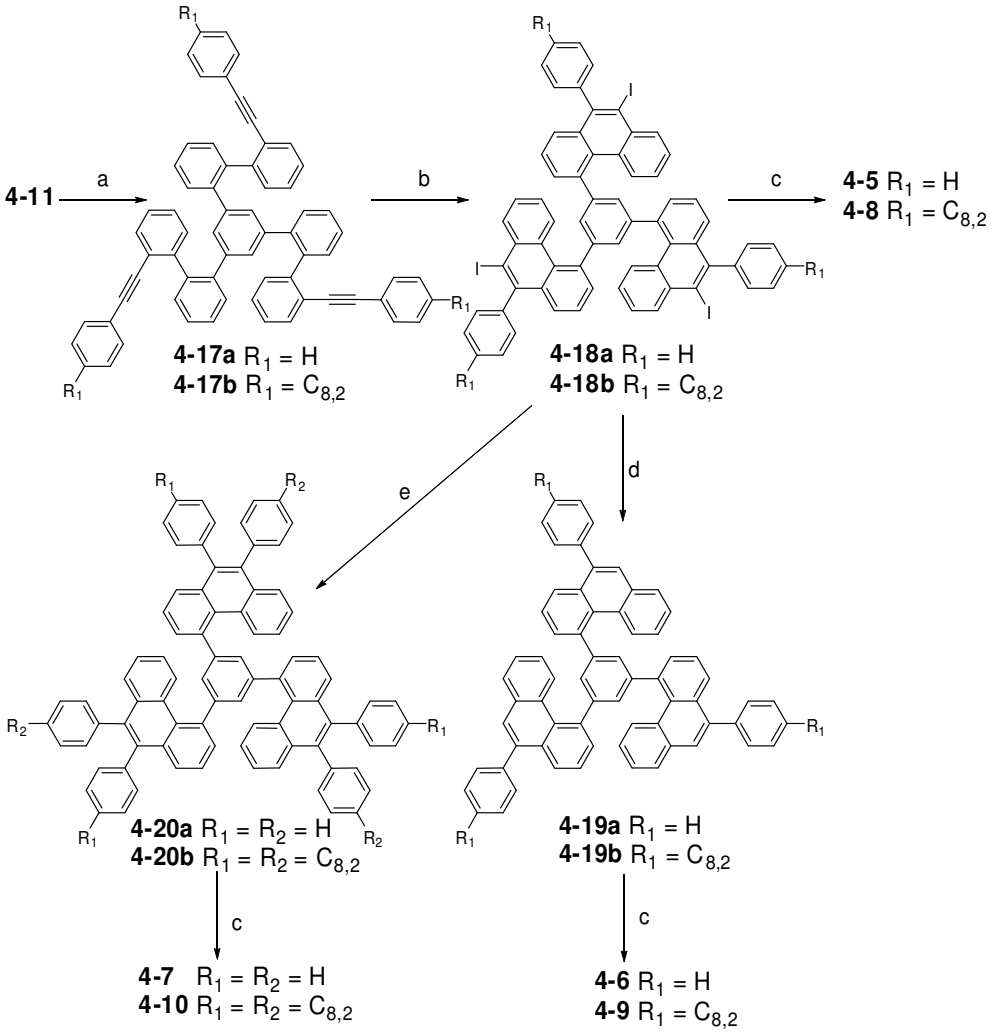

Scheme 4-2. Synthesis of trizigzagHBCs, **4-5—4-10**: a) *o*-phenylethynylbenzeneboronic acid, $Pd(PPh_3)_4$, toluene, K_2CO_3 (aq.), reflux, 82% for **4-17a**, 86% for **4-17b**; b) ICl, CH_2Cl_2, -78°C, 92% for **4-18a**, 95% for **4-18b**; c) $FeCl_3$, CH_3NO_2/CH_2Cl_2, 86% for **4-5**, 88% for **4-6**, 76% for **4-7**, 72% for **4-8**, 78% for **4-9**, 85% for **4-10**; d) *s*-BuLi, THF, -78°C, MeOH, 98% for **4-19a**, 97% for **4-19b**; e) phenylboronic acid, $Pd(PPh_3)_4$, toluene, K_2CO_3 (aq.), reflux, 81% for **4-20a**, 83% for **4-20b**.

Therefore, here we developed an alternative and enhanced strategy to synthesize a great diversity of trizigzagHBCs (**4-5—4-10**). The synthesis of these semi-triangle shaped molecules was also based on the same precursor **4-11**. As shown in Scheme 4-2, Suzuki coupling of **4-11** with *o*-phenylethynylbenzeneboronic acids afforded **4-17a** and **4-17b** in good yields. Iodine monochloride induced ring cyclization at low temperature gave precursors **4-18a** and **4-18b** with three phenanthrene units in high yields.[7] Cyclodehydrogenations of **4-18a** and **4-18b** by treatment with $FeCl_3$ also worked smoothly and provided **4-5** and **4-8** with three "zig-zag" peripheries. Compounds **4-5**, **4-8** and **4-18** possess reactive iodide functional groups, and therefore allowed further functionalizations. The iodides in **4-18a** and **4-18b** could be easily replaced by protons using *sec*-BuLi mediated lithium-halogen exchange followed by quenching with methanol gave **4-19a** and **4-19b** in almost quantitative yields**.** Afterwards, Suzuki coupling of **4-18a** and **4-18b** with phenylboronic acids afforded precursors **4-20a** and **4-20b** in good yields. Finally, cyclodehydrogenation of **4-19** and **4-20** by treatment with $FeCl_3$ under mild conditions gave **4-6**, **4-7**, **4-9** and **4-10** respectively. It should be noted that no further cyclization took place at the peripheral phenyl rings during the cyclodehydrogenation of **4-20** even under extended reaction time or under UV irradiation.[8] Molecules **4-8—4-10** are well soluble in normal organic solvents including THF, dichloromethane and chloroform, and thus can be purified by column chromatography to remove residual inorganic impurities and partially fused products. Molecules **4-5—4-7** were excluded from chromatography due to the low solubilities, and were thus purified by repeated washing with water and

methanol.

MALDI-TOF MS (TCNQ matrix) of **4-2—4-10,** using a solid-state sample preparation method, revealed single species with isotopic distribution, which were in accordance with calculations (Figure 4-1).[9]

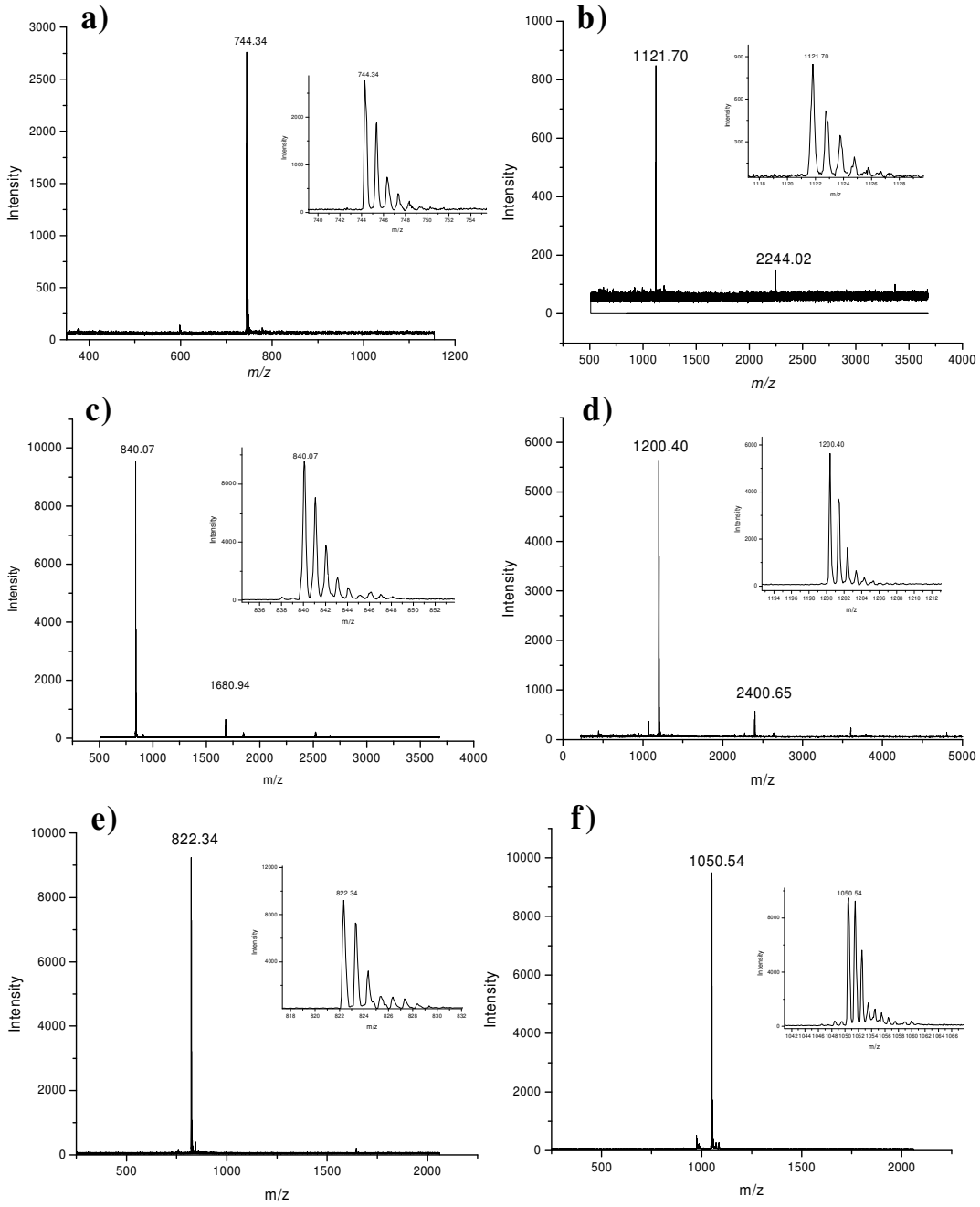

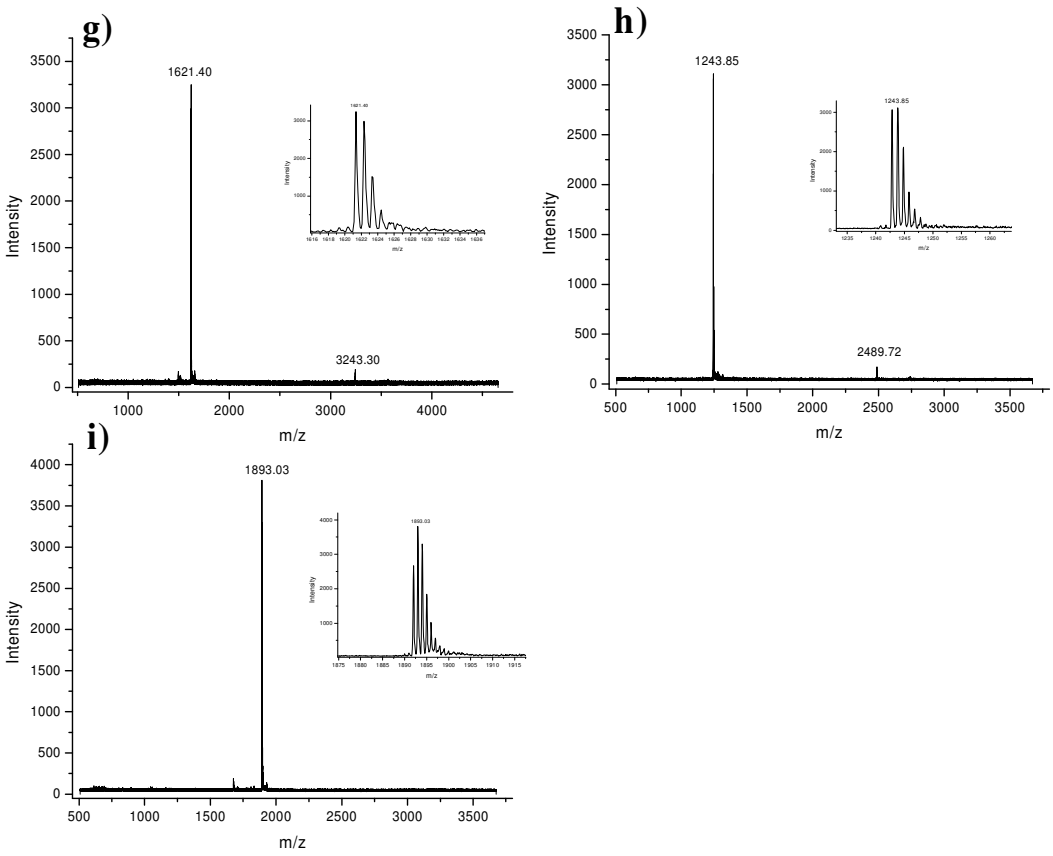

Figure 4-1: MALDI-TOF mass spectra of **4-2 (a), 4-3 (b), 4-4 (c), 4-5 (d), 4-6 (e), 4-7 (f), 4-8 (g), 4-9 (h), 4-10 (i).**

UV-vis absorption spectra of **4-4—4-7** were in good agreement with the excitation spectra. UV-vis absorption spectra of trinaphthoHBCs **4-2** and **4-3** were obtained from thin-films, which could be obtained by simply smearing the samples onto quartz plate. The spectrum of **4-2** (Figure 4-2) showed three types of bands (α, β, p) that are characteristic of large polycyclic aromatic hydrocarbons.[10] In contrast to an elongated D_{2h} symmetrical PAH molecule (***D*$_{2h}$-C60**, inset in Figure 4-2), which can be regarded as a structural isomer of molecule **4-2**, a 10 nm blue shift of the absorption maximum was observed for **4-2**. This value is consistent with ZINDO/S calculations (Table 4-1), suggesting that the electronic properties depend also on the symmetry of the PAHs.[11] The peaks of UV-vis and fluorescence spectra of **4-4** in solution (Figure 4-3) showed a blue shift of 10 nm and ca. 30 nm respectively, as

compared to HBC molecules. This was probably because the sulfur atoms in fused oligothiophene rings did not improve conjugation, but instead led to a non-planar molecular conformation (Figure 4-4).[12] Compound **4-4** represents the first example of large PAHs fused with electron-rich thiophene rings, which would be promising candidate for organic electronic devices, further functionalization based on this discotic core with phase forming behavior will be our next focus.

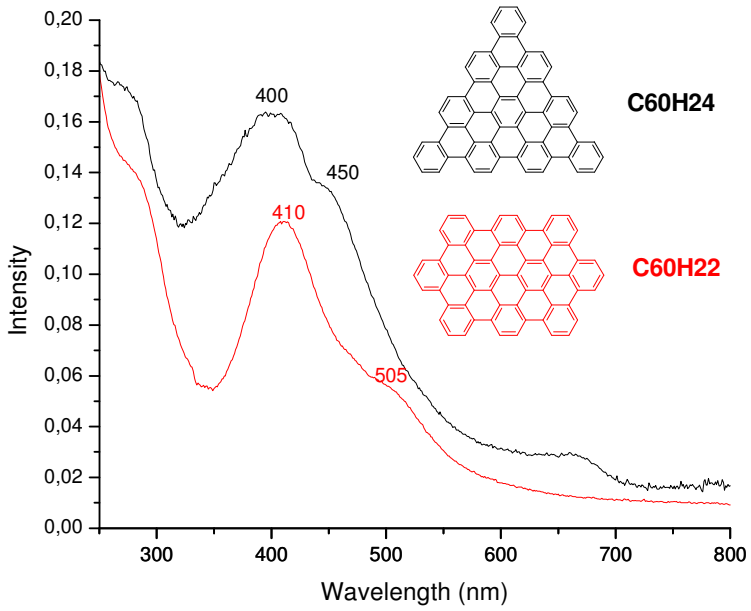

Figure 4-2. Solid-state UV-vis spectrum of **4-2** (black line) and elongated D_{2h}-C_{60} (red line).

Table 4-1. Computed B3LYP/3-21G energy differences between the LUMO and the HOMO orbitals and ZINDO/S-CIS energy of the B type state.

compound	ΔE(HOMO-LUMO)/eV	Number of carbon atoms	symmetry	B type state ZINDO/S(exp)/nm
4-1	3.67	42	D6h	338(359)
C60H22	2.99	60	D2h	373(410)
4-2	3.27	60	D3h	369(400)

The UV-vis and fluorescence spectra of **4-6** and **4-7** (recorded in 1,2,4-trichlorobenzene) exhibited three types of bands (α, β, p) (Figure 4-5). The

absorption maximum of **4-6** (401 nm, ε = 2.50×10^5 M^{-1} cm^{-1}) and **4-7** (405 nm, ε = 3.58×10^5 M^{-1} cm^{-1}) showed a significant bathochromic shift with respect to the corresponding band of parent HBC **4-1** (λ_{max} = 359 nm) and HBC with one C2 unit as "zigzag" periphery ($C_{44}H_{18}$, λ_{max} = 380 nm).[5b] The 4 nm bathochromic shift of absorption and emission maximum of **4-7** with respect to **4-6** can be ascribed to the additional three-phenyl groups at the periphery.

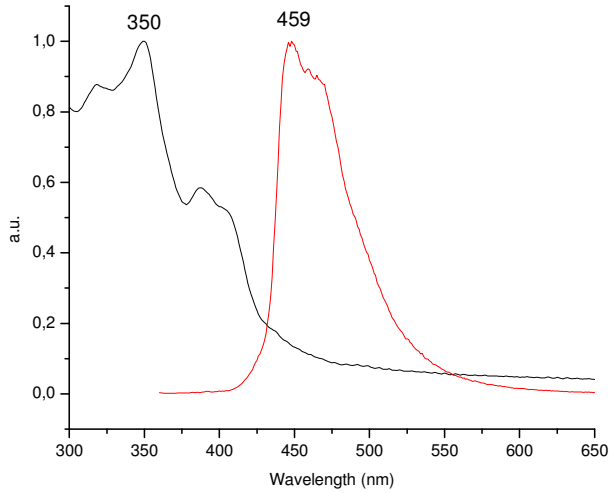

Figure 4-3. UV-visible absorption and photoluminescence spectra of 4-4 (in $CHCl_2CHCl_2$)

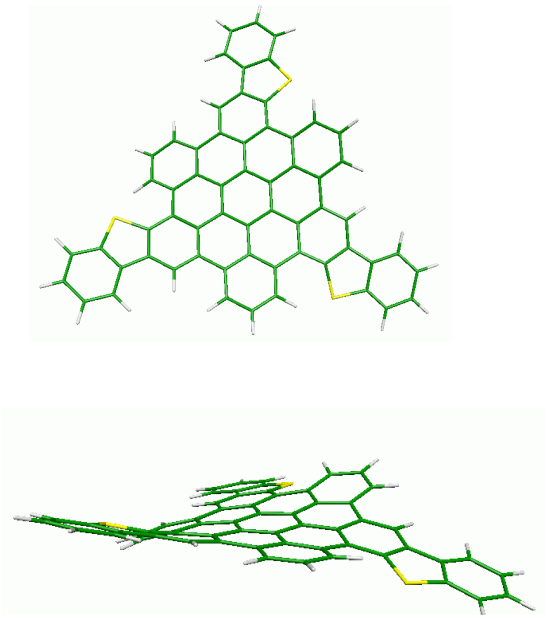

Figure 4-4. B3LYP/6-31G** equilibrium structure of compound **4-4**.

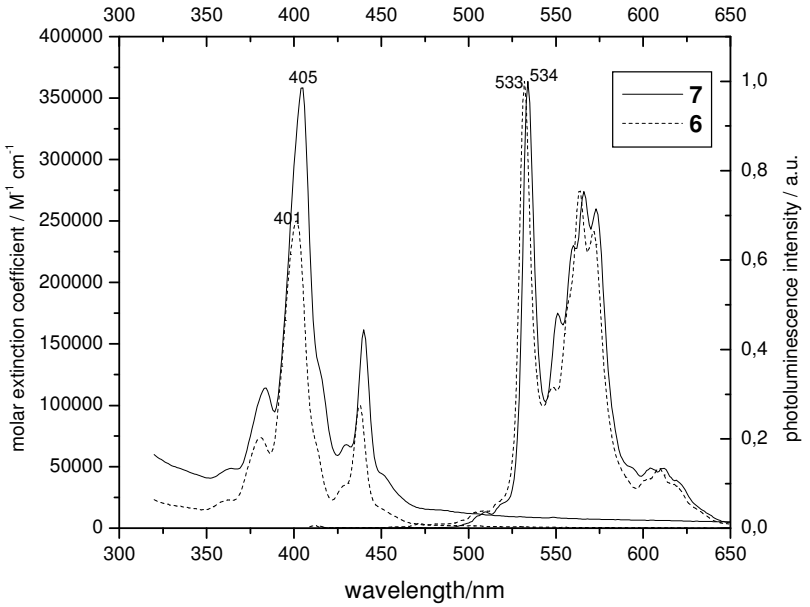

Figure 4-5. UV-vis and photoluminescence spectra of **4-6** and **4-7** (1.0×10^{-6} M in 1,2,4-trichlorobenzene). Dashed line: **4-6**, black line: **4-7**.

The ^{1}H NMR spectra of **4-10** at different temperatures together with the signal assignments are given in Figure 4-6. The signal assignment is based on the comparison with related compounds,[13] the dynamic behavior (see below) and NOESY measurements (not shown here). Although the signals are broad, the resolution of the spectra is already remarkable with respect to other large soluble PAHs, since the ^{1}H NMR signals of many larger, but soluble analogues of **4-10** are broadened into the baseline due to pronounced aggregation effects.[13] The chemical shifts of core protons (H_c around 8.68 and H_d around 9.14) are clearly resolved. The signals of the phenyl protons H_a and H_b, however, showed a temperature-dependent line broadening which was more pronounced for the signal of the ortho protons H_b. This suggested that an intramolecular rotation of the phenyl rings around the neighbouring single bond occurred.

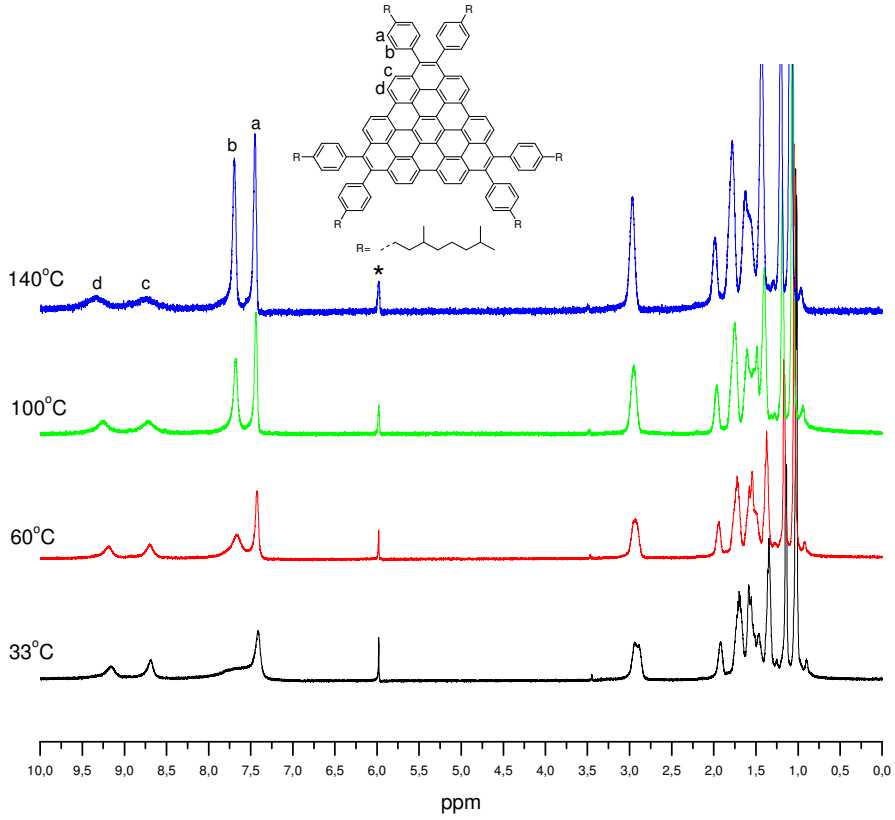

Figure 4-6. Temperature-dependent ^{1}H NMR (500 MHz) spectra of **4-10** in [D_2]tetrachloroethane(*).

4.1.3 Bulk characterization and self-assembly at solid-liquid interface

The bulk thermotropic properties of **4-10** were investigated in cooperation with W. Pisula in the Müllen group. Differential scanning calorimetry (DSC), polarized optical microscopy (POM), and two-dimensional wide-angle X-ray scattering (2D-WAXS). DSC and POM did not show any phase transition over the investigated temperature range between –150 °C and 250 °C. The 2D-WAXS pattern of filament extruded [14] **4-10** in Figure 4-7a indicated a supramolecular organization with helical discotic columnar structures characteristic for a 3D ordered plastic crystalline phase. This kind of phase, reported also for other discotic PAHs,[15] could be clearly distinguished from the typical crystalline phase and disordered liquid crystalline phase. The positions of the reflections in the meridional axis of the X-ray pattern implied a correlation of 1.1

nm between every 4th triangle disc along the column, being a multiple distance of the π-stacking distance of 0.36 nm, which is usually not formed in the liquid crystalline state.[16] The C_3 symmetry of the aromatic core is reflected in the molecular packing since every disc is successively rotated by an angle of 40°. The helical stacking is induced by the sterically demanding out-of-plane arrangement of the attached phenyl rings, as schematically illustrated in Figure 4-7b, whereby the molecular planes are oriented perpendicular to the columnar axis. Due to the helical packing an enhanced columnar and phase stability was observed over a remarkable temperature range. POM experiments showed an isotropization temperature far above 500 °C, which has not been reported for any discotics before. It is known that a helical organization improves the intracolumnar order and leads to high charge-carrier mobilities for discotic columnar systems, which was also expected for **4-10**.[1a]

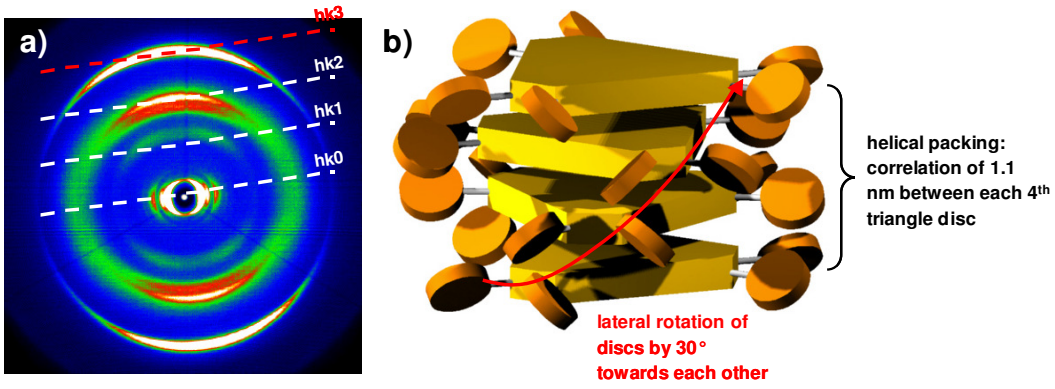

Figure 4-7. a) 2D-WAXS of an extruded fibre of **4-10** including the Miller's indices for the intracolumnar packing and b) schematic illustration of a helical pitch (the alkyl side chains are omitted for simplicity).

An interesting effect on the intercolumnar arrangement was monitored upon annealing at higher temperatures. The positions of the equatorial reflections describe the organization of the columns. At 180 °C, a characteristic hexagonal unit cell was assigned with a packing parameter of a = 3.41 nm (Figure 4-8) when cooling back the sample to room temperature, new, but weak reflections appeared in comparison to the

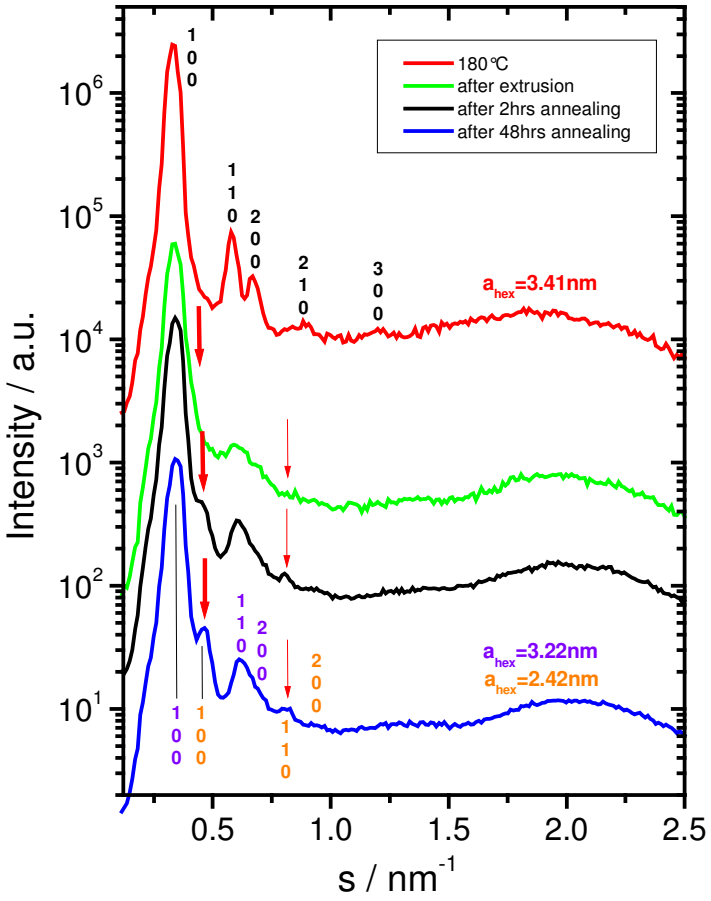

Figure 4-8: Scattering intensity as a function of the scattering vector of **4-10**. The experiments after annealing were performed at 30 °C.

X-ray pattern for the sample measured directly after mechanical alignment. After further annealing for 48 hours at 180 °C, the intensity of these reflections increased significantly indicating a structure modification. Interestingly, the positions of the equatorial scattering intensities for the annealed sample could not be fitted to one single unit cell. Thus, the reflections, which appeared after the thermal procedure, were clearly attributed to a hexagonal unit cell with a=2.42 nm, whereas the former ones indicated an identical lattice, but with a significantly larger packing parameter of a=3.22 nm (Figure 4-8). It could be assumed that the annealing enhances the order of the alkyl substituents in the columnar periphery resulting in a smaller packing parameter. This slight change of the arrangement might not take place homogenously over the sample, but only in specific areas, being an explanation for the coexistence of

two hexagonal unit cells, what has not been reported so far for a discotic columnar organization. However, it should be noted that the meridional reflections were not influenced by the variation of the temperature suggesting no effect on the molecular packing and thus confirming once again the assumed modification of the order of the alkyl side chains, which nevertheless remain disordered after the thermal treatment.

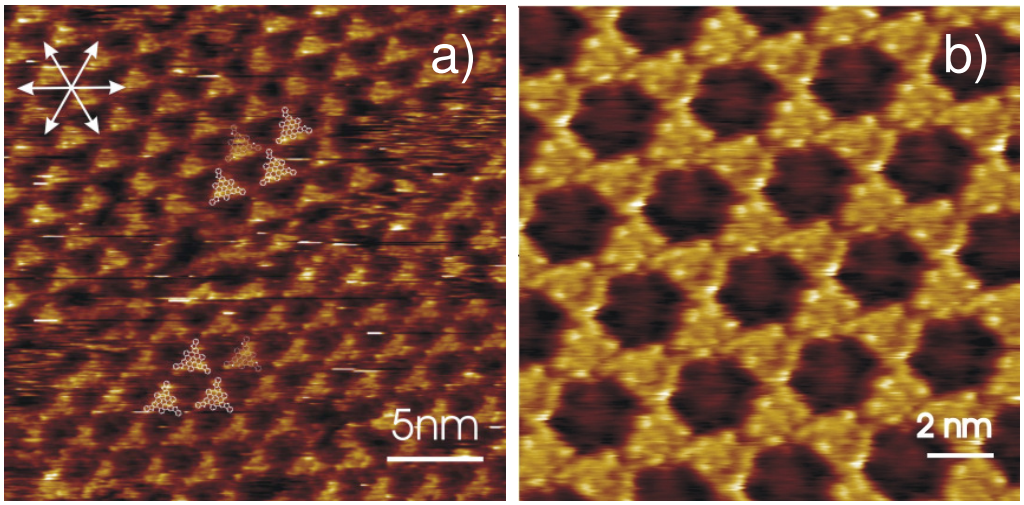

Figure 4-9. STM current images of a) **4-4** and b) **4-10** at the HOPG-solution.

A powerful method to investigate the two-dimensional (2D) organization of functionalized organic molecules on surfaces is STM at a solid-liquid interface in cooperation with M. Ai in Prof. Rabe group, which provides access to molecular and supramolecular structure and dynamics at the single molecule level.[17] To date the largest C_3 symmetrical discs investigated are derivatized triphenylenes.[18] We expected that the larger novel triangle-shaped discs might be exploited to form new 2D superstructures at interfaces. Consequently, the 2D self-assembly of **4-4** (Figure 4-9a) was investigated at the interface between a concentrated solution of 1,2,4-trichlorobenzene and the basal plane of highly oriented pyrolytic graphite (HOPG), a two-dimensional polycrystal, where the single crystallites were oriented epitaxially along one of the three graphite axes. In each grain, the two-dimensional crystal exhibited a hexagonal unit cell with one triangular molecule. The unit cell[19] was about twice as large as a footprint of the molecule (~ 2.85 nm^2), indicating that the self-assembled molecules lay completely flat on the substrate, all oriented in the

same direction with the interstices filled by solvent molecules. On the other hand, Figure 4-9b reveals that **4-10** packed highly regular within a honeycomb lattice, with the determined unit cell[19] being smaller than required for two molecules lying totally flat on the graphite surface (6.95 nm^2 per molecule). This indicated that the alkyl chains dissolved partially in the supernatant organic solution. The honeycomb pattern, which was only observed for molecules **4-8—4-10** and formed by weak intermolecular and interfacial forces, represents the first visualization in a series of substituted PAHs by STM.[20] Thereby, substituted trizigzagHBCs gave rise to a new superstructure, which may be employed for the design of molecular electronic devices based on PAHs as a host and a second molecular species as a guest.

4.1.4 Conclusion

In summary, we have established a novel synthetic method towards large PAHs with C_3 symmetrical triangle shape and multiple "zig-zag" peripheries. The title compounds serve as models for describing the relationship between the molecular structure and the electronic absorption and photoluminescence properties. Further, they reveal a unique self-assembly behavior in solution, solid state, and at the solution-substrate interface. A mesophase stability over an extremely large temperature range has been obtained as a result of the helical supramolecular arrangement of the discs, reflecting the C_3 symmetry. The honeycomb pattern with "holes" observed for monolayers of **4-10** suggests a potential molecular engineering with host-guest recognition and surface pattering. Attachment of long alkyl chains onto molecules **4-3**, **4-5** and **4-8** by transition metal catalyzed coupling reactions was feasible and will provide a new series of discotic liquid crystalline materials with novel self-assembling behavior and promising applications in organic electronics.[21]

4.2 Supramolecular Organization and Photovoltaics of Triangle-shaped Discotic Graphenes with Swallow-tailed Alkyl Substituents

4.2.1 Introduction

Polycyclic aromatic hydrocarbons (PAHs) as molecularly defined nanographenes with columnar superstructures formed by π-stacking,[22] exhibit the highest local charge-carrier mobilities for discotics, which allowed the successful implementation in field-effect transistors (FETs),[23] photovoltaic devices,[24] and molecular electronic devices.[25] It is expected that larger aromatic cores will lead to discotic liquid crystals with enhanced columnar stability and supramolecular order and thus to materials with improved charge-carrier mobilities due to the more extended π-orbital overlap. However, the increased π-orbital overlap is typically accompanied by a drastic limitation in processibility from both solution and vacuum.[26] The introduction of alkyl substituents, possessing a pronounced steric demand, is an effective tool to enhance the solubility which is also crucial for the purification, and device fabrication. Additionally, the variation of alkyl side chains (linear vs. branched) allows a precise control over the thermotropic properties of the material.[27] The formation of the liquid crystalline state represents a significant advantage for the implementation of discotic graphenes into electronic devices. For instance, upon annealing at elevated temperatures, self-healing occurs improving (macro)molecular packing and diminishing the number of local defects and macroscopic grain boundaries which impede the charge carrier transport through organic semiconductors.[28] Monodomain formation of small liquid crystalline molecules prevents film shrinkage and ensures in this way an enhanced operation of solution processed FET devices.[29] On the other hand, as far as we know, there is no example of large discotics reported which possess a liquid crystalline state over a broad temperature range including ambient conditions.[30]

In order to elucidate the influence of the molecular design on the self-organization behavior and further to understand the relationship between the bulk organization and device performance after thermal annealing, bulk heterojunction photovoltaic cells provide meaningful test experiments.[31] For example, the efficiency of photovoltaic devices, which were fabricated from a blend of donor (hexa-*peri*-hexabenzocoronene, HBC) and acceptor (*N*,*N*′-Bis(1-ethylpropyl)-3,4,9,10-perylenetetracarboxydiimide,

PDI), displayed a strong dependence on the substituents' architecture, supramolecular order and macroscopic morphology.[24] Hereby, we focus our attention on the triangle-shaped discotic graphenes with three swallow-tailed alkyl substituents (benzo[o]bistriphenyleno[2,1,12,11-efghi:2',1',12', 11'-uvabc] ovalene, **4-22**),[32] because of their simplest triangle-shaped benzenoid graphene unit with the same number of carbons as fullerene C_{60} and their large D_{3h} symmetric discotic core. Additionally their straightforward synthesis and functionalization on the periphery with branched alkyl chains allow efficient solution purification and facile device fabrication. Furthermore, the π-conjugated chromophore with a relatively low number of "diluting" bulky substituents results in close molecular stacking and high mesophase stability over an extremely broad temperature range.

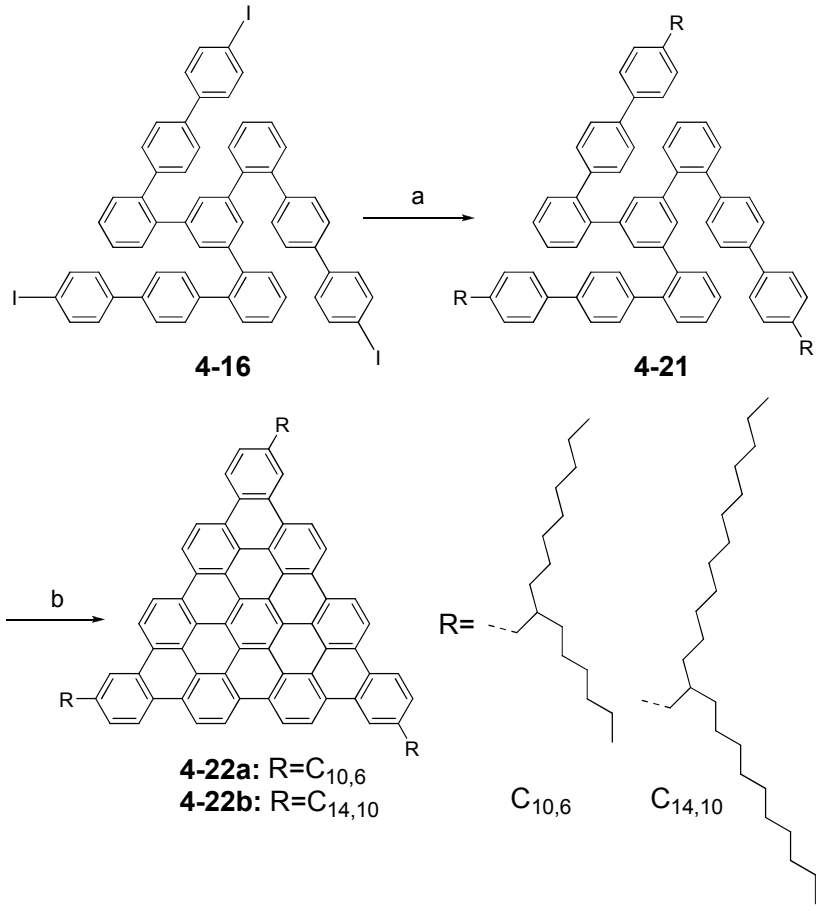

Scheme 4-3. Synthesis of triangle-shaped discotic graphenes **4-22**. a) RBrZn, $Pd(dppf)Cl_2$, DMA, 50°C, 43% for **4-21a**, 30% for **4-21b**; b) $FeCl_3/CH_3NO_2$, CH_2Cl_2, 89% for **4-22a**, 86% for **4-22b**. dppf: 1,1′-bis(diphenylphosphino)ferrocene; DMA: dimethylacetamide.

4.2.2 Synthesis and structural characterizations

The synthetic approach was based on the useful building block **4-16** (1,3,5-tris[2'-(4''-(4'''-iodophenyl))biphenyl]benzene, Scheme 4-3), which allowed further functionalization via metal-catalyzed coupling reactions.[6,33] We firstly attempted to prepare precursors **4-21** via Kumada coupling from the magnesium reagents of branched alkyl chains,[27a] however, only minor amounts of product could be detected, apparently this could be ascribed to the inactivity and severe homo-coupling of the magnesium reagents. Therefore, we considered the application of the corresponding zinc reagents,[33] which could be easily prepared under mild conditions, and indeed allowed the synthesis of **4-21** in reasonable yields. Subsequently oxidative cyclodehydrogenation reactions were carried out under mild conditions by treating precursors **4-21** with $FeCl_3$ to afford the final triangle-shaped discotic graphenes **4-22** in good yields after purification by column chromatography. Further characterization by MALDI-TOF MS (TCNQ matrix) and elemental analysis were in accordance with expectation (Figure 4-10 and 4-11). Compound **4-22b** was soluble enough for ^1H NMR characterization at high temperature (Figure 4-12).[34]

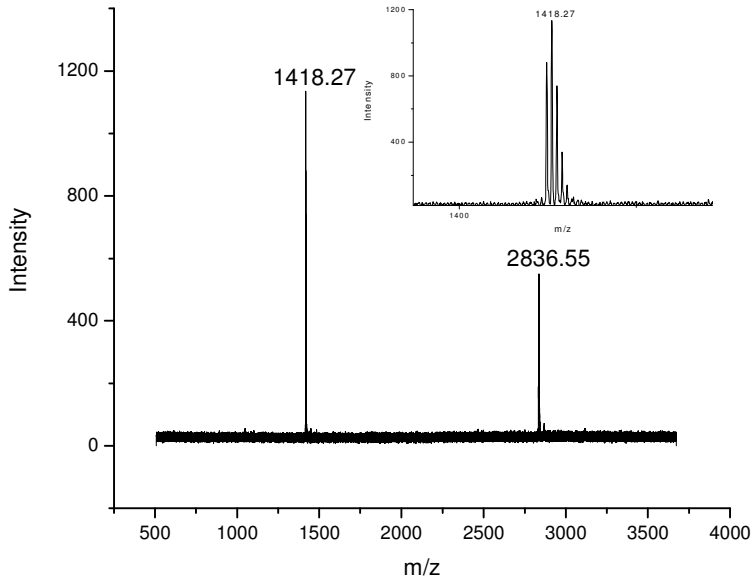

Figure 4-10. MALDIT-TOF MS spectrum of **4-22a**.

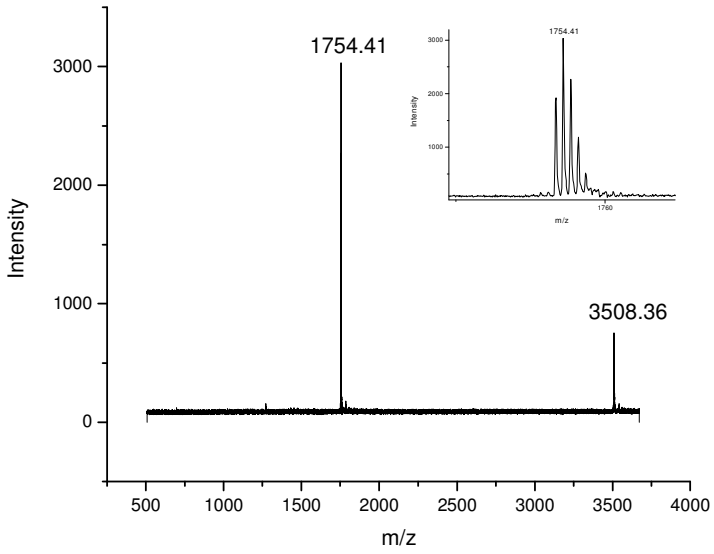

Figure 4-11. MALDIT-TOF MS spectrum of **4-22b**.

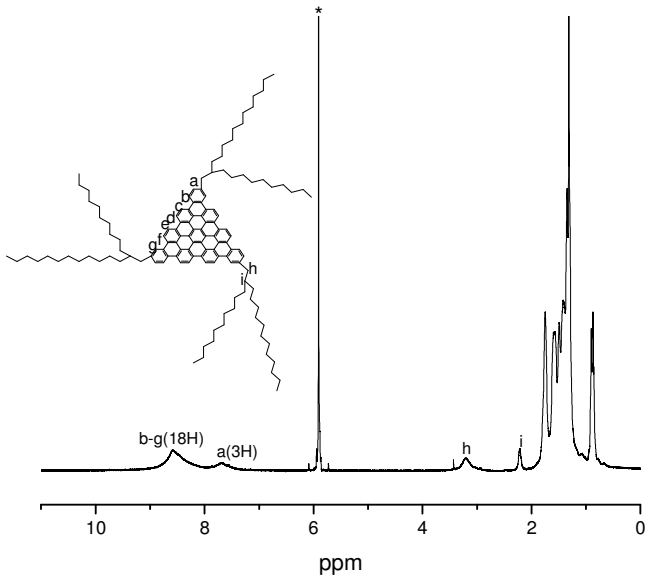

Figure 4-12. ^{1}H NMR spectrum of **4-22a** at 140^{o}C in $CDCl_2CDCl_2$ (*).

The UV-vis spectrum of **4-22b** in $CHCl_3$ exhibited three types of bands (α, β, p, λ_{max}= 391 nm, $\varepsilon = 1.48\times10^5$ $M^{-1}cm^{-1}$), which are typical for aromatic hydrocarbons (Figure 4-13).[35] It was comparable to the solid state UV-vis spectrum of the parent insoluble compound.[32] As expected, a spin-coated thin film of **4-22a** revealed a higher

absorbance than **4-22b** at the same film thickness due to higher chromophore concentrations in **4-22a**, which is also an important parameter for light harvesting in the photovoltaic device (Figure 4-14). The p-band (455 nm) and α-band (not clearly resolvable) for both **4-22a** and **4-22b** were distinctly bathochromically shifted in the solid state with respect to solution spectra, indicating high sensitivity of the p-band and α-band toward aggregation. After annealing the thin films at 120 ^{o}C for one hour, the UV-vis spectrum of **4-22a** did not show apparent differences (Figure 4-14). In contrast, the peak intensity for **4-22b** was markedly enhanced after thermal treatment and the corresponding p-band and α-band were further broadened (Figure 4-14). The intensity increase was attributed to an improved long-range order after annealing. This annealing effect above the thermal transition was only observed for **4-22b**.

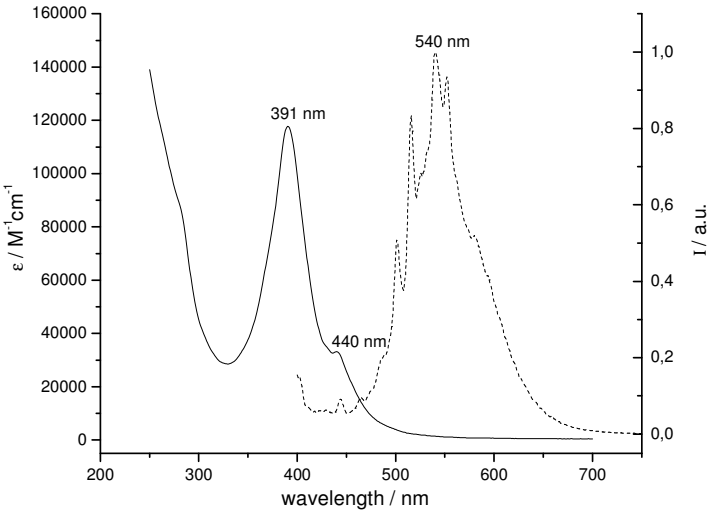

Figure 4-13. UV-vis absorption (solid line, 1.0×10^{-6} M) and fluorescence (dashed line, 1.0×10^{-7} M) spectra of **4-22b** in $CHCl_3$.

The design of bulk heterojunction photovoltaic devices requires a consideration of the potential energy levels of both donor and acceptor components. Cyclic voltammetry (CV) was carried out to obtain the electronic levels of compounds **4-22a** and **4-22b** on thin films. Similar to other alkyl-substituted HBC derivatives, quasi-reversible oxidation peaks were observed in positive scans, while no reduction peaks were

detected in the scanned range. For **4-22a**, a highest occupied molecular orbital (HOMO) level of –5.1 eV was calculated from the onset values of oxidation peak (E_{ox}^{onset} = 0.3 V vs. Fc/Fc$^+$), while **4-22b** showed the level at –5.2 eV. With the optical bandgap of 2.3 eV (onset of the p-band in solid state UV-vis spectra), the lowest unoccupied molecular orbitals (LUMOs) of –2.8 eV for **4-22a** and –2.9 eV for **4-22b** have been calculated. The determined levels suggested that **4-22a** and **4-22b** are suitable donor materials for PDI, which exhibited HOMO and LUMO energy levels at -5.8 and -3.8 eV, respectively.

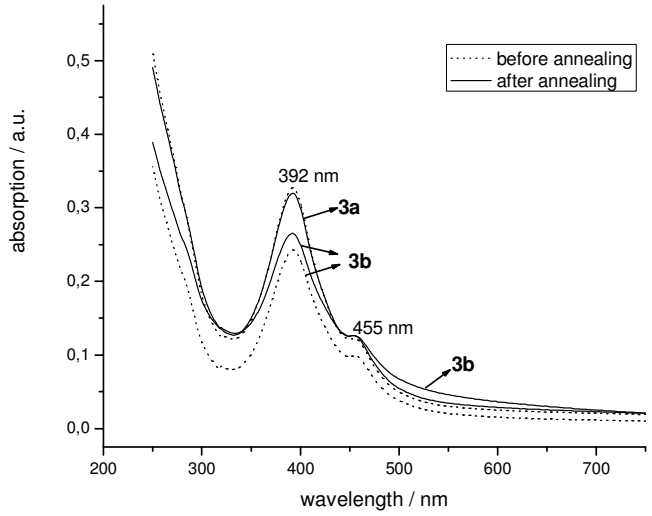

Figure 4-14. UV-vis absorption spectra of **4-22a** and **4-22b** in thin films (thickness of 100 ± 10 nm) before (dotted line) and after annealing at 120°C (solid line).

4.2.3 Bulk characterizations

It has been reported that besides the optical properties and energy levels, the self-organization and molecular packing of the compounds play a key role for the photovoltaic efficiency.[36] Therefore, a particular focus was put on the thermotropic properties of both compounds **4-22a** and **4-22b**. The thermal behavior was investigated by using differential scanning calorimetry which revealed a phase transition for **4-22b** at 24 °C (7.4 J/g during 2nd heating cycle, 45 °C during 1st heating). Compound **4-22a** did not show any phase transition in the investigated temperature range. In cooperation with W. Pisula in the Müllen group,

two-dimensional wide-angle X-ray scattering (2D-WAXS) measurements[14] on extruded samples gave an insight into the supramolecular organization. Before annealing the scattering patterns of both compounds **4-22a** and **4-22b** indicated a characteristic discotic liquid crystalline phase (inset Figure 4-15a for **4-22b**).[22] Thereby, the molecules were arranged in columnar structures with their disc planes perpendicular to the stacking axis possessing a π-stacking distance of 0.35 nm for both cases, as characterized by the meridional wide-angle reflections (schematic illustration in Figure 4-15c). The well-aligned columns organized in a lateral 2D hexagonal array with packing parameters of a_{hex} = 2.77 nm for **4-22a** and a_{hex} = 3.49 nm for **4-22b**. While **4-22a** did not display any change of the supramolecular arrangement upon thermal treatment, compound **4-22b** exposed an enhanced degree of order, as suggested by much more distinct reflections in the pattern during annealing at 100 °C and after cooling back the sample to 30 °C (Figure 4-15a). Especially the wide-angle meridional reflection became more intense and sharp (see comparison of the azimuthal integration, Figure 4-15b) proving a significant improvement of the intracolumnar packing within the columns. The unit cell parameters decreased to a_{hex} = 3.22 nm. Apparently, the phase transition observed for **4-22b** played an important role for the self-healing procedure. The high degree of order remained after cooling back the sample to –70 °C. In general, self-healing involves two effects; on the one hand it reduces macroscopic domain boundaries and promotes the formation of a monodomain, whereas on the other hand the local arrangement of molecules is enhanced. In contrast, compound **4-22a** did not reveal such behavior due to the absence of a phase transition with distinct molecular dynamics. Therefore, the improved supramolecular order of **4-22b** can be explained in terms of longer branched side chains which led to higher molecular dynamics at temperatures above the phase transition and allowed a reorganization of the molecules into a more favorable packing.[27b] Both phases of **4-22b** were assigned as liquid crystalline, whereas the higher temperature phase was accompanied by higher molecular dynamics being responsible for the order improvement, which was crucial for the device processing, as discussed below. Diffraction on thin films of spin-coated

4-22a and **4-22b** confirmed the 2D WAXS results (Figure 4-16). While the scattering intensity for the film of **4-22b** increased significantly after annealing, the diffractogram of **4-22a** remained after the thermal treatment unchanged. Finally, it should be noted that both compounds did not undergo an isotropic phase up to 500 °C indicating an extreme liquid crystalline stability. Up to now, we have observed such thermal mesophase stabilities only for systems with improved organization, e.g helical arrangement in plastic phases.[30] In this case, we can relate the exceptionally broad temperature range of the liquid crystalline phase of both compounds also with an improved packing of molecules and their unique triangle shape of the aromatic core.

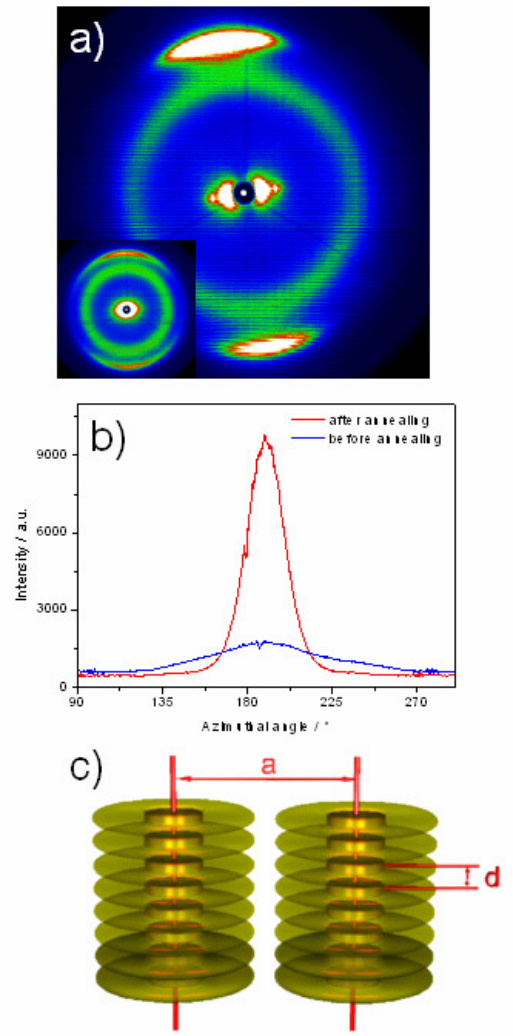

Figure 4-15. a) 2D-WAXS pattern of **4-22b** after annealing (inset shows before annealing), b) azimuthal integration of the meridional reflection related to the π-stacking, c) schematic illustration of the columnar organization of **4-22a** and **4-22b**.

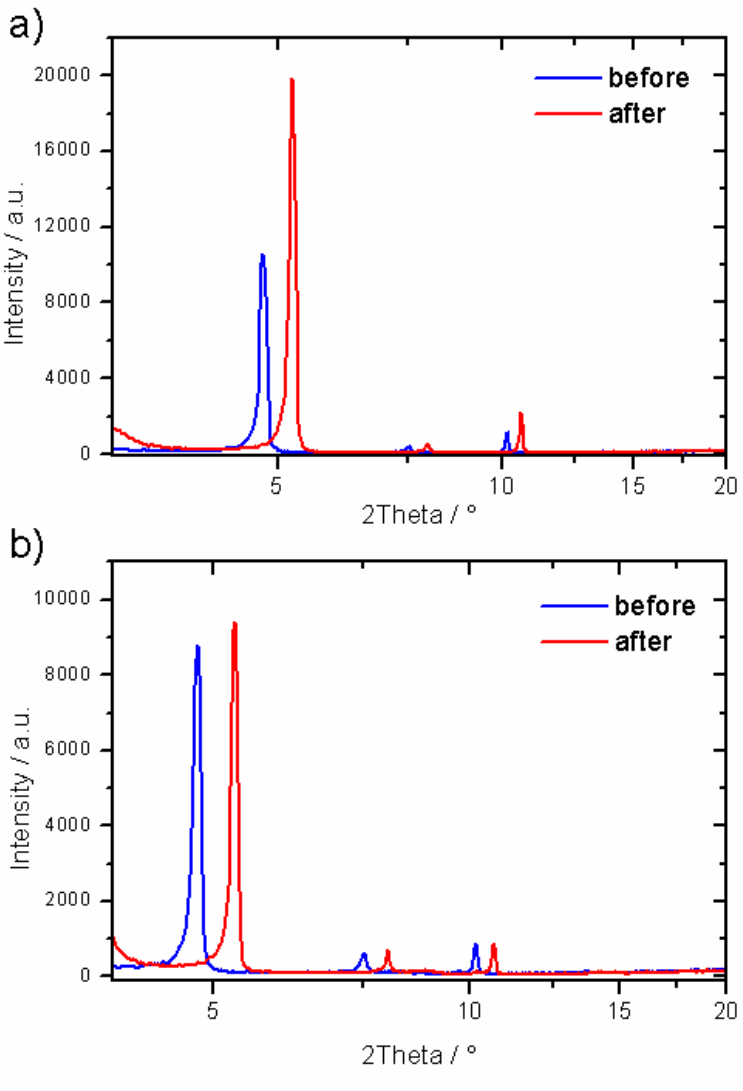

Figure 4-16. Thin film diffraction of) **4-22b** and b) **4-22a** before and after annealing of spin-coated layers. For comparisons, the diffractorgram before annealing (blue plot) is shifted by 0.5° to lower angles.

4.2.4 Photovoltaic device characterizations

The influence of the thermotropic behavior of **4-22a** and **4-22b** on device properties was further investigated on bulk heterojunction photovoltaics in cooperation with M. Liu in the Müllen group. The photovoltaic devices consisted of indium tin oxide (ITO)/(**4-22**+PDI)/Ag and were fabricated by spin-coating a chloroform solution made from a mixture of **4-22** and PDI. Before the measurement, the samples were

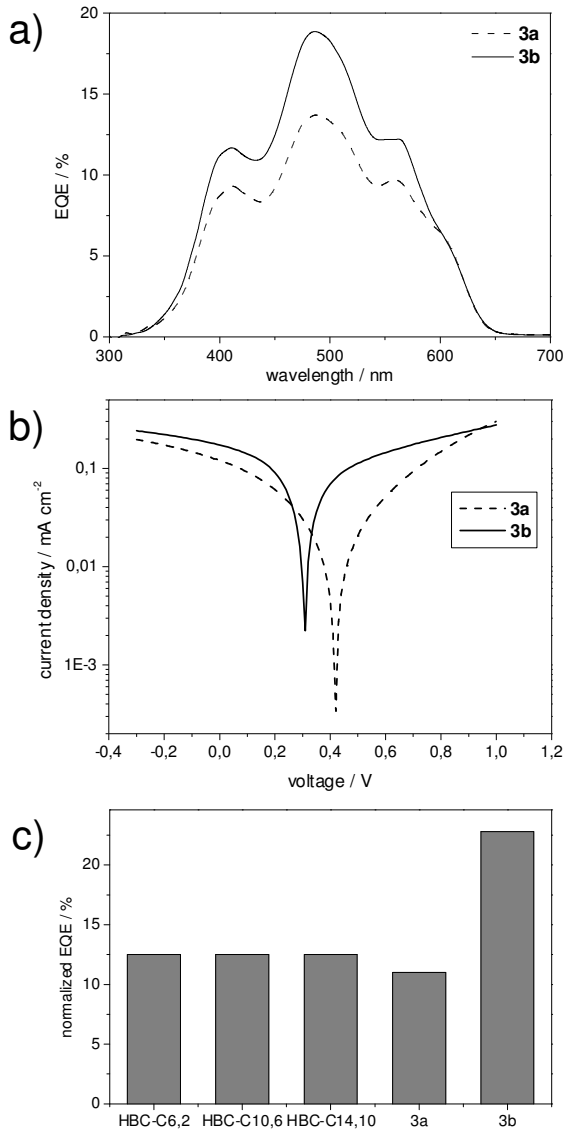

Figure 4-17. a) *EQE* plots for ITO/ **4-22b**(solid line) and **4-22a** (dotted line):PDI (4:6)/ Ag device; b) corresponding I –V characteristics under one sun illumination at 490 nm; c) normalized *EQE* by the chromophore density for previously reported swallow-tailed HBCs[24b] and compounds **4-22**. The chromophore density was determined by ratio between the number of carbon atoms of the aromatic core and the side chains.

annealed at 120 °C for 1 hr under a nitrogen atmosphere in order to self-heal the thin films. The highest device efficiency was observed for blends with the ratio of **4-22**:PDI = 4:6. Interestingly, the same ratio was determined for the best photovoltaics based on discotic HBCs and PDI.[24b] In this study, it is remarkable that the highest external quantum efficiency (*EQE*) of 19% was achieved at 490 nm for the blend containing **4-22b**, while **4-22a** showed a lower *EQE* of 14% (Figure 4-17a). The performance difference between the compounds was attributed to the improved intracolumnar packing of **4-22b** upon thermal annealing favoring the charge-carrier transport and exciton diffusion length, which are both key parameters for device efficiency.[24] This assumption was manifested in a higher short-circuit current for **4-22b**, which was extracted from the current–voltage (I–V) curve (Figure 4-17b). The higher device efficiency of **4-22b** in comparison to **4-22a** is quite impressive, since **4-22b** showed poorer light harvesting (Figure 4-14) due to a lower chromophore concentration (defined as the ratio of carbon atoms between aromatic core and alkyl side chains).

The inspection of the thin layers in the devices consisting of blends of **4-22a** and **4-22b**, respectively, and PDI by scanning electron microscopy (SEM) revealed similar top view images and bulk morphologies in the cross-section (Figure 4-18). In both cases a 'homogeneous' bicontinuous phase was observed across the thickness with cylindrical PDI crystals evenly dispersed within the liquid crystalline matrix of **4-22a** and **4-22b**, respectively, from bottom to top of the film. This kind of morphology is considered to be favorable for better charge transport of holes and electrons in the corresponding separated continuous percolation pathway. It is well known that the bulk heterojunction morphology is important for the photovoltaic performance.[31] Since films of **4-22b**:PDI and **4-22a**:PDI revealed identical morphologies, it is reasonable to assume that the above discussed parameters, such as the improvement of molecular packing after annealing, play the main role for the performance difference between **4-22a** and **4-22b**.

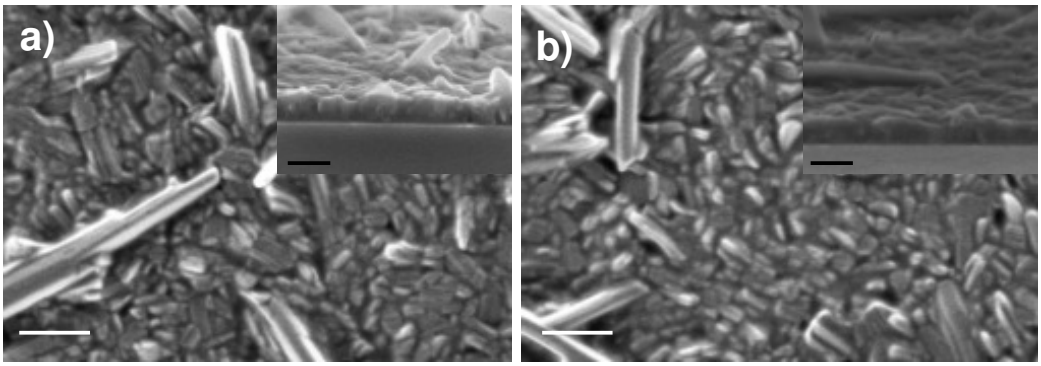

Figure 4-18. SEM images: top view images (scale bar for 100 nm) and cross-section view (inset, scale bar for 500 nm) of a) **4-22b**:PDI and b) **4-22a**:PDI (both in a ratio of 4:6). All the films were annealed at 120 °C for 1h.

It has to be stressed that both **4-22a** and **4-22b** exhibited a better photovoltaic performance in comparison to the swallow-tailed HBC analogues. Figure 4-17b presents the *EQE* normalized by the chromophore concentration for the previously reported HBCs and compounds **4-22a** and **4-22b**. Interestingly, despite the differences of the HBC derivatives in the thermotropic properties, light harvesting and morphology, the normalized *EQE* is equal for the three materials. However, this is not the case for **4-22a** and **4-22b**. Compound **4-22a** exposed a slightly lower value than the swallow-tailed HBCs, whereby for **4-22b** the highest normalized *EQE* was determined. This comparison indicates again the great impact of the self-healing process on the photovoltaic device, which was only observed for **4-22b**.

4.2.5 Conclusion

In conclusion, we have demonstrated the synthesis of novel triangle-shaped discotics with swallow alkyl tails, which consist of a high D_{3h} symmetric extended graphene corona. The introduction of the swallow tailed substituents allowed a facile purification, control over the thermotropic properties and finally solution fabrication into efficient photovoltaic devices. The unique design of the large aromatic core

provided a material with an extremely broad liquid crystalline range, whereby the adequate choice of the substituents permitted self-healing at low processing temperatures. It has been revealed that the latter aspect played a key role for improved photovoltaic cells. The control over thermotropic properties by molecular design and the substitution pattern of liquid crystalline semiconductors capable to monodomain formation opens an alternative route towards optimized organic electronics.

4.2.6 References:

[1] a) Adam, D.; Schuhmacher, P.; Simmerer, J.; Häussling, L.; Siemensmeyer, K.; Etzbach, K. H.; Ringsdorf, H.; Haarer, D. *Nature*. **1994**, *371*, 141-143; b) Kumar, S. *Chem. Soc. Rev*. **2006**, *35*, 83-109; c) Kumar, S. *Liq. Cryst*. **2005**, *32*, 1089-1113; d) b) Laschat, S.; Baro, A.; Steinke, N.; Giesselmann, F.; Hagele, C.; Scalia, G.; Judele, R.; Kapatsina, E.; Sauer, S.; Schreivogel, A.; Tosoni, M. *Angew. Chem.* **2007**, *119*, 4916-4973; *Angew. Chem. Int. Ed.* **2007**, *46*, 4837-4887.

[2] Kumar, S. *Liq, Cryst*. **2004**, *31*, 1037-1059.

[3] Yasuhiro, F. *Bull. Chem. Soc. Jpn*. **1985**, *58*, 481-489.

[4] a) Watson, M. D.; Fechtenkötter, A.; Müllen, K. *Chem. Rev*. **2001**, *101*, 1267-1300; b) Grimsdale, A. C.; Müllen, K. *Angew. Chem*. **2005**, 117, 5732-5772; *Angew. Chem., Int. Ed*. **2005**, *44*, 5592-5629; c) Wu, J.; Tomovic, Z.; Enkelmann, V.; Müllen, K. *J. Org. Chem*. **2004**, *69*, 5179-5186; d) Tomovic, Z.; Watson, M. D.; Müllen, K. *Angew. Chem*. **2004**, *116*, 773-777; *Angew. Chem. Int. Ed*. **2004**, *43*, 755-758.

[5] a) Stein, S. E.; Brown, R. L. *J. Am. Chem. Soc*. **1987**, *109*, 3721-3728; b) Wang, Z.; Tomovic, Z.; Kastler, M.; Pretsch, R.; Negri, F.; Enkelmann, V.; Müllen, K. *J. Am. Chem. Soc*. **2004**, *126*, 7794-7795; c) Kastler, M.; Schimidt, J.; Pisula, W.; Sebastiani, D.; Müllen, K. *J. Am. Chem. Soc*. **2006**, *128*, 9526-9534.

[6] Feng, X.; Wu, J.; Enkelmann, V.; Müllen, K. *Org. Lett*. **2006**, *8*, 1145-1148.

[7] Yao, T.; Campo, M. A.; Larock, R. C. *J. Org. Chem*. **2005**, *70*, 3511-3517; b) Goldfiner, M. B.; Swager, T. M. *J. Am. Chem. Soc*. **1994**, *116*, 7895-7896; c)

Goldfinger, M. B.; Crawford, K. B.; Swager, T. M. *J. Am. Chem. Soc*. **1997**, *119*, 4578-4593.

[8] Fischer, E.; Larsen, J.; Christensen, J. B.; Fourmigue, M.; Madsen, H. G.; Harrit, N. *J. Org. Chem*. **1996**, *61*, 6997-7005.

[9] Przybilla, L.; Brand, J. D. ; Yoshimura, K.; Räder, J.; Müllen, K. *Anal. Chem*. **2000**, **72**, 4591-4597.

[10]The detection of the α-band is difficult because of the extremely low intensity of this band. However, the β-band at 400 nm and the p-band as the shoulder at 450 nm are clearly resolved and show significant bathochromic shifts compared to the parent HBC (the β-band at 359 nm).

[11] Simpson, C. PhD thesis. Mainz University, **2006**.

[12] a) Zhang, X.; Matzger, A. J. *J. Org. Chem*. **2003**, *68*, 9813-9815; b) Zhang, X.; Cote, A. P.; Matzger, A. J. *J. Am. Chem. Soc*. **2005**, *127*, 10502-10503; c) Xiao, K.; Liu, Y.; Qi, T.; Zhang, W.; Wang, F.; Gao, J.; Qiu, W.; Ma, Y.; Cui, G.; Chen, S.; Zhan, X.; Yu, G.; Qin, J.; Hu, W.; Zhu, D. *J. Am. Chem. Soc*. **2005**, *127*, 13281-13286.

[13] Kastler, M.; Pisula, W.; Wasserfallen, D.; Pakula, T.; Müllen, K. *J. Am. Chem. Soc*. **2005**, *127*, 4286-4296.

[14] Pisula, W.; Tomovic, Z.; Simpson, C. D.; Kastler, M.; Pakula, T.; Müllen, K. *Chem. Mater*. **2005**, *17*, 4296.

[15] a) Wu, J.; Watson, M. D.; Müllen, K. *Angew. Chem*. **2003**, *115*, 5487-5491; *Angew. Chem. Int. Ed*. **2003**, *42*, 5329-5333; b) Glusen, B.; Heitz, W.; Kettner, A.; Wendorff, J. H. *Liquid Crystals,* **1996**, *20* (5), 627.

[16] a) Nolde, F.; Pisula, W.; Müller, S.; Kohl, C.; Müllen, K. *Chem. Mater*. **2006**, *18*, 3715-3725; b) Pisula, W.; Kastler, M.; Wasserfallen, D.; Robertson, J. W. F.; Nolde, F.; Kohl, C.; Müllen, K. *Angew. Chem*. **2006**, *118*, 834-838; *Angew. Chem. Int. Ed.* **2006**, *45*, 819 –823.

[17] a) Rabe, J. P.; Buchholz, S. *Science*. **1991**, *253*, 424; b) Rabe, J. P.; Buchholz, S. *Phys. Rev. Lett*. **1991**, *66*, 2096.

[18] Askadskaya, L.; Boeffel, C.; Rabe, J.P. *Ber. Bunsenges. Phys. Chem.* **1993**, *97*, 517-521.

[19] For **4**, the unit cell parameters a = (2.42 ± 0.10) nm, b = (2.55 ± 0.13) nm and = (61 ± 4)° correspond to a unit cell area of A = (5.40 ± 0.28) nm2; For **10**, the unit cell parameters a = (3.34 ± 0.14) nm, b = (3.49 ± 0.16) nm and = (62 ± 2) ° correspond to a unit cell area of A = (10.25 ± 0.80) nm2.

[20] Hydrogen bonding induced honeycomb: a) Ishikawa, Y.; Ohira, A.; Sakata, M.; Hirayama, C.; Kunitake, M. *Chem. Commun*. **2002**, 2652-2653; b) Dmitriev, A.; Lin, N.; Weckesser, J.; Barth, J. V.; Kern, K. *J. Phys. Chem. B*. **2002**, *106*, 6907-6912; c) Theobald, J. A.; Oxtoby, N. S.; Phillips, M. A.; Champness, N. R.; Beton, P. H. *Nature*, **2003**, 1029-1031; Van der Waals interaction induced honeycomb: d) Furukawa, S.; Uji-I, H.; Tahara, K.; Ichikawa, T.; Sonoda, M.; De Schryver, F. C.; Tobe, Y.; De Feyter, S. *J. Am. Chem. Soc*. **2006**, *128*, 3502-3503.

[21] a) Wu, J.; Fechtenkötter, A.; Gauss, J.; Watson, M. D.; Kastler, M.; Fechtenkötter, C.; Wagner, M.; Müllen, K. *J. Am. Chem. Soc*. **2004**, *126*, 11311-11321; b) Wu, J.; Watson, M. D.; Zhang, L.; Wang, Z.; Müllen, K. *J. Am. Chem. Soc*. **2004**, *126*, 177-186.

[22] a) Wu, J.; Pisula, W.; Müllen, K. *Chem. Rev*. **2007**, *107*, 718-747.

[23] a) van de Craats, A. M.; Stutzmann, N.; Bunk, O.; Nielsen, M. M.; Watson, M.; Müllen, K.; Chanzy, H. D.; Sirringhaus, H.; Friend, R. H. *Adv. Mater.* **2003**, *15*, 495-499; b) Pisula, W.; Menon, A.; Stepputat, M.; Lieberwirth, I.; Kolb, U.; Tracz, A.; Sirringhaus, H.; Pakula, T.; Müllen, K. *Adv. Mater*. **2005**, *17*, 684; c) Xiao, S.; Tang, J.; Beetz, T.; Guo, X.; Tremblay, N.; Siegrist, T.; Zhu, Y.; Steigerwald, M.; Nuckolls, C. *J. Am. Chem. Soc*. **2006**, *128*, 10700-10701.

[24] a) Schmidt-Mende, L.; Fechtenkötter, A.; Müllen, K.; Moons, E.; Freind, R. H.; MacKenzie, J. D. *Science*. **2001**, *293*, 1119-1122; b) Li, J.; Kastler, M.; Pisula, W.; Fobertson, J. W. F.; Wasserfallen, D.; Grimsdale, A. C.; Wu, J.; Müllen, K. *Adv. Funct. Mater.* **2007**, *17*, 2528-2533.

[25] Jäckel, F.; Watson, M. D.; Müllen, K.; Rabe, J. P. *Phys. Rev. Lett*. **2004**, *92*, 188303.

[26] a) Murphy, A. R.; Frechet, J. M. J. *Chem. Rev*. **2007**, *107*, 1066-1096; b) Gunes, S.; Neugebauer, H.; Sariciftci, N. S. *Chem. Rev*. **2007**, *107*, 1324-1338.

[27] a) Pisula, W.; Kastler, M.; Wasserfallen, D.; Pakula, T.; Müllen, K. *J. Am. Chem. Soc*. **2004**, *126*, 8074; b) Pisula, W.; Kastler, M.; Wasserfallen, D.; Mondeshki, M.; Piris, J.; Schnell, I.; Müllen, K. *Chem. Mater*. **2006**, *18*, 3634.

[28] a) Mcculloch, I.; Heeney, M.; Bailey, C.; Genevicius, K.; Macdonald, I.; Shkunov, M.; Sparrowe, D.; Tierney, S.; Wagner, R.; Zhang, W.; Chabinyc, M. L.; Kline, R. J.; Mcgehee, M. D.; Toney, M. F. *Nature. Mater*, **2006**, *5*, 328; b) Ong, B. S.; Wu, Y.; Liu, P.; Gardner, S. *J. Am. Chem. Soc*, **2004**, *126*, 3378-3379; c) Maunoury, J. C.; Howse, J. R.; Turner, M. L. *Adv. Mater*. **2007**, *19*, 805–809.

[29] a) Funahashi, M.; Zhang, F.; Tamaoki, N. *Adv. Mater*. **2007**, *19*, 353–358; b) Oikawa, K.; Monobe, H.; Nakayama, K.; Kimoto, T.; Tsuchiya, K.; Heinrich, B.; Guillon, D.; Shimizu, Y.; Yokoyama, M. *Adv. Mater.* **2007**, *19*, 1864–1868; c) van Breemen, A. J. J. M.; Herwig, P. T.; Chlon, C. H. T.; Sweelssen, J.; Schoo, H. F. M.; Setayesh, S.; Hardeman, W. M.; Martin, C. A.; de Leeuw, D. M.; Valeton, J. J. P.; Bastiaansen, C. W. M.; Broer, D. J.; Popa-Merticaru, A. R.; Meskers, S. C. J.; *J. Am. Chem. Soc*. **2006**, *128*, 2336-2345]

[30] Only the plastic crystalline phase was observed over a broad temperature range. Examples see : a) Pisula, W.; Tomović, Ž.; Watson, M. D.; Müllen, K.; Kussmann, J.; Ochsenfeld, C.; Metzroth, T.; Gauss, J.; *J. Phys. Chem. B.* **2007**, *111*, 7481; b) Feng, X.; Pisula, W.; Müllen, K.; *J. Am. Chem. Soc*. **2007**, *129*, 14116-14117.

[31] Yang, X.; Loos, J.; *Macromolecules*. **2007**, *40*, 1353-1362.

[32] Feng, X.; Wu, J.; Ai, M.; Pisula, W.; Zhi, L.; Rabe, J. P.; Müllen, K. *Angew. Chem*. **2007**, *119*, 3093-3096; *Angew. Chem. Int. Ed*. **2007**, *46*, 3033-3036.

[33] Huo, S. *Org. Lett.* **2003**, *5*, 423-425.

[34] Simpson, C. PhD thesis, Mainz University, **2004**. The ^{1}H NMR characterizations of large PAHs are so far only available for the carbon number within 60.

[35] The intensity of the α-band is too low to be detected. However, the β-band at 391 nm and the p-band as the shoulder at 440 nm are clearly resolved and show a significant bathochromic shift with respect to the hexa-*peri*-hexabenzocoronenes (the

β-band at 360 nm).

[36] a) Peet, J.; Kim, J. Y.; Coates, N. E.; Ma, W. L.; Moses, D.; Heeger, A. J.; Bazan, G. C. *Nature. Mater.* **2007**, *6*, 497-500. See recent reviews: b) Thompson, B. C.; Frechet, J. M. J. *Angew. Chem. Int. Ed.* **2008**, *47*, 58–77; c) Lloyd, M. T.; Anthony, J. E.; Malliaras, G. G. *Materials Today* **2007**, *10*, 34; d) Brabec, C. J.; Sariciftci, N. S.; Hummelen, J. C. *Adv. Funct. Mater.* **2001**, *11*, 15-26.

Chapter 5. Controlling the Helical and Staggered Stacking of Nanographenes

In 1994, it was reported that hexa-hexylthioether substituted triphenylenes with helical organization showed the highest charge carrier mobility in all triphenylene discotics.[1] It is expected that the helical self-organization for hexa-*peri*-hexabenzocoronenes (HBCs) and other large discotics will also be favorable for the charge carrier transport.[2] However, the question to which extent the nature of the stacking behavior between two intracolumnar discotic molecules has not yet been answered. Theoretical studies predict that the face-to-face stacking of triphenylenes leads to the highest charge carrier mobility, whereas the staggered stacking (60^o rotation) will be detrimental.[3] On the other hand, for the HBC systems, the staggered stacking (30^o rotation) will be detrimental for the charge transport, whereas the face-to-face stacking is beneficial.[3] Therefore, a conceptual challenge is initiated to understand and manipulate the intermolecular packing of discotic system consisting of extended polycyclic aromatic hydrocarbons.

Hereby, for the first time in this chapter we will illustrate the introduction of two "zig/zag" peripheries into the HBCs. The so formed D_2 symmetric bizigzagHBCs not only reveal interesting electronic properties with respect to benzenoid HBC molecules, but also allow a facile control of supramolecular organization from helical stacking to the staggered stacking of discs.

For another system, we have presented in the last chapter that the trizigzagHBC derivative (**4-10**) exhibits a highly ordered helical superstructure with every three molecules in one helical pitch, corresponding to a 40^o rotation for each disc molecules. By applying a supramolecular chemistry approach, we will demonstrate here the introduction of alternating hydrophilic/hydrophobic substituents in the same system. Thereby weak non-covalent interactions will significantly influence the supramolecular organization in the bulk with highly regularly staggered stacking, which corresponds to 60^o rotation for every two molecules. In cooperation with the group of Prof. Kremer group for the theoretical simulations, it was possible to confirm

that this self-organization is dynamically favourable and predicted that this packing should lead to the highest charge carrier mobility for all discotics already known, with even one order higher than that of HBCs.

5.1 From Helical to Staggered Stacking of Biszigzag Nanographenes

5.1.1 Introduction

Discotic liquid crystalline materials with high one-dimensional charge carrier mobility along columnar superstructures show potential as active components in organic electronics,[4,5] whereby the control of their molecular packing and long-range organization through the design of the building block represents a prime concern for the performance in devices.[6] It has been shown for triphenylene derivatives that a helical arrangement of discotic molecules results in a significantly improved intracolumnar packing and in high mobility of charge carriers.[1,7]

Recently, we have described the introduction of alkyl-substituted phenyl groups on the periphery of hexa-*peri*-hexabenzocoronenes (HBCs) and C_3 symmetric zigzag nanographenes leading to the formation of helical self-assembly of the molecules accompanied with considerable mesophase stability over an extremely broad temperature range.[2,8] The intracolumnar arrangement of these extended PAHs could be related to the symmetry and substitution of the aromatic cores yielding a helical pitch with three building blocks. However, a strategy to control the helical packing within columnar structures by the substitution pattern of PAHs has not been reported so far. Herein, we introduce novel dodecyl-phenyl substituted D_2 symmetric zigzag nanographenes (dibenzo[*hi,uv*]phenanthro-[3,4,5,6-*bcdef*]-ovalene, **dizigzagHBC 5-1**)[9] which open the opportunity to manipulate the packing of discs. For the first time a modification of the supramolecular organization from helical stacking to a staggered superstructure has been observed simply upon changing the substitution pattern.

5.1.2 Synthesis and structure characterizations

M. Kastler in the Müllen group has demonstrated the synthesis of a variety of zigzagHBC derivatives including the alkyl-substituted dizigzagHBC,[9] however the necessary alkylphenyl substituents at the periphery which are expected to induce the helical organization is restricted by his synthetic route. Therefore, the concept here is to synthesize title dizigzagHBC derivatives by using the similar strategy as for trizigzagHBCs which was described in Chapter 4, where two phenanthrene units should be introduced properly in this case and can undergo a intramolecular ring-fusion under the cyclodehydrogenation conditions.

The detailed synthetic route towards **5-1** is outlined in Scheme 1. The key building blocks **5-5** were synthesized via three steps from **5-2** followed by Suzuki coupling, trimethylsiyl-iodide exchange and another regioselective Suzuki coupling in good yields, and allowed the synthesis of different 1,4-bis-2'-diaryl-2,5-diphenylbenzene precursors.[10]. A subsequent Suzuki coupling afforded **5-6** in good yields, whereby various substituents R_2 could be introduced in this step. Afterwards, ICl induced ring cyclization under mild conditions provided precursors **5-7** with two phenanthrene units and iodo substituents in high yields.[11] Further Suzuki coupling yielded precursors **5-8** in good yields. The final cyclodehydrogenation were performed with appropriate $FeCl_3$ to give **5-1** with two "zig/zag" edges. It should be noticed here that the additional cyclodehydrogenation did not occur between the periphery phenyl groups even under extended reaction time or UV irradiation due to the higher oxidation potentials. All compounds, **5-1a**, **5-1b** and **5-1c**, are well soluble in common organic solvents including THF, dichloromethane, toluene and can thus be purified by column chromatography.

Similar to the versatile synthesis of trizigzagHBC as described in Chapter 4, it should be mentioned here that the present strategy for dizigzagHBC should also allow the introduction of various functional groups as well as different substitution fashions. For example, precursors **5-7** can also be transformed into corresponding dizigzagHBC derivatives via the oxidative cyclodehydrogenation, where the functional iodide groups bear the feasibility for a variety of metal-catalyzed coupling reactions.

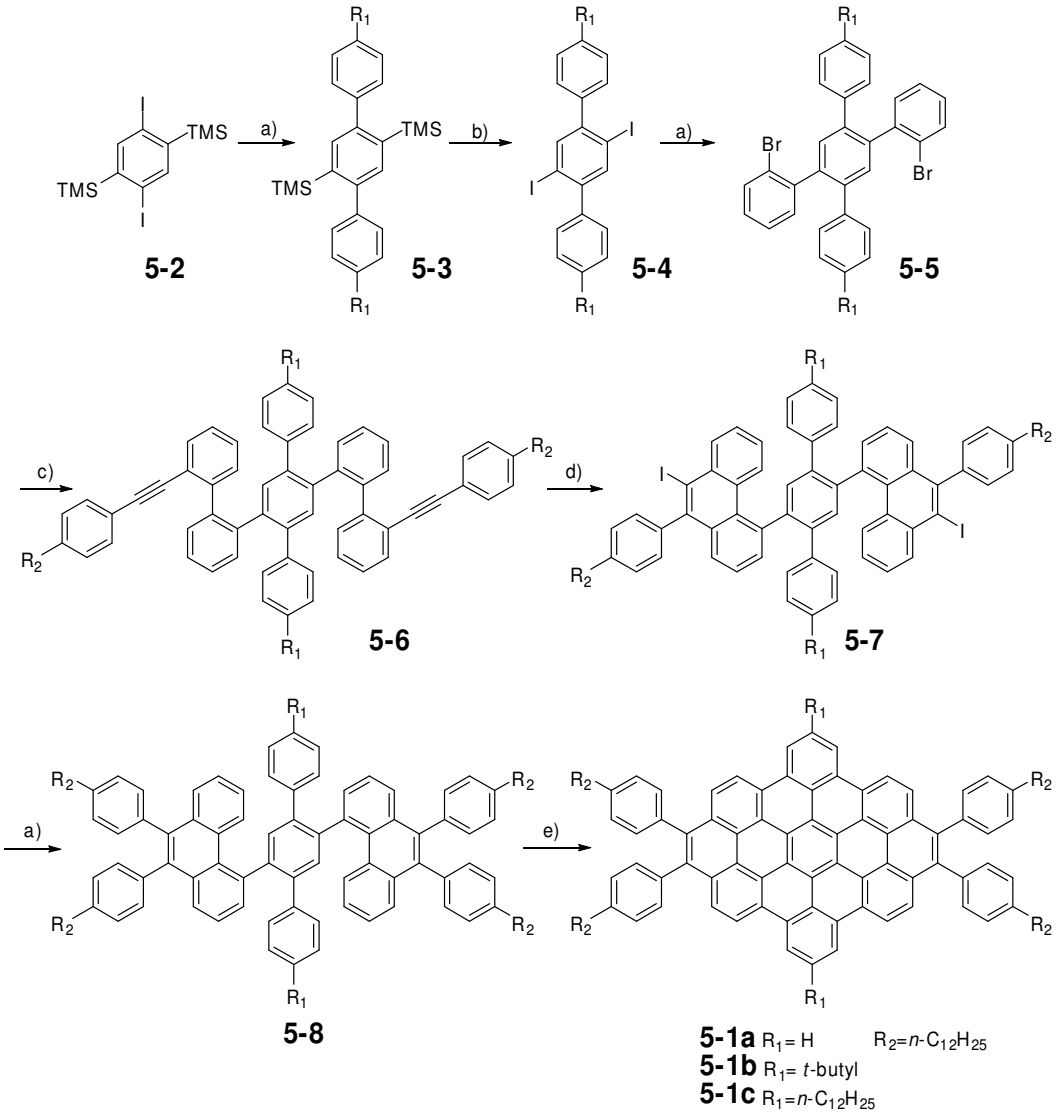

[a] Conditions: (a) Aryl boronic acid, $Pd(PPh_3)_4$, THF, K_2CO_3, EtOH, H_2O, reflux, 84% for **5-3a**, 92% for **5-3b**, 79% for **5-3c**, 80% for **5-5a**, 81% for **5-5b**, 90% for **5-5c**, 89% for **5-8a**, 91% for **5-8b**, 76% for **5-8c**; (b) ICl, $CHCl_3$, 95% for **5-4a**, 92% for **5-4b**, 91% for **5-4c**; (c) Aryl boronic acid, $Pd(PPh_3)_4$, Toluene, K_2CO_3, EtOH, H_2O, reflux, 83% for **5-6a**, 85% for **5-6b**, 76% for **5-6c**; (d) ICl, CH_2Cl_2, -78 °C, 86% for **5-7a**, 91% for **5-7b**, 86% for **5-7c**; (e) $FeCl_3$, CH_3NO_2, CH_2Cl_2, 66% for **5-1a**, 87% for **5-1b**, 37% for **5-1c**.

Scheme 5-1. Synthetic strategy towards **5-1**.

MALDI-TOF MS (TCNQ matrix) of **5-1a**—**5-1c**, using a solid-state sample preparation revealed single species with isotopic distribution, which were in accordance with the calculations. UV-vis absorption spectra of **5-1a**—**5-1c** were measured in chloroform (1.0×10^{-6} M) and exhibited essentially similar structured spectra with three types of bands (α, β, γ), and with absorption maxima at 394 nm, 396 nm and 397 nm respectively, which were significantly bathochromically shifted compared to HBCs (Figure 5-1). The reduction of symmetry in comparison to HBCs allowed the 0-0 transitions for **5-1a**—**5-1c**, where the α bands were significantly intensified. The Stokes shift was in all cases small (< 7 nm) and independent of the used solvents.

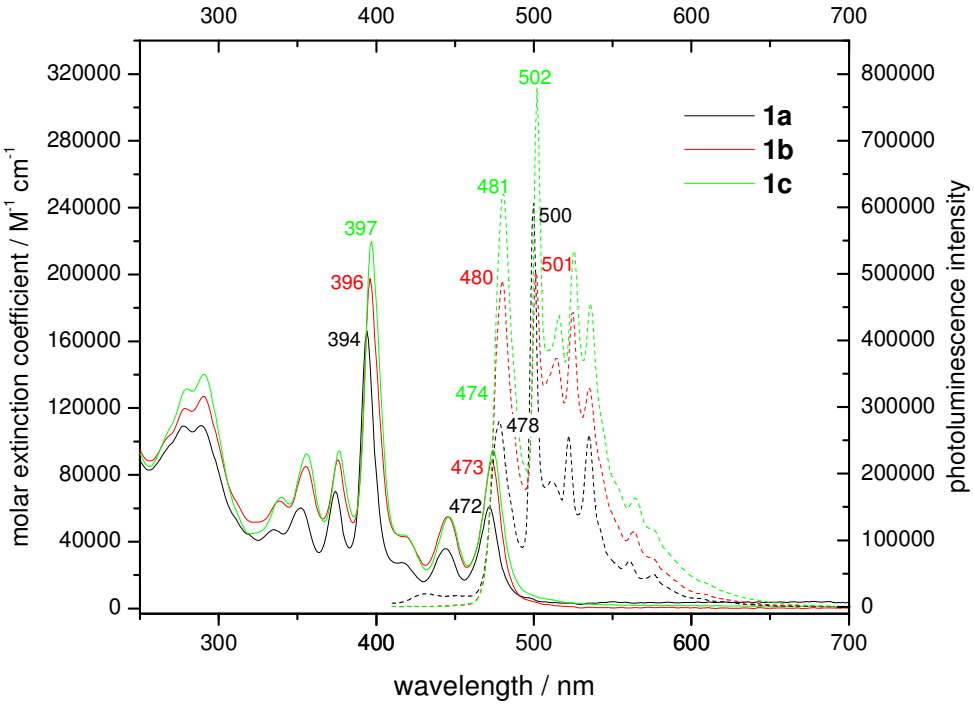

Figure 5-1. UV-vis and photoluminescence spectra of **5-1a** (black), **5-1b** (red) and **5-1c** (green) (1.0×10^{-6}M in $CHCl_3$).

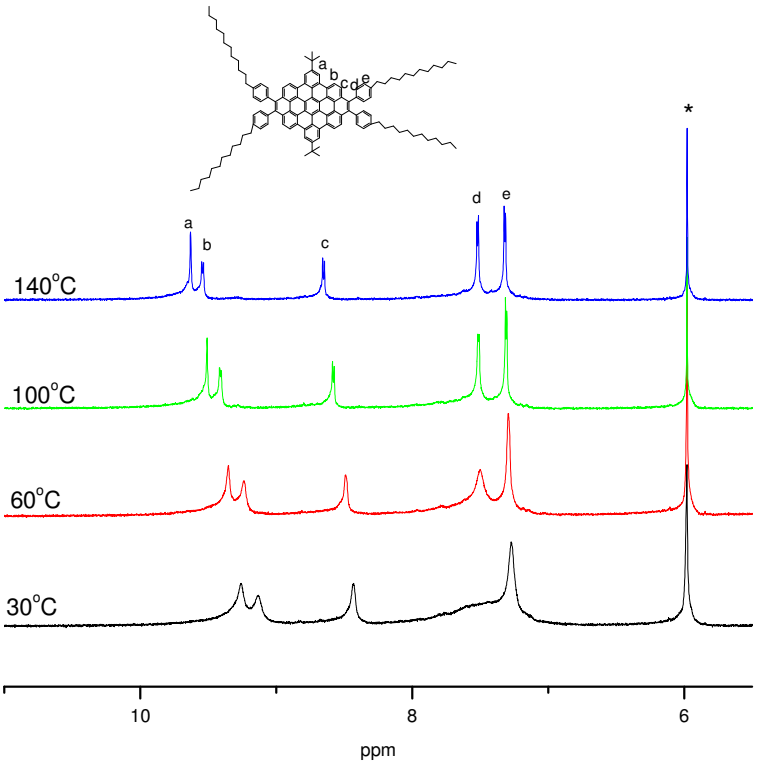

Figure 5-2. Temperature-dependant ^{1}H NMR (500MHz) spectra of **5-1b** in *d*-$CD_2Cl_2CD_2Cl_2$.

The ^{1}H NMR spectra of **5-1b** at different temperatures together with signal assignments are shown in Figure 5-2. Similar to the self-association behavior of trizigzagHBC derivative **4-10** as reflected in the last chapter, at low temperatures, the ^{1}H NMR signals are broadened into the baseline due to pronounced aggregation effects. With increasing of temperature, the resolution of the spectra enhances remarkably. The signals of the phenyl protons, exhibit obviously temperature-dependant line broadening, which was more pronounced for the signal of the *ortho* protons close to the core. This effect suggested that an intramolecular rotation of the phenyl rings around the neighbouring single bond and an interlocking between these pendant phenyl rings occurred.

5.1.3 Self-organization in the bulk

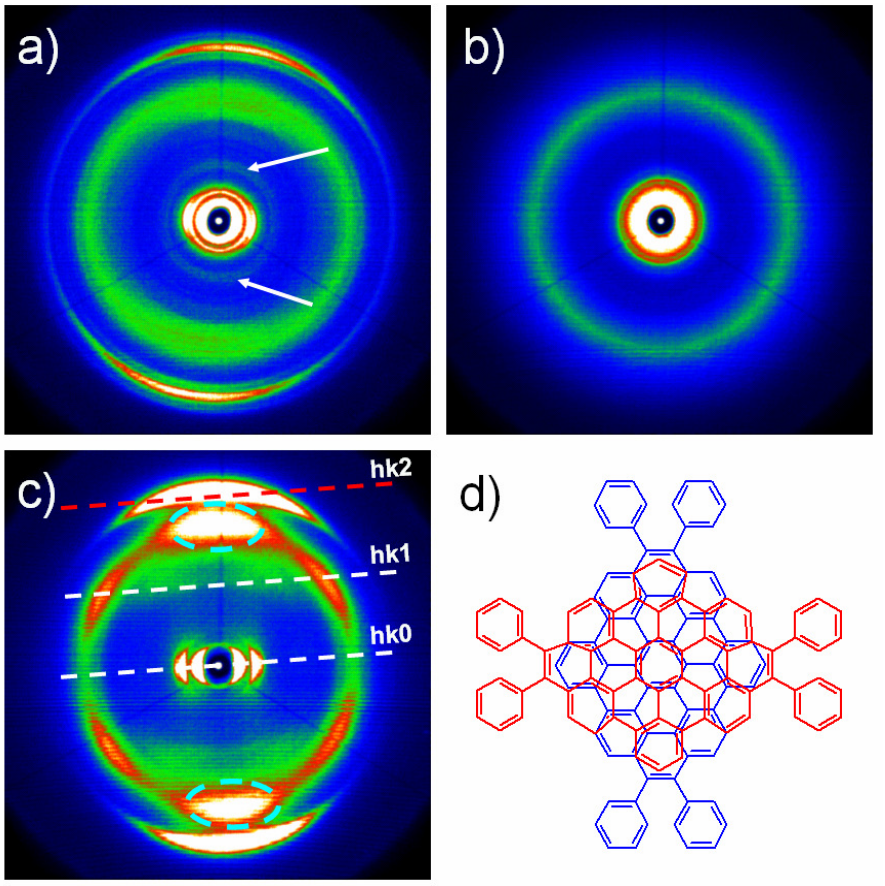

Figure 5-3. 2D-WAXS patterns of a) **5-1a** (arrows indicate intracolumnar periods of 1 nm), b) **5-1b**, c) **5-1c** (Miller's indices for the intracolumnar stacking and the higher order reflections are indicated) and d) illustration of the rotation assigned for **5-1c**.

In cooperation with W. Pisula in the Müllen group for the thermal and self-organization studies. Differential scanning calorimetry (DSC) measurements of **5-1a**—**5-1c** revealed phase transitions in the temperature range of -150 °C to 220 °C, and TGA proved a pronounced thermal stability up to 400 °C, which could be related to the enhanced supramolecular organization which will be discussed in the following. Two-dimensional wide-angle X-ray scattering (2D-WAXS) experiments on extruded fibers[12] of the three derivatives **5-1a**—**5-1c** showed no significant changes of the organization at the phase transitions. However, strong differences in the supramolecular order among the three compounds were indicated by reflections of varying intensity and shape (Figure 5-3). It could be concluded that **5-1a** and **5-1c**

self-assemble into hexagonal columnar structures over the whole temperature range and are well aligned in the extrusion direction of the sample, characterized by distinct equatorial scattering intensities (Figures 5-3 a,c). The hexagonal unit cell parameters are slightly dependent on the molecular design and the corresponding temperature (Table 5-1). In both cases, **5-1a** and **5-1c**, two meridional wide-angle high intensity

Table 5-1. Phase transitions of **5-1a**, **5-b** and **5-1c** determined by DSC and unit cells for **5-1a** and **5-1c**.

compound	2nd heating	Cooling	hexagonal unit cell parameter
5-1a	16 °C (8.4 J/g)	10 °C (8.6 J/g)	3.91 nm
	111 °C (5.4 J/g)	99 °C (6.4 J/g)	4.59 nm
5-1b	8 °C (2.0 J/g)	-8 °C (1.9 J/g)	-
5-1c	14 °C (10 J/g)	4 °C (11.2 J/g)	3.27 nm
	108 °C (1.6 J/g)	96 °C (2.0 J/g)	3.36 nm

reflections were attributed to a face-to-face π-stacking distance of 0.35 nm between individual ovalenes, whereby their molecular planes are arranged perpendicularly to the columnar axis. Additional meridional and off-meridional reflections at different positions for **5-1a** and **5-1c** implied significant variations in the intracolumnar arrangement of the molecules. For **5-1a**, meridional reflections related to a further intracolumnar period of 1 nm and thus between every 4th unit suggested a helical packing with a molecular rotation of 60° (Figure 5-3a).[8] A similar organization has already been experimentally observed for hexaphenyl HBCs and C_3 symmetric zigzag nanographenes and confirmed by quantum-chemical calculations.[13] In sharp contrast, compound **5-1c** revealed a staggered packing characterized by off-meridional reflections corresponding to a period of 0.72 nm, being twice the stacking distance and leading to a correlation of every second molecule along the columns (Figure 5-3c). Figure 1d illustrates that this molecular packing is in good accordance with the ovalene architecture of **5-1c**. The lateral rotation of the ovalenes by 90° to each other is initiated not only by the hindrance of the phenyl rings at the aromatic core as for

5-1a, but intriguingly enough, additionally by the introduction of alkyl side chains at the *para* position. The different lateral rotation angle of the molecules **5-1a** and **5-1c** is attributed to a different filling of the peripheral space by side chains. Since compound **5-1a** carries only four alkyl substituents in comparison to **5-1c** with six chains, the resulting rotation of **5-1a** is smaller to fill the peripheral space by the attached phenyls. The additional 2D-WAXS patterns of **5-1a** and **5-1c** at the high temperatures and with the respective Miller indexes are shown in Figure 5-4 and Figure 5-5.

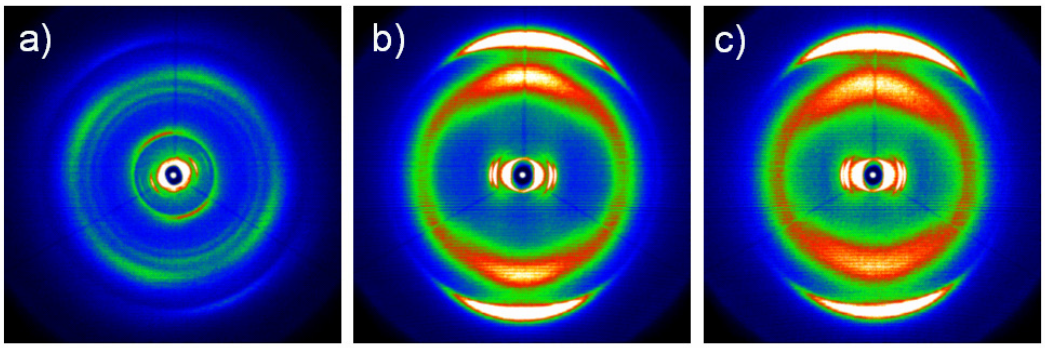

Figure 5-4. 2D-WAXS patterns of a) **5-1a** at 180 °C, and **5-1c** at b) 30 °C and c) at 160 °C.

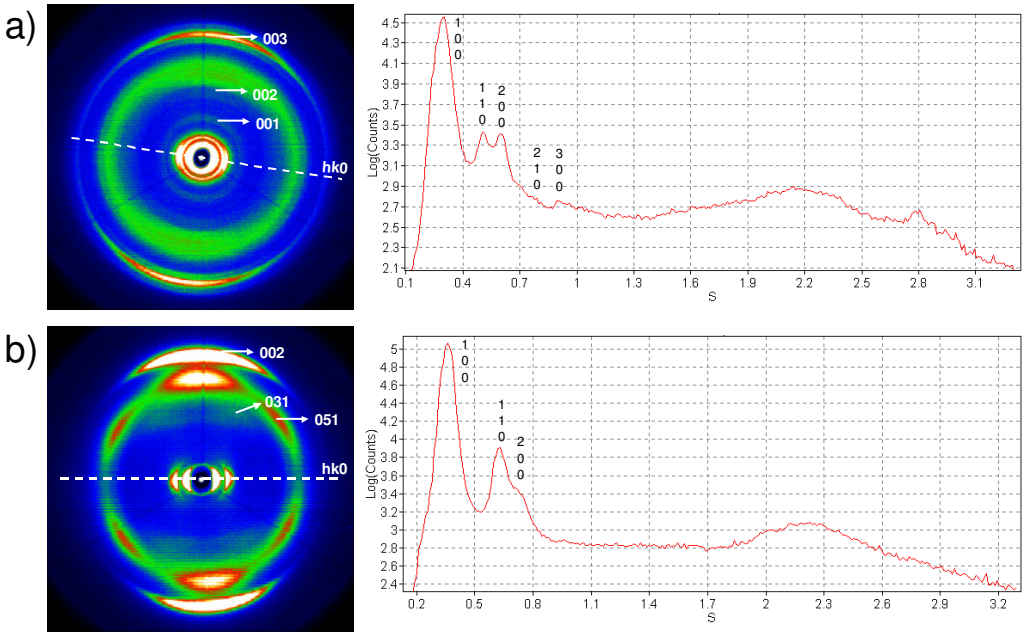

Figure 5-5. Indexed 2D-WAXS patterns of a) **5-1a** and b) **5-1c.**

Cooling samples of **5-1c** to low temperatures (-100 °C) resulted in a higher supramolecular order as expressed by a higher intensity of the reflections and the appearance of new doublet reflections at a scattering vector s=2.32 nm^{-1} (Figure 5-3c), which have been also observed for discotic triphenylenes with a similar staggered packing and a plastic crystalline phase.[14] We assigned **5-1a** and **5-1c** also as plastic crystalline over the whole temperature range attributable to their waxy/soft state and their above described exceptional three-dimensional organization, which can be clearly distinguished from a typical crystalline and disordered liquid crystalline phase. On the other hand, poor order was observed only for **5-1b** caused by the *t*-butyl groups hindering a stacking of the molecules (Figure 5-3b). The weak interaction between the building blocks of **5-1b** was also reflected by the isotropization temperature (T_i) of 320 °C. This stood in contrast to **5-1a** and **5-1c** which failed to show a T_i up to 500 °C, thus reflecting the strongly improved stability of the mesophase over a broad temperature range due to helical packing. It should be noted that birefringence in the polarized optical microscopy and the isotropic small-angle reflection implied columnar structures for **5-1b** which are, however, established only over short-range, whereby **5-1a** and **5-1c** exhibited self-assembly over long-range.

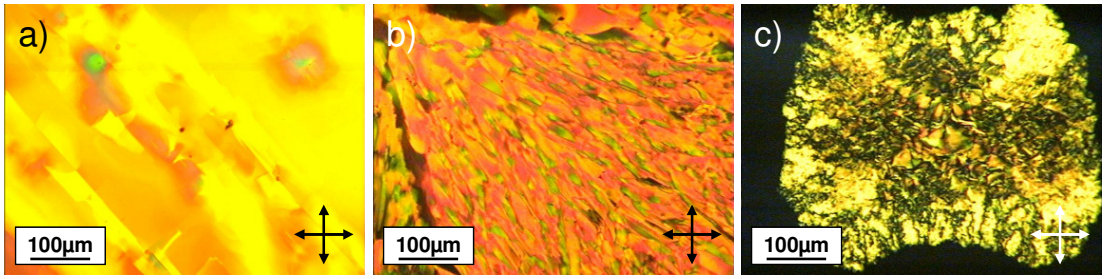

Figure 5-6. Polarized optical microscopy images of **5-1b** cooled from the isotropic phase by a) 0.1 °C/min, b) 1 °C/min and c) 10 °C/min.

5.1.4 Conclusion

In conclusion, we have developed a synthetic protocol yielding the novel D_2 symmetric zigzag nanographenes, and allowing a specific substitution of the ovalene corona. The latter appeared as a key feature to modify the intracolumnar arrangement in a facile way. It thus became possible to modify the supramolecular organization of

an extended PAH from helical to a unique staggered superstructure. For example in the future, one may consider to intentionally introducing additional non-covalent forces such as hydrogen-bonding and hydrophilic-hydrophobic interactions in one PAH system to manipulate the stacking behavior from a supramolecular chemistry approach. It is expected that the variation of the molecular packing for one system is accompanied by a different performance in electronic devices.[3]

5.2 Rational Design of the Shape and Periphery of Discotic Liquid Crystals: a synthetic way towards high charge carrier mobilities

5.2.1 Introduction

Discotic thermotropic liquid crystals combine unique material properties, such as fluidity and inability to support shear stress with anisotropic mechanical and optical properties.[15] This combination is a consequence of the molecular self-organization into columnar structures, where the molecules stack on top of each other into columns which then arrange in a regular lattice. The anisotropy of macroscopic properties arises from the anisotropy of the molecules, in our case flat aromatic cores with aliphatic chains attached at the edges, and the global orientational ordering of molecules.

The most striking property of discotics, however, is their ability to conduct charges along the stacks of aromatic cores, which can be used in various organic devices, such as field-effect transistors[4b,5b] and photovoltaic cells.[16-17] To guarantee efficient operation, high charge mobilities along the columns are required.[18] To achieve high mobilities, two distinct but related problems must be addressed: first, compounds must have good self-organizing abilities, which would guarantee defect-free mesophases on a large spatial scale. Second, the local molecular arrangement in these mesophases has to be optimal for the charge transport.

Hence, to rationally design these compounds, one has to (i) identify the best local molecular arrangement of all (synthesizable) aromatic cores (ii) manipulate the

periphery (side chains) to achieve this arrangement and at the same time to obtain good self-organizing abilities.

We will first discuss the optimal choice of local molecular arrangements for charge transport. Charge transport in discotic liquid crystals can be described using a hopping formalism and the rate for hops can be described within semiclassical non-adiabatic high-temperature Marcus theory. The higher this rate, the faster an electron (hole) moves along the column, and the higher is the corresponding mobility. According to Marcus' theory the transfer rate ω depends on two key parameters: the reorganization energy λ and the transfer integral J.[19,20]

$$\omega = \frac{J^2}{\hbar}\sqrt{\frac{\pi}{\lambda kT}}\exp\left[-\frac{\lambda}{4kT}\right].$$

Here $\hbar$ is Planck's constant, k Boltzmann's constant and T the temperature.

The reorganization energy λ is strongly related to the self trapping energy of a charge and decreases with the increase of the size of the conjugated core[21] and is not sensitive to the relative positions/orientations of neighboring molecules.[3b,21] Larger conjugated cores favor higher hopping rates and hence higher charge carrier mobilities.[22]

The transfer integral J describes the strength of the interaction between two neighboring molecules. Since it is intimately related to molecular overlap, it is very sensitive to relative positions and orientations of neighboring molecules. J decays exponentially as a function of intermolecular separation (for example for HBC this dependence is $J \sim \exp\left(-2.2z/\mathring{\mathrm{A}}\right)$). Hence, compounds with smaller intermolecular distance should have higher charge mobility. The azimuthal angle dependence of the transfer integral is shown in Figure 5-7 for a set of symmetric cores. It is clear that the most favorable for the charge transport molecular alignment is either a co-facial (0 deg twist) or 60 deg twisted one (except triphenylene, for the coronene and HBC, the 60 deg twisting has the same conformation as 0 deg; see the illustration in Chart 5-1). In addition, the maxima of the overlap integral (at 0 and 60 deg) decrease with the

increase of the core size and the value of the transfer integral decreases very rapidly with the angle, e.g. for a 10 deg twist the value is two times smaller than for 0 deg.

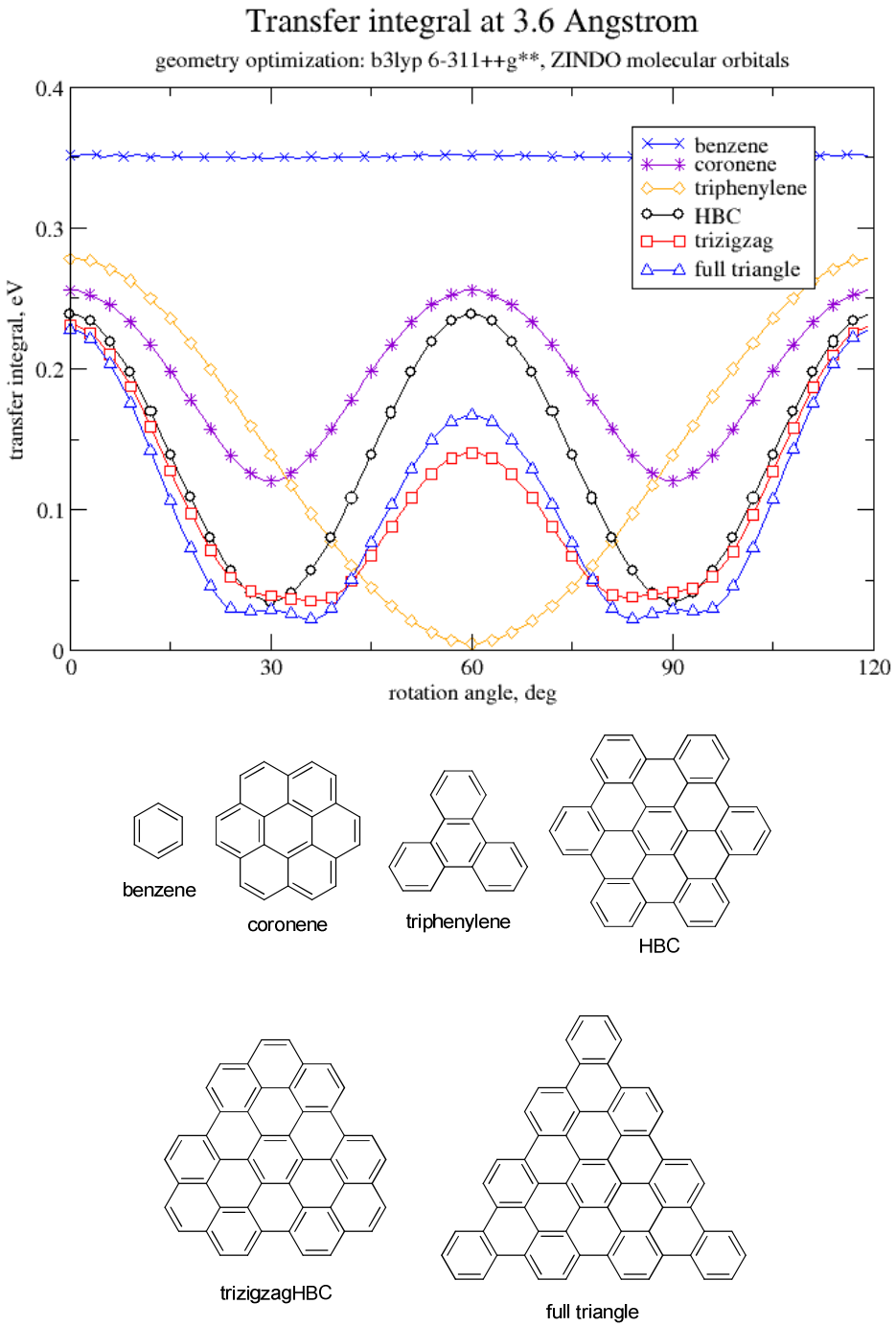

Figure 5-7. Absolute value of the transfer integral *J* as a function of the azimuthal rotation angle.

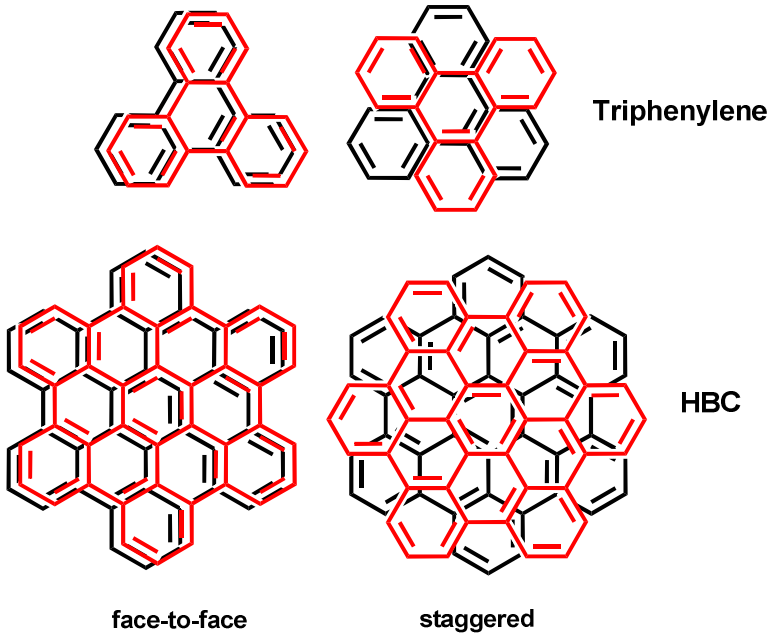

Chart 5-1. Illustration of the face-to-face and staggered stacking of two typical discotic molecules: triphenylene (staggered twisting angle is 60^{o}); HBC (staggered twisting angle is 30^{o}).

Summarizing the predictions of the Marcus' theory, we can narrow down the tasks of the side chains on large discotic systems (except triphenylene): apart from providing good self-assembling properties they should (i) favor small intermolecular separation with good π-stacking interactions and (ii) provide either a face-to-face or 60 degrees twist molecular arrangement. The face-to-face arrangement, however, will result in a steric repulsion of the side chains and lead to larger intermolecular separations as well as widening of the distribution of transfer integrals, which will decrease the mobility. Naturally, compounds with the six-fold symmetry (e.g. HBC with alkane side chains) are in a face-to face arrangement for both 0 and 60 deg twist between the neighbors, and have the same drawbacks. Hence, our conclusion is that, among these class of compounds, molecules of threefold symmetry (e.g. triangularly-shaped PAH) with a *helical packing structure* and 60 degrees twist provide optimal local arrangement for the charge transfer.

To achieve helical molecular packing, one can borrow the examples from nature, where the helical organization can be found in the double helices formed by DNA and

the α-helical motives in proteins.[23] Theses biopolymers adopt helical conformations spontaneously, because of the molecular information present in their building blocks, and have already inspired an extensive amount of work on synthetic helical nanostructures.[24]

Nature exploits a great variety of interactions to control the self-organization, from steric repulsion, hydrogen bonding, van der Waals forces, π-π stacking, and electrostatic interactions.[25] A minor change in the molecular architecture may dramatically influence the subtle balance of non-covalent interactions between molecules.[26] In the case of polyaromatic hydrocarbons, one can vary the size and the shape of the conjugated core as well as the type of the attached side chains.[5a] By tuning these "molecular parameters" compounds with different ability to self-organize and conduct charge carriers can be obtained.[27,28]

In this work, we present a facile control of the helical to staggered stacking of large graphene-like discotics (**4-10** and **5-9**, Figure 5-8) within columnar assemblies. Semi-triangle shaped molecule **4-10** has been reported previously to show highly ordered helical superstructures including three molecules in one helical pitch, corresponding to the twist of 40° of the discs to each other.[8] On the other hand, for molecule **5-9** possessing a similar molecular structure but with alternating hydrophobic and hydrophilic substituents, staggered stacking with a twist of 60° has been achieved. This novel assembly is believed to be induced through complementary hydrophobic-hydrophilic and π-π interactions.

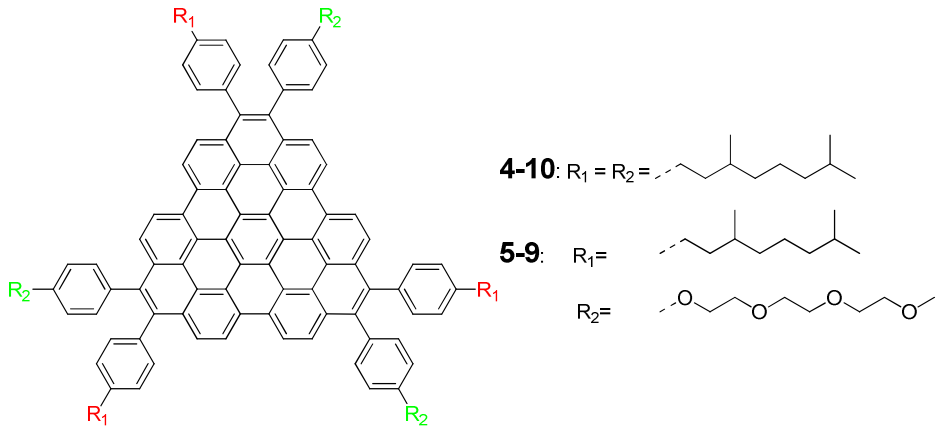

Figure 5-8. Structures of studied triangle-shaped discotics.

5.2.2 Synthesis and structure characterization

The synthetic route towards molecule **5-9** is outlined in Scheme 5-2. Precursor **4-18b** which has been described to allow the further functionalization in Chapter 4, by using the same strategy, Suzuki coupling of **4-18b** with 4-methoxyphenylboronic acid yielded **5-10** in 90% yield. Afterwards, BBr_3 mediated demethylation under mild conditions provided **5-11** in 82% yield. Subsequent reaction with (4-toluenesulfonyl)triethylene glycol monomethyl ether under the base afforded precursor **5-12** in 93% yield. Finally $FeCl_3$ mediated oxidative cyclodehydrogenation gave **5-9** as yellow solid in 72% yield. Compound **5-9** is soluble in normal organic solvents including THF, dichloromethane, chloroform and so on, thus can be purified by column chromatography.

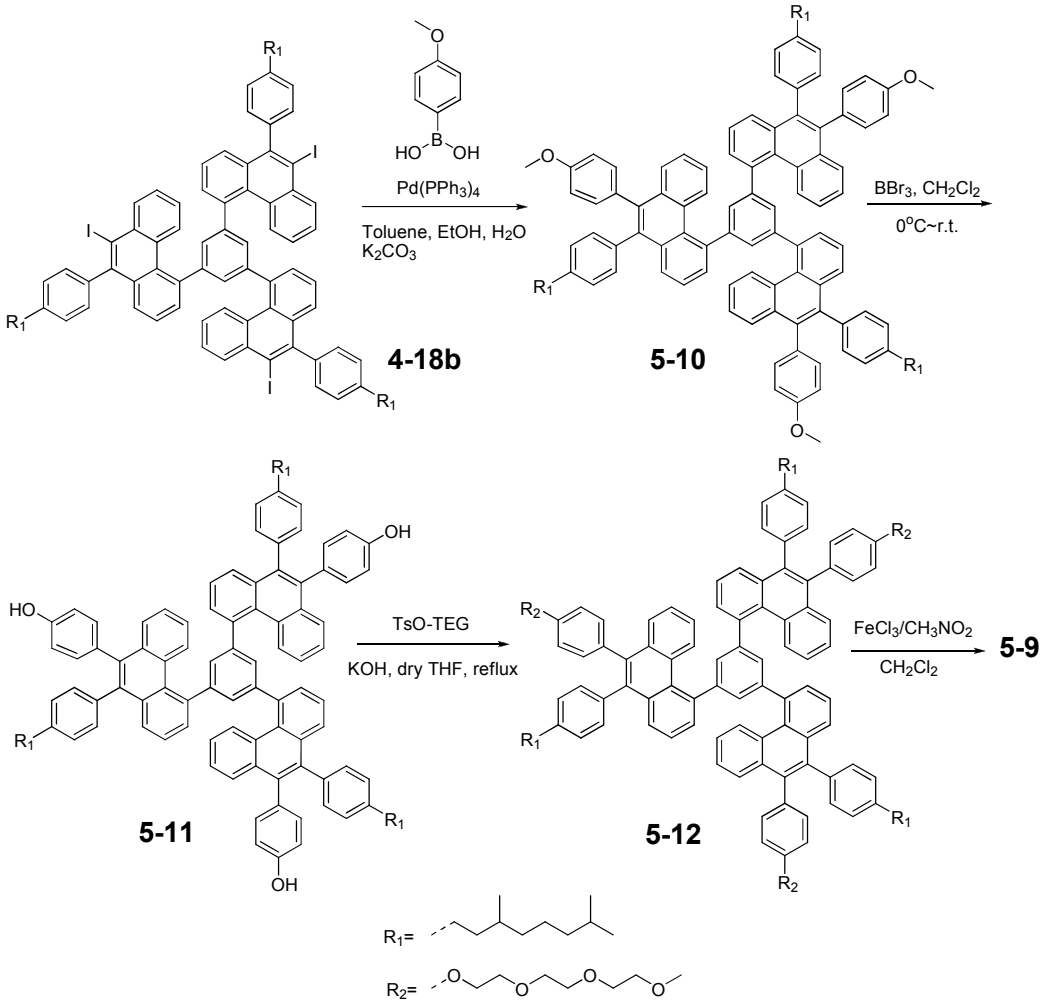

Scheme 5-2. Synthetic route towards **5-9**.

MALDI-TOF MS (TCNQ matrix) of **5-9** revealed single species with isotopic distribution, which was in accordance with calculations (Figure 5-9). Temperature dependant ^{1}H NMR further demonstrated the purity of compound (Figure 5-10). All the protons in the corona and substituted phenyl groups are indicated. Due to the molecular symmetry and different chemical environments, protons *e* and *f* could be identified at the low temperature by the different chemical shifts, whereas they merged in one signal at high temperature. Comparatively, protons *g* and *h* can not be identified at all temperatures due to the very similar chemical environments. With the increase of temperature, the proton signals of peripheral phenyl groups become remarkably resolved, whereas at low temperature the broadening of the signals into the baseline indicates the strong aggregation effects which are be presented in solution.

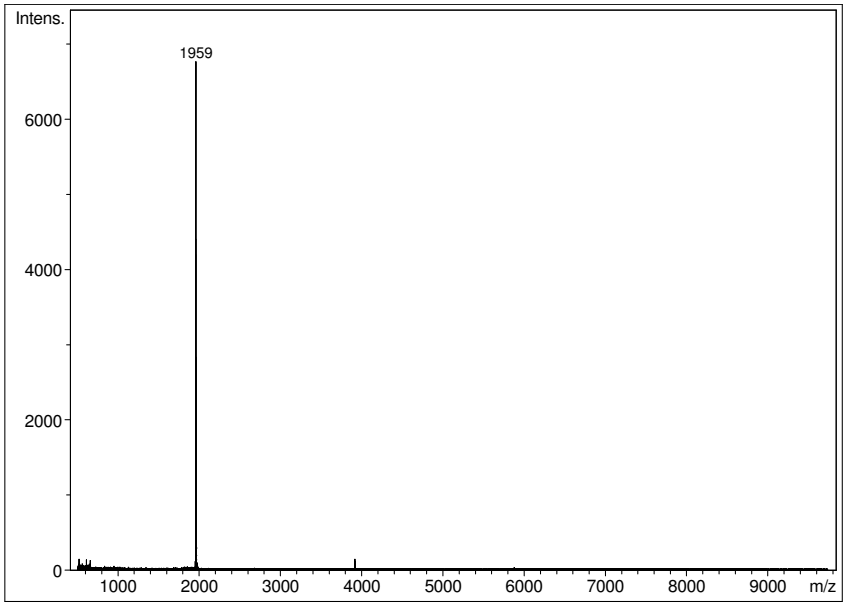

Figure 5-9. MALDI-TOF mass spectrum of **5-9.**

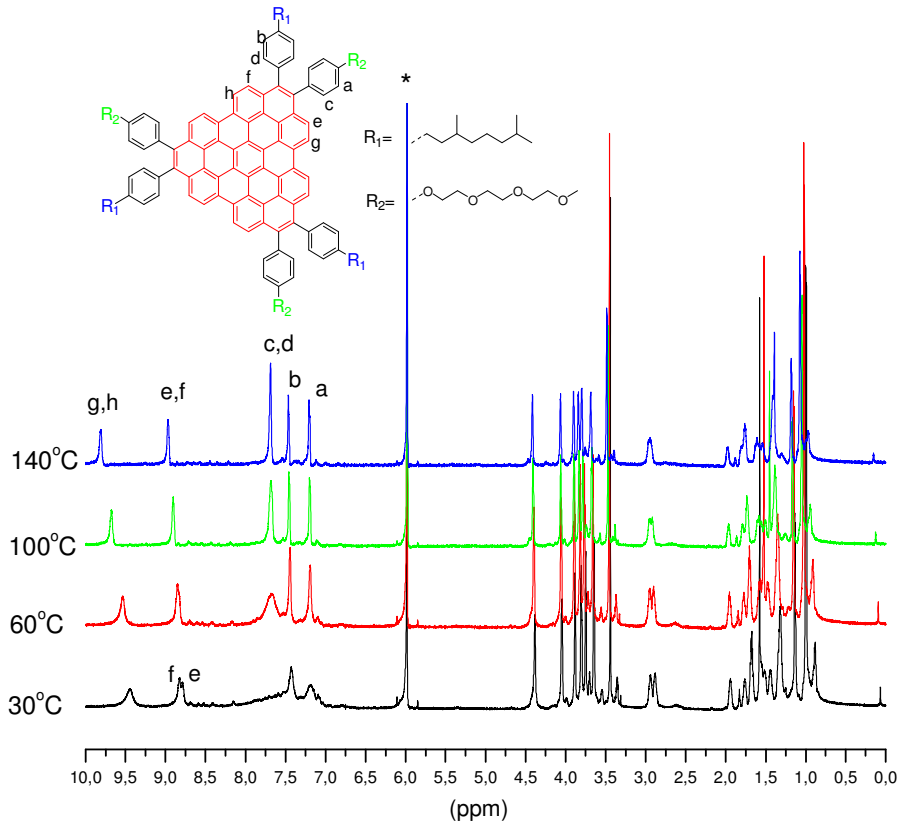

Figure 5-10. Temperature-dependent ^{1}H NMR (700 MHz) spectra of **5-9** in [D_2]tetrachloroethane(*).

5.2.3 Bulk chacterizations

In cooperation with W. Pisula in the Müllen group, two-dimensional wide-angle scattering X-ray scattering (2D-WAXS) experiments on mechanically aligned filaments were performed to gain an insight into the influence of the different substitution patterns on supramolecular organization of both compounds **4-10** and **5-9**.[12] The 2D patterns at 30 °C in Figures 5-11a and 5-11b indicate in both cases well oriented hexagonal columnar structures characterized by equatorial reflections at relative reciprocal spacing of $1:\sqrt{3}:2$ which are typical for liquid crystalline phases of discotic systems. The derived unit cell parameters are a_{hex} = 3.41 nm for **4-10** and a_{hex} = 3.19 for **5-9**. The disc-shaped molecules are arranged in the stacks with their molecular planes perpendicular to the columnar axis. The intracolumnar π-stacking distance of 0.36 nm for **4-10** and **5-9** is represented by the sharp wide-angle

meridional reflections. Furthermore, the appearance of additional meridional reflections in the middle-angle scattering range of both patterns suggests more complex superstructures. The first (off-)meridional reflections at a related distance of 1.1 nm (Figure 5-11a) indicate an identical lateral order of every 4^{th} molecule along the stacking direction. Therefore, every neighbouring two molecules in the column are rotated laterally by 40° towards each other leading to a helical stacking with 3 molecules per pitch. Figure 5-11a presents a schematic illustration of a top-viewed stack with three molecules of **4-10**. In contrast, the 2D pattern of compound **5-9** showed only one middle-angle reflection corresponding to a distance of 0.72 nm, which is the double value of a simple π-stacking distance (Figure 5-11b). The molecules of **5-9** perform a rotation of 60° leading to a staggered packing with every 2^{nd} disc in an identical position. The schematic illustration in Figure 5-11b displays that the substituents of same character of neighbouring discs fall together at this rotational angle. The smaller rotational angle for **4-10** in comparison to **5-9** results in a denser alkyl mantle around the aromatic stack and thus in a larger hexagonal unit cell. Therefore, considering their similar molecular structures and substitution pattern, the difference in intracolumnar packing between **4-10** and **5-9** can only be explained in terms of the hydrophobic/hydrophilic interactions of the side chains in the disc periphery which favor the staggered stacking of **5-9**. On the other hand, X-ray measurements of **4-10** at high temperatures indicate that the disc symmetry and the bulky phenyl substituents play also an additional role. The pattern in Figure 5-11c recorded at 180 °C shows a similar staggered packing for **4-10** as observed for **5-9** at ambient conditions. This is quite surprising, since **4-10** does not bear hydrophilic/hydrophobic interactions in the periphery. Therefore, it is assumed that the staggered packing of **5-9** at high molecular dynamic is due to increased steric hindrance of the attached phenyl groups. On heating, the flexible alkylphenyl chains with higher thermal motion relative to that of rigid discs require a larger interfacial area to reduced enhanced space crowding in the flexible domains. This spatial requirement enforces the stacked discs of **4-10** to be more rotated to each other with a larger twist angle. Therefore, the staggered stacking with the largest twisting angle of

60° is dynamically more favorable. This is further confirmed by the simulations of both molecules **4-10** and **5-9**.

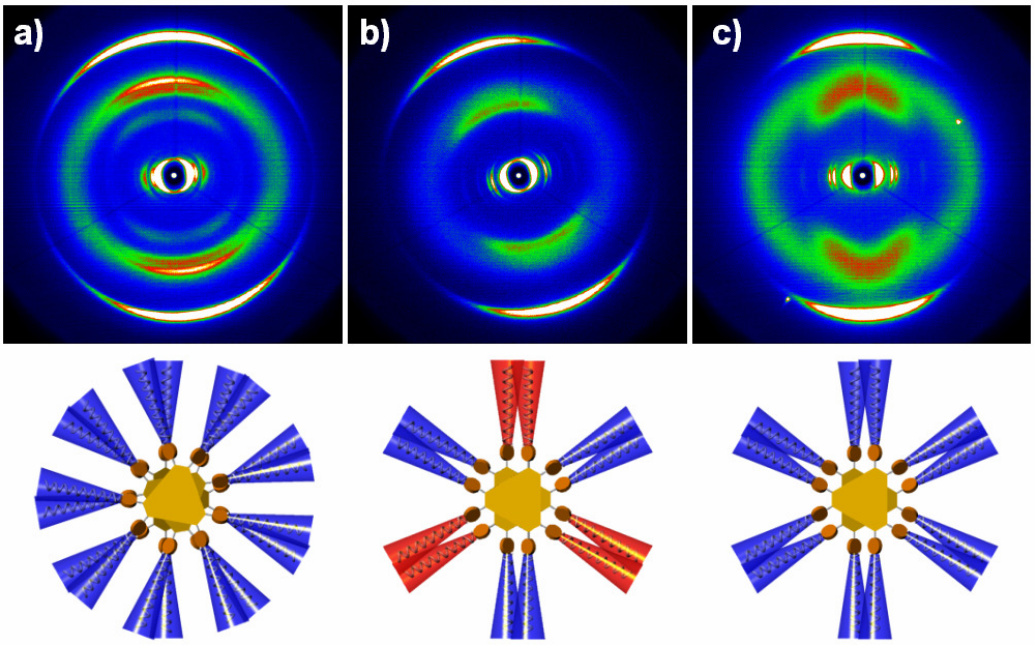

Figure 5-11 2D-WAXS patterns and corresponding schematic illustrations of top-viewed molecules stacked on top of each other, a) **4-10**, b) **5-9** (both patterns recorded at 30 °C) and c) **4-10** at 180 °C. Blue and red substituents indicate alkyl and glycol chains respectively.

5.2.4 Computer simulations

In cooperation with V. Marcon and D. Andrienko in the Prof. Kremer group, computer simulations of molecular organizations and charge carrier transport were investigated in detail as described below.

960 molecules were arranged in columns of sixty molecules each, with hexagonal arrangement of the columns. Within the columns, the molecules were aligned in a helical fashion, with initial twist angles of 0, 30, 40, and 60 deg between the neighboring molecules.

5.2.4.1 Molecular model and simulation details

We adopt the OPLS-united atom approach for the side chains and consider explicitly only the hydrogen atoms belonging to the aromatic rings of the central core.[29-31] The

initial distances between the columns and between the molecules in the columns were slightly increased to avoid site superposition. After the energy minimization, a 4 ns equilibrating run was performed at a constant pressure P = 0.1 MPa and temperature T = 200 K using the method of Berendsen et al.[32] with anisotropic pressure coupling. The simulation box angles were fixed at 90°. The electrostatic interactions were treated with the smooth particle-mesh Ewald (PME) method, spacing for PME grid 0.12 nm, cutoff 0.9 nm. The time step of 2 fs was used to integrate equations of motion using the velocity Verlet algorithm with a 0.9 nm cutoff for short-range interactions. Bond lengths were constrained using the LINCS algorithm. All calculations were performed with the GROMACS program. The 40 ns production runs were performed at a constant pressure (P =0.1 Mpa) and temperature (T=400K) fixed using the method of Berendsen et al. with time constant 5 ps and compressibility 4.5×10^{-5} bar $^{-1}$ (both isotropic).

For charge transport, the internal part of the reorganization energy λ for the hole transport was calculated as:[33]

$$\lambda=E_{+}^{n}-E_{0}^{n}+E_{0}^{c}-E_{+}^{c},$$

where E_0^n and E_+^c represent the energies of the neutral and cation species in their lower energy geometries, while E_0^c and E_+^n represent the energies of the neutral and cation species with the geometries of the cation and neutral species, respectively. The geometry of a single molecule and its cation was optimized using B3LYP functional and 6-311g(d,p) basis set. Transfer integrals *J* where calculated using molecular orbital overlap method.[34]

The charge dynamics was simulated either using kinetic Monte Carlo technique, or master equation, with the charge transfer rates obtained from Marcus expression, as described in Refs.[35]

5.2.4.2 Results and discussion

We will first discuss the helical molecular ordering of the system. After equilibration we observed that the molecules are well-ordered within the columns, with their molecular planes oriented perpendicular to the columnar axes. Small undulations of

the columns were also observed, which is due to thermal fluctuations of the director. The representative snapshots of the studied systems are shown in Figure 5-12.

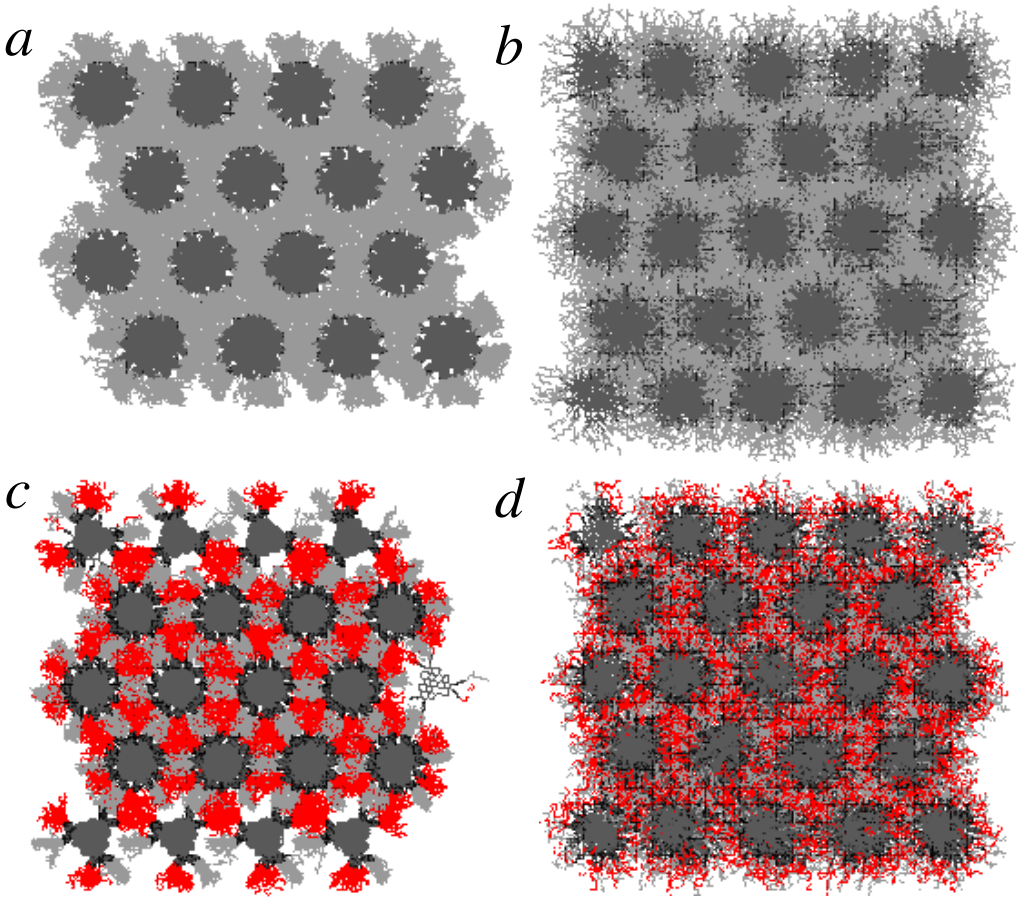

Figure 5-12. Representative simulation snapshots (top view). (a) and (b) alkane side chains (**4-10**), with 30 and 60 deg initial twist angle, correspondingly. (c) and (d) alkane and glycol side chains (**5-9**), with 30 and 60 deg initial twist angle. Glycol side chains are shown in red.

To quantify the degree of positional order in the systems, we calculated two distribution functions, $g_z(r)$ and $g_{xy}(r)$. $g_z(r)$ gives the distribution of distances between molecules in a column while $g_{xy}(r)$ provides information about the arrangement of the columns with respect to each other. Both distributions functions are shown in Figure 5-13.

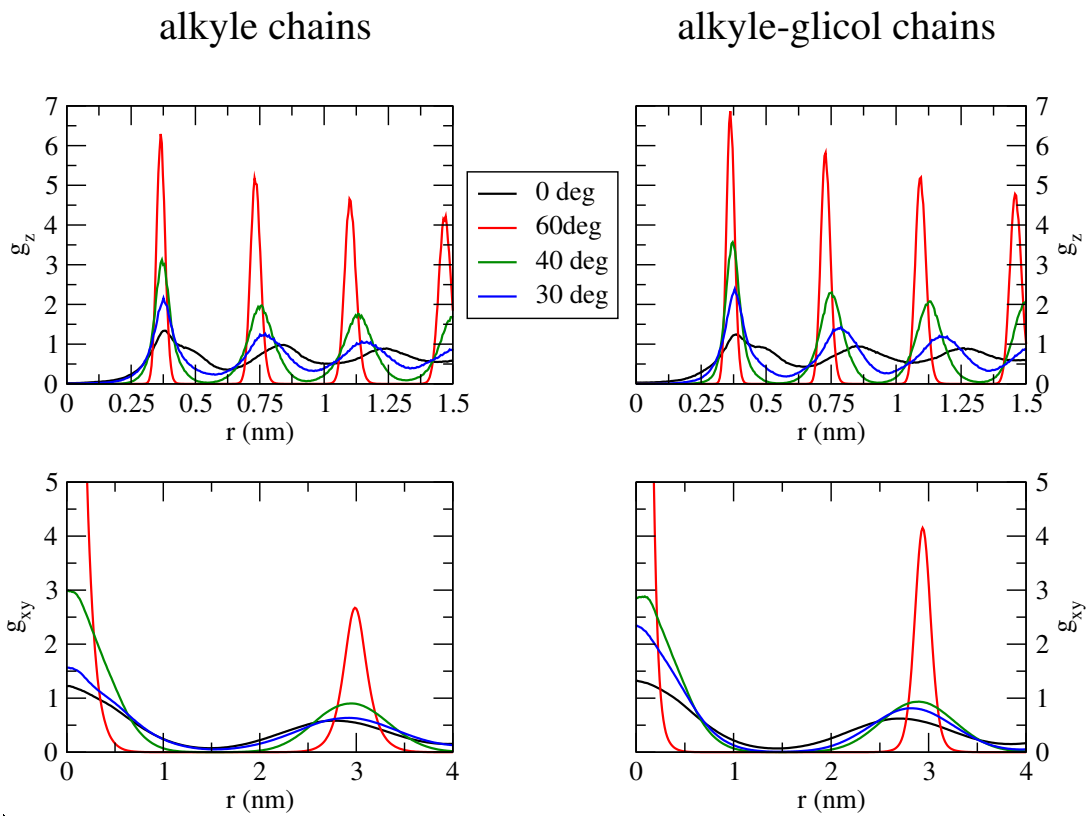

Figure 5-13. Distribution functions for the intracolumnar, g_z, and intercolumnar, g_{xy}, distances; **4-10** (left) and **5-9** (right).

Analysis of the orientational order parameter shows that the systems with the initial twist angle of 60 deg have the highest value of the order parameter and therefore the best ordering of the molecules, for both types of side chains (Figure 5-13, up). The better alignment also manifests itself in a zero average tilt angle of the molecules in the columns, 0 deg for the systems starting with 60deg and about 10 deg for the other systems, as well as results in a closer intracolumnar packing of the molecules, with a distance between the molecules of 0.36 nm, in a good agreement with the experimental data.

For what concerns the hexagonal lattice, there is a trend for both the system of **4-10** and **5-9** (with glycol chains) to have a smaller lattice constant and a higher density (Figure 5-13, down), what is also in accordance with the X-ray scattering results.

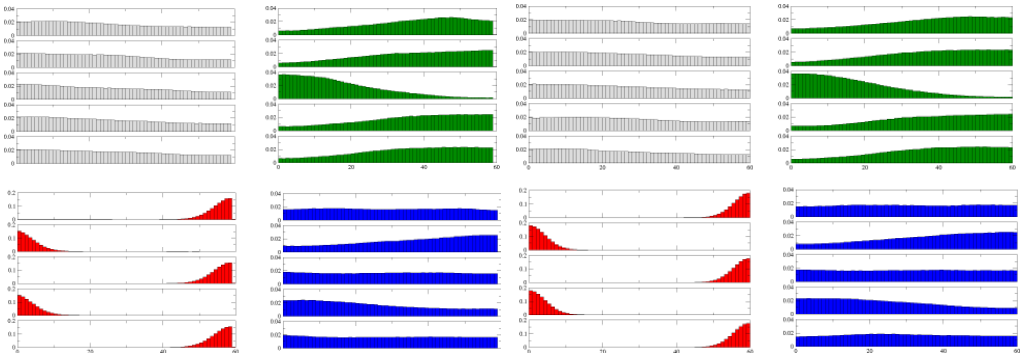

Figure 5-14. Distribution functions of the relative orientations between the nearest neighbors, next nearest neighbors, etc. Left (**4-10**) and right (**5-9**); grey (0°), green

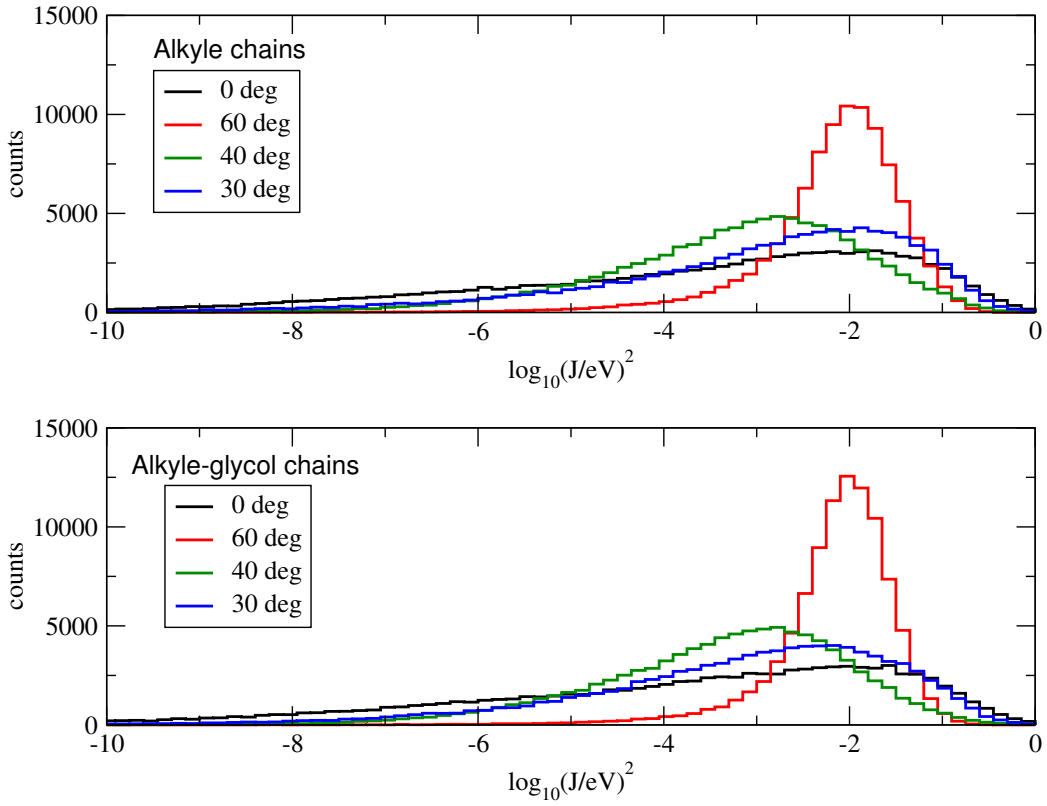

Figure 5-15. Distribution functions of the transfer integrals for two different systems and four different initial twist angles. Up (**4-10**) and down (**5-9**).

To obtain the value of the helical pitch, we calculated an average twisting angle between neighbouring two molecules in the column. They indicate that the systems starting with a twist angle of 60 deg, keep this twist and the helical pitch of 2 molecules, the other two starting configurations converge to an average twist of 30

deg between nearest neighbours but no helical structure is observed. No difference in behavior is observed due to the different type of side chains.

5.2.5 Charge transport

We will first discuss the distribution of transfer integrals for all systems, which are shown in Figure 5-15. These distributions will affect the charge mobility, since the transfer integral is very sensitive to the rotational angle and even small variations of relative molecular orientations can lead to significant changes of hopping rates.[36,37] Since we are dealing with one-dimensional transport, the value of the mobility is limited by the tail of the small transfer integrals, i.e. the width of the distribution is important: the sharper the peak, the higher is the mobility (provided the position of the peak does not change). This is an additional factor which shall be taken to the parametric dependence of the transfer integral on the relative molecular orientations, which is discussed in the introduction.

Figure 5-15 shows that the systems with zero initial twist angle has the highest maximum value of the transfer integral, in agreement with the predictions of parametric dependence on the azimuthal angle. The 60 degrees twist has slightly lower maximum (note logarithmic scale on the axes). However, the distribution of the transfer integrals is significantly sharper for the 60 deg twist, due to locking of the rotational molecular motion. This immediately reflects on the mobility of the system, which is several orders of magnitude higher for the 60 deg twist, as summarized in Table 5-2.

4-10	0 deg	30 deg	40 deg	60 deg
μ, $cm^2V^{-1}s^{-1}$	0.000767	0.0177	0.208	15.6

5-9	0 deg	30 deg	40 deg	60 deg
μ, $cm^2V^{-1}s^{-1}$	0.00137	0.0619	0.195	15.9

Table 5-2. Hole mobilites for all starting configurations.

5.2.6 Conclusions

In conclusion, we have presented a facile approach to control the intracolumnar stacking of triangle-shaped discotics via a supramolecular strategy. X-ray and computer simulation both demonstrate the staggered staking for these triangle-shaped discotics is dynamically favourable fashion. The transition from the helical to staggered stacking of discotics resulted in a significant influence of intrinsic electronic properties. The charge-carrier mobility of 15.9 $cm^2V^{-1}s^{-1}$ which is so far the highest for all discotics as predicted for the molecule **5-9** with specified staggered stacking, paving the way for the extreme broadness of discotic semiconductor materials in the future.

5.2.7 References:

(1) Adam, D.; Schuhmacher, P.; Simmerer, J.; Häussling, L.; Siemensmeyer, K.; Etzbach, K. H.; Ringsdorf, H.; Haarer, D. *Nature*. **1994**, *371*, 141-143.

(2) (a) Fechtenkötter, A.; Saalwachter, K.; Harbison, M. A.; Müllen, K.; Spiess, H. W. *Angew. Chem., Int. Ed.* **1999**, *38*, 3039-3042; (b) Wu, J.; Fechtenkötter, A.; Gauss, J.; Watson, M. D.; Kastler, M.; Fechtenkötter, C.; Wagner, M.; Müllen, K. *J. Am. Chem. Soc*. **2004**, *126*, 11311-11321.

(3) (a) Cornil, J.; Lemaur, V.; Calbert, J. P.; Bredas, J. L. *Adv. Mater.* **2002**, *14*, 726-729; (b) Lemaur, V.; Filho, D. A. S.; Coropceanu, V.; Lehmann, M.; Geerts, Y.; Piris, J.; Debije, M. G.; van de Craats, A. M. ; Senthilkumar, K. ; Siebbeles, L. D. A.; Warmann, J. M.; Bredas, J. L.; Cornil, J. *J. Am. Chem. Soc.* **2004**, *126*, 3271-3279

(4) (a) van de Cratts, A. M.; Warmam, J. M. *Adv. Mater*. **2001**, *13*, 130-133.; (b) Pisula, W.; Menon, A.; Stepputat, M.; Lieberwirth, I.; Kolb, U.; Tracz, A.; Sirringhaus, H.; Pakula, T.; Müllen, K. *Adv. Mater*. **2005**, *17*, 684.; (c) Xiao, S.; Myers, M.; Miao, Q.; Sanaur, S.; Pang, K.; Steigerwald, M. L.; Nuckolls, C. *Angew. Chem. Int. Ed*. **2005**, *44*, 7390-7394.

(5) (a) Wu, J.; Pisula, W.; Müllen, K. *Chem. Rev.* **2007**, *107*, 718-747; (b) Xiao, S.; Tang, J.; Beetz, T.; Guo, X.; Tremblay, N.; Siegrist, T.; Zhu, Y.; Steigerwald, M.; Nuckolls, C. *J. Am. Chem. Soc*. **2006**, *128*, 10700-10701.

(6) (a) Pisula, W.; Tomović, Z.; Stepputat, M.; Kolb, U.; Pakula, T.; Müllen, K. *Chem. Mater*. **2005**, *17*, 2641; (b) Pisula, W.; Kastler, M.; Wasserfallen, D.; Nolde, F.; Kohl, C.; Pakula, T.; Müllen, K. *Angew. Chem. Int. Ed*. **2006**, *45*, 819; (c) Tracz, A.; Jeszka, J. K.; Watson, M. D.; Pisula, W.; Müllen, K.; Pakula T. *J. Am. Chem. Soc*. **2003**, *125*, 1682-1683.

(7) (a) Ikeda, M.; Takeuchi, M.; Shinkai, S. *Chem. Commun*. **2003**, 1354-1355; (b) Arikainen, E. O.; Boden, N.; Bushby, R. J.; Lozman, O. R.; Vinter, J. G.; Wood, A. *Angew. Chem. Int. Ed.* **2000**, 39, 2333-2336.

(8) Feng, X.; Wu, J.; Ai, M.; Pisula, W.; Zhi, L.; Rabe, J. P.; Müllen, K. *Angew. Chem. Int. Ed*. **2007**, *46*, 3033-3046.

(9) Kastler, M.; Schmidt, J.; Pisula, W.; Sebastiani, D.; Müllen, K. *J. Am. Chem. Soc*. **2006**, *128*, 9526-9534.

(10) Feng, X.; Wu, J.; Enkelmann, V.; Müllen, K. *Org. Lett*. **2006**, *8*, 1145-1148;

(11) Yao, T.; Campo, M. A.; Larock, R. C. *J. Org. Chem*. **2005**, *70*, 3511-3517.

(12) (a) Pisula, W.; Tomović Ž., Simpson, C.; Kastler, M.; Pakula, T.; Müllen. K. *Chem. Mater*. **2005**, *17*, 4296-4303; (b) Pisula, W.; Kastler, M.; Wasserfallen, D.; Mondeshki, M.; Piris, J.; Schnell, I.; Müllen K. *Chem. Mater.* **2006** *18*, 3634. (c) Barbera, J.; Cavero, E.; Lehmann, M.; Serrano, J. L.; Sierra, T.; Vazquez, J. T. *J. Am. Chem. Soc*. **2003**, *125*, 4527-4533.

(13) Pisula, W.; Tomović, Ž.; Watson, M. D.; Müllen, K.; Kussmann, J.; Ochsenfeld, C.; Metzroth, T.; Gauss, J. *J. Phys. Chem B* 2007, *111*, 7481-7487.

(14) (a) Bayer, A.; Zimmermann, S.; Wendorff, J. H.; *Mol. Cryst. Liq. Cryst.* **2003**, *396*, 1–22; (b) Glusen, B.; Heitz, W.; Kettner, A.; Wendorff, J. H. *Liq. Cryst*. **1996**, *20*, 627.

(15) Laschat, S.; Baro, A.; Steinke, N.; Giesselmann, F.; Hagele, C.; Scalia, G.; Judele, R.; Kapatsina, E.; Sauer, S.; Schreivogel, A.; Tosoni, M. *Angew. Chem*. **2007**, *119*, 4916-4973; *Angew. Chem. Int. Ed*. **2007**, *46*, 4837-4887.

(16) Schmidt-Mende, L.; Fechtenkotter, A.; Müllen, K.; Moons, E.; Friend, R. H.; MacKenzie, J. D. *Science* **2001**, *293*, 1119-1122.

(17) Li, J.; Kastler, M.; Pisula, W.; Fobertson, J. W. F.; Wasserfallen, D.; Grimsdale, A. C.; Wu, J.; Müllen, K. *Adv. Funct. Mater.* **2007**, *17*, 2528-2533.

(18) van de Craats, A. M.; Warman, J. M.; Fechtenkotter, A.; Brand, J. D.; Harbison, M. A.; Mullen, K., *Adv. Mater.* **1999,** 11, (17), 1469-1472.

(19) Freed, K. F.; Jortner, J., *J. Chem. Phys.* **1970,** 52, (12), 6272-&.

(20) Marcus, R. A., *Rev. Mod. Phys.* **1993,** 65, (3), 599-610.

(21) Andrienko, D.; Kirkpatrick, J.; Marcon, V.; Nelson, J.; Kremer, K. *Phys. Stat. Solidi B.* **2008**, -.

(22) Coropceanu, V.; Cornil, J.; Filho, D. A.; Olivier, Y.; Silbey, R.; Breda, J. L. *Chem. Rev*. **2007**, *107*, 926-952.

(23) (a) Bell, T. W.; Jousselin, H. *Nature* **1994**, *367*, 441-444. (b) Prins, J. J.; Huskens, J.; de Jong, F.; Timmerman, P.; Reinhoudt, D. N. *Nature* **1999**, *398*, 498-502. (c) Percec, V.; Dulcey, A. E.; Balagurusamy, V. S. K.; Miura, Y.; Smidrkal, J.; Peterca, M.; Nummelin, S.; Edlund, U.; Hudson, S. D.; Heiney, P. A.; Hu, D. a.; Magonov, S. N.; Vinogradov, S. A. *Nature* **2004**, *430*, 764-768.

(24) Papapostolou, D.; Smith, A. M.; Atkins, E. D. T.; Oliver, S. J.; Ryadnov, M. G.; Serpell, L. C.; Woolfson, D. N., *Proc. Natl. Acad. Sci. U. S. A.* **2007,** 104, (26), 10853-10858. (b) Martinek, T. A.; Mandity, I. M.; Fulop, L.; Toth, G. K.; Vass, E.; Hollosi, M.; Forro, E.; Fulop, F., *J. Am. Chem. Soc.* **2006,** 128, (41), 13539-13544.

(25) (a) Hoeben, F. J. M.; Jonkheijm, P.; Meijer, E. W.; Schenning, A., *Chem. Rev.* **2005,** 105, (4), 1491-1546.; (b) Shimizu, T.; Masuda, M.; Minamikawa, H., *Chem. Rev.* **2005,** 105, (4), 1401-1443. (c) Percec, V.; Glodde, M.; Bera, T. K.; Miura, Y.; Shiyanovskaya, I.; Singer, K. D.; Balagurusamy, V. S. K.; Heiney, P. A.; Schnell, I.; Rapp, A.; Spiess, H. W.; Hudson, S. D.; Duan, H., *Nature* **2002,** 419, (6905), 384-387.

(26) (a) Wagner, D. E.; Phillips, C. L.; Ali, W. M.; Nybakken, G. E.; Crawford, E. D.; Schwab, A. D.; Smith, W. F.; Fairman, R., *Proc. Natl. Acad. Sci. U. S. A.* **2005,** 102,

(36), 12656-12661. (b) Percec, V.; Dulcey, A. E.; Peterca, M.; Ilies, M.; Sienkowska, M. J.; Heiney, P. A., *J. Am. Chem. Soc.* **2005,** 127, (50), 17902-17909.

(27) Xiao, S. X.; Myers, M.; Miao, Q.; Sanaur, S.; Pang, K. L.; Steigerwald, M. L.; Nuckolls, C., *Angew. Chem.-Int. Edit.* **2005,** 44, (45), 7390-7394.

(28) (a) Kastler, M.; Pisula, W.; Laquai, F.; Kumar, A.; Davies, R. J.; Baluschev, S.; Garcia-Gutierrez, M. C.; Wasserfallen, D.; Butt, H. J.; Riekel, C.; Wegner, G.; Mullen, K., *Adv. Mater.* **2006,** 18, (17), 2255-+. (b) Pisula, W.; Kastler, M.; Wasserfallen, D.; Mondeshki, M.; Piris, J.; Schnell, I.; Mullen, K., *Chem. Mater.* **2006,** 18, (16), 3634-3640.

(29) Andrienko, D.; Marcon, V.; Kremer, K., *J. Chem. Phys.* **2006,** 125, (12), -.

(30) Marcon, V.; Vehoff, T.; Kirkpatrick, J.; Jeong, C.; Yoon, D. Y.; Kremer, K.; Andrienko, D., *J. Chem. Phys.* **2008**, submitted.

(31) Cinacchi, G.; Colle, R.; Tani, A., *J. Phys. Chem. B.* **2004,** 108, (23), 7969-7977.

(32) Berendsen, H. J. C.; Postma, J. P. M.; Vangunsteren, W. F.; Dinola, A.; Haak, J. R., *J. Chem. Phys.* **1984,** 81, (8), 3684-3690.

(33) Hutchison, G. R.; Ratner, M. A.; Marks, T. J., *J. Am. Chem. Soc.* **2005,** 127, (48), 16866-16881.

(34) Kirkpatrick, J., *Int. J. Quant. Chem.* **2008,** 108, (1), 51-56.

(35) Kirkpatrick, J.; Marcon, V.; Nelson, J.; Kremer, K.; Andrienko, D., *Phys. Rev. Lett.* **2007,** 98, (22), -.

(36) Deng, W. Q.; Goddard, W. A., *J. Phys. Chem. B.* **2004,** 108, (25), 8614-8621.

(37) Senthilkumar, K.; Grozema, F. C.; Bickelhaupt, F. M.; Siebbeles, L. D. A., *J. Chem. Phys.* **2003,** 119, (18), 9809-9817.

Chapter 6. Summary and Outlook

The results of the present work "C_3-symmetric Discotic Liquid Crystalline Materials for Molecular Electronics: Versatile Synthesis and Self-organization" can be summarized as follows:

I. A novel synthetic strategy starting from the key building block 1,3,5-tris-2'-bromophenylbenzene (**2-9**) towards the versatile synthesis of novel C_3 symmetric hexa-*peri*-hexabenzocoronenes (HBCs) and a series of triangle-shaped polycyclic aromatic hydrocarbons (PAHs) has been developed (Scheme 1). Compound **2-9** was synthesized firstly in an efficient way, and allowed single or multi-steps transition-metal catalyzed coupling reactions to provide a series of C_3 symmetric 1,3,5-tri-2'-biphenylbenzene, 1,3,5-tris-9'- phenanthrenylbenzene as well as substituted 1,3,5-tri-2'-arylbenzene precursors. After the final treatment with $FeCl_3$ under mild conditions, it became possible to access a variety of new discotic molecules based on C_3 symmetry or triangle shape.

1. For the synthesis of substituted HBCs from 1,3,5-tris-2'-biphenylbenzene precursors, the substitution patterns were shown to be important for the cyclodehydrogenation. D_3 symmetric HBC with three alkyl substituents (**2-14**) and C_2 symmetric HBC with two alkyl substituents (**2-15**) were both obtained from this route, which showed the unusual thermal behavior with a surprising decrease of isotropic points with respect to their D_{6h} symmetric analogues. The self-assembly of **2-14** and **2-15** at the solid-liquid interface displayed a strong symmetry dependant behavior, which allowed the observation of novel zigzag and flower patterns.

2. The triangle shaped discotics serve as models for describing the relationship between the molecular structure and the electronic absorption and photoluminescence properties. Compound **4-2** is a simple triangle-shaped benzenoid PAH with the same number of carbons as fullerene. Compound **4-4** with a triangle shape as reflected by STM, was a first example of large PAHs fused with electron-rich thiophene rings. The semi-triangle shaped discotics **4-9** and **4-10** revealed a unique self-assembly behavior

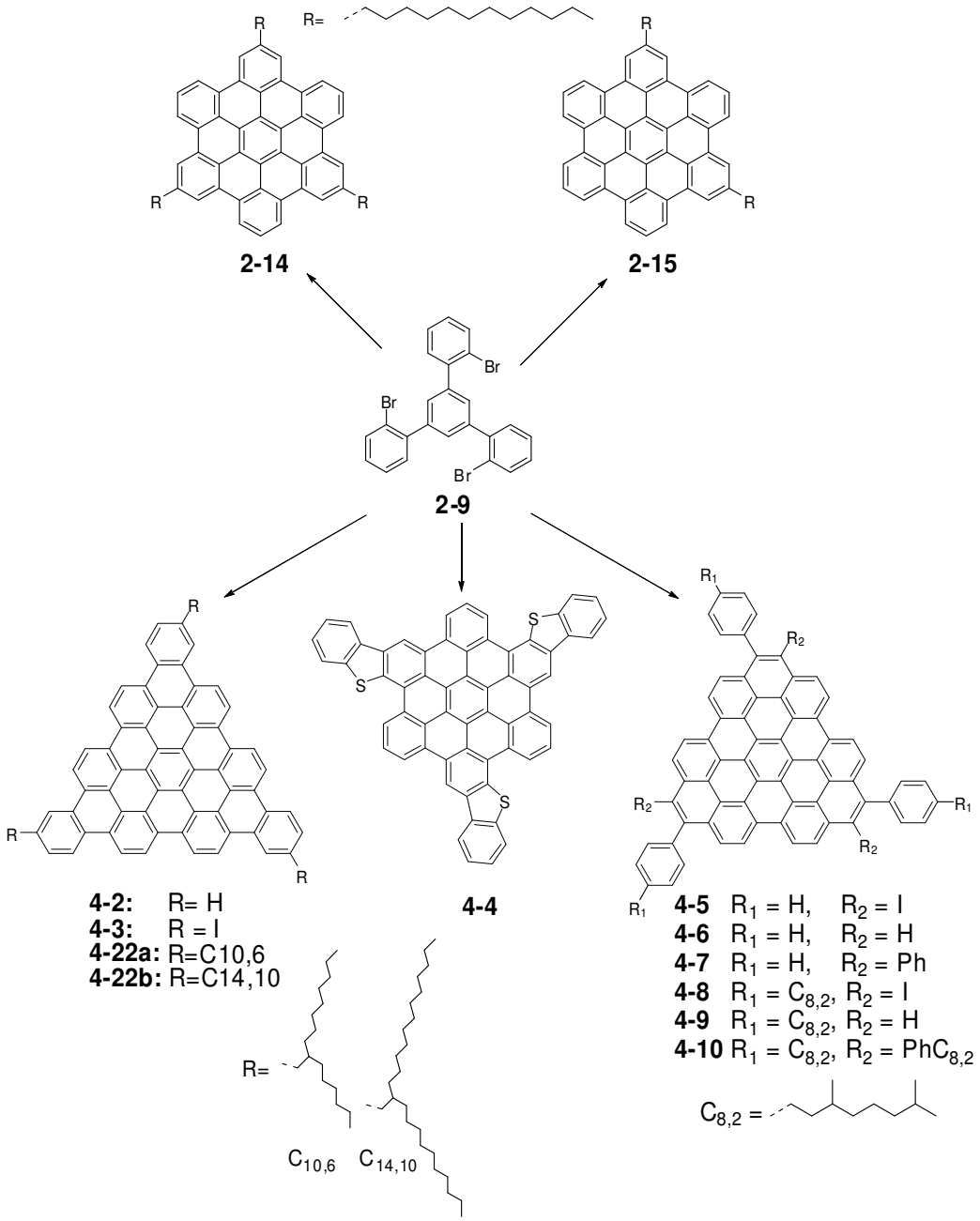

Scheme 6-1. The versatile synthesis of C_3 symmetric HBCs and triangle-shaped discotics based on the key building block **2-9**.

in solution, solid state, as well as at the solution-substrate interface. A mesophase stability over an extremely large temperature range has been obtained as a result of the helical supramolecular arrangement of the discs by a rotational angle of 40° between every two neighboring molecules in the column. For the first time, a

honeycomb pattern with "holes" observed for monolayers of **4-9** and **4-10** suggests a molecular recognition with host-guest interaction and surface pattering (Figure 6-1).

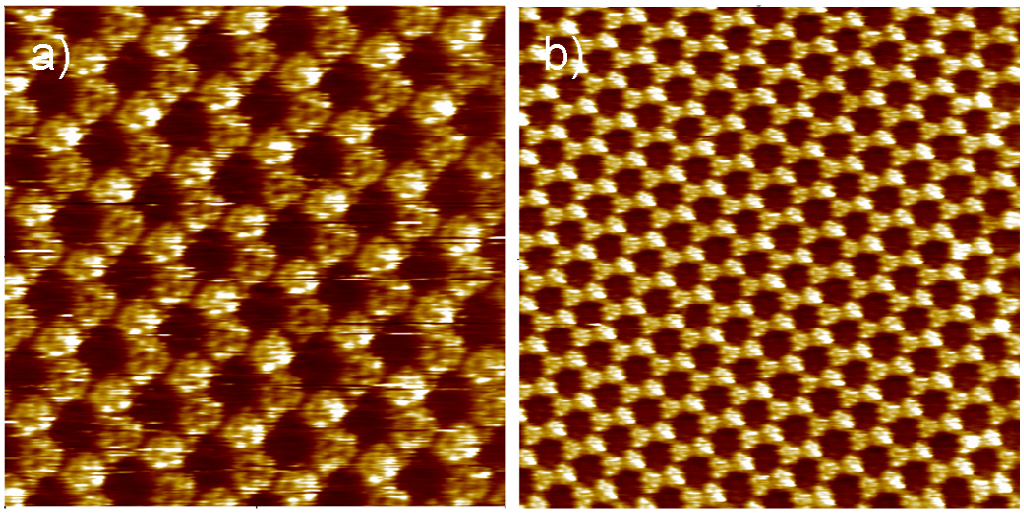

Figure 6-1. STM current images of a) **4-9** and b) **4-10** at the HOPG-solution.

3. Triangle shaped discotics with swallow alkyl tails **4-22a** and **4-22b**, allowed a facile purification, solution physical characterizations, control over the thermotropic properties and finally solution fabrication into efficient photovoltaic devices. Surprisingly, this unique design of the large aromatic core provided a material with an extremely broad temperature range of liquid crystalline, whereby the adequate choice of the substituents permitted self-healing at low processing temperatures. While compound **4-22a** did not display any phase transition and change of the supramolecular arrangement upon thermal treatment, compound **4-22b** with longer swallow tails showed the phase transition at 24 ^{o}C and exposed enhanced degree of order, as suggested by much more distinct reflections in the pattern during annealing at 100 °C and after cooling back the sample to 30 °C (Figure 6-2). The latter aspect was further demonstrated to play a key role in the photovoltaic cell devices, being the higher efficiency for **4-22b** than that for **4-22a**. .

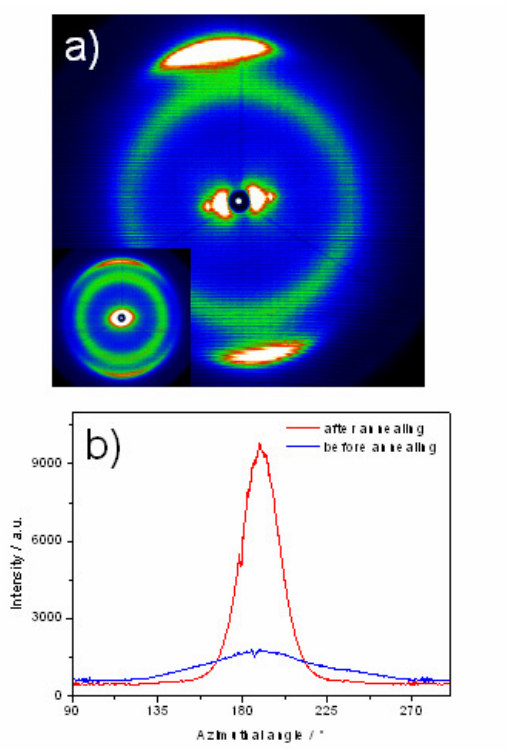

Figure 6-2. a) 2D-WAXS pattern of **4-22b** after annealing (inset shows before annealing), b) azimuthal integration of the meridional reflection related to the π-stacking.

II. A novel class of C_3 symmetric HBCs with alternating polar/apolar substituents was synthesized. The synthetic strategy was based on the cyclotrimerization of asymmetric diphenylacetylenes, where the obtained two isomers could be separated by column chromatography, thus it became possible to provide both C_3 symmetric HBCs and asymmetric HBCs upon the further $FeCl_3$ meditated oxidation. Functional groups such as ester and methoxy groups could be introduced directly on the HBC skeleton or via the additional phenyl units. Compound **3-1a** with the functional ester substitutions directly on the hexaphenyl-substituted HBCs, displayed stronger self-association both in the solution and in the solid state with respect to **3-1b**, which could be attributed to the local dipole moments and nanoscale phase separation between the polar and apolar substituents. The peculiar self-association properties of **3-1a** were additionally manifested by the reversed columnar orientation upon the

extrusion as well as the fibrous nanostructure formation on the surface upon drop-casting from appropriate solutions. The methoxy-substituted HBC **3-11b** showed strong self-association in the solution. Interestingly, the exceptional long-range helical packing in the solid state is for the first time observed for HBC derivatives. Remarkably, upon the drop-casting from different solvents, including THF, toluene, $CHCl_3$, and o-dichlorobenzene, **3-11b** could self-assembly into several hundred micrometers length of fibers.

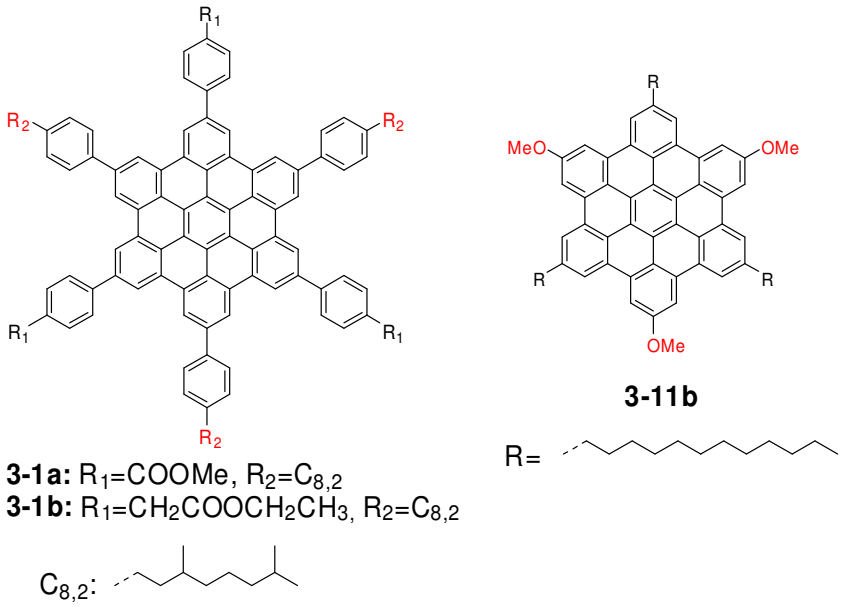

Scheme 6-2. Molecular structures of C_3 symmetric HBCs with alternating polar/apolar substituents.

III. The concept for manipulating the intracolumnar stacking of discotics and thus for controlling the helical pitch has been developed. Compound **5-1a** showed a helical packing with every four molecules in one pitch, however with additional *t*-butyl groups at the *para* position of corona, **5-1b** did not exhibit any pronounced π-stacking. Otherwise, with additional *n*-dodecyl substituents for **5-1b**, a staggered stacking of discotics was achieved. With the alternating hydrophilic and hydrophobic substituents on the trizigzagHBC **5-9**, weak non-covalent interactions significantly influenced the supramolecular organization in the bulk, leading to a highly regularly staggered stacking. Theoretical simulations have confirmed this self-organization and predicted

that this packing should show the highest charge carrier mobility for all discotics.

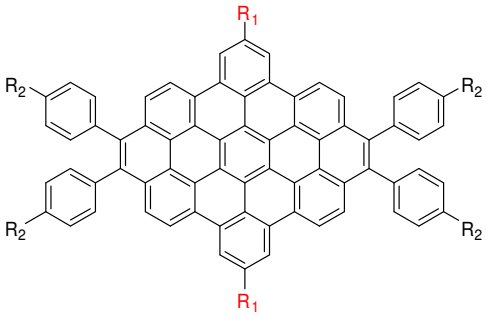

5-1a: R_1= H R_2=*n*-$C_{12}H_{25}$
5-1b: R_1= *t*-butyl
5-1c: R_1=*n*-$C_{12}H_{25}$

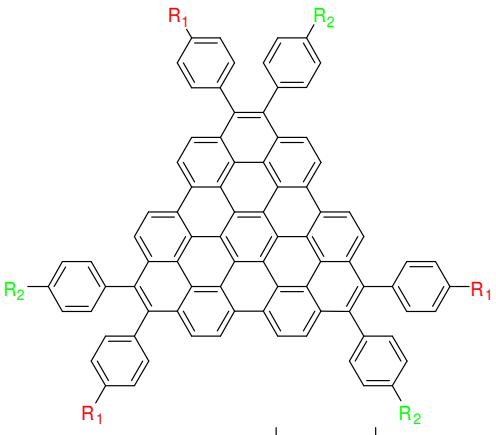

5-9: R_1=

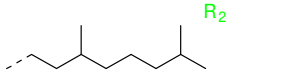

R_2=

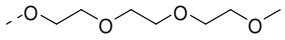

It is no doubt that the above new synthetic strategies have extended the general synthetic protocols toward HBCs and large PAHs through the standard oxidative cyclodehydrogenation of corresponding oligophenylene precursors. The functionalization based on the discotic building blocks is a useful synthetic approach to widen the class of discotic liquid crystalline materials. With the development of new techniques for morphology control and electronic device fabrication, intelligent and circumspective design of functional PAHs is extremely important in the future. Based on the present results, several extensions can be summarized as follows:

1. Small conjugated π-systems are attractive for organic field-effect transistors due to their semiconductor properties. It is believed that the introduction of electron-rich thiophene rings or sulfur atoms in the π-system will not only increase the materials stability, which can be reflected by the decrease of HOMO level, but also increase the dimensionality of hole transporting through the enhanced intermolecular interactions, and thus leading to an improved device performance. Therefore, the future work will focus on the derivatization and functionalization based on the HBC corona with more surrounding thiophene rings or sulfur atoms (besides compound **4-4**) which may pave the way to utilizing these new semiconductor materials in devices.

2. The host-guest interactions based molecular recognition and molecular switch are

extremely important in the fields of biotechnology, nanotechnology and supramolecular chemistry. Compounds **4-9** and **4-10** can self-assembly into the ordered honeycomb network at the liquid-solid interface, thus represent the potential applications as molecular templates. The C_3 symmetry in the case of **4-9** and **4-10** is demonstrated to be extremely important for this self-assembly, with the consideration of molecular-substrate interactions, molecular-molecular interactions as well as interdigitation of the substituents, the molecular design and synthesis based on extended PAHs core with C_3 symmetry are expected to be important in the future. Additionally, the substitution effects on the self-assembly should be also taken in to account, in which they should allow the molecules to easily form host networks on the surface and leave enough spaces for guest molecules to be transported inside. Furthermore, with the appended functional units such as azobenzene or electron acceptor groups on this core, the function based on single molecular device would be feasible in the future.

3. Compounds **3-1** with ester groups can be hydrolyzed into their acid analogues, the unique C_3 symmetric tri-acids on HBCs will allow the future epitaxial growth of mono and multi-layers on the surface through intermolecular hydrogen-bonding dimerizations. The further derivatization with three amide groups on HBCs will give a new class of discotics with confined hydrogen bonding units in the two dimensions, which will not only influence the intrinsic π-π interactions along the columnar superstructure, but also lead to interesting nanostructures in the solution as well as on the surface.

4. In order to find attractive alternatives for carbon nanotubes, the construction of suprmolecular fibrous or tubular nanostructures of conjugated π-systems are a crucial bottom-up strategy. HBCs with strong π-interactions are surely good candidates. Although hexadodecyl-HBC and **3-11b** can self-assembly into the longest fibers, which are presumably due to the mainly strong intermolecular π-interactions as well as van der Waals interactions, a secondary non-covalent interactions such as hydrogen-bonding, dipole-interactions or hydrophilic/hydrophobic interactions are necessary in order to control the self-assembly in a facile approach. Therefore, with

the established synthetic methods as described above, C_3 symmetric HBCs with alternating hydrophilic and hydrophobic substituents can be synthesized, the self-assembly of these novel materials should allow the promising engineering of nanofibrous structures on the surface. In addition, the effect of hydrophilic/hydrophobic interactions at the liquid-solid interface for these materials will be the future objective.

5. Future works will be considered with the modification of substituents on the trizigzagHBC core (**4-10** and **5-9**), in order to systematically study the helical-staggered stacking regulation upon the influence of substitution effects. Regarding the logics of helical stacking for discotic HBCs observed so far, peripheral alkyl-phenyl substituents are believed to be very important due to the steric driving forces. Future work on extended PAHs with proper architectures of alkyl-phenyl substituents may also allow the realization of the unique helical and staggered stacking. The most charming case will be to achieve the unique staggered stacking of one large discotic system in the crystalline state, which is expected to be the high performance organic materials for one-dimensional charge carrier transport.

Chapter 7. Experimental Section

Materials:

All starting materials, solvents and catalysts for chemical reactions were purchased from Aldrich, Acros, Fluka, Strem etc. and used as received without purification.

NMR spectroscopy:

^{1}H NMR and ^{13}C NMR spectra were recorded in CD_2Cl_2, $C_2D_2Cl_4$, d_8-THF or $CDCl_3$ on a Bruker DPX 250, Bruker AMX 300, Bruker DRX 500 or Bruker DRX 700 spectrometer with use of the solvent proton or carbon signal as an internal standard.

Mass spectrometry:

FD mass spectra were obtained on a VG Instruments ZAB 2-SE-FPD spectrometer. MALDI-TOF mass spectra were measured on a Bruker Reflex IITOF spectrometer using a 337 nm nitrogen laser and 7,7,8,8-tetracyanoquinodimethane (TCNQ) as matrix. The mass instrument is not dedicated to isotopic measurements, and the deviations of relative intensities of peaks, from those calculated, can be more than 10%.

UV/Vis spectroscopy:

UV/Vis spectra were recorded at room temperature on a Perkin-Elmer Lambda 9 spectrophotometer.

Fluorescence spectroscopy:

Fluorescence spectra were recorded on a SPEX–Fluorolog II (212) spectrometer.

Melting points:

Melting points were determined using a Büchi B-545 apparatus in open capillaries and are uncorrected.

Chromatography:

Preparative column chromatography was performed on silica gel from Merck with a particle size of 0.063-0.200 mm (Geduran Si 60). For analytical thin layer chromatography (TLC) silica gel coated substrates 60 F254 from Merck were used. Compounds were detected by fluorescence quenching at 254 nm and selffluorescence at 366 nm.

Elemental analysis:

Elemental analyses were carried out on a Foss Heraeus Vario EL as a service of the Institute for Organic Chemistry, Johannes-Gutenberg-University of Mainz. Because of the high carbon content of large, non-alkylated PAHs, combustion may be incomplete (soot formation), resulting in values lower than expected for the carbon content.

Differential scanning calorimetry (DSC) and thermogravimetric analysis (TGA):

DSC was measured on a Mettler DSC 30 with heating and cooling rates of 10 °C/min in the range from -150 °C to 250 °C. For TGA a Mettler TG 50 thermogravimetric analyzer was used.

Polarization microscopy:

A Zeiss Axiophot with a nitrogen flushed Linkam THM 600 hot stage was used to perform polarization microscopy.

X-ray:

Powder X-ray diffraction experiments were performed using a Siemens D 500 Kristalloflex diffractometer with a graphite-monochromatized CuKα X-ray beam, emitted from a rotating Rigaku RV-300 anode. 2D WAXS measurements of oriented filaments were conducted using a rotating anode (Rigaku 18 kW) X-ray beam (CuKα, pinhole collimation, double graphite monochromator) and CCD camera. The patterns were recorded with vertical orientation of the filament axis and with the beam perpendicular to the filament.

Single crystal analysis

The single crystal analysis was performed on a Nonius-KCCD diffractometer with a Mo-Kα (λ = 0.71923 Å, graphite monochromatized) at a temperature of 150 K. The structures were solved by direct methods (Shelxs) and refined on F with anisotropic temperature factors for all non-hydrogen atoms. The H atoms were refined with fixed isotropic temperature factors in the riding mode.

Scanning electron microscope (SEM) and transmission electron microscope (TEM)

SEM measurements were performed on a LEO 1530 field emission scanning electron microscope. TEM studies were conducted on a Philips Tecnai F20 electron microscope at an operating voltage of 200 kV.

Scanning Tunneling Microscopy (STM)

STM imaging has been carried out at the interface between a freshly cleaved highly oriented pyrolytic graphite (HOPG) substrate and an almost saturated solution in 1,2,4-trichlorobenzene (Aldrich). Measurements have been executed at room temperature employing a home-made set-up. After the visulization of the HOPG lattice, a drop of an almost saturated solution was applied to the basal plane of HOPG. The scan speeds were 10-50 lines/s. The STM images have been corrected with respect to the hexagonal HOPG lattice underneath exploiting SPIP software. In this way the unit cell of the adsorbate crystal could be defined with a high degree of precision.

Synthesis:

1,3,5-Tris-2'-bromophenylbenzene (2-9)

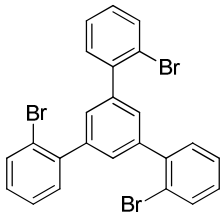

2-Bromoacetophenone (20.g, 100.0 mmol) and trifluoromethanesulfonic acid 10 mol% were stirred at 130 ^{o}C until the total conversion of starting material (7 h). The resulting black solution was allowed to cool to room temperature and quenched by adding water. The mixture was then extracted with CH_2Cl_2, and the organic layer was washed with water and brine, dried over $MgSO_4$. The solvents were removed under vacuum and the residue was purified by column chromatography (silica gel, PE/ DCM = 6/1) to afford 13.0g (72%) slight-yellow solid. Further recrystallization afforded the white powder. Mp: 159~160 ^{o}C. FD-MS (8 KV): m/z = 543.80, calcd.: 543.09 (M^+). ^{1}H NMR (250MHz, CD_2Cl_2): δ ppm 7.69 (d, J = 7.8Hz, 3H), 7.51~7.26 (m, 9H), 7.22 (m, 3H). ^{13}C NMR (62.5 MHz, CD_2Cl_2): δ ppm 142.26, 140.90, 133.59, 131.92, 130.05, 129.44, 127.99, 122.85. Elemental Analysis: Calculated: C 53.08, H 2.78, Br 44.14; Found: C 53.36, H 2.93.

1,3,5-Tris(2'-biphenyl)ylbenzene (2-4a)

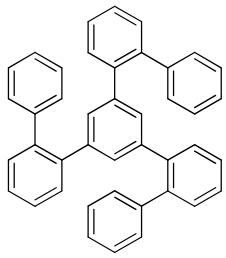

400 mg **2-9** (0.737mmol), 326 mg phenylboronic acid (2.652 mmol), 26 mg (3mol%) $Pd(PPh_3)_4$, 1.02 g K_2CO_3, 25 ml toluene, 6ml ethanol and 6ml H_2O were added into a 50 ml Schlenk flask. The mixture was degassed by two "freeze-pump-thaw" cycles and then heated to reflux under argon overnight. After standard work-up and purification by column chromatography (silica gel, PE/DCM = 6/1), 339 mg white solid was obtained (86%). FD-MS (8 KV): m/z = 534.0, calcd.: 534.69 (M^+). ^{1}H NMR (250 MHz, CD_2Cl_2): δ ppm 7.33~7.21 (m, 18H), 7.02~6.98 (m, 6H), 6.81~6.78 (m, 3H), 6.71~6.68(m, 3H). ^{13}C NMR (62.5 MHz, CD_2Cl_2): δ ppm 141.95, 141.16, 140.87, 140.60, 130.71, 130.60, 130.50, 130.10, 128.20, 127.71, 127.61, 126.80. Elemental Analysis: Calculated: C 94.34, H 5.66; Found: C 94.29, H 5.62.

1,3,5-Tris[3"-(trimethylsilyl)-2'-biphenyl]ylbenzene (2-10a)

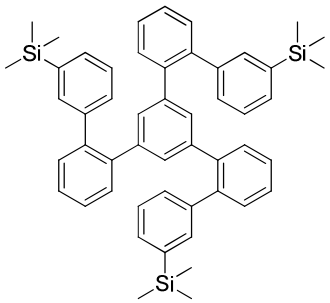

400 mg **2-9** (0.737 mmol), 515 mg *m*-TMS phenylboronic acid (2.652 mmol), 26 mg (3 mol%) $Pd(PPh_3)_4$, 1.02 g K_2CO_3, 25 ml toluene, 6ml ethanol and 6ml H_2O were added into a 50 ml Schlenk flask. The mixture was degassed by two "freeze-pump-thaw" cycles and then heated to reflux under argon overnight. After standard work-up and purification by column chromatography (silica gel, PE/DCM = 10/1), 498 mg white solid was obtained (90%). FD-MS (8 KV): m/z = 750.9, calcd.: 751.23 (M^+). ^{1}H NMR (250 MHz, CD_2Cl_2): δ ppm 7.55~6.72 (m, 27H, Ar-H), 0.27 (s, 27H, TMS). ^{13}C NMR (62.5 MHz, CD_2Cl_2): δ ppm 141.41, 141.26, 140.81, 140.74, 135.45, 131.80, 130.68, 130.56, 130.32,

127.67, 127.59, -0.99. Elemental Analysis: Calculated: C 81.54, H 7.25, Si 11.22; Found: C 81.38, H 7.28.

1,3,5-Tris[4''-(trimethylsilyl)-2'-biphenyl]ylbenzene (2-10b)

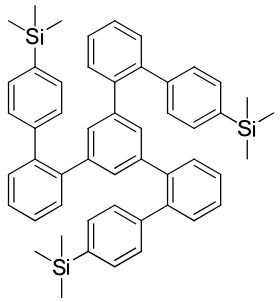

400mg **2-9** (0.737 mmol), 515 mg *p*-TMS phenylboronic acid (2.652 mmol), 26 mg (3mol%) $Pd(PPh_3)_4$, 1.02 g K_2CO_3, 25ml toluene, 6ml EtOH and 6ml H_2O were added into a 50ml Schlenk flask. The mixture was degassed by two "freeze-pump-thaw" cycles and then heated to reflux under argon overnight. After standard work-up and purification by column chromatography (silica gel, PE/DCM = 6/1), 514 mg white solid was obtained (93%). FD-MS (8 KV): m/z = 750.8, calcd.: 751.23 (M^+). ^{1}H NMR (250 MHz, CD_2Cl_2): δ ppm 7.47 (d, J = 8.2Hz, 6H), 7.33~7.30 (m, 6H), 7.25~7.16 (m, 3H), 7.02 (d, J=7.8Hz, 6H), 6.74~6.70 (m, 6H), 0.25 (s, 27H, TMS). ^{13}C NMR (75 MHz, CD_2Cl_2): δ ppm 142.36, 141.11, 140.83, 140.61, 138.71, 133.23, 130.63, 130.20, 129.90, 127.74, 127.66, 0.988. Elemental Analysis: Calculated: C 81.54, H 7.25, Si 11.22; Found: C 81.45, H 7.18.

1,3,5-Tris(4''-iodo-2'-biphenyl)ylbenzene (2-4c)

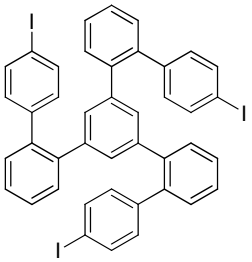

500 mg **2-10b** (0.665mmol) was dissolved in 130 ml $CHCl_3$ and then degassed by bubbling through argon for 20 min; afterwards, 2.4 ml iodine monochloride (1.0 M in CH_2Cl_2) was added slowly. After stirring for 1h, the reaction was quenched by adding aqueous sodium disulfite. The organic layer was washed by water three times and dried

over $MgSO_4$. The solution was concentrated to 10 ml and then 100 ml MeOH was added to precipitate the product. The white solid was collected and dried under vacuum to afford 564 mg product (93%). Mp: 258~259 ^oC. FD-MS (8 KV): m/z = 912.8, calcd.: 912.38 (M^+). ^1H NMR (300 MHz, CD_2Cl_2): δ ppm 7.66~7.61 (m, 6H), 7.41~7.30 (m, 9H), 6.86~6.83 (m, 3H), 6.76~6.72 (m, 6H), 6.67 (s, 3H). ^{13}C NMR (75 MHz, CD_2Cl_2): δ ppm 141.66, 141.08, 140.45, 139.77, 137.37, 132.43, 130.78, 130.25, 130.18, 128.23, 127.97, 92.43. Elemental Analysis: Calculated: C 55.29, H 2.98, I 41.73; Found: C 54.94, H 3.03.

HBC 2-6a prepared from 2-4a

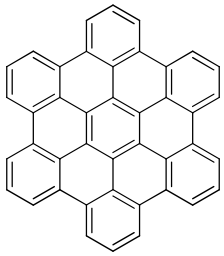

100 mg **2-4a** (0.184mmol) was dissolved in 80 ml dichloromethane, the solution was degassed by bubbling through argon for 20 min, and then 1.08g $FeCl_3$ in 4ml CH_3NO_2 was added dropwise. After being stirred for 1 h, the reaction was quenched by adding 100 ml methanol, the yellow precipitate was collected, washed by methanol repeatedly and dried under vacuum to afford 76 mg yellow powder (80%). MALDI-TOF-MS (TCNQ as matrix): m/z = 521.93, calcd. 522.14 for $C_{42}H_{18}$.

Tribenzo[b,n,pqr]perylene, 2,8-diiodo-16-(4'-iodo[1,1'-biphenyl]-2-yl)- (9CI) (2-11)

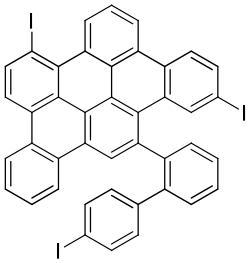

500mg **2-4c** (0.548mmol) was dissolved in 150 ml CH_2Cl_2. The solution was then degassed by bubbling through argon for 20 min. Then 3.2g $FeCl_3$ in 10ml CH_3NO_2 was added dropwise in 10 min. After being stirred for 21 h, the reaction was quenched by adding the methanol, the yellow precipitate was collected, washed by methanol and dried under vacuum to afford 450 mg yellow powder (91%). Mp: >400 ^oC. MALDITOF-MS

(TCNQ as matrix): m/z = 904.88, calcd. 906.33 for $C_{42}H_{21}I_3$. Elemental Analysis: Calculated: C 55.66, H 2.34, I 42.01; Found: C 51.71, H 2.06.

Silane, [[16-[4'-[(trimethylsilyl)ethynyl][1,1'-biphenyl]-2-yl]tribenzo[b,n,pqr] perylene-2,8-diyl]di-2,1-ethynediyl]bis[trimethyl- (9CI) (2-12)

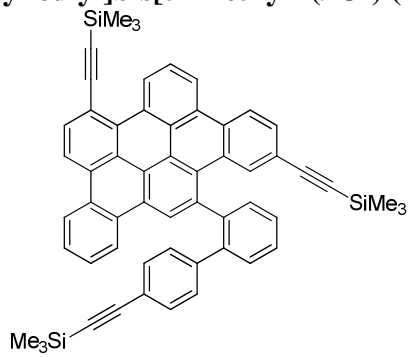

To a 25 ml Schlenk flask was added 150 mg **2-11** (0.165mmol), 20mg $Pd(PPh_3)_4$, 9mg CuI, and 10ml piperidine. The mixture was degassed by two "freeze-pump-thaw" cycles, then 147mg TMS-acetylene (1.48mmol) was added. The solution was heated to 42^{o}C overnight, cooled to room temperature, and then methanol was added to quench the reaction. The yellow precipitate was collected and further purified by column chromatography (silica gel, PE/DCM = 3/1) to afford 56 mg yellow solid (42%). Mp: 280~284 ^{o}C. FD-MS (8 KV): m/z = 817.4, calcd.: 817.25 (M^+). ^{1}H NMR (250 MHz, CD_2Cl_2): δ ppm 10.19(d, J = 8.2Hz, 0.6H), 9.86(d, J = 8.2Hz, 0.4H), 8.73~7.19(m, 16H), 6.37(d, J = 8.2Hz, 1H), 6.18(d, J = 8.2Hz, 1H), 6.10(d, J = 8.2Hz, 1H), 5.84(d, J = 8.2Hz, 1H), 0.50(s, 5H), 0.43(s, 4H), 0.38(s, 4H), 0.36(s, 5H), 0.10(s, 1H), 0.048(s, 8H).

Dibenzo[f,j]naphtho[1,2,3,4-pqr]picene, 11-(1,1-dimethylethyl)- 20-[4-(1,1-dimethyl ethyl)phenyl] (2-13)

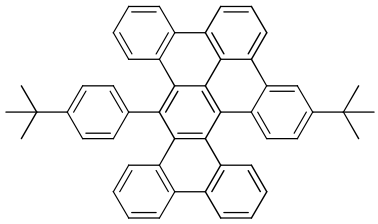

200 mg **2-5b** was dissolved in 120 ml CH_2Cl_2. The solution was then bubbled through argon for 20min, then 1.5g $FeCl_3$ in 10ml CH_3NO_2 was added dropwise in 10 min. After 30 min, the reaction was quenched by adding methanol and a black solution was

obtained. After several hours, the slowly formed precipitate was extracted with CH_2Cl_2 and the organic layer was washed by water and brine, dried over $MgSO_4$. The solvents were removed and the residue was purified by column chromatography (silica gel, PE/DCM = 4/1) to provide 135 mg yellow solid (68%). Mp: 240~245 ^oC. FD-MS (8 KV): m/z = 641.0, calcd.: 640.85 (M^+). ^1H NMR (500 MHz, $CDCl_2CDCl_2$): δ ppm 9.11~6.97 (m, 22H), 1.49 (s, 9H), 1.44 (s, 9H).

1, 10-Di(tert-butyl)-Hexa-*peri*-hexabenzocoronene 7

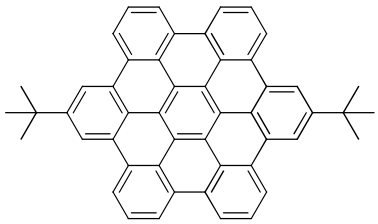

15 mg **2-13** was dissolved in 15ml CH_2Cl_2. The solution was then bubbled through argon for 20min, and then 46 mg $FeCl_3$ in 0.3 ml CH_3NO_2 was added dropwise in 5 min. After stirring for 30 min, methanol was added to quench the reaction. The formed precipitate was collected and washed by methanol, dried under vacuum to afford yellow powder in quantitative yield. MALDI-TOF-MS (TCNQ as matrix): m/z = 633.95, calcd. 634.80 for $C_{50}H_{34}$.

1,4-Bis(2'-biphenyl)yl-2,5-diphenylbenzene (2-5a)

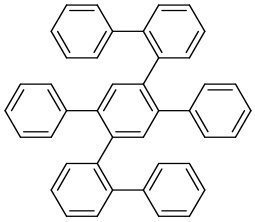

300 mg 1,4-bis(2'-biphenyl)-2,5-dibromobenzene (0.555mmol), 271mg phenylboronic acid (2.22mmol), 767mg K_2CO_3, 19mg $Pd(PPh_3)_4$, 13ml toluene, 3ml EtOH and 3ml H_2O were added to a 50 ml Schlenk flask. The mixture was degassed by two "freeze-pump-thaw" cycles, and then heated to reflux under argon overnight. After standard work-up and purification by column chromatography (silica gel, PE/DCM = 4/1), 277 mg white solid was obtained (92%). Mp: 244~246 ^oC. FD-MS (8 KV): m/z =

534.9, calcd.: 534.69 (M^+). ^{1}H NMR (250 MHz, CD_2Cl_2): δ ppm 7.47~6.58 (m, 30H). ^{13}C NMR (75 MHz, CD_2Cl_2): δ ppm 141.36, 140.82, 140.25, 139.89, 139.39, 133.85, 132.02, 130.26, 129.58, 129.46, 127.83, 127.57, 126.43, 126.39. Elemental Analysis: Calculated: C 94.34, H 5.66; Found: C 94.21, H 5.76.

1,3,5-Tris-2'-(3"-dodecyl)biphenylbenzene (2-16) and **1,3-bis-2'-(3"-dodecyl)biphenyl-5-2'-biphenyl-benzene (2-17)**

816mg (0.89mmol) **2-4b,** 73mg (10%) $Pd(dppf)Cl_2$ and 10ml THF were added into 50ml Schlenk flask. The mixture was carefully degassed by pump and refilled with argon. The Gringard reagent 7.1 ml (1M in Et_2O) was then slowly added dropwise. The resulting mixture was heated at 50^{o}C overnight. After standard work-up and purification by column chromatography (Silica gel, PE:DCM = 6:1), afforded 567mg (61%) **5** and 249mg (32%) **6** as colorless oil respectively. (It should be noted here that the yield of **5** could be improved up to 86% by optimizing the reaction condition with the exclusion of oxygen and reducing the catalyst).

2-16:

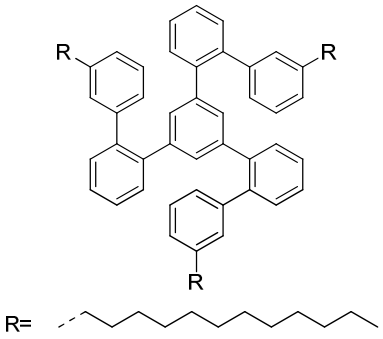

FD-MS (8 KV): m/z 1039.4, calcd.: 1039.64 (M^+). ^{1}H NMR (250 MHz, CD_2Cl_2): δ ppm.7.32~7.01(m, 18H), 6.76~6.68(m, 9H), 2.54(t, 6H, J=7.58Hz), 1.47(m, 6H), 1.35~1.15(m, 54H), 0.89~0.84(m, 9H). ^{13}C NMR (62.5 MHz, CD_2Cl_2): δ ppm 143.38, 142.06, 141.11, 140.77, 140.55, 130.70, 130.56, 130.47, 130.12, 127.93, 127.53, 126.88, 36.30, 32.32, 32.21, 30.07, 29.94, 29.89, 29.76, 29.67, 23.09, 14.27.

2-17:

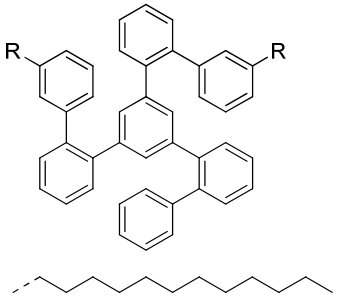

.FD-MS (8 KV): m/z 873.1, calcd.: 871.33 (M^+). ^{1}H NMR (300 MHz, CD_2Cl_2): δ ppm.7.32~6.98(m, 20H), 6.73~6.70(m, 8H), 2.54(t, 4H, J=7.53Hz), 1.47(m, 4H), 1.35~1.18(m, 36H), 0.89~0.83(m, 6H). ^{13}C NMR (75 MHz, CD_2Cl_2): δ ppm 143.60, 142.10, 141.99, 141.16, 140.88, 140.56, 130.88, 130.62, 130.53, 130.44, 130.04, 128.23, 127.97, 127.56, 126.89, 36.28, 32.30, 30.03, 29.92, 29.74, 29.66, 23.07, 14.26

1,7,13-Trisdodecyl-hexa-*peri*-hexabenzocoronene (2-14)

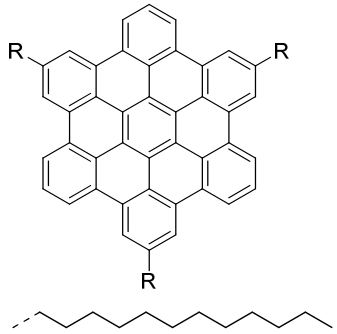

280 mg (0.269mmol) **2-16** was dissolved in 110ml dichloromethane, the solution was then degassed by bubbling through argon for 20 min, and then 30eq $FeCl_3$ 1.31g in 5ml CH_3NO_2 was added dropwise. After being stirred for 45 min, the reaction was quenched by adding methanol, the yellow precipitate was collected, washed by methanol repeatedly, redissolved in hot toluene and passed through a short silica column, the solution was collected and dried under vacuum and then reprecipitated from methanol to afford 241 mg yellow powder (87%). MALDITOF-MS (TCNQ as matrix): m/z=1026.40, calcd. 1027.55 for $C_{78}H_{90}$. ^{1}H NMR (500 MHz, $CDCl_2CDCl_2$, 140^{o}C): 8.64(brs, 6H), 8.48(brs, 6H), 3.08(brs, 6H), 2.02(m, 6H), 1.66~1.33(m, 54H), 0.89(m, 9H). ^{13}C NMR can not be well resolved because of the poor solubility. Elemental Analysis: Calculated: C 91.17, H 8.73; Found: C 91.45, H 8.34..

1,7-Bisdodecyl-hexa-*peri*-hexabenzocoronene (2-15)

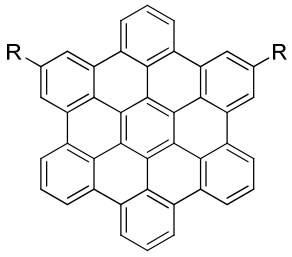

180 mg (0.206mmol) **2-17** was dissolved in 100ml dichloromethane, the solution was then degassed by bubbling through argon for 20 min, and then 30eq $FeCl_3$ 1.0g in 4ml CH_3NO_2 was added dropwise. After being stirred for 45 min, the reaction was quenched by adding methanol, the yellow precipitate was collected, washed by methanol repeatedly, redissolved in hot toluene and passed through a short silica column, the solution was collected and dried under vacuum and then reprecipitated from methanol to afford 153 mg yellow powder (86%). MALDITOF-MS (TCNQ as matrix): m/z=858.36, calcd. 859.23 for $C_{66}H_{66}$. ^{1}H NMR (500 MHz, $CDCl_2CDCl_2$, 140^{o}C): 8.72(brs, 12H), 7.88(brs, 4H), 3.13(brs, 4H), 2.03(m, 4H), 1.67~1.32(m, 36H), 0.89(m, 6H). ^{13}C NMR can not be well resolved because of the poor solubility. Elemental Analysis: Calculated: C 92.26 , H 7.24; Found: C 92.47, H 7.15.

4-(4'-Methylcarbonylphenyl)-4''-(4'''-(3'''',7''''-dimethyloctanyl)phenyl)-diphenylacetylene (3-3a)

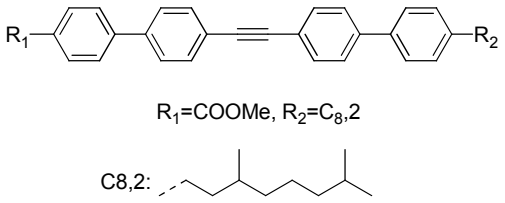

5.0 g (15.7 mmol) 4-(4'-(3''-7''-dimethyloctanyl)biphenylacetylene and 4.35 g (14.9 mmol) 4'-bromo-biphenyl-4-carboxylic acid methyl ester were dissolved in 100 ml triethylamine, the mixture was degassed by bubbling through argon for 20 min and then 314 mg (3mol%) $Pd(PPh_3)_2Cl_2$ and 173 mg CuI (6mol%) were added. The mixture was stirred at 80^{o}C overnight, poured into aqueous HCl and extracted with dichloromethane. The organic layer was washed by water and dried over $MgSO_4$. The solvent was removed under vacuum and the residue was purified by column chromatography (DCM:Hex=1:1

then hot $CHCl_3$) to provide 5.85 g light yellow solid (74%). FD-MS (8 KV): m/z 528.1, calcd.: 528.72 (M^+). ^1H NMR (CD_2Cl_2, 250 MHz): δ ppm 8.09(d, 2H, J=8.2Hz), 7.72~7.52(m, 12H), 7.26(d, 2H, J=8.2Hz), 3.90(s, 3H), 2.62(m, 2H), 1.53~1.12(m, 10H), 0.94~0.84(m, 9H). ^{13}C NMR (62.5 MHz, CD_2Cl_2): δ ppm 167.00, 144.87, 143.55, 141.45, 139.98, 137.69, 132.44, 132.34, 130.04, 129.30, 127.58, 127.26, 127.17, 127.11, 121.96, 90.86, 89.87, 39.68, 39.30, 37.48, 33.44, 32.92, 28.35, 25.05, 22.81, 22.72, 19.73. Elemental Analysis: Calculated: C 86.32, H 7.63, O 6.05; Found: C 86.25, H 7.65.

4-(4'-Ethylacetate)phenyl)- ''-(4'''-(3'''',7''''-dimethyloctanyl)phenyl)-diphenylacetylene (3-3b)

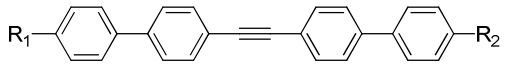

R_1=$CH_2COOCH_2CH_3$, R_2=C_8,2

C8,2: 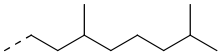

2.10g (5.73 mmol) 4-ethylacetate-4'-(4''-iodo)phenylbenzene and 2.0g 4-(4'-(3''-7''-dimethyloctanyl)biphenylacetylene were dissolved in 100 ml triethylamine, the mixture was degassed by bubbling through argon for 20 min and then 120 mg (3mol%) $Pd(PPh_3)_2Cl_2$ and 66 mg CuI (6mol%) were added. The mixture was stirred at 80^oC overnight, poured into aqueous HCl and extracted with dichloromethane. The organic layer was washed by water and dried over $MgSO_4$. The solvent was removed under vacuum and the residue was purified by column chromatography (DCM:Hex=1:1) to provide 2.78 g light yellow solid (87%). FD-MS (8 KV): m/z 556.9, calcd.: 556.78 (M^+). ^1H NMR (CD_2Cl_2, 250 MHz): δ ppm 7.60~7.52(m, 12H), 7.35(d, 2H, J=8.22Hz), 7.27(d, 2H, J=8.22Hz), 4.12(q, 2H), 3.64(s, 2H), 2.63(m, 2H), 1.56~1.12(m, 13H), 0.95~0.85(m, 9H). ^{13}C NMR (62.5 MHz, CD_2Cl_2): δ ppm 171.71, 143.53, 141.33, 140.88, 139.27, 137.75, 134.43, 132.34, 132.33, 130.26, 129.31, 127.16, 127.12, 122.58, 122.14, 90.38, 90.12, 61.25, 41.24, 39.70, 39.32, 37.50, 33.46, 32.94, 28.37, 25.07, 22.83, 22.74, 19.75, 14.38. Elemental Analysis: Calculated: C 86.29, H 7.97, O 5.75; Found: C 86.22, H 7.95.

Synthesis of **3-4a** and **3-5a**:

3.80 g (7.19 mmol) **3-3a** was dissolved in 140 ml dioxane, the mixture was degassed by bubbling through argon for 30min and 10 mmol% $Co_2(CO)_8$ 245 mg were added, the reaction mixture was mixed under reflux for 7hrs. After stop the reaction, the solvent was removed under vacuum, the residue was purified by column chromatography (DCM:PE=2:1) to get the final product **3-4a** in 30% yield as white solid and **3-5a** in 63% yield as white solid.

1,3,5-Trikis(4'-methylcarbonylphenyl)phenyl-2,4,6-trikis(4'-(3"-7"-dimethyloctanyl phenyl))phenyl)-benzene (3-4a)

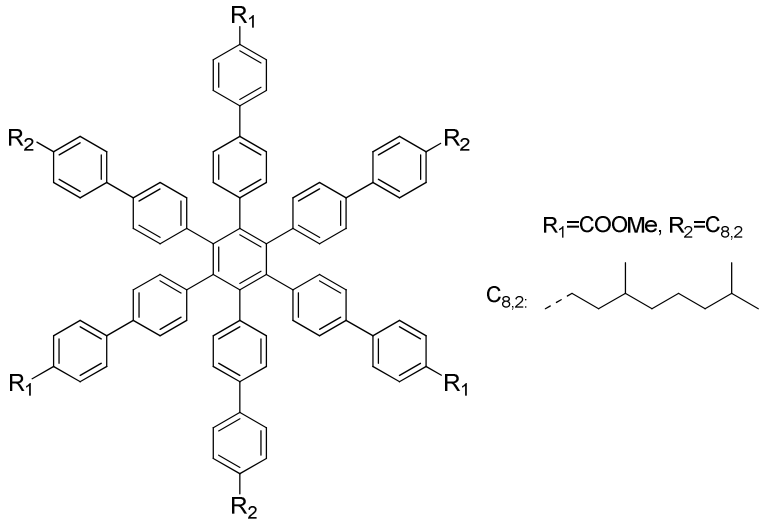

Mp: 228~231°C. FD-MS (8 KV): m/z 1586.0, calcd.: 1586.17 (M^+). ^{1}H NMR (CD_2Cl_2, 250 MHz): δ ppm 7.94(d, 6H, J=8.48Hz), 7.47(d, 6H, J=8.48Hz), 7.31~6.96(m, 36H), 3.84(s, 9H), 2.53(m, 6H), 1.50~1.08(m, 30H), 0.88~0.80(m, 27H). ^{13}C NMR (62.5 MHz, CD_2Cl_2): δ ppm: 167.07, 145.24, 142.75, 140.75, 140.53, 139.68, 138.12, 137.87, 136.90, 132.25, 130.10, 128.99, 126.93, 126.72, 125.80, 125.37, 52.23, 39.66, 37.44, 33.31, 32.82, 25.02, 22.86, 22.77, 19.69. Elemental Analysis: Calculated: C 86.32, H 7.63, O 6.05; Found: C 86.32, H 7.60.

1,2,5-Trikis(4'-methylcarbonylphenyl)phenyl-3,4,6-trikis(4'-(3"-7"-dimethyloctanyl phenyl))phenyl)-benzene (3-5a)

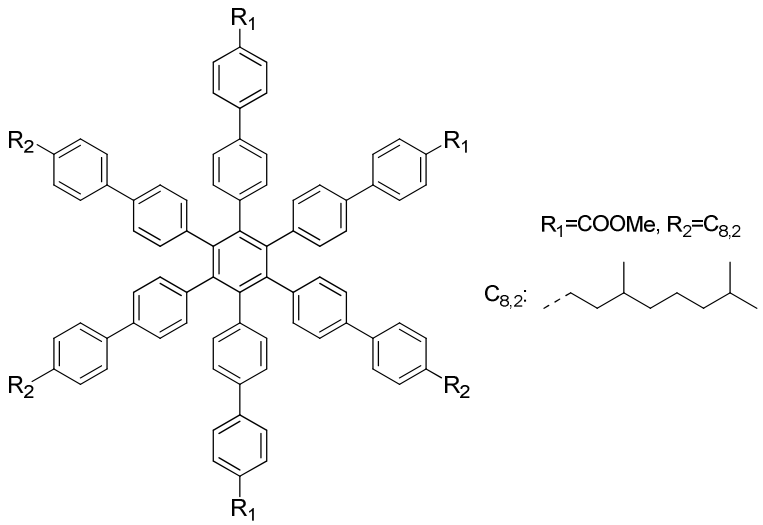

Mp: 221~223°C. FD-MS (8 KV): m/z 1586.0, calcd.: 1586.17 (M^+). ^{1}H NMR (CD_2Cl_2, 250 MHz): δ ppm 7.92(d, 6H, J=8.48Hz), 7.47(d, 6H, J=8.48Hz), 7.32~6.97(m, 36H), 3.84(s, 9H), 2.53(m, 6H), 1.50~1.08(m, 30H), 0.88~0.80(m, 27H). ^{13}C NMR (62.5 MHz, CD_2Cl_2): δ ppm: 167.05, 145.19, 142.70, 141.22, 140.64, 140.41, 139.68, 138.12, 137.92, 136.93, 132.48, 132.25, 130.11, 129.07, 128.98, 126.89, 126.74, 125.82, 125.35, 52.24, 39.66, 39.27, 37.45, 33.32, 32.82, 28.33, 25.02, 22.80, 22.71, 19.69. Elemental Analysis: Calculated: C 86.32, H 7.63, O 6.05; Found: C 86.28, H 7.55.

Synthesis of **3-4b** and **3-5b**:

2.80 g (5.03 mmol) **3-3b** was dissolved in 100 ml dioxane, the mixture was degassed by bubbling through argon for 30min and 10 mmol% $Co_2(CO)_8$ 172 mg was added, the reaction mixture was mixed under reflux for 7hrs. After cooling down the reaction, the solvent was removed under vacuum, the residue was purified by column chromatography (DCM:PE=2:1) to get the final product **3-4b** in 31% yield as waxy sticky solid and **3-5b** in 63% yield as waxy sticky solid.

1,3,5-Trikis(4'-ethylacetatephenyl)phenyl-2,4,6-trikis(4'-(3"-7"-dimethyloctanylphenyl))phenyl)-benzene (3-4b)

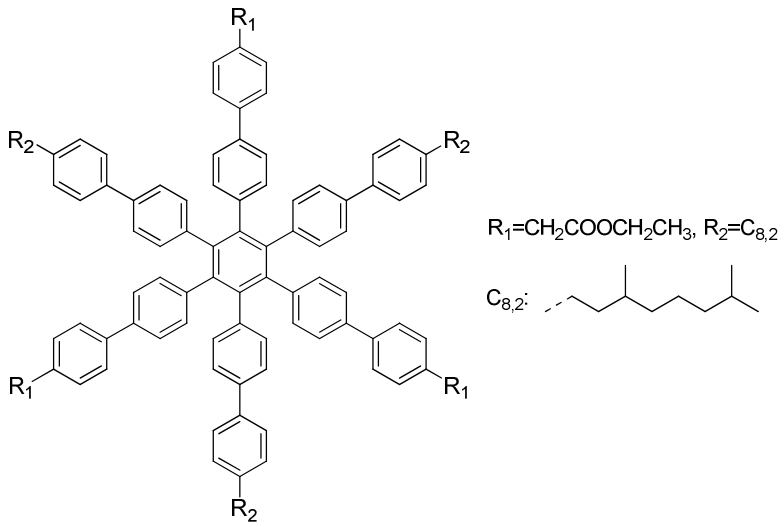

FD-MS (8 KV): m/z 1671.3, calcd.: 1670.33 (M^+). ^{1}H NMR (CD_2Cl_2, 250 MHz): δ ppm 7.33(m, 12H), 7.15(m, 24H), 6.99(m, 12H), 4.06(q, 6H), 3.55(s, 6H), 2.54(m, 6H), 1.53~1.09(m, 38H), 0.90~0.82(m, 27H). ^{13}C NMR (62.5 MHz, CD_2Cl_2): δ ppm:.171.71, 142.62, 140.72, 140.66, 140.31, 139.88, 139.59, 138.05, 137.65, 133.57, 132.35, 132.30, 129.86, 128.95, 127.06, 126.79, 125.42, 125.30, 61.11, 41.20, 39.67, 39.29, 37.46, 33.33, 32.84, 28.33, 25.02, 22.80, 19.69, 14.33. Elemental Analysis: Calculated: C 86.29, H 7.97, O 5.75; Found: C 86.22, H 7.91.

1,2,5-Trikis(4'-ethylacetatephenyl)phenyl-3,4,6-trikis(4'-(3"-7"-dimethyloctanylphenyl))phenyl)-benzene (3-5b)

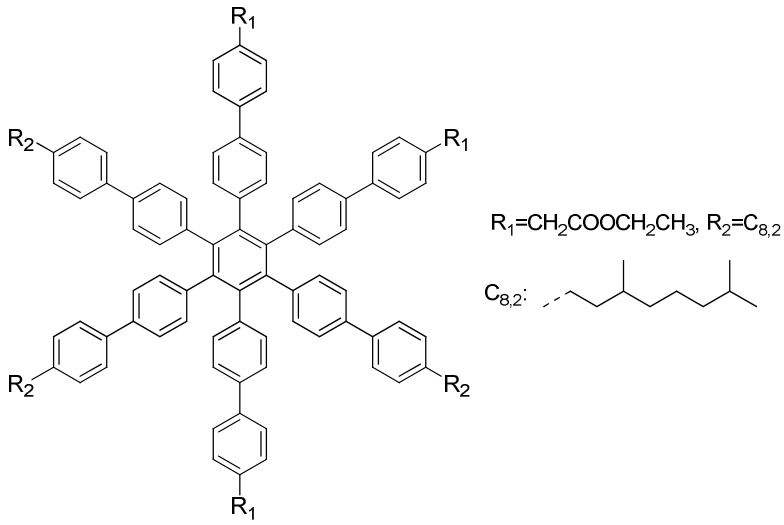

FD-MS (8 KV): m/z 1671.2, calcd.: 1670.33 (M^+). ^{1}H NMR (CD_2Cl_2, 250 MHz): δ ppm 7.35(m, 12H), 7.16(m, 24H), 7.00(m, 12H), 4.07(q, 6H), 3.55(s, 6H), 2.54(m, 6H),

1.53~1.09(m, 38H), 0.90~0.82(m, 27H). ^{13}C NMR (62.5 MHz, CD_2Cl_2): δ ppm: 171.72, 142.62, 140.70, 140.30, 139.90, 139.60, 138.05, 137.66, 133.59, 132.31, 129.87, 128,96, 127.07, 126.80, 125.45, 125.31, 61.12, 41.21, 39.68, 39.29, 37.47, 33.34, 32.85, 28.34, 25.04, 22.82, 22.73, 19.71, 14.35. Elemental Analysis: Calculated: C 86.29, H 7.97, O 5.75; Found: C 86.24, H 7.90.

1,7,13-Trikis(4'-methylcarbonylphenyl)-4,10,16-trikis(4'-(3"-7"-dimethyloctanylphenyl)-hexa-peri-hexabenzocoronene (3-1a)

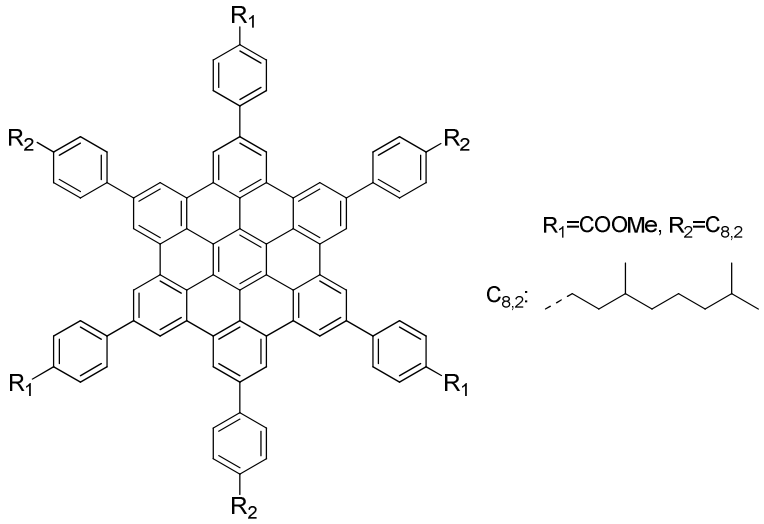

100 mg (0.0631 mmol) **3-4a** was dissolved in 50ml dichloromethane, the solution was then degassed by bubbling through argon for 20 min, and then 368 mg $FeCl_3$ (36eqv) in 1.5ml CH_3NO_2 was added dropwise. After being stirred for 1hr, the reaction was quenched by adding methanol, the yellow precipitate was collected, washed by water and methanol repeatedly and dried under vacuum to afford 80.4 mg yellow powder (81%). MALDITOF-MS (TCNQ as matrix): m/z=1573.85, calcd. 1574.07 for $C_{114}H_{108}O_6$. ^{1}H NMR ($CDCl_2CDCl_2$, 500 MHz, 140^{o}C): δ ppm 7.56(brs, 12H), 6.77(br, 24H), 3.98(s, 9H), 2.60(brs, 6H), 1.67~0.99(m, 57H). ^{13}C NMR can not be clearly resolved due to poor solubility. Elemental Analysis: Calculated: C 86.99, H 6.92, O 6.10; Found: C 86.16, H 7.03.

1,4,13-Trikis(4'-methylcarbonylphenyl)-7,10,16-trikis(4'-(3"-7"-dimethyloctanylphenyl)-hexa-peri-hexabenzocoronene (3-2a)

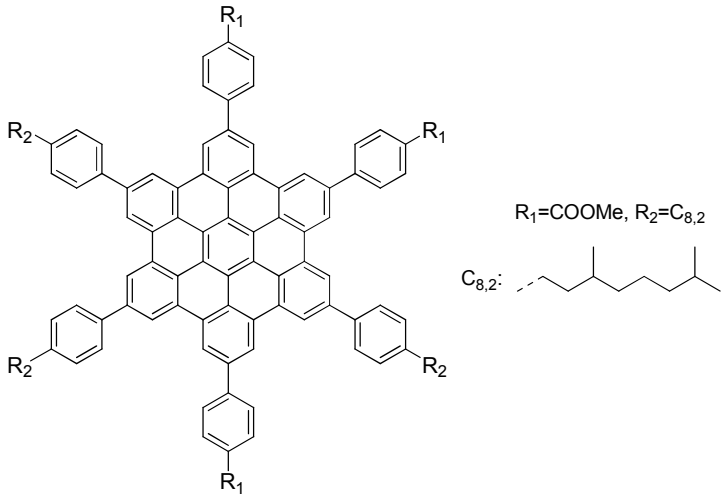

100 mg (0.0631 mmol) **3-5a** was dissolved in 50ml dichloromethane, the solution was then degassed by bubbling through argon for 20 min, and then 368 mg $FeCl_3$ (36eqv) in 1.5ml CH_3NO_2 was added dropwise. After being stirred for 1hr, the reaction was quenched by adding methanol, the yellow precipitate was collected, washed by water and methanol repeatedly and dried under vacuum to afford 83.4 mg yellow powder (84%). MALDITOF-MS (TCNQ as matrix): m/z=1573.95, calcd. 1574.07 for $C_{114}H_{108}O_6$. ^{1}H NMR ($CDCl_2CDCl_2$, 500 MHz, 140^{o}C): δ ppm 7.50(brs, 12H), 6.75(br, 24H), 3.96(s, 9H), 2.61(brs, 6H), 1.67~0.91(m, 57H). ^{13}C NMR can not be clearly resolved due to poor solubility. Elemental Analysis: Calculated: C 86.99, H 6.92, O 6.10; Found: C 85.89, H 6.99.

1,7,13-Trikis(4'-ethylacetatephenyl)-4,10,16-trikis(4'-(3"-7"-dimethyloctanylphenyl) -hexa-peri-hexabenzocoronene (3-1b)

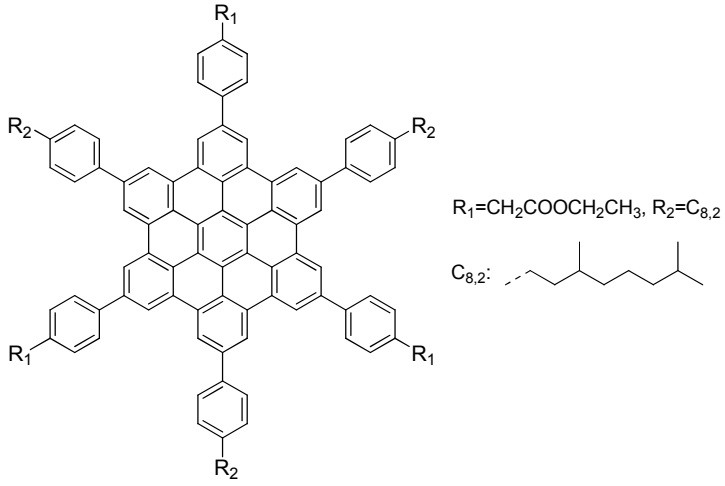

184 mg (0.108 mmol) **3-4b** was dissolved in 100ml dichloromethane, the solution was then degassed by bubbling through argon for 20 min, and then 644 mg $FeCl_3$ (36eqv) in 3ml CH_3NO_2 was added dropwise. After being stirred for 45min, the reaction was quenched by adding methanol, the yellow precipitate was collected, washed by methanol repeatedly and purified by column chromatography (Silica, Ethylacetate:Tolune=1:1), dried under vacuum to afford 152 mg yellow powder (85%). MALDITOF-MS (TCNQ as matrix): m/z=1657.82, calcd. 1658.23 for $C_{120}H_{120}O_6$. ^{1}H NMR ($CDCl_2CDCl_2$, 500 MHz, 140^{o}C): δ ppm 8.21(brs, 12H), 7.53(brs, 12H), 7.42(brs, 6H), 7.34(brs, 6H), 4.44(q, 6H), 3.91(brs, 6H), 2.95(brs, 6H), 2.01(m, 3H), 2.00~1.23(m, 48H), 1.04(m, 15H). ^{13}C NMR (125MHz, CD_2Cl_2, 100^{o}C): δ ppm 170.98, 141.85, 139.83, 138.43, 136.15, 135.63, 132.95, 129.62, 128.68, 128.38, 127.45, 127.34, 121.95, 118.96, 117.52, 60.46, 40.94, 39.45, 36.10, 37.35, 33.33, 33.12, 27.85, 24.73, 22.53, 22.46, 19.68, 14.30. Elemental Analysis: Calculated: C 86.92, H 7.29, O 5.79; Found: C 86.34, H 6.81.

1,4,13-Trikis(4'-ethylacetatephenyl)-7,10,16-trikis(4'-(3"-7"-dimethyloctanylphenyl) -hexa-peri-hexabenzocoronene (3-2b)

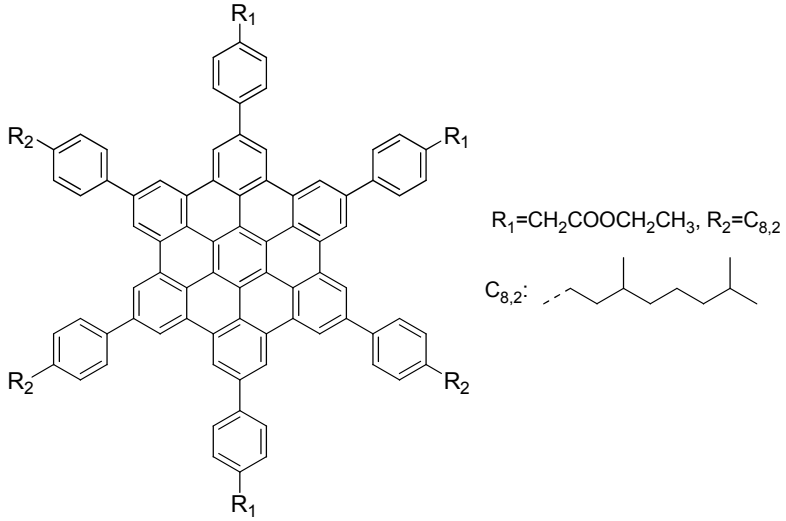

586 mg (0.344 mmol) **3-5b** was dissolved in 279ml dichloromethane, the solution was then degassed by bubbling through argon for 20 min, and then 2.05g $FeCl_3$ (36eqv) in 7ml CH_3NO_2 was added dropwise. After being stirred for 45min, the reaction was quenched by adding methanol, the yellow precipitate was collected, washed by methanol repeatedly and purified by column chromatography (Silica, Ethylacetate:Tolune=1:1),

dried under vacuum to afford 496 mg yellow powder (87%). MALDITOF-MS (TCNQ as matrix): m/z=1657.80, calcd. 1658.23 for $C_{120}H_{120}O_6$. ^{1}H NMR ($CDCl_2CDCl_2$, 500 MHz, 140^{o}C): δ ppm 8.27(brs, 12H), 7.56(brs, 12H), 7.43(brs, 6H), 7.36(brs, 6H), 4.44(q, 6H), 3.91(brs, 6H), 2.96(brs, 6H), 2.02(m, 3H), 2.00~1.23(m, 48H), 1.04(m, 15H). ^{13}C NMR (125MHz, CD_2Cl_2, 100^{o}C): δ ppm 170.99, 141.84, 139.84, 138.43, 136.17, 135.64, 132.97, 129.63, 128.68, 128.39, 127.44, 127.35, 121.97, 118.96, 117.53, 60.49, 40.95, 39.48, 39.10, 37.36, 33.32, 33.11, 27.88, 24.74, 22.54, 22.47, 19.69, 14.30. Elemental Analysis: Calculated: C 86.92, H 7.29, O 5.79; Found: C 86.40, H 7.09.

4-Methoxy-4'-(*t*-butyl)-diphenylacetylene (3-13a)

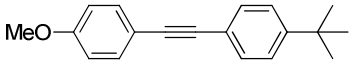

3.0 g (12.8 mmol) 4-methoxyiodobenzene and 2.44 g 4-*t*-butylphenyacetylene were dissolved in 30 ml triethylamine, the mixture was degassed by bubbling through argon for 20 min and then 270 mg (3mol%) $Pd(PPh_3)_2Cl_2$ and 146 mg CuI (6mol%) were added. The mixture was stirred at room temperature overnight, poured into aqueous HCl and extracted with dichloromethane. The organic layer was washed by water and dried over $MgSO_4$. The solvent was removed under vacuum and the residue was purified by column chromatography (DCM:Hex=1:3) to provide 3.11 g white solid (92%). Mp: 122-124^{o}C. FD-MS (8 KV): m/z 263.7, calcd.: 264.36 (M^+). ^{1}H NMR (CD_2Cl_2, 250 MHz): δ ppm 7.44(m, 6H), 6.86(d, 2H, J=8.82Hz), 3.79(s, 3H), 1.30(s, 9H). ^{13}C NMR (62.5 MHz, CD_2Cl_2): δ ppm 160.02, 151.75, 133.24, 131.37, 125.77, 120.79, 115.77, 114.35, 88.88, 88.35, 35.01, 31.26. Elemental Analysis: Calculated: C 86.32, H 7.63, O 6.05; Found: C 86.26, H 7.62.

Synthesis of 3-14a and 3-15a

3.5 g (13.2 mmol) **3-13a** was dissolved in 100 ml dioxane, the mixture was degassed by bubbling through argon for 30min and 10 mmol% $Co_2(CO)_8$ 452 mg were added, the reaction mixture was mixed under reflux for 7hrs. After stop the reaction, the solvent was removed under vacuum, the residue was purified by column chromatography (DCM:PE=1:1) to get the final product **3-14a** in 30% yield as white solid and **3-15a** in 58% yield as white solid.

1,3,5-Trikis(4'-methoxy)phenyl-2,4,6-trikis(4'-(*t*-butyl)phenyl)-benzene (3-14a)

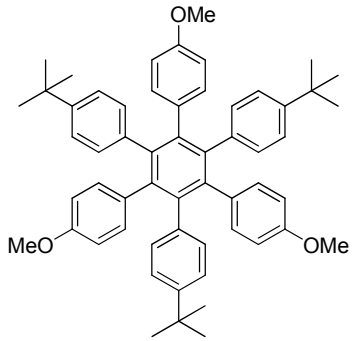

Mp: 298-301°C. FD-MS (8 KV): m/z 793.9, calcd.: 793.08 (M^+). ^{1}H NMR (CD_2Cl_2, 250 MHz): δ ppm 6.86(d, 6H, J=8.22Hz), 6.66(t, 12H, J=8.22Hz), 6.33(d, 6H, J=8.22Hz), 3.54(s, 9H), 1.11(s, 27H). ^{13}C NMR (62.5 MHz, CD_2Cl_2): δ ppm 157.35, 148.19, 141.01, 140.36, 138.56, 133.85, 132.80, 131.49, 123.68, 112.18, 34.38, 31.31. Elemental Analysis: Calculated: C 86.32, H 7.63, O 6.05; Found: C 86.23, H 7.58.

1,2,4-Trikis(4'-methoxy)phenyl-3,5,6-trikis(4'-(*t*-butyl)phenyl)-benzene (3-15a)

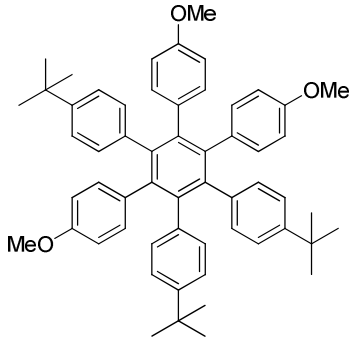

Mp: 256~258°C. FD-MS (8 KV): m/z 793.7, calcd.: 793.08 (M^+). ^{1}H NMR (CD_2Cl_2, 250 MHz): δ ppm 6.88~6.63(m, 18H), 6.36(m, 6H), 3.56(s, 6H), 3.54(s, 3H), 1.11(s, 18H), 1.09(s, 9H). ^{13}C NMR (62.5 MHz, CD_2Cl_2): δ ppm 157.39, 148.18, 148.09, 141.20, 140.48, 140.21, 140.12, 138.52, 133.91, 133.84, 132.82, 131.47, 131.39, 123.68, 123.56, 112.28, 112.22, 34.35, 31.31. Elemental Analysis: Calculated: C 86.32, H 7.63, O 6.05; Found: C 86.27, H 7.61.

4-Methoxy-4'-(*n*-dodecyl)-diphenylacetylene (3-13b)

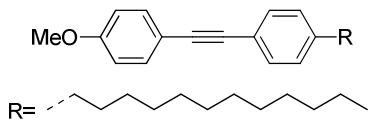

1.5 g (6.41 mmol) 4-methoxyiodobenzene and 1.91g 4-dodecylphenyacetylene were dissolved in 20 ml triethylamine, the mixture was degassed by bubbling through argon for 20 min and then 135 mg (3mol%) $Pd(PPh_3)_2Cl_2$ and 73 mg CuI (6mol%) were added. The mixture was stirred at room temperature overnight, poured into aqueous HCl and extracted with dichloromethane. The organic layer was washed by water and dried over $MgSO_4$. The solvent was removed under vacuum and the residue was purified by column chromatography (DCM:Hex=1:3) to provide 2.30 g white solid (95%). Mp: 52-54^oC. FD-MS (8 KV): m/z 376.8, calcd.: 376.57 (M^+). ^1H NMR (CD_2Cl_2, 250 MHz): δ ppm 7.44(m, 4H), 7.14(d, 2H, J=8.20Hz), 6.86(d, 2H, J=8.20Hz), 3.80(s, 3H), 2.60(t, 2H, J=7.90Hz), 1.58(m, 2H), 1.24(m, 18H), 0.86(m, 3H). ^{13}C NMR (62.5 MHz, CD_2Cl_2): δ ppm 160.02, 143.75, 138.53, 133.23, 131.56, 128.86, 120.95, 116.71, 115.79, 114.36, 88.87, 88.43, 55.66, 36.18, 32.29, 31.67, 30.01, 29.95, 29.84, 29.72, 29.63, 23.06,14.25. Elemental Analysis: Calculated: C 86.12, H 9.64, O 4.25; Found: C 86.17, H 9.68.

Synthesis of 3-14b and 3-15b:

2.2 g (5.84 mmol) **3-13b** was dissolved in 55 ml dioxane, the mixture was degassed by bubbling through argon for 30min and 10 mmol% $Co_2(CO)_8$ 198 mg were added, the reaction mixture was mixed under reflux for 7hrs. After stop the reaction, the solvent was removed under vacuum, the residue was purified by column chromatography (DCM:PE=1:1) to get the final product **3-14b** in 28% yield as sticky oil and **3-15b** in 62% yield as sticky oil.

1,3,5-Trikis(4'-methoxy)phenyl-2,4,6-trikis(4'-(*n*-dodecyl)phenyl)-benzene (3-14b)

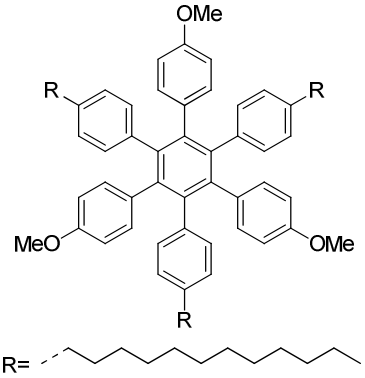

FD-MS (8 KV): m/z 1129.5, calcd.: 1129.72 (M^+). ^1H NMR (CD_2Cl_2, 250 MHz): δ ppm

6.68(m, 18H), 6.35(d, 6H, J=8.82Hz), 3.56(s, 9H), 2.36(t, 6H, J=7.25Hz), 1.43~1.13(m, 60H), 0.86(m, 9H). ^{13}C NMR (62.5 MHz, CD_2Cl_2): δ ppm 157.32, 141.09, 140.32, 139.84, 138.80, 133.85, 132.79, 131.62, 126.96, 112.16, 55.17, 35.57, 32.31, 31.51, 30.09, 30.07, 30.04, 29.98, 29.82, 29.75, 29.21, 23.08, 14.26.

1,2,4-Trikis(4'-methoxy)phenyl-3,5,6-trikis(4'-(*n*-dodecyl)phenyl)-benzene (3-15b)

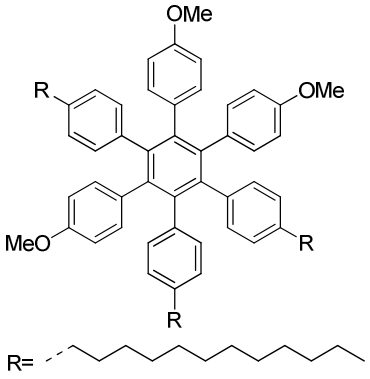

FD-MS (8 KV): m/z 1129.6, calcd.: 1129.72 (M^+). ^{1}H NMR (CD_2Cl_2, 250 MHz): δ ppm 6.72~6.65(m, 18H), 6.37(m, 6H), 3.58(d, 9H), 2.34(m, 6H), 1.39~1.13(m, 60H), 9.86(m, 9H). ^{13}C NMR (62.5 MHz, CD_2Cl_2): δ ppm 157.34, 141.07, 141.00, 140.46, 140.22, 139.81, 138.74, 133.91, 133.86, 132.81, 131.61, 126.97, 126.88, 112.25, 112.18, 35.63, 32.32, 31.64, 30.11, 30.07, 29.98, 29.88, 29.77, 29.27, 29.21, 23.08, 14.26.

Synthesis of 3-16a and 3-17a

590 mg (0.744mmol) **3-15a** was dissolved in 200ml dichloromethane, the solution was then degassed by bubbling through argon for 20 min, and then 2.89g $FeCl_3$ (24eqv) in 7ml CH_3NO_2 was added dropwise. After being stirred for 45 min, the reaction was quenched by adding methanol, the yellow precipitate was collected, washed by methanol repeatedly and reprecipitated and dried under vacuum to afford **3-16a** 212mg yellow powder (36%) with strongly chlorination (+Cl, 2Cl, 3Cl) Water was added to the filtrate solution, the organic fraction was separated and dried under $MgSO_4$, solvent was removed under vacuum, the residue was purified by column chromatography (PE:EA=4:1) to get the final product **3-17a** in 54% yield as white solid

1,7,13-Trikis(4'-methoxy)-4,10,16-trikis(4'-(*t*-butyl))-hexa-*peri*-hexabenzocoronene

(3-16a)

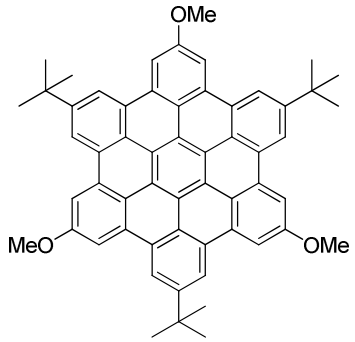

MALDITOF-MS (TCNQ as matrix): m/z=780.35, calcd. 780.99 for $C_{57}H_{48}O_3$. Additonally strong chlorination was observed.

5-Methoxyphenyl-11-(*t*-butyl)phenyl-2,8-di(*t*-butyl)-10,12-bis(spiro(6'-oxo-cyclohexa-1'-4'-diene)-3')indeno[1,2-b]fluorene (3-17a)

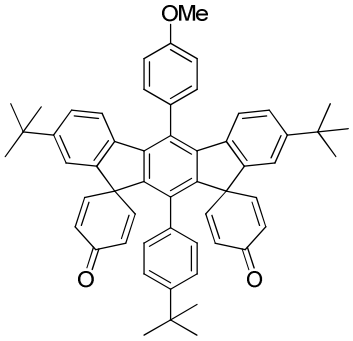

Mp: >350°C. FD-MS (8 KV): m/z 761.3, calcd.: 761.00 (M^+). ^{1}H NMR (CD_2Cl_2, 250 MHz): δ ppm 7.44(d, 2H, J=8.52Hz), 7.20(d, 2H, J=8.52Hz), 7.23(d, 2H, J=8.52Hz), 6.99(m, 6H), 6.44(m, 6H), 5.92(d, 4H, J=8.52Hz), 3.98(s, 3H), 1.24(s, 9H), 1.18(s, 18H). ^{13}C NMR (62.5 MHz, CD_2Cl_2): δ ppm 185.49, 160.27, 152.25,151.80, 149.60, 143.49, 141.35, 140.95, 140.17, 138.97, 137.73, 131.04, 130.85, 130.55, 129.40, 125.99, 123.66, 123.25, 121.38, 115.48, 57.03, 55.78, 35.12, 34.69, 31.36, 31.20. Elemental Analysis: Calculated: C 86.81, H 6.89, O 6.31; Found: C 86.72, H 7.00.

Synthesis of 3-16b and 3-17b

250 mg (0.221mmol) **3-15b** was dissolved in 120ml dichloromethane, the solution was then degassed by bubbling through argon for 20 min, and then 646 mg $FeCl_3$ (18eqv) in 3ml CH_3NO_2 was added dropwise. After being stirred for 35 min, the reaction was

quenched by adding methanol, the yellow precipitate was collected, washed by methanol repeatedly and reprecipitated and dried under vacuum to afford **3-16b** 108mg yellow powder (43%). Water was added to the filtrate solution, the organic fraction was separated and dried under $MgSO_4$, solvent was removed under vacuum, the residue was purified by column chromatography (PE:EA=4:1) to get the final product **3-17b** in 50% yield as sticky solid.

1,7,13-Trikis(4'-methoxy)-4,10,16-trikis(4'-(*n*-dodecyl))-hexa-*peri*-hexabenzocorone (3-16b)

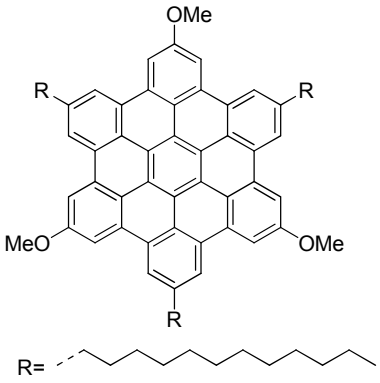

MALDITOF-MS (TCNQ as matrix): m/z=1117.62, calcd. 1117.63 for $C_{81}H_{96}O_3$. ^{1}H NMR ($CDCl_2CDCl_2$, 500 MHz): δ ppm 7.90(s, 6H), 7.66(s, 6H), 3.99(s, 9H), 2.72(br, 6H), 1.77~1.19(m, 60H), 0.85(m, 9H). ^{13}C NMR (62.5 MHz, $CDCl_2CDCl_2$): δ ppm 156.69, 139.17, 130.58, 128.32, 122.50, 120.83, 118.98, 118.58, 116.76, 105.78, 55.18, 36.79, 31.99, 31.89, 30.03, 29.84, 29.78, 29.71, 29.37, 22.68, 14.19. Elemental Analysis: Calculated: C 87.05, H 8.66, O 4.29; Found: C 85.93, H 8.78.

5-Methoxyphenyl-11-(*n*-dodecyl)phenyl-2,8-di(*n*-dodecyl)-10,12-bis(spiro(6'-oxo-cyclohexa-1'-4'-diene)-3')indeno[1,2-b]fluorene (3-17b)

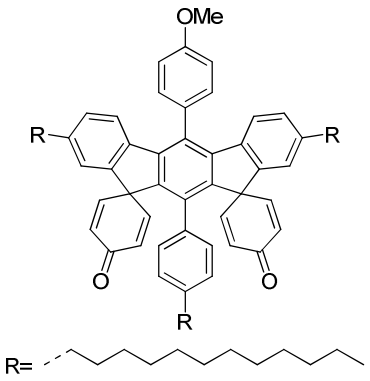

FD-MS (8 KV): m/z 1098.1, calcd.: 1097.64 (M^+). ^{1}H NMR (CD_2Cl_2, 250 MHz): δ ppm 7.45(d, 2H, J=8.52Hz), 7.20(d, 2H, J=8.52Hz), 6.88(m, 8H), 6.45(m, 6H), 5.94(d, 4H, J=8.52Hz), 2.46(m, 6H), 1.33~1.21(m, 60H), 0.85(m, 9H). ^{13}C NMR (62.5 MHz, CD_2Cl_2): δ ppm 185.54, 160.27, 149.77, 143.68, 143.55, 141.48, 141.06, 139.20, 131.70, 131.51, 131.09, 131.02, 130.55, 129.23, 128.92, 126.48, 124.58, 123.92, 115.51, 56.86, 55.77, 36.13, 32.29, 31.92, 30.09, 30.00, 29.91, 29.78, 29.71, 29.62, 23.06, 14.25.

1,3,5-Tris(2'-(4"-phenyl)biphenyl)benzene (4-12)

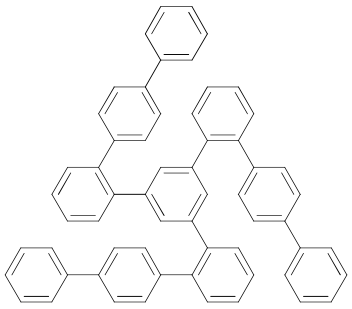

420 mg (0.773mmol) 1,3,5-tris-2'-bromophenylbenzene, 919mg (4.64mmol) 4-biphenyl boronic acid, 91mg (10mol%) $Pd(PPh_3)_4$, 2.14g K_2CO_3, 25ml toluene, 6ml EtOH and 6ml H_2O were added into 50ml Schlenk flask. The mixture was degassed by two "freeze-pump-thaw"cycles and then heated to reflux overnight. After standard work-up and purification by column chromatography (Silica gel, PE/DCM =6/1), 489mg white solid was obtained (83%). Mp: 263~266^{o}C. FD-MS (8 KV): m/z 763.4, calcd.: 762.98 (M^+). ^{1}H NMR (300 MHz, CD_2Cl_2): δ ppm 7.38~7.31 (m, 27H), 7.21 (m, 3H), 6.96 (d, 9H, J=8.1Hz), 6.80 (s, 3H). ^{13}C NMR (75 MHz, CD_2Cl_2): δ ppm141.56, 141.10, 141.01, 140.97, 140.72, 139.43, 130.76, 130.43, 130.03, 129.24, 127.44, 127.62, 127.58, 127.31, 127.01. Elemental analysis: Calcd.: C 94.45, H 5.55; Found: C 94.30, H 5.40.

Benzo[o]bistriphenyleno[2,1,12,11-efghi:2',1',12',11'-uvabc]ovalene
(**TrinaphthoHBC 4-2**)

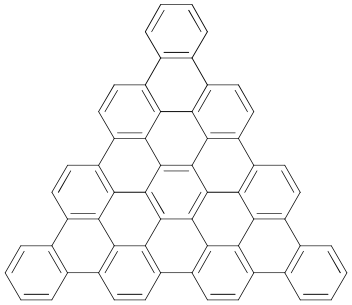

110 mg (0.144mmol) **4-12** was dissolved in 50ml dichloromethane, the solution was then degassed by bubbling through argon for 20 min, and then 2.14g $FeCl_3$ in 11ml CH_3NO_2 was added dropwise. After being stirred for 50 min, the reaction was quenched by adding 100ml methanol, the yellow precipitate was collected, washed by water and methanol repeatedly and dried under vacuum to afford 76mg red powder (71%). MALDITOF-MS (TCNQ as matrix): m/z=744.34, calcd. 744.83 for $C_{60}H_{24}$.

1,3,5-Tris[2'-(4"-(4"'-trimethylsilyl)phenyl))biphenyl]benzene (4-15)

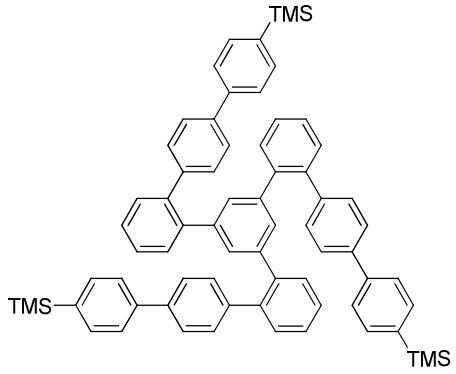

418 mg (0.458mmol) 1,3,5-tris(4"-iodo-2'-biphenyl)ylbenzene, 400mg (2.06mmol) 4-trimethylsilylphenyl boronic acid, 54mg (10mol%) $Pd(PPh_3)_4$, 1.27g K_2CO_3, 17ml THF, 4.5ml EtOH and 4.5ml H_2O were added into 50ml Schlenk flask. The mixture was degassed by two "freeze-pump-thaw"cycles and then heated to reflux overnight. After standard work-up and purification by column chromatography (Silica gel, PE/DCM =5/1), 314mg white solid was obtained (70%). Mp: 291~293^oC. FD-MS (8 KV): m/z 979.8, calcd.: 979.52 (M^+). ^1H NMR (250 MHz, CD_2Cl_2): δ ppm 7.54 (d, 6H, J=6.25Hz), 7.31~7.21 (m, 15H), 7.13 (d, 6H, J= 6.62Hz), 7.04 (d, 3H, J= 7.25Hz), 6.78(m, 9H), 0.31

(s, 27H). ^{13}C NMR (62.5 MHz, CD_2Cl_2): δ 141.81, 141.39, 141.15, 141.08, 140.93, 139.54, 139.11, 134.30, 130.77, 130.61, 130.40, 129.86, 127.69, 127.52, 127.06, 126.60, -0.95. Elemental analysis: Calcd.: C 84.61, H 6.79, Si 8.60; Found: C 84.33, H 6.74.

1,3,5-Tris[2'-(4"-(4"'-iodophenyl))biphenyl]benzene (4-16)

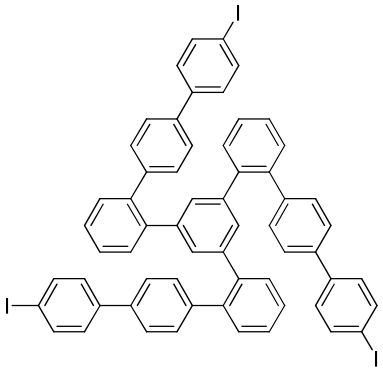

302mg (0.308mmol) **4-15** was dissolved in 25ml $CHCl_3$, then degassed by bubbling through argon for 20 min, then 2.5 ml iodine monochloride (1.0 M in CH_2Cl_2) was added slowly. After stirring for 1h, the reaction was quenched by adding aqueous sodium disulfite. The organic layer was washed by water three times and dried over $MgSO_4$. The solution was concentrated to 5 ml and then 50 ml MeOH was added to precipitate the product. The white solid was collected and dried under vacuum to get 349mg product (99%). Mp: >275°C, decompose. FD-MS (8 KV): m/z 1140.8, calcd.: 1140.67 (M^+). ^1H NMR (250 MHz, CD_2Cl_2): δ ppm 7.74(m, 6H), 7.31~6.65(m, 33H). ^{13}C NMR (62.5 MHz, CD_2Cl_2): δ ppm 141.64, 141.50, 140.97, 140.79, 140.57, 138.73, 138.46, 138.16, 130.78, 130.40, 129.94, 129.23, 127.77, 127.65, 126.85, 93.18. Elemental analysis: Calcd.: C 63.18, H 3.45, I 33.38; Found: C 62.99, H 3.47.

Tri(iodonaphtho)HBC (4-3)

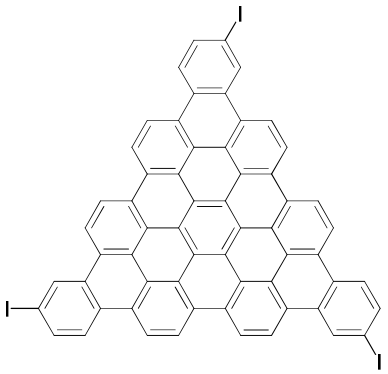

50 mg (0.0438mmol) **4-16** was dissolved in 40ml dichloromethane, the solution was then degassed by bubbling through argon for 20 min, and then 0.64g $FeCl_3$ in 1.5ml CH_3NO_2 was added dropwise. After being stirred for 4h, the reaction was quenched by adding 50ml methanol, the yellow precipitate was collected, washed by water and methanol repeatedly and dried under vacuum to afford 41mg yellow powder (83%). MALDITOF-MS (TCNQ as matrix): m/z=1121.7, calcd. 1122.52 for $C_{60}H_{21}I_3$.

1,3,5-Tris(2'-(4"-dibenzothiophene)phenyl)benzene (4-13)

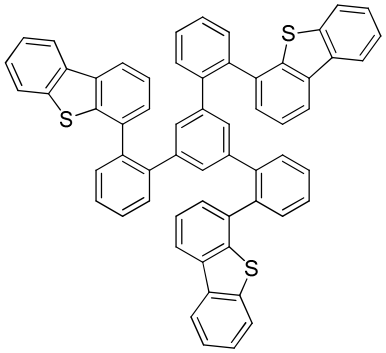

400 mg (0.735mmol) 1,3,5-tris-2'-bromophenylbenzene, 754mg (3.31mmol) 4-dibenzothiopheneboronic acid, 86mg (10mol%) $Pd(PPh_3)_4$, 2.00g K_2CO_3, 26ml toluene, 6ml EtOH and 6ml H_2O were added into 50ml Schlenk flask. The mixture was degassed by two "freeze-pump-thaw"cycles and then heated to reflux overnight. After standard work-up and purification by column chromatography (Silica gel, PE/DCM =2/1), 546mg white solid was obtained (87%). Mp: 200~203°C. FD-MS (8 KV): m/z 853.3, calcd.: 853.12 (M^+). ^{1}H NMR (250 MHz, CD_2Cl_2): δ ppm 8.20 (d, 3H, J= 5.75Hz), 8.02 (d, 3H, J= 7.75Hz), 7.75 (d, 3H, J= 8.15 Hz), 7.48 (m, 9H), 7.22 (m, 3H), 6.96 (s, 6H), 6.61(s, 6H), 6.36(s, 3H). ^{13}C NMR (62.5 MHz, CD_2Cl_2): δ ppm 140.83, 140.30, 140.10, 139.99, 138.78, 137.02, 136.13, 135.89, 130.56, 130.10, 129.06, 128.87, 128.45, 127.45, 127.11, 124.80, 124.74, 123.13, 122.06, 120.19. Elemental analysis: Calcd.: C 84.47, H 4.25, S 11.28; Found: C 84.46, H 4.24, S 11.28.

TribenzothiopheneHBC (4-4)

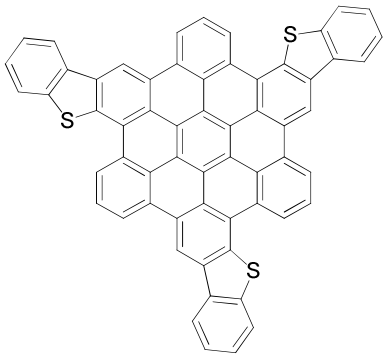

200 mg (0.234mmol) **4-13** was dissolved in 80ml dichloromethane, the solution was then degassed by bubbling through argon for 20 min, and then 1.37g $FeCl_3$ in 12ml CH_3NO_2 was added dropwise. After being stirred for 40 min, the reaction was quenched by adding 100ml methanol, the yellow precipitate was collected, washed by methanol and water repeatedly and dried under vacuum to afford 159mg yellow powder (81%). MALDITOF-MS (TCNQ as matrix): m/z=840.1, calcd. 841.03 for $C_{60}H_{24}S_3$.

1,3,5-Tris(2'-(2"-phenylethynyl)biphenyl)benzene (4-17a)

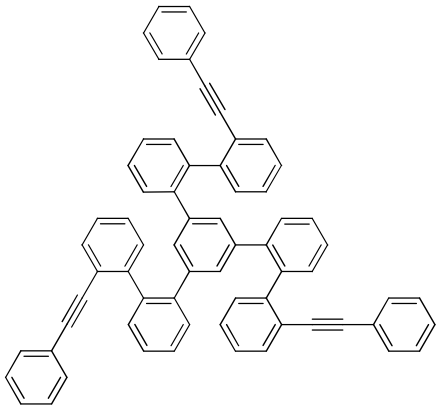

859mg (1.58mmol) 1,3,5-tris-2'-bromophenylbenzene, 1.30g (5.85mmol) o-phenylethynylbenzeneboronic acid, 55mg (3mol%) $Pd(PPh_3)_4$, 2.18g K_2CO_3, 50ml toluene, 10ml EtOH and 10ml H_2O were added into 100ml Schlenk flask. The mixture was degassed by two "freeze-pump-thaw"cycles and then heated to reflux overnight. After standard work-up and purification by column chromatography (Silica gel, PE/DCM =2/1), 1.072g of little yellow oil was obtained (82%). FD-MS (8 KV): m/z 835.8, calcd.: 835.04 (M^+). ^1H NMR (250 MHz, CD_2Cl_2): δ ppm 7.54~7.10 (m, 33H), 6.70 (s, br, 9H). ^{13}C NMR (62.5 MHz, CD_2Cl_2): δ ppm 144.52, 141.32, 140.47, 139.41, 132.25, 131.59, 131.31, 130.18, 129.87, 128.47, 128.34, 128.09, 127.99, 126.97, 126.76, 123.57, 123.28,

92.70, 89.43.

1,3,5-Tris(2'(2"-(3,7-dimethyloctanyl)phenylethynyl)benzene (4-17b)

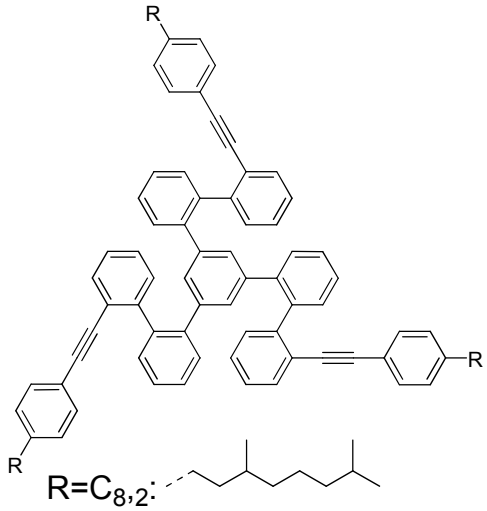

4-17b was synthesized as the little yellow oil by using the same procedure as above. 86%). FD-MS (8 KV): m/z 1255.6, calcd.: 1255.84 (M^+). ^{1}H NMR (250 MHz, CD_2Cl_2): δ ppm 7.51~6.93 (m, 30H), 6.69(s, br. 9H), 2.52(m, 6H), 1.52~1.10(m, 30H), 0.89~0.84(m, 27H). ^{13}C NMR (62.5 MHz, CD_2Cl_2): δ ppm 144.38, 144.00, 141.32, 140.47, 139.48, 132.19, 131.52, 131.29, 130.18, 129.86, 128.59, 127.92, 126.92, 126.68, 123.51, 120.65, 93.03, 88.81, 39.69, 39.07, 37.48, 33.67, 31.96, 28.36, 25.06, 22.83, 22.73, 19.68, 14.24.

1,3,5-Tris(9'-(4"-iodo-5"-phenyl)phenanthrenyl)benzene (4-18a)

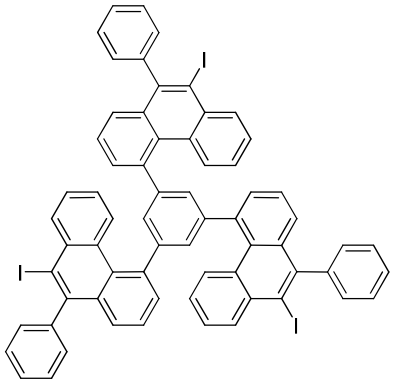

1.041g (1.246mmol) **4-17a** in 24ml dry dichloromethane was cooled down to –78^{o}C in dry ice-acetone bath, then 3.9eq ICl (4.86mmol, 1M in dichloromethanee) was added

dropwise over 5min. The mixture was kept at –78°C for 2h and then quenched by adding aqueous $Na_2S_2O_3$ solution. The organic layer was washed with water two times and dried over $MgSO_4$. After the solvent was removed to leave 5ml and 50ml cold methanol was added to give white precipitate, the white solid was collected and washed by methanol without further purification, dried under vacuum to afford 1.42g in 92% yield. Mp: >350°C. FD-MS (8 KV): m/z 1212.7, calcd.: 1212.73 (M^+). ^{1}H NMR (250 MHz, $CDCl_2CDCl_2$): δ ppm 8.98 (d, 0.89H, J=7.5Hz), 8.45(m, 4.30H), 8.00(d, 0.71H, J=8.5Hz), 7.73~7.28(m, 33H). ^{13}C NMR (62.5 MHz, $CDCl_2CDCl_2$): δ ppm 146.87, 146.17, 145.36, 145.25, 139.20, 139.16, 134.23, 133.76, 133.67, 133.44, 133.36, 133.21, 131.43, 130.26, 129.88, 129.38, 128.91, 128.55, 128.48, 127.78, 126.22, 125.18, 107.19(C-I). Elemental Analysis: Calculated: C 65.37, H 3.24, I 31.39; Found: C 64.57, H 3.48.

1,3,5-Tris(9'-(4"-iodo-5"-(3,7-dimethyloctanyl)phenyl)phenanthrenyl)benzene (18b)

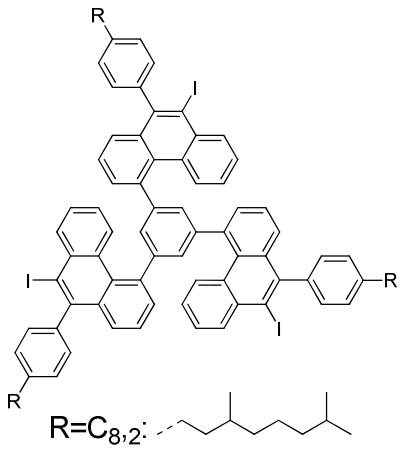

4-18b was synthesized as a slightly yellow solid by using the same procedure as above. 95%). FD-MS (8 KV): m/z 1633.4, calcd.: 1633.53 (M^+). ^{1}H NMR (250 MHz, CD_2Cl_2): δ ppm 8.93(d, 0.65H, J=8.22Hz), 8.51~8.38(m, 4.34H), 8.00(d, 0.73H, J=8.44Hz), 7.77~7.12(m, 29.94H), 2.78(m, 6H), 1.79~1.16(m, 30H), 0.98(d, 9H, J=6.0Hz), 0.87(d, 18H, J=6.62Hz). ^{13}C NMR (62.5 MHz, CD_2Cl_2): δ ppm 147.44, 145.95, 143.48, 143.21, 139.84, 134.61, 134.47, 134.37, 134.03, 131.97, 131.76, 131.49, 130.73, 130.24, 130.17, 129.97, 129.16, 129.07, 128.79, 128.08, 126.52, 125.57, 107.49(C-I), 39.69, 39.31, 37.55, 33.02, 28.40, 25.12, 22.86, 22.78, 19.84.

1,3,5-Tris(9'-(5"-phenyl)phenanthrenyl)benzene (4-19a)

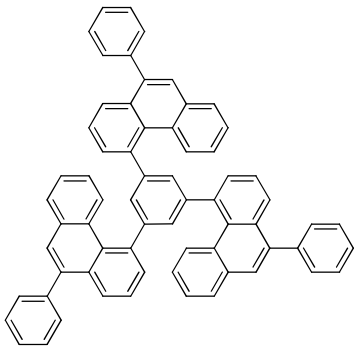

A solution of (247mg, 0.203mmol) **4-18a** in 50ml dry THF was cooled to –78°C, and s-BuLi (6.2ml, 1.3M, 8.1mmol) was added resulting in the formation of deep black solution. After 5 min of stirring, the reaction was quenched by rapid addition of 16ml methanol. The mixture was then diluted with 100ml $CHCl_3$, washed with 5% HCl (50ml×2) and H_2O, and dried under Na_2SO_4. The solvent was removed under vacuum to afford 166mg as white solid (98%yield). Mp: >350°C. FD-MS (8 KV): m/z 834.1, calcd.: 835.04 (M^+). ^1H NMR (250 MHz, $CDCl_2CDCl_2$): δ ppm 9.14(d, 1.03H, J=8.5Hz), 8.66(d, 1.21H, J=8.78Hz), 8.08(d, 0.69H, J=8.5Hz), 7.96~7.34(m, 39.04H). ^{13}C NMR (62.5 MHz, $CDCl_2CDCl_2$): δ ppm 147.09, 147.00, 146.36, 140.79, 140.76, 139.92, 139.87, 138.76, 138.69, 132.84, 132.78, 132.66, 132.56, 131.22, 130.94, 130.05, 129.64, 129.60, 129.51, 129.01, 128.71, 128.67, 128.50, 128.31, 127.36, 126.65, 126.55, 125.64, 124.61. Elemental analysis: Calcd.: C 94.93, H 5.07; Found: C 94.94, H 5.00.

1,3,5-Tris(9'-(5"-(3,7-dimethyloctanyl)phenyl)phenanthrenyl)benzene (19b)

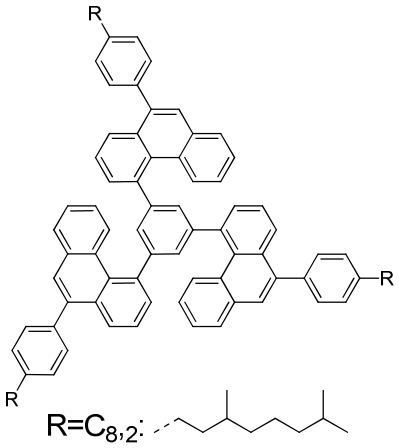

4-19b was synthesized as the little yellow solid by using the same procedure as above.

97%). FD-MS (8 KV): m/z 1254.6, calcd.:1255.84 (M^+). ^{1}H NMR (250 MHz, CD_2Cl_2): δ ppm 9.08(d, 0.73H, J=8.48Hz), 8.62(d, 1.39H, J=8.48Hz), 8.03(d, 0.77H, J=8.78Hz), 7.91~7.27(m, 35.65H), 2.76(m, 6H), 1.75~1.17(m, 30H), 0.98(d, 9H, J=5.95Hz), 0.90(d, 18H, J=6.58Hz). ^{13}C NMR (62.5 MHz, CD_2Cl_2): δ ppm 147.72, 147.60, 146.96, 143.00, 140.55, 140.41, 139.33, 139.25, 138.56, 133.50, 133.37, 133.27, 131.48, 131.30, 130.94, 130.35, 130.12, 129.63, 129.31, 129.24, 129.07, 128.90, 128.80, 128.69, 128.53, 127.16, 126.84, 126.76, 125.97, 124.92, 39.73, 39.44, 37.55, 33.63, 33.01, 28.41, 25.12, 22.88, 22.79, 19.83.

1,3,5-Tris(9'-(4"-5"-diphenyl)phenanthrenyl)benzene (20a)

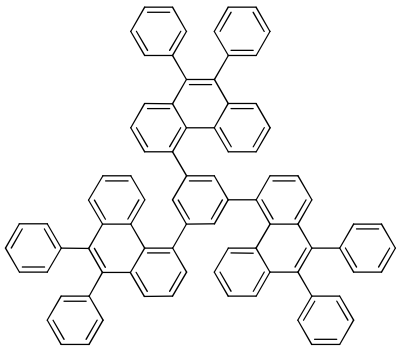

500mg (0.412 mmol) **4-18a**, 226mg (1.86 mmol) phenylboronic acid, 20mg (4 mol%) $Pd(PPh_3)_4$, 569 mg K_2CO_3, 20 ml toluene, 5ml EtOH and 5 ml H_2O were added into 50 ml Schlenk flask. The mixture was degassed by two "freeze-pump-thaw"cycles and then heated to reflux overnight. After standard work-up and purification by recrystallization from chloroform, 355 mg white solid was obtained (81%). Mp: >350^{o}C. FD-MS (8 KV): m/z 1063.5, calcd.: 1063.33 (M^+). ^{1}H NMR (250 MHz, $CDCl_2CDCl_2$): δ ppm 9.16(d, 1.18H, J=8.18Hz), 8.70(d, 1.09H, J=8.48Hz), 8.17(d, 0.53H, J=8.48Hz), 7.83~7.14(m, 52.20H). ^{13}C NMR (62.5 MHz, $CDCl_2CDCl_2$): δ ppm 147.24, 147.19, 139.60, 139.55, 139.51, 139.33, 139.29, 139.25, 137.57, 137.53, 137.48, 137.12, 133.49, 133.44, 133.33, 133.25, 133.18, 133.05, 130.93, 130.86, 130.45, 129.69, 129.12, 128.59, 128.36, 128.28, 128.24, 127.71, 127.56, 127.48, 126.28, 125.70, 124.17, 124.00.

1,3,5-Tris(9'-(4"-5"-di(3,7-dimethyloctanyl)phenyl)phenanthrenyl)benzene (4-20b)

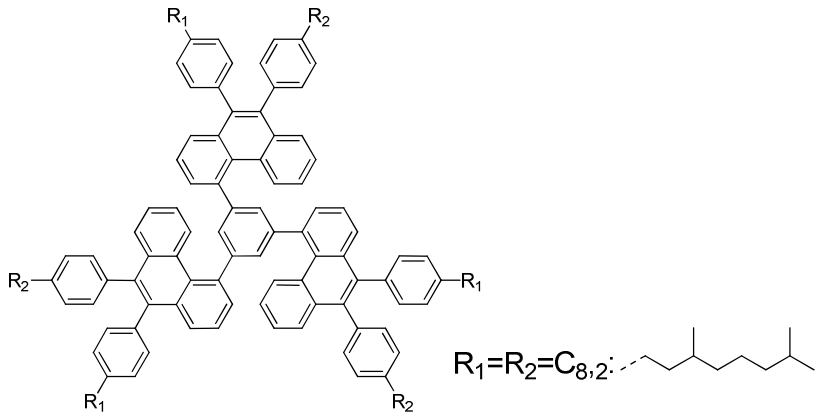

4-20b was synthesized as the little yellow solid by using the same procedure as above. 83%). FD-MS (8 KV): m/z 1905.6, calcd.: 1904.92 (M^+). ^{1}H NMR (250 MHz, CD_2Cl_2): δ ppm 9.14(d, 0.82H, J=8.48Hz), 8.68(d, 1.31H, J=8.56Hz), 8.14(d, 0.65H, J=8.48Hz), 7.84(s, 0.81H), 7.72~7.19(m, 20.97H), 7.04(d, 23.56H, J=4.38Hz), 2.56(m, 12H), 1.61~1.14(m, 60H), 0.91~0.85(m, 54H). ^{13}C NMR (62.5 MHz, CD_2Cl_2): δ ppm 147.81, 147.66, 147.05, 141.71, 140.09, 139.92, 138.08, 137.70, 137.48, 137.31, 137.16, 134.28, 134.16, 134.01, 133.89, 131.29, 131.19, 130.82, 130.35, 130.15, 129.84, 129.10, 128.97, 128.80, 128.71, 127.87, 126.48, 126.02, 124.42, 39.72, 39.16, 37.51, 33.49, 32.86, 28.38, 25.09, 22.85, 22.78, 19.81.

TrizigzagHBC(PhI)$_3$ (4-5)

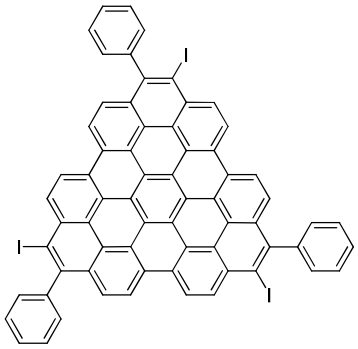

150 mg (0.123 mmol) **4-18a** was dissolved in 100 ml dichloromethane, the solution was then degassed by bubbling through argon for 20 min, and then 722mg $FeCl_3$ in 6ml CH_3NO_2 was added dropwise. After being stirred for 30 min, the reaction was quenched by adding 100 ml methanol, the yellow precipitate was collected, washed by methanol repeatedly and dried under vacuum to afford 127mg red brown powder (86%). MALDITOF-MS (TCNQ as matrix): m/z=1200.40, calcd. 1200.63 for $C_{66}H_{27}I_3$.

TrizigzagHBC(Ph)$_3$ (4-6)

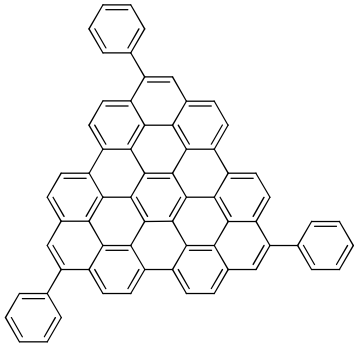

200 mg (0.239 mmol) **4-19a** was dissolved in 150 ml dichloromethane, the solution was then degassed by bubbling through argon for 20 min, and then 1.40 g $FeCl_3$ in 7 ml CH_3NO_2 was added dropwise. After being stirred for 35 min, the reaction was quenched by adding 100 ml methanol, the red brown precipitate was collected, washed by methanol repeatedly and dried under vacuum to afford 172 mg yellow powder (88%). MALDITOF-MS (TCNQ as matrix): m/z=822.34, calcd. 822.23 for $C_{66}H_{30}$.

TrizigzagHBC(Ph)$_6$ (4-7)

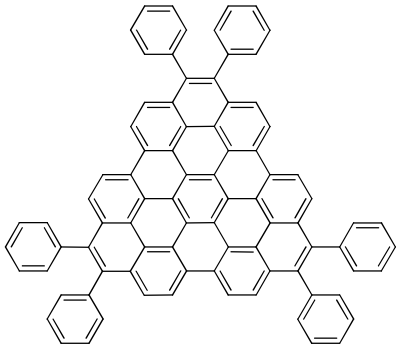

250 mg (0.235mmol) **4-20a** was dissolved in 200 ml dichloromethane and 50 ml CS_2, the solution was then degassed by bubbling through argon for 20 min, and then 2.06 g $FeCl_3$ in 11ml CH_3NO_2 was added dropwise. After being stirred for 1.5 h, the reaction was quenched by adding 200 ml methanol, the red brown precipitate was collected, washed by methanol repeatedly and dried under vacuum to afford 188mg yellow powder (76%). MALDITOF-MS (TCNQ as matrix): m/z=1050.6, calcd. 1051.23 for $C_{84}H_{42}$.

TrizigzagHBC(PhC$_{8,2}$I)$_3$ (4-8)

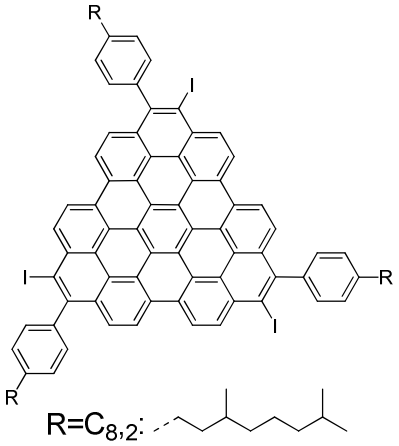

50 mg (0.0306mmol) **4-18b** was dissolved in 40 ml dichloromethane, the solution was then degassed by bubbling through argon for 20 min, and then 60eq $FeCl_3$ in 1ml CH_3NO_2 was added dropwise. After being stirred for 35 min, the reaction was quenched by adding 50 ml methanol, the yellow precipitate was collected, washed by methanol repeatedly, redissolved in THF and precipitated by adding the methanol, the precipitate was dried under vacuum to afford 35 mg yellow powder (72%). MALDITOF-MS (TCNQ as matrix): m/z=1621.40, calcd. 1621.43 for $C_{96}H_{87}I_3$. ^{1}H NMR (700 MHz, $CDCl_2CDCl_2$, 140^{o}C): δ ppm 7.91~7.26 (m, 24H), 3.11(t, 6H), 1.95~1.12(m, 57H). ^{13}C NMR can not be well resolved because of the large disc.

TrizigzagHBC(Ph$C_{8,2}$)$_3$ (4-9)

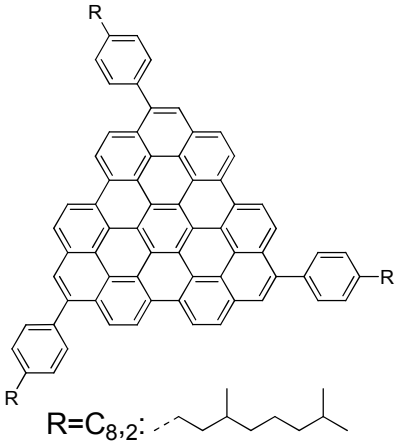

150 mg (0.119 mmol) **4-19b** was dissolved in 100 ml dichloromethane, the solution was then degassed by bubbling through argon for 20 min, and then 36eq $FeCl_3$ in 2 ml CH_3NO_2 was added dropwise. After being stirred for 35 min, the reaction was quenched

by adding 50 ml methanol, the yellow precipitate was collected, washed by methanol repeatedly, redissolved in THF passed through a short silica column, the solution was collected and dried under vacuum to afford 116 mg yellow powder (78%). MALDITOF-MS (TCNQ as matrix): m/z=1243.85, calcd. 1243.74 for $C_{96}H_{90}$. ^{1}H NMR (700 MHz, $CDCl_2CDCl_2$, 140^{o}C): δ ppm 8.60~8.04(m, 15H), 7.89(s, 6H), 7.76(s, 6H), 3.13 (t, 6H), 2.16~1.12(m, 57H). ^{13}C NMR can not be well resolved because of the large disc.

TriszigzagHBC($PhC_{8,2}$)$_6$ (4-10)

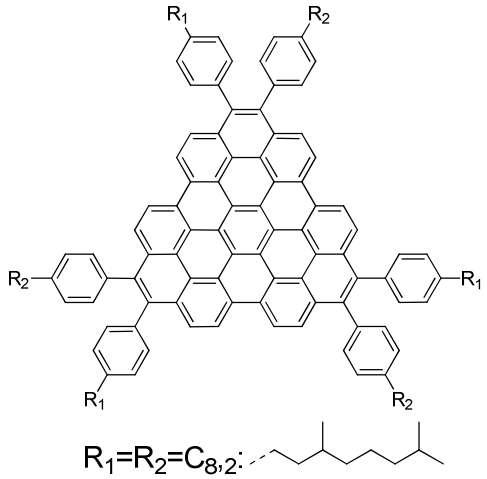

150 mg (0.0787 mmol) **4-20b** was dissolved in 100 ml dichloromethane, the solution was then degassed by bubbling through argon for 20 min, and then 24eq $FeCl_3$ in 2ml CH_3NO_2 was added dropwise. After being stirred for 60 min, the reaction was quenched by adding 50 ml methanol, the yellow precipitate was collected, washed by methanol repeatedly, redissolved in THF passed through a short silica column, the solution was collected and dried under vacuum to afford 127 mg yellow powder (85%). MALDITOF-MS (TCNQ as matrix): m/z=1893.03, calcd. 1892.83 for $C_{114}H_{162}$. ^{1}H NMR (500 MHz, $CDCl_2CDCl_2$, 140 ^{o}C): 9.27(s, 6H), 8.65(s, 6H), 7.62(s, 12H), 7.37(s, 12H), 2.88(m, 12H), 1.90~0.89(m, 114H). ^{13}C NMR can not be well resolved because of the large disc.

1,3,5-Tris(2'-(4"-(4"'-(2""-hexyl-decyl))phenyl)biphenyl)benzene (4-21a)

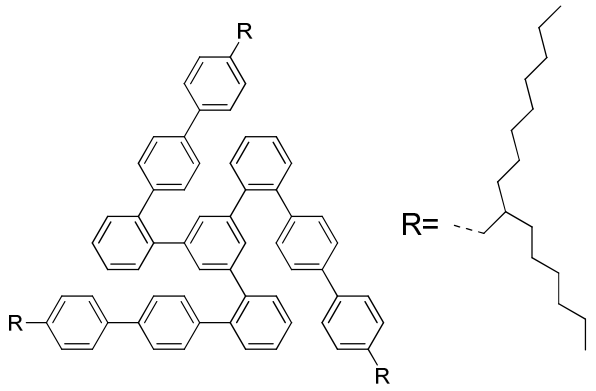

Preparation of Negishi reagent:

In a dry flask, 384 mg (15.9 mmol) Zn powder were initially treated with 60 mg (5%) iodine-crystals in 8 ml DMA, then 1.15 g (3.94 mmol) 2-hexyl-decylbromide was added and the resulting mixture was mixed at 80^{o}C for 24 h.

The above Negishi reagent was transferred *via* cannula to the flask which contained with 500 mg (0.438 mmol) 1,3,5-tris[2'-(4''-(4'''-iodophenyl))biphenyl]benzene and 36 mg (10 mol%) dichloro[1,1'-bis(diphenylphosphino)ferrocene]palladium(II). The mixture was stirred overnight under 50 °C. The reaction was quenched by adding aqueous HCl solution, and extracted with dichloromethane, the organic solvent was removed under vacuum, and purified by column chromatography (silica gel, Hexane to Hexane:DCM=6:1) to afford 270 mg (43%) of target compound as a colorless oil. FD-MS (8 KV): m/z 1437.3, calcd.: 1436.25 (M^+). ^{1}H NMR (250 MHz, CD_2Cl_2): δ ppm 7.38~7.16(m, 27H), 6.94~6.91(m, 9H), 6.78(s, 3H), 2.57(d, 6H, J=6.62Hz), 1.65(m, 3H), 1.40~1.22(m, 72H), 0.84(m, 18H). ^{13}C NMR (62.5 MHz, CD_2Cl_2): δ ppm 141.57, 141.53, 140.98, 140.83, 140.64, 139.38, 138.19, 130.74, 130.40, 130.07, 130.43, 130.07, 127.69, 127.57, 126.94, 126.71, 40.62, 40.15, 33.59, 32.31, 30.44, 30.09, 30.04, 29.74, 26.97, 26.94, 23.08, 14.27.

1,3,5-Tris(2'-(4"-(4"'-(2""-decyl-tetradecyl))phenyl)biphenyl)benzene (4-21b)

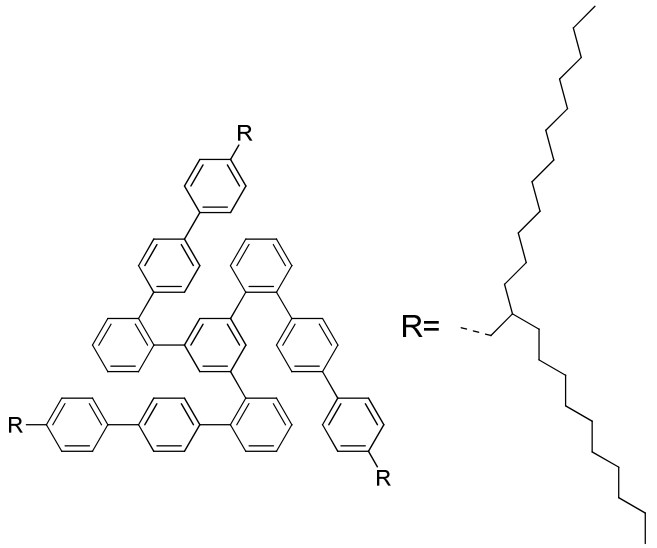

The above Negishi reagent was transferred *via* cannula to the flask which contained with 500mg (0.438mmol) 1,3,5-tris[2'-(4''-(4'''-iodophenyl))biphenyl]benzene and 36mg (10mol%) dichloro[1,1'-bis(diphenylphosphino)ferrocene]palladium(II). The mixture was stirred overnight under 50 °C. The reaction was quenched by adding aqueous HCl solution, and extracted with dichloromethane, the organic solvent was removed under vacuum, and purified by column chromatography (silica gel, Hexane to Hexane:DCM=6:1) to afford 230 mg (30%) of target compound as a colorless oil. FD-MS (8 KV): m/z 1774.0, calcd.: 1772.89 (M^+). ^{1}H NMR (250 MHz, CD_2Cl_2): δ ppm 7.35~7.16(m, 27H), 6.97~6.88(m, 9H), 6.78(s, 3H), 2.58(d, 6H, J=6.62Hz), 1.66(m, 3H), 1.41~1.23(m, 120H), 0.86(m, 18H). ^{13}C NMR (62.5 MHz, CD_2Cl_2): δ ppm 141.59, 141.55,141.02, 140.87, 140.62,139.32, 138.18, 130.70, 130.40, 130.07, 129.99, 127.67, 127.55, 126.94, 126.71, 40.64, 40.16, 33.59, 32.33, 30.45, 30.11, 30.07, 29.78, 26.99, 23.08, 14.27.

Triangle-($C_{10, 6}$)$_3$ (4-22a)

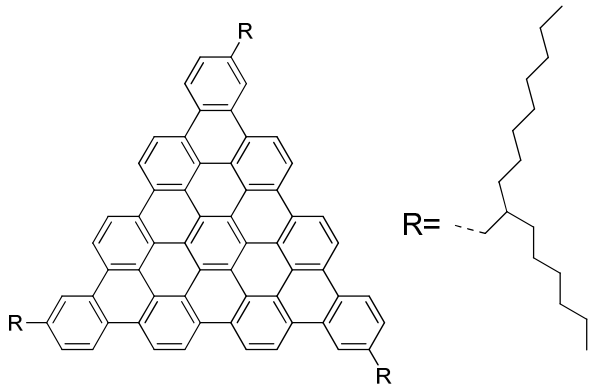

156 mg (0.109mmol) **4-21a** was dissolved in 60ml dichloromethane, the solution was then degassed by bubbling through argon for 20 min, and then 1.58g (5eq/H) $FeCl_3$ in 4ml CH_3NO_2 was added dropwise. After being stirred for 45min, the reaction was quenched by adding 50ml methanol. The yellow precipitate was collected, washed by methanol, and passed through the short column (Silica gel, hot toluene), the most organic solvent was removed under vaccum and methanol was added to precipitate the yellow solid, the final yellow sticky powder was dried under vaccum (89%). MALDITOF-MS (TCNQ as matrix): m/z=1418.2701, calcd. 1418.11 for $C_{108}H_{120}$. ^1H NMR can not be measured due to the less solubility. ^{13}H NMR can not be measured due to the large disc core and less solubility.

Triangle-$(C_{14,\ 10})_3$ (4-22b)

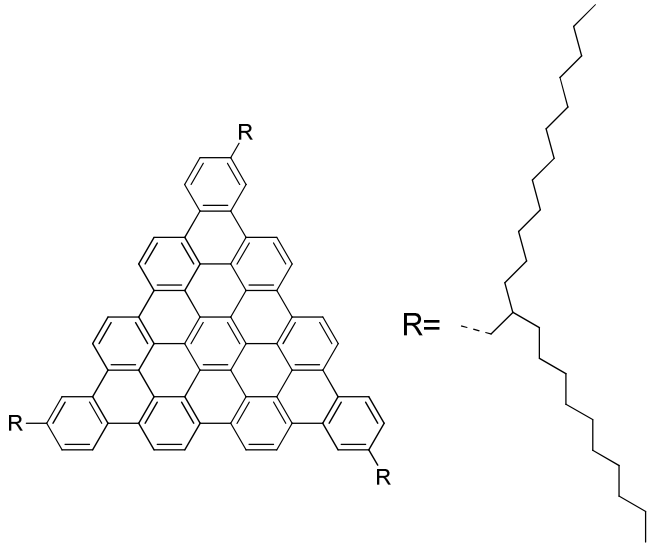

126 mg (0.0711mmol) **4-21b** was dissolved in 60ml dichloromethane, the solution was then degassed by bubbling through argon for 20 min, and then 1.04g (5eq/H) $FeCl_3$ in

4ml CH_3NO_2 was added dropwise. After being stirred for 45min, the reaction was quenched by adding 50ml methanol. The yellow precipitate was collected, washed by methanol, and passed through the short column (Silica gel, hot toluene), the most organic solvent was removed under vaccum and methanol was added to precipitate the yellow solid, the final yellow sticky powder was dried under vaccum (86%). MALDITOF-MS (TCNQ as matrix): m/z=1754.4110, calcd. 1574.75 for $C_{132}H_{168}$. ^{1}H NMR (500MHz, CD_2Cl_2, 140^{o}C) : δ ppm 8.57(br, 18H), 7.70(br, 3H), 3.20(br, 6H), 2.22(m, 3H), 1.75~1.31(m, 120H), 0.89(m, 18H). ^{13}H NMR can not be measured due to the large disc core and less solubility.

1,4-Di(trimethylsilyl)-2,5-diphenylbenzene (5-3a)

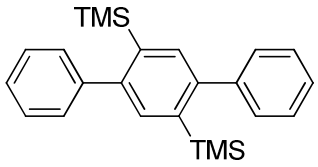

3.00g (6.32mmol) 1,4-diiodo-2,5-bis(trimethylsilyl)benzene**,** 2.31g (18.9mmol) phenylboronic acid, 584mg (0.505mmol) $Pd(PPh_3)_4$, 5.24g (37.9mmol) K_2CO_3, 50ml THF, 12ml EtOH and 12ml H_2O were added into 100ml Schlenk flask. The mixture was degassed by two "freeze-pump-thaw"cycles and then heated to reflux overnight. After standard work-up and purification by column chromatography (Silica gel, PE (petroleum ether):DCM (dichloromethane) = 6:1), 1.99g (5.31mmol) white solid was obtained (84%). FD-MS (8 KV): m/z 373.1, calcd.: 374.67 (M^+). ^{1}H NMR (250 MHz, CD_2Cl_2): δ ppm 7.41~7.31(m, 12H), 0.02(s, 18H). ^{13}C NMR (62.5 MHz, CD_2Cl_2): δ ppm 147.33, 144.96, 139.17, 135.90, 129.86, 128.11, 127.37, 0.542. Elemental Analysis: Calculated: C 76.94, H 8.07, Si 14.99; Found: C 76.91, H 8.08.

1,4-Di(trimethylsilyl)-2,5-di(4'-*t*-butyl)phenylbenzene (5-3b)

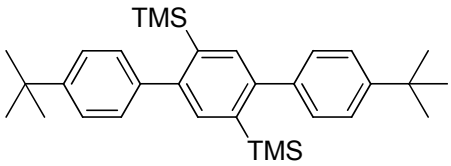

3.00g (6.32mmol) 1,4-diiodo-2,5-bis(trimethylsilyl)benzene**,** 3.38g (18.9mmol)

t-butylphenylboronic acid, 584mg (0.505mmol) $Pd(PPh_3)_4$, 5.24g (37.9mmol) K_2CO_3, 50ml THF, 12ml EtOH and 12ml H_2O were added into 100ml Schlenk flask. The mixture was degassed by two "freeze-pump-thaw"cycles and then heated to reflux overnight. After standard work-up and purification by column chromatography (Silica gel, PE:DCM = 10:1) , 2.85g (5.85mmol) white solid was obtained (92%). Mp: 284-287°C. FD-MS (8 KV): m/z 486.5, calcd.: 486.88 (M^+). ^{1}H NMR (250 MHz, CD_2Cl_2): δ ppm 7.43(m, 6H), 7.25(m, 4H), 1.36(s, 18H), -0.03(s, 18H). ^{13}C NMR (62.5 MHz, CD_2Cl_2): δ ppm 150.52, 147.16, 141.99, 139.28, 135.95, 129.43, 124.97, 34.80, 31.55, 0.56. Elemental Analysis: Calculated: C 78.94, H 9.52, Si 11.54; Found: C 78.92, H 9.50.

1,4-Di(trimethylsilyl)-2,5-di(4'-*n*-dodecyl)phenylbenzene (5-3c)

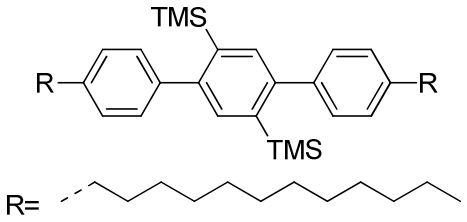

1.06 (2.23mmol) 1,4-diiodo-2,5-bis(trimethylsilyl)benzene**,** 1.42g (4.89mmol) *n*-dodecylphenylboronic acid, 129mg (0.111mmol) $Pd(PPh_3)_4$, 1.85g (13.4mmol) K_2CO_3, 20ml THF, 5ml EtOH and 5ml H_2O were added into 50ml Schlenk flask. The mixture was degassed by two "freeze-pump-thaw"cycles and then heated to reflux overnight. After standard work-up and purification by column chromatography (Silica gel, PE), 1.25g (1.76mmol) white solid was obtained (79%). Mp: 93-95°C. FD-MS (8 KV): m/z 711.0, calcd.: 711.30 (M^+). ^{1}H NMR (250 MHz, CD_2Cl_2): δ ppm 7.41(s, 2H), 7.21(s, 8H), 2.65(t, 4H, J=8.20Hz), 1.61(m, 4H), 1.31~1.26(m, 36H), 0.86(m, 6H), -0.02(s, 18H). ^{13}C NMR (62.5 MHz, CD_2Cl_2): δ ppm 147.25, 142.28, 139.26, 129.68, 128.15, 35.96, 32.31, 32.01, 30.07, 30.03, 29.89, 29.74, 29.60, 23.07, 14.26, 0.60. Elemental Analysis: Calculated: C 81.05, H 11.05, Si 7.90; Found: C 81.02, H 10.99.

1,4-Diiodo-2,5-diphenylbenzene (5-4a)

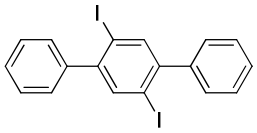

500mg (1.33mmol) **5-3a** was dissolved in 60ml $CHCl_3$, the solution was degassed by bubbling through argon for 20 min, then 4eq ICl (1M in dichloromethane) was added dropwise. After stirring for 1hr, the reaction was quenched by adding aqueous $Na_2S_2O_3$. After standard work-up and purification by column chromatography (Silica gel, PE:DCM= 5:1), 611mg (1.27mmol) white solid was obtained (95%). Mp: 269-272^oC. FD-MS (8 KV): m/z 482.3, calcd.: 482.10 (M^+). ^1H NMR (250 MHz, CD_2Cl_2): δ ppm 7.87(s, 2H), 7.45~7.34(m, 10H). ^{13}C NMR (75 MHz, CD_2Cl_2): δ ppm 147.43, 142.75, 140.55, 129.54, 128.47, 98.37. Elemental Analysis: Calculated: C 44.84, H 2.51, I 52.65; Found: C 44.83, H 2.56.

1,4-Diiodo-2,5-di(4'-*t*-butyl)phenylbenzene (5-4b)

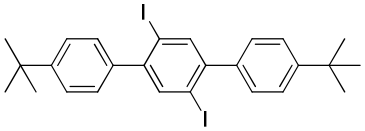

2.44g (5.01mmol) **5-3b** was dissolved in 300ml $CHCl_3$, the solution was degassed by bubbling through argon for 20 min, then 4eq ICl (1M in dichloromethane) was added dropwise. After stirring for 1hr, the reaction was quenched by adding aqueous $Na_2S_2O_3$. After standard work-up and purified by precipitation from methanol, 2.74g (4.61mmol) white solid was obtained (92%). Mp: >300^oC. FD-MS (8 KV): m/z 594.1, calcd.: 594.31 (M^+). ^1H NMR (250 MHz, CD_2Cl_2): δ ppm 7.86(s, 2H), 7.46(d, 4H, J=8.22Hz), 7.30(d, 4H, J-8.22Hz), 1.36(s, 18H). ^{13}C NMR (62.5 MHz, CD_2Cl_2): δ ppm 151.54, 147.06, 140.77, 139.69, 129.19, 125.38, 98.35, 34.94, 31.45. Elemental Analysis: Calculated: C 52.54, H 4.75, I 42.71; Found: C 52.50, H 4.71.

1,4-Diiodo-2,5-di(4'-*n*-dodecyl)phenylbenzene (5-4c)

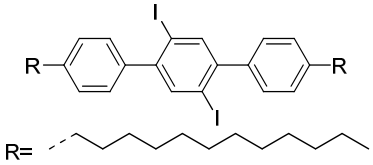

811.g (1.14mmol) **5-3c** was dissolved in 20ml $CHCl_3$, the solution was degassed by bubbling through argon for 20 min, then 4eq ICl (1M in dichloromethane) was added dropwise. After stirring for 1hr, the reaction was quenched by adding aqueous $Na_2S_2O_3$. After standard work-up and purified by column chromatography (Silica gel, PE), 849mg (1.04mmol) white solid was obtained (91%). Mp: 98~99^oC. FD-MS (8 KV): m/z 818.3, calcd.: 818.73 (M^+). ^1H NMR (250 MHz, CD_2Cl_2): δ ppm 7.85(s, 2H), 8.00(s, 8H), 2.65(t, 4H, J=7.56Hz), 1.65(m, 4H), 1.25(m, 36H), 0.84(m, 6H). ^{13}C NMR (62.5 MHz, CD_2Cl_2): δ ppm 147.23, 143.52, 140.64, 140.01, 129.39, 128.44, 98.54, 36.06, 32.32, 31.82, 30.04, 29.99, 29.88, 29.74, 23.08, 14.27. Elemental Analysis: Calculated: C 69.95, H 5.56, Br 24.49; Found: C 69.92, H 5.55.

1,4-Di(2'-bromo)phenyl-2,5-diphenylbenzene (5-5a)

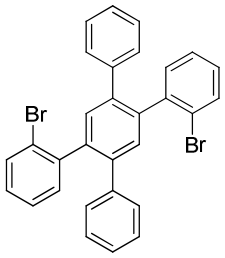

670mg (1.39mmol) **5-4a**, 586mg (2.92mmol) 2-bromophenylboronic acid, 80.0mg (0.0690mmol) $Pd(PPh_3)_4$, 1.15g (8.32mmol) K_2CO_3, 25ml Toluene, 6ml EtOH and 6ml H_2O were added into 50ml Schlenk flask. The mixture was degassed by two "freeze-pump-thaw"cycles and then heated to reflux overnight. After standard work-up and purification by column chromatography (Silica gel, PE:DCM = 4:1) , 600mg (1.11mmol) white solid was obtained (80%). Mp: 230~231^oC. FD-MS (8 KV): m/z 540.3, calcd.: 540.29 (M^+). ^1H NMR (250 MHz, CD_2Cl_2): δ ppm 7.57 (t, 2H, J=7.6Hz), 7.42 (d, 2H, J=6.95Hz), 7.32~7.10 (m, 16H). ^{13}C NMR (62.5 MHz, CD_2Cl_2): δ ppm 142.30, 142.18, 140.71, 139.93, 139.81, 139.63, 139.56, 133.09, 132.96, 132.88, 132.72, 132.52, 129.85, 129.06, 128.17, 128.12, 127.29, 127.10, 124.09. Elemental Analysis: Calculated: C 66.69, H 3.73, Br 29.58; Found: C 66.68, H 3.74.

1,4-Di(2'-bromo)phenyl-2,5-di(4'-*t*-butyl)phenylbenzene (5-5b)

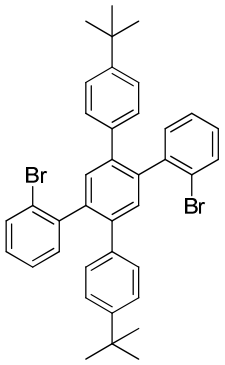

.3.24g (5.45mmol) **5-4b**, 2.30g (11.4mmol) 2-bromophenylboronic acid, 315mg (0.272mmol) $Pd(PPh_3)_4$, 4.52g (32.7mmol) K_2CO_3, 55ml THF, 12ml EtOH and 12ml H_2O were added into 100ml Schlenk flask. The mixture was degassed by two "freeze-pump-thaw"cycles and then heated to reflux overnight. After standard work-up and purification by column chromatography (Silica gel, PE:DCM = 6:1) , 2.88g (4.44mmol) white solid was obtained (81%). Mp: 318~320^oC. FD-MS (8 KV): m/z 652.5, calcd.: 652.50 (M^+). ^1H NMR (250 MHz, CD_2Cl_2): δ ppm: 7.58(t, 2H, J=7.25Hz), 7.38(d, 2H, J=6.32Hz), 7.16(m, 14H), 1.24(s, 18H). ^{13}C NMR (62.5 MHz, CD_2Cl_2): δ ppm 150.10, 142.47, 139.43, 139.37, 137.76, 133.35, 133.13, 132.91, 129.79, 129.34, 127.64, 125.50, 124.15, 34.66, 31.77. Elemental Analysis: Calculated: C 69.95, H 5.56, Br 24.49; Found: C 69.92, H 5.55.

1,4-Di(2'-bromo)phenyl-2,5-di(4'-*n*-dodecyl)phenylbenzene (5-5c)

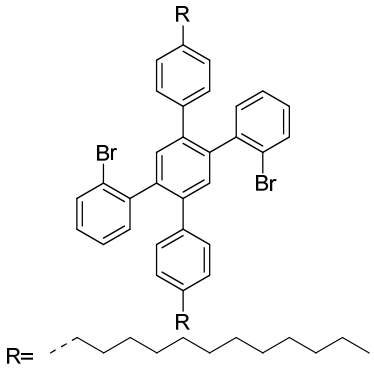

935mg (1.14mmol) **5-4c**, 482mg (2.40mmol) 2-bromophenylboronic acid, 66mg (0.057mmol) $Pd(PPh_3)_4$, 950mg (6.87mmol) K_2CO_3, 22ml THF, 5ml EtOH and 5ml H_2O were added into 50ml Schlenk flask. The mixture was degassed by two "freeze-pump-thaw"cycles and then heated to reflux overnight. After standard work-up

and purification by column chromatography (Silica gel, PE:DCM = 6:1) , 900mg (1.03mmol) white solid was obtained (90%). Mp: 84~86°C. FD-MS (8 KV): m/z 875.9, calcd.: 876.93 (M^+). ^{1}H NMR (250 MHz, CD_2Cl_2): δ ppm: 7.57(t, 4H, J=7.58Hz), 7.39(d, 4H, J=8.2Hz), 7.21~7.09(m, 10H), 7.00(d, 4H, J=8.2Hz), 2.52(t, 4H, J=7.25Hz), 1.51(m, 4H), 1.32~1.24(m, 36H), 0.86(t, 6H, J=6.0Hz). ^{13}C NMR (62.5 MHz, CD_2Cl_2): δ ppm 142.60, 142.47, 141.99, 139.56, 137.99, 133.11, 132.95, 132.77, 132.56, 129.66, 128.94, 128.24, 127.27, 124.15, 35.85, 32.30, 31.68, 30.05, 29.97, 29.85, 29.65, 23.07, 14.26. Elemental Analysis: Calculated: C 73.96, H 7.82, Br 18.22; Found: C 73.74, H 7.78.

1,4-Di(2'-(2"-(4"'-*n*-dodecyl)phenylethynyl)biphenyl)-2,5-diphenylbenzene (5-6a)

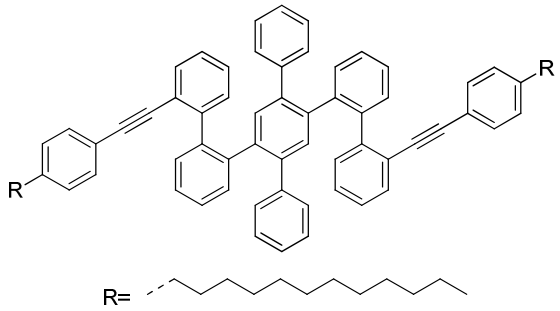

1.00g (1.85mmol) **5-5a**, 2.00g (5.12mmol) *o*-(4-dodecyl)phenylethynylbenzeneboronic acid, 107mg (0.0925mmol) $Pd(PPh_3)_4$, 1.53g (11.1mmol) K_2CO_3, 45ml Toluene, 11ml EtOH and 11ml H_2O were added into 100ml Schlenk flask. The mixture was degassed by two "freeze-pump-thaw"cycles and then heated to reflux overnight. After standard work-up and purification by column chromatography (Silica gel, PE:DCM = 4:1) , 1.65g (1.54mmol) of light yellow oil was obtained (83%). FD-MS (8 KV): m/z 1072.5, calcd.: 1071.56 (M^+). ^{1}H NMR (250 MHz, CD_2Cl_2): δ ppm 7.35~6.99(m, 34H), 2.54(t, 4H, J=7.58Hz), 1.55(m, 4H), 1.25(m, 38H), 0.86(m, 6H). ^{13}C NMR (62.5 MHz, CD_2Cl_2): δ ppm 143.57, 141.00, 138.95, 134.40, 131.76, 130.98, 130.46, 130.21, 129.91, 128.67, 128.00, 127.77, 127.31, 126.71, 126.55, 123.26, 121.09, 92.39, 89.47, 36.19, 32.30, 31.69, 30.04, 29.96, 29.87, 29.73, 29.65, 23.07, 14.26. Elemental Analysis: Calculated: C 91.91, H 8.09; Found: C 91.83, H 8.10.

1,4-di(2'-(2"-(4"'-*n*-dodecyl)phenylethynyl)biphenyl)-2,5-di(4'-*t*-butyl)phenylbenzene (5-6b)

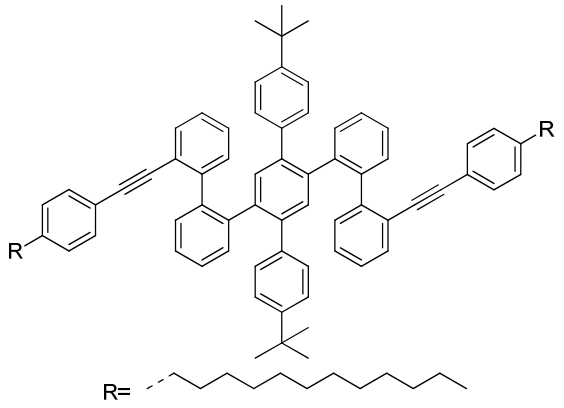

500mg (0.766mmol) **5-5b**, 897mg (2.30mmol) *o*-(4-dodecyl)phenylethynyl-benzeneboronic acid, 44mg (0.038mmol) $Pd(PPh_3)_4$, 638mg (4.62mmol) K_2CO_3, 25ml Toluene, 6ml EtOH and 6ml H_2O were added into 50ml Schlenk flask. The mixture was degassed by two "freeze-pump-thaw"cycles and then heated to reflux overnight. After standard work-up and purification by column chromatography (Silica gel, PE:DCM = 4:1) , 771mg (0.651mmol) of light yellow oil was obtained (85%). FD-MS (8 KV): m/z 1185.0, calcd.: 1183.77 (M^+). ^{1}H NMR (250 MHz, CD_2Cl_2): δ ppm 7.43~6.96(m, 32H), 2.55(t, 4H, J=7.58Hz), 1.56(m, 4H), 1.25(m, 56H), 0.86(m, 6H). ^{13}C NMR (62.5 MHz, CD_2Cl_2): δ ppm 143.54, 138.90, 134.50, 132.06, 131.65, 130.28, 129.65, 128.63, 127.78, 126.56, 124.74, 89.84, 82.28, 36.21, 34.47, 32.29, 31.79, 31.36, 30.01, 29.95, 29.72, 23.07, 14.25. Elemental Analysis: Calculated: C 91.32, H 8.68; Found: C 91.42, H 8.54.

1,4-Di(2'-(2"-(4"'-*n*-dodecyl)phenylethynyl)biphenyl)-2,5-di(4'-*n*-dodecyl)phenylbenzene (5-6c)

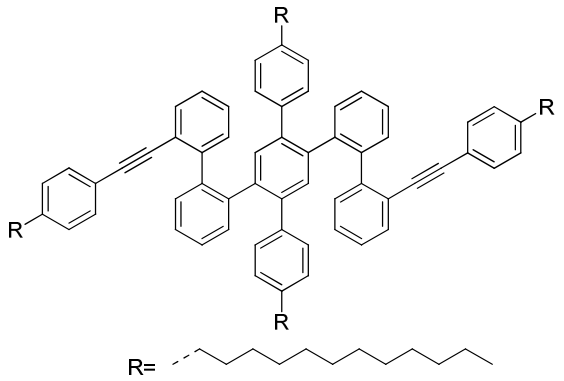

885mg (1.01mmol) **5-5c**, 1.02g (2.61mmol) *o*-(4-dodecyl)phenylethynylbenzeneboronic acid, 35mg (0.030mmol) $Pd(PPh_3)_4$, 830mg (6.01mmol) K_2CO_3, 22ml Toluene, 5ml

EtOH and 5ml H_2O were added into 50ml Schlenk flask. The mixture was degassed by two "freeze-pump-thaw"cycles and then heated to reflux overnight. After standard work-up and purification by column chromatography (Silica gel, PE:DCM = 6:1) , 1.08g (0.767mmol) of light yellow oil was obtained (76%). FD-MS (8 KV): m/z 1406.5, calcd.: 1408.20 (M^+). ^{1}H NMR (250 MHz, CD_2Cl_2): δ ppm 7.35~6.97(m, 32H), 2.52(m, 8H), 1.52(m, 8H), 1.25(m, 74H), 0.84(m, 12H). ^{13}C NMR (62.5 MHz, CD_2Cl_2): δ ppm 143.50, 142.97, 141.45, 138.92, 134.33, 131.59, 130.50, 129.76, 128.61, 127.81, 126.60, 123.06, 89.61, 36.25, 35.79, 32.31, 31.82, 30.11, 30.08, 30.04, 29.44, 29.89, 29.77, 29.75, 23.08, 14.27. Elemental Analysis: Calculated: C 90.41, H 9.59; Found: C 90.50, H 9.52.

1,4-Di(9'-(4"-iodo-5"-(4"'-*n*-dodecyl)phenyl)phenanthrenyl)-2,5-diphenylbenzene (5-7a)

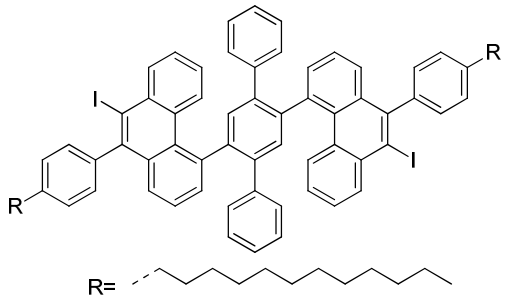

1.38g (1.29mmol) **5-6a** in 65ml dry dichloromethane was cooled down to –78°C in dry ice-acetone bath, then 4eq ICl (5.1mmol, 1M in dichloromethanee) was added dropwise over 5min. The mixture was kept at –78°C for 3h and then quenched by adding aqueous $Na_2S_2O_3$ solution. The organic layer was washed with water two times, dried over $MgSO_4$. The solvent was removed and the residue was purified by column chromatography (Silica gel, PE:DCM= 10:1), 1.46g (1.10mmol) light yellow solid was obtained (86%). FD-MS (8 KV): m/z 1323.4, calcd.: 1323.35 (M^+). ^{1}H NMR (250 MHz, CD_2Cl_2): atropisomer, δ ppm 8.66(d, 1.09H, J=8.22Hz), 8.40~24(m, 2.49H), 7.66~7.28(m, 20.83H), 7.17~6.77(m, 9.61H), 2.74(t, 4H, J=7.85Hz), 1.73(m, 4H), 1.50~1.23(m, 38H), 0.87(m, 6H). ^{13}C NMR (62.5 MHz, CD_2Cl_2): δ ppm 145.84, 145.72, 143.39, 143.25, 143.15, 140.71, 140.57, 138.94, 134.59, 134.10, 133.69, 133.01, 132.66, 132.58, 131.05, 130.26, 130.17, 130.07, 129.99, 129.31, 128.79, 128.53, 128.32, 128.20, 127.85, 127.59, 126.69, 126.26, 125.95, 107.25, 36.22, 32.32, 31.91, 30.06, 30.02, 29.93, 29.79, 29.76, 23.09, 14.27. Elemental

Analysis: Calculated: C 74.42, H 6.40, Br 19.18; Found: C 74.41, H 6.38.

1,4-Di(9'-(4"-iodo-5"-(4"'-*n*-dodecyl)phenyl)phenanthrenyl)-2,5-di(4'-*t*-butyl)phenylbenzene (5-7b)

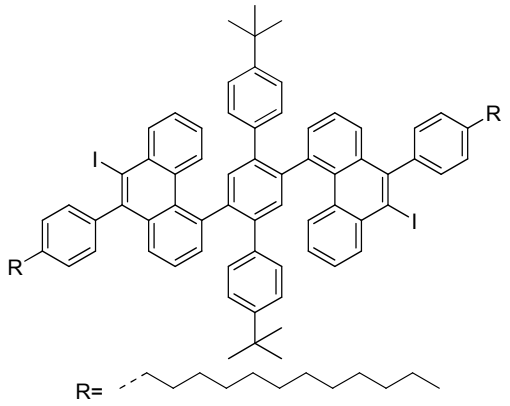

200mg (0.169mmol) **5-6b** in 20ml dry dichloromethane was cooled down to –78°C in dry ice-acetone bath, then 4eq ICl (0.68mmol, 1M in dichloromethanee) was added dropwise over 5min. The mixture was kept at –78°C for 3h and then quenched by adding aqueous $Na_2S_2O_3$ solution. The organic layer was washed with water two times, dried over $MgSO_4$. The solvent was removed and the residue was purified by column chromatography (Silica gel, PE:DCM= 4:1), 221mg (0.159mmol) light yellow solid was obtained(91%). FD-MS (8 KV): m/z 1435.4, calcd.: 1435.57 (M^+). ^{1}H NMR (250 MHz, CD_2Cl_2): atropisomer, δ ppm 8.55(d, 1.14H, J=8.48Hz), 8.27(d, 1.7H, J=8.20Hz), 7.73(s, 1.15H), 7.61~6.69(m, 23.34H), 6.51(d, 2.59H, J=8.20Hz), 2.75(t, 4H, J=7.85Hz), 1.73(m, 4H), 1.50~1.23(m, 38H), 1.13(s, 18H), 0.87(m, 6H) ^{13}C NMR (62.5 MHz, CD_2Cl_2): δ ppm 149.60, 145.49, 143.37, 143.32, 143.07, 140.83, 139.14, 137.46, 134.29, 133.89, 133.48, 132.52, 132.27, 131.07, 130.35, 130.26, 130.13, 130.02, 129.87, 128.78, 128.67, 128.38, 128.07, 127.74, 126.38, 125.67, 124.38, 124.15, 107.09, 36.21, 34.44, 32.32, 31.91, 31.43, 31.38, 30.09, 30.06, 30.01, 29.93, 29.79, 29.75, 23.08, 14.27. Elemental Analysis: Calculated: C 75.30, H 7.02, Br 17.68; Found: C 75.43, H 6.98.

1,4-Di(9'-(4"-iodo-5"-(4"'-*n*-dodecyl)phenyl)phenanthrenyl)-2,5-di(4'-*n*-dodecyl)phenylbenzene (5-7c)

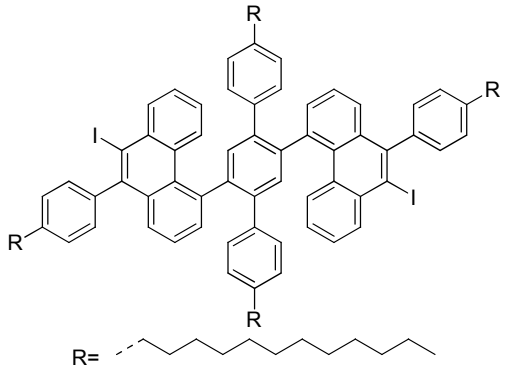

813mg (0.577mmol) **5-6c** in 55ml dry dichloromethane was cooled down to –78°C in dry ice-acetone bath, then 4eq ICl (2.31mmol, 1M in dichloromethanee) was added dropwise over 5min. The mixture was kept at –78°C for 3h and then quenched by adding aqueous $Na_2S_2O_3$ solution. The organic layer was washed with water two times, dried over $MgSO_4$. The solvent was removed and the residue was purified by column chromatography (Silica gel, PE:DCM= 10:1), 824mg (0.496mmol) light yellow sticky solid was obtained(86%). FD-MS (8 KV): m/z 1657.4, calcd.: 1659.99 (M^+). ^{1}H NMR (250 MHz, CD_2Cl_2): antropisomer, δ ppm 8.64(d, 1.30H, J=8.48Hz), 8.34(d, 2.06H, J=8.20Hz), 7.66~6.62(m, 28.64H), 2.75(t, 4H, J=7.52Hz), 2.37(m, 4H), 1.73~1.23(m, 80H), 0.85(m, 12H). ^{13}C NMR (62.5 MHz, CD_2Cl_2): δ ppm 145.64, 143.43, 143.32, 143.09, 141.74, 140.65, 139.20, 137.75, 134.47, 134.19, 134.02, 133.63, 132.72, 132.45, 131.13, 130.34, 130.21, 130.09, 129.94, 129.09, 128.96, 128.76, 128.39, 128.31, 128.18, 127.70, 126.26, 125.84, 107.20, 36.23, 35.80, 32.32, 31.99, 31.92, 30.06, 30.04, 29.95, 29.82, 29.77, 23.09, 14.27. Elemental Analysis: Calculated: C 76.70, H 8.01, I 15.29; Found: C 76.83, H 8.13.

1,4-Di(9'-(4",5"-di(4"'-*n*-dodecyl)phenyl)phenanthrenyl)-2,5-diphenylbenzene (5-8a)

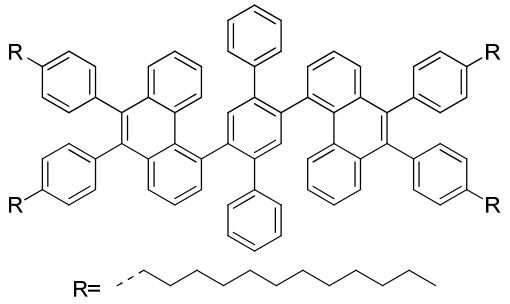

470mg (0.355mmol) **5-7a**, 310mg (1.07mmol) *n*-dodecylphenylboronic acid, 12mg

(0.010mmol) $Pd(PPh_3)_4$, 300mg (2.17mmol) K_2CO_3, 16ml THF, 4ml EtOH and 4ml H_2O were added into 50ml Schlenk flask. The mixture was degassed by two "freeze-pump-thaw"cycles and then heated to reflux overnight. After standard work-up and purification by column chromatography (Silica gel, PE:DCM = 4:1) , 493mg (0.316mmol) of light yellow solid was obtained (89%). FD-MS (8 KV): m/z 1558.9, calcd.: 1560.39 (M^+). ^1H NMR (250 MHz, CD_2Cl_2): atroipsomer, δ ppm 8.75(d, 1.17H, J=8.22Hz), 8.34(d, 0.58H, J=8.20Hz), 7.74~6.89(m, 40,22H), 2.56(m, 8H), 1.58(m, 8H), 1.27~1.20(m, 72H), 0.87(m, 12H). ^{13}C NMR (62.5 MHz, CD_2Cl_2): δ ppm 143.66, 143.56, 141.40, 141.35, 141.10, 140.99, 140.70, 139.11, 138.95, 137.64, 137.60, 137.46, 137.33, 133.93, 133.67, 133.31, 133.04, 131.69, 131.32, 131.19, 131.05, 130.48, 129.78, 129.42, 129.32, 128.10, 127.89, 127.59, 126.60, 126.27, 125.76, 124.73, 35.96, 32.34, 31.81, 30.12, 30.08, 29.94, 29.78, 29.62, 23.09, 14.28. Elemental Analysis: Calculated: C 90.83, H 9.17; Found: C 91.03, H 9.17.

1,4-Di(9'-(4",5"-di(4"'-*n*-dodecyl)phenyl)phenanthrenyl)-2,5-di(4'-*t*-butyl) phenylbenzene (5-8b)

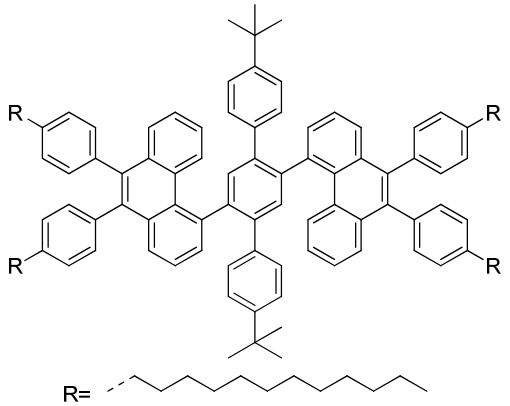

400mg (0.278mmol) **5-7b**, 243mg (0.837mmol) *n*-dodecylphenylboronic acid, 10mg (0.0086mmol) $Pd(PPh_3)_4$, 400mg (2.89mmol) K_2CO_3, 14ml THF, 3ml EtOH and 4ml H_2O were added into 50ml Schlenk flask. The mixture was degassed by two "freeze-pump-thaw"cycles and then heated to reflux overnight. After standard work-up and purification by column chromatography (Silica gel, PE:DCM = 4:1) , 423mg (0.253mmol) of light yellow solid was obtained (91%). FD-MS (8 KV): m/z 1672.4, calcd.: 1672.60 (M^+). ^1H NMR (250 MHz, CD_2Cl_2): atroipsomer, δ ppm 8.81(d, 1.07H,

J=8.22Hz), 8.33(d, 0.59H, J=8.20Hz), 7.63~7.34(m, 14.99H), 7.04~6.94(m, 23.44H), 2.56(m, 8H), 1.57(m, 8H), 1.27~1.1(m, 90H), 0.86(m, 12H). ^{13}C NMR (62.5 MHz, CD_2Cl_2): δ ppm 149.76, 143.56, 141.36, 139.99, 139.39, 138.01, 137.77, 137.67, 134.03, 133.75, 133.47, 131.28, 130.58, 129.63, 129.04, 128.16, 127.87, 127.74, 127.47, 126.24, 124.75, 35.93, 34.54, 32.32, 31.79, 31.34, 30.11, 30.06, 29.92, 29.76, 29.61, 23.08, 14.27. Elemental Analysis: Calculated: C 90.48, H 9.52; Found: C 90.57, H 9.53.

1,4-Di(9'-(4",5"-di(4"'-*n*-dodecyl)phenyl)phenanthrenyl)-2,5-di(4'-*n*-dodecyl)phenyl benzene (5-8c)

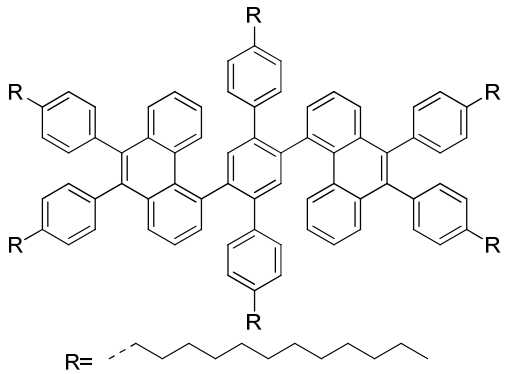

350mg (0.211mmol) **5-7c**, 184mg (0.634mmol) *n*-dodecylphenylboronic acid, 7.3mg (0.0063mmol) $Pd(PPh_3)_4$, 290mg (2.10mmol) K_2CO_3, 12ml THF, 3ml EtOH and 3ml H_2O were added into 50ml Schlenk flask. The mixture was degassed by two "freeze-pump-thaw"cycles and then heated to reflux overnight. After standard work-up and purification by column chromatography (Silica gel, PE:DCM = 10:1) , 303mg (0.160mmol) of light yellow sticky solid was obtained (76%). FD-MS (8 KV): m/z 1896.2, calcd.: 1897.03 (M^+). ^{1}H NMR (250 MHz, CD_2Cl_2): atroipsomer, δ ppm 8.78(d, 1.11H, J=8.48Hz), 8.32(d, 0.43H, J=8.32Hz), 7.66~6.61(m, 38.45H), 2.58~2.39(m, 12H), 1.57~1.27(m, 120H), 0.85(m, 18H). ^{13}C NMR (62.5 MHz, CD_2Cl_2): δ ppm 143.56, 141.55, 141.39, 141.34, 140.36, 139.29, 138.26, 137.69, 137.52, 137.41, 137.35, 133.96, 133.68, 133.14, 131.74, 131.25, 130.57, 129.72, 129.19, 128.16, 127.86, 127.43, 126.23, 125.70, 124.74, 35.96, 32.33, 31.81, 30.12, 30.07, 29.94, 29.88, 29.78, 29.74, 29.63, 23.09, 14.27. Elemental Analysis: Calculated: C 89.90, H 10.10; Found: C 90.03, H 9.98.

3,4,12,13-Tetrakis-(4'-*n*-dodecylphenyl)-dibenzo[*hi,uv*]phenanthro-[3,4,5,6-*bcdef*]-ovalene (5-1a)

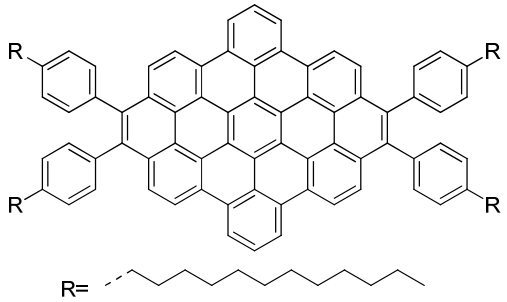

60.0mg (0.0384mmol) **5-8a** was dissolved in 40ml dichloromethane, the solution was then degassed by bubbling through argon for 20 min, and then 18eq $FeCl_3$ in 0.5ml CH_3NO_2 was added dropwise. After being stirred for 30 min, the reaction was quenched by adding 50ml methanol, the yellow precipitate was collected, washed by methanol repeatedly, redissolved in THF and passed through a short silica column, the solution was collected and dried under vacuum and then reprecipitated to afford 39.0mg (0.0252 mmol) yellow powder (66%). MALDITOF-MS (TCNQ as matrix): m/z=1548.15, calcd. 1548.29 for $C_{118}H_{130}$. ^{1}H NMR (500 MHz, $CDCl_2CDCl_2$, 140^{o}C): 9.25(brs, 4H), 9.17(brs, 4H), 8.49(brs, 4H), 8.21(s, 2H), 7.47(d, 8H, J=7.14Hz), 7.29(d, 8H, J=7.63Hz), 2.80(t, 8H, J=7.49Hz), 1.81~1.28(m, 90H), 0.93(m, 12H). ^{13}C NMR can not be well resolved because of the large disc. Elemental Analysis: Calculated: C 91.54, H 8.46; Found: C 90.94, H 8.48.

3,4,12,13-Tetrakis-(4'-*n*-dodecylphenyl)-8,17-bis-*t*-butyl-dibenzo[*hi,uv*]phenanthro-[3,4,5,6-*bcdef*]-ovalene (1b)

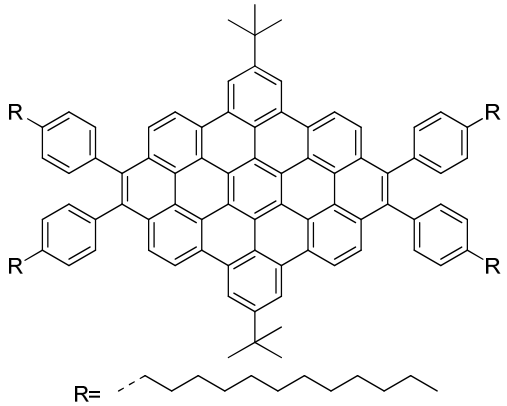

150mg (0.0896mmol) **5-8b** was dissolved in 70ml dichloromethane, the solution was

then degassed by bubbling through argon for 20 min, and then 30eq $FeCl_3$ in 1.5ml CH_3NO_2 was added dropwise. After being stirred for 45 min, the reaction was quenched by adding methanol, the yellow precipitate was collected, washed by methanol repeatedly, redissolved in THF and passed through a short silica column, the solution was collected and dried under vacuum and then reprecipitated to afford 129mg (0.0777mmol) yellow powder (87%). MALDITOF-MS (TCNQ as matrix): m/z=1661.04, calcd. 1660.51 for $C_{126}H_{146}$. ^{1}H NMR (500 MHz, $CDCl_2CDCl_2$, 140^{o}C): 9.56(s, 4H), 9.47(d, 4H, J=8.80Hz), 8.58(d, 4H, J=8.80Hz), 7.45(d, 8H, J=7.14Hz), 7.25(d, 8H, J=7.49Hz), 2.76(t, 8H, J=7.84Hz), 1.94~1.33(m, 98H), 0.91(m, 12H). ^{13}C NMR can not be well resolved because of the large disc. Elemental Analysis: Calculated: C 91.14, H 8.86; Found: C 90.98, H 8.75.

3,4,12,13-Tetrakis-(4'-*n*-dodecylphenyl)-8,17-bis-*n*-dodecyl-dibenzo[*hi,uv*]phenanthro-[3,4,5,6-*bcdef*]-ovalene (1c)

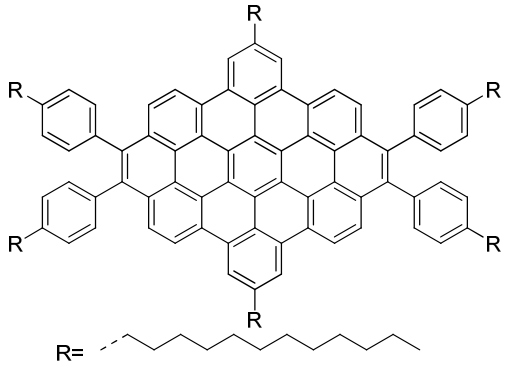

30.0mg (0.0158mmol) **5-8c** was dissolved in 20ml dichloromethane, the solution was then degassed by bubbling through argon for 20 min, and then 24eq $FeCl_3$ in 0.4ml CH_3NO_2 was added dropwise. After being stirred for 45 min, the reaction was quenched by adding methanol, the yellow precipitate was collected, washed by methanol repeatedly, redissolved in THF and passed through a short silica column, the solution was collected and dried under vacuum and then reprecipitated to afford 11mg (0.0058mmol) yellow powder (37%). MALDITOF-MS (TCNQ as matrix): m/z=1884.42, calcd. 1884.93 for $C_{142}H_{178}$. ^{1}H NMR (500 MHz, $CDCl_2CDCl_2$): 9.48(s, 4H), 9.27(brs, 4H), 8.59(brs, 4H), 7.44(d, 8H, J=7.14Hz), 7.25(d, 8H, J=7.48Hz), 3.39(m, 2H), 2.75(t, 8H, J=7.84Hz), 2.15(m, 2H), 1.77~0.83(m, 138H). ^{13}C NMR can not be well resolved because of the

large disc. Elemental Analysis: Calculated: C 90.48, H 9.52; Found: C 90.73, H 9.45.

1,3,5-Tris(9'-(4"-(4"'-methoxyphenyl)-5"-(3"',7"'-dimethyloctanyl)phenyl)phenanthrenyl)benzene (5-10)

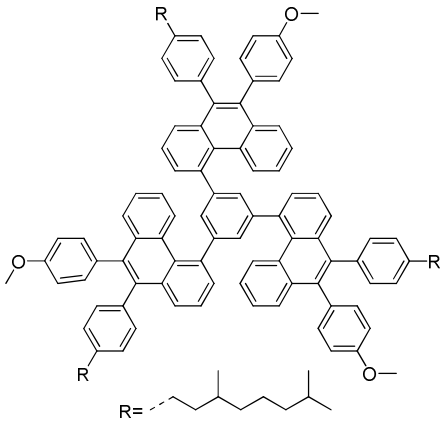

800mg (0.489mmol) **4-18b**, 334mg (1.5eq/I) 4-methoxyphenylboronic acid, 17mg (3mol%) $Pd(PPh_3)_4$, 680mg K_2CO_3, 32ml Toluene, 8ml EtOH and 8ml H_2O were added into 100ml Schlenk flask. The mixture was degassed by two "freeze-pump-thaw"cycles and then heated to reflux overnight. After standard work-up and purification by column chromatography (Hex:DCM=2:1), 690mg white solid was obtained (90%). Mp: 242~245^{o}C. FD-MS (8 KV): m/z 1570.4, calcd.: 1574.20 (M^+). ^{1}H NMR (250 MHz, $CDCl_2CDCl_2$): δ ppm 9.05(d, 1.24H, J=8.48H), 8.60(d, 1.06H, J=8.50Hz), 8.07(d, 0.54H, J=8.48Hz), 7.66~7.32(m, 21.06H), 6.99(m, 18H), 6.68(d, 6H, J=8.48Hz), 3.69(s, 9H), 2.50(m, 6H), 1.51~1.06(m, 30H), 0.84~0.78(m, 27H). ^{13}C NMR (62.5 MHz, $CDCl_2CDCl_2$): δ ppm 157.57, 140.95, 139.44, 137.54, 137.18, 133.63, 133.54, 132.19, 132.01, 131.69, 130.75, 129.66, 128.61, 128.41, 128.23, 128.19, 127.54, 112.89, 55.15, 39.23, 38.48, 37.04, 33.07, 32.29, 27.85, 24.61, 22.71, 22.64, 19.65. Elemental Analysis: Calculated: C 89.27, H 7.68, O 3.05; Found: C 89.29, H 7.64.

1,3,5-Tris(9'-(4"-(4"'-hydroxyphenyl)-5"-(3"',7"'-dimethyloctanyl)phenyl)phenanthrenyl)benzene (5-11)

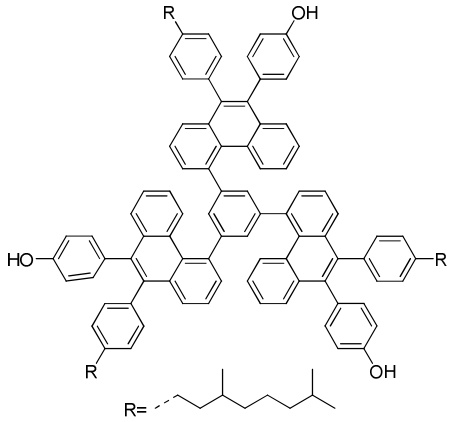

690mg (0.438mmol) **5-10** was dissolved in 35ml dry dichloromethane and cooled down to 0°C, 2.5ml BBr_3 (1M in dichloromethane) was added dropwise, the mixture was stirred overnight and poured into mixture of ice/THF and extracted with dichloromethane, the combined organic solvent was washed with brine and dried under $MgSO_4$, the organic solvent was removed under vacuum and the residue was purified by column chromatography (Silica gel, Hex:EA=2:1) then hot $CHCl_3$ to afford 550mg white solid (82%). Mp: >300°C, decomposed. FD-MS (8 KV): m/z 1531.4, calcd.: 1532.12 (M^+). ^1H NMR (CD_2Cl_2, 250 MHz): δ ppm 9.05(d, 1.24H, J=8.80Hz), 8.60(d, 1.06H, J=8.15Hz), 8.07(d, 0.54H, J=8.78Hz), 7.65~7.32(m, 21.6H), 6.94(m, 18H), 6.61(d, 6H, J=8.48H), 4.61(s, br, 3H, OH), 2.51(m, 6H), 1.52~1.17(m, 30H), 0.84~0.78(m, 27H). ^{13}C NMR can not be measured due to poor solubility. Elemental Analysis: Calculated: C 89.37, H 7.50, O 3.13; Found: C 89.18, H 7.60.

1,3,5-Tris(9'-(4"-(4"'-{2''''-[2''''-(2''''-methoxyethoxy)ethoxy]ethoxy}phenyl)-5"-(3"',7"'-dimethyloctanyl)phenyl)phenanthrenyl)benzene (5-12)

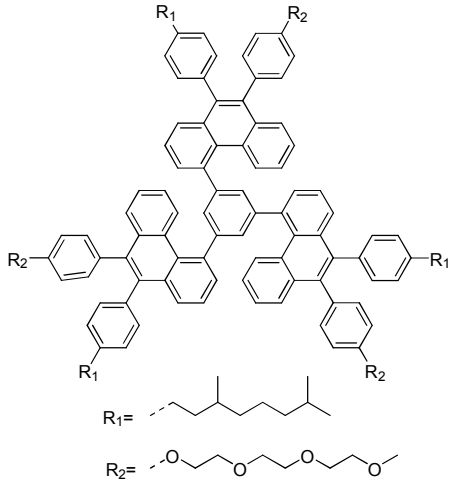

A THF solution (10 ml) of a mixture of **5-11** (255 mg, 0.166mmol) and (4-toluenesulfonyl)triethylene glycol monomethyl ether (335 mg, 6eq) was added NaOH (40 mg, 1 mmol), and the resulting suspension was refluxed for 14 h under argon. The reaction mixture was allowed to cool to room temperature and evaporated to dryness. A CH_2Cl_2 solution of the residue was washed with water, dried over anhydrous $MgSO_4$, and evaporated to dryness. The residue was subjected to column chromatography (Silica gel, ethyl DCM:EA=3:1) to afford final 304mg white waxy solid (93%). FD-MS (8 KV): m/z 1970.1, calcd.: 1970.68 (M^+). ^{1}H NMR (250 MHz, CD_2Cl_2): δ ppm 9.12(d, 0.77H, J=8.52Hz), 8.66(d, 1.37H, J=8.20Hz), 8.12(d, 0.70Hz, J=8.20Hz), 7.80~7.35(m, 21.16H), 7.05(m, 18H), 6.77(d, 6H, J=7.40Hz), 4.10(m, 6H), 3.70~3.44(m, 30H), 3.32(s, 9H), 2.59(m, 6H), 1.51~1.06(m, 30H), 0.92~0.85(m, 27H). ^{13}C NMR (62.5 MHz, CD_2Cl_2): δ ppm. 157.67, 147.80, 147.03, 145.46, 141.80, 140.79, 137.94, 137.63, 137.49, 134.29, 132.41, 131.24, 131.07, 130.24, 130.17, 128.97, 128.81, 128.24, 127.98, 127.83, 126.50, 126.02, 124.42, 113.94, 72.28, 72.25, 71.15, 71.05, 70.89, 70.82, 70.75, 70.03, 69.85, 68.96, 67.71, 58.99, 39.70, 39.09, 37.48, 33.51, 32.97, 28.36, 25.08, 22.83, 22.76, 19.81. Elemental Analysis: Calculated: C 82.28, H 7.98. O 9.74; Found: C 82.20, H 7.63.

TrizigzagHBC (5-9)

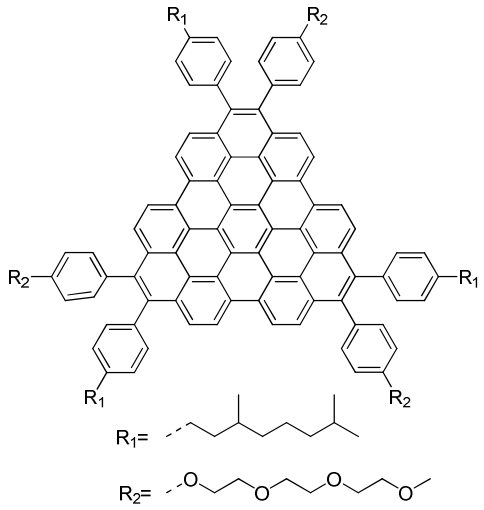

60 mg (0.0304mmol) **5-12** was dissolved in 50ml dichloromethane, the solution was then degassed by bubbling through argon for 20 min, and then 118mg $FeCl_3$ (24eqv) in 0.5ml CH_3NO_2 was added dropwise. After being stirred for 1h, the reaction was quenched by adding methanol, the yellow precipitate was collected, washed by methanol repeatedly

and reprecipitated and dried under vacuum to afford 43 mg yellow-orange powder (72%). MALDITOF-MS (TCNQ as matrix): m/z=, calcd. 1958.58 for $C_{135}H_{144}O_{12}$. ^{1}H NMR ($CDCl_2CDCl_2$, 500 MHz, 100^{o}C): δ ppm 9.60 (s, 6H), 8.83(s, 6H), 7.60(s, 12H), 7.38(s, 6H), 7.12(s, 6H), 4.33(s, 6H), 3.99(s, 6H), 3.82(s, 6H), 3.75(s, 6H), 3.71(s, 6H), 3.60(s, 6H), 3.40(s, 9H), 2.88(m, 6H), 1.89~0.87(m, 57H). ^{13}C NMR can not be resolved due to the large disc. Elemental Analysis: Calculated: C 82.79, H 7.41. O 9.80; Found: C 82.52, H 7.59.